Publishing House ASV
begell house, inc. publishers
PAACH
Scientific coordination is carried out by the Russian Academy of Architecture and Construction Sciences (RAACS)

Volume 16 • Issue 2 • 2020

ISSN 2588-0195 (Online)
ISSN 2587-9618 (Print) Continues ISSN 1524-5845

International Journal for

Computational Civil and Structural Engineering

Международный журнал по расчету гражданских и строительных конструкций

http://raasn.ru/public.php
http://ijccse.iasv.ru/index.php/IJCCSE

DOI: 10.22337/2587-9618
GICID: 71.0000.1500.2830

Scientific coordination is carried out by the Russian Academy of Architecture and Construction Sciences (RAACS)

PUBLISHER

ASV Publishing House (ООО «Издательство АСВ»)
19/1,12, Yaroslavskoe Shosse, 120338, Moscow, Russia
Tel. +7(925)084-74-24; E-mail: iasv@iasv.ru; Интернет-сайт: http://iasv.ru/

ADVISORY EDITORIAL BOARD

TECHNICAL EDITOR

EDITORIAL TEAM

INVITED REVIEWERS

AIMS AND SCOPE

The aim of the Journal is to advance the research and practice in structural engineering through the application of computational methods. The Journal will publish original papers and educational articles of general value to the field that will bridge the gap between high-performance construction materials, large-scale engineering systems and advanced methods of analysis.

The scope of the Journal includes papers on computer methods in the areas of structural engineering, civil engineering materials and problems concerned with multiple physical processes interacting at multiple spatial and temporal scales. The Journal is intended to be of interest and use to researches and practitioners in academic, governmental and industrial communities.

ОБЩАЯ ИНФОРМАЦИЯ О ЖУРНАЛЕ

International Journal for Computational Civil and Structural Engineering

(Международный журнал по расчету гражданских и строительных конструкций)

Международный научный журнал “International Journal for Computational Civil and Structural Engineering (Международный журнал по расчету гражданских и строительных конструкций)” (IJCCSE) является ведущим научным периодическим изданием по направлению «Инженерные и технические науки», издаваемым, начиная с 1999 года (ISSN 2588-0195 (Online); ISSN 2587-9618 (Print) Continues ISSN 1524-5845). В журнале на высоком научно-техническом уровне рассматриваются проблемы численного и компьютерного моделирования в строительстве, актуальные вопросы разработки, исследования, развития, верификации, апробации и приложений численных, численно-аналитических методов, программно-алгоритмического обеспечения и выполнения автоматизированного проектирования, мониторинга и комплексного наукоемкого расчетно-теоретического и экспериментального обоснования напряженно-деформированного (и иного) состояния, прочности, устойчивости, надежности и безопасности ответственных объектов гражданского и промышленного строительства, энергетики, машиностроения, транспорта, биотехнологий и других высокотехнологичных отраслей.

В редакционный совет журнала входят известные российские и зарубежные деятели науки и техники (в том числе академики, члены-корреспонденты, иностранные члены, почетные члены и советники Российской академии архитектуры и строительных наук). Основной критерий отбора статей для публикации в журнале − их высокий научный уровень, соответствие которому определяется в ходе высококвалифицированного рецензирования и объективной экспертизы, поступающих в редакцию материалов.

Журнал входит в Перечень ВАК РФ ведущих рецензируемых научных изданий, в которых должны быть опубликованы основные научные результаты диссертаций на соискание ученой степени кандидата наук, на соискание ученой степени доктора наук по научным специальностям и соответствующим им отраслям науки:

- 01.02.04 – Механика деформируемого твердого тела (технические науки),
- 05.13.18 – Математическое моделирование численные методы и комплексы программ (технические науки),
- 05.23.01 – Строительные конструкции, здания и сооружения (технические науки),
- 05.23.02 – Основания и фундаменты, подземные сооружения (технические науки),
- 05.23.05 – Строительные материалы и изделия (технические науки),
- 05.23.07 – Гидротехническое строительство (технические науки),
- 05.23.17 – Строительная механика (технические науки).

В Российской Федерации журнал индексируется Российским индексом научного цитирования (РИНЦ).

Журнал входит в базу данных Russian Science Citation Index (RSCI), полностью интегрированную с платформой Web of Science. Журнал имеет международный статус и высылается в ведущие библиотеки и научные организации мира.

Издатели журнала – *Издательство Ассоциации строительных высших учебных заведений /АСВ/* (Россия, г. Москва) и до 2017 года *Издательский дом Begell House Inc.* (США, г. Нью-Йорк). Официальными партнерами издания является *Российская академия архитектуры и строительных наук* (*РААСН*), осуществляющая научное курирование издания, и *Научно-исследовательский центр СтаДиО* (ЗАО НИЦ СтаДиО).

Цели журнала – демонстрировать в публикациях российскому и международному профессиональному сообществу новейшие достижения науки в области вычислительных методов решения фундаментальных и прикладных технических задач, прежде всего в области строительства.

Задачи журнала:

- предоставление российским и зарубежным ученым и специалистам возможности публиковать результаты своих исследований;
- привлечение внимания к наиболее актуальным, перспективным, прорывным и интересным направлениям развития и приложений численных и численно-аналитических методов решения фундаментальных и прикладных технических задач, совершенствования технологий математического, компьютерного моделирования, разработки и верификации реализующего программно-алгоритмического обеспечения;
- обеспечение обмена мнениями между исследователями из разных регионов и государств.

Тематика журнала. К рассмотрению и публикации в журнале принимаются аналитические материалы, научные статьи, обзоры, рецензии и отзывы на научные публикации по фундаментальным и прикладным вопросам технических наук, прежде всего в области строительства. В журнале также публикуются информационные материалы, освещающие научные мероприятия и передовые достижения Российской академии архитектуры и строительных наук, научно-образовательных и проектно-конструкторских организаций.

Тематика статей, принимаемых к публикации в журнале, соответствует его названию и охватывает направления научных исследований в области разработки, исследования и приложений численных и численно-аналитических методов, программного обеспечения, технологий компьютерного моделирования в решении прикладных задач в области строительства, а также соответствующие профильные специальности, представленные в диссертационных советах профильных образовательных организациях высшего образования.

Редакционная политика. Политика редакционной коллегии журнала базируется на современных юридических требованиях в отношении авторского права, законности, плагиата и клеветы, изложенных в законодательстве Российской Федерации, и этических принципах, поддерживаемых сообществом ведущих издателей научной периодики.

За публикацию статей плата с авторов не взымается. Публикация статей в журнале бесплатная. На платной основе в журнале могут быть опубликованы материалы рекламного характера, имеющие прямое отношение к тематике журнала.

Журнал предоставляет непосредственный открытый доступ к своему контенту, исходя из следующего принципа: свободный открытый доступ к результатам исследований способствует увеличению глобального обмена знаниями.

Индексирование. Публикации в журнале входят в системы расчетов индексов цитирования авторов и журналов. «Индекс цитирования» — числовой показатель, характеризующий значимость данной статьи и вычисляющийся на основе последующих публикаций, ссылающихся на данную работу.

Авторам. Прежде чем направить статью в редакцию журнала, авторам следует ознакомиться со всеми материалами, размещенными в разделах сайта журнала (интернет-сайт Российской академии архитектуры и строительных наук (http://raasn.ru); подраздел «Издания РААСН» или интернет-сайт Издательства АСВ (http://iasv.ru); подраздел «Журнал IJCCSE»): с основной информацией о журнале, его целями и задачами, составом редакционной коллегии и редакционного совета, редакционной политикой, порядком рецензирования направляемых в журнал статей, сведениями о соблюдении редакционной этики, о политике авторского права и лицензирования, о представлении журнала в информационных системах (индексировании), информацией о подписке на журнал, контактными данными и пр. Журнал работает по лицензии Creative Commons типа cc by-nc-sa (Attribution Non-Commercial Share Alike) – Лицензия «С указанием авторства – Некоммерческая – Копилефт».

Рецензирование. Все научные статьи, поступившие в редакцию журнала, проходят обязательное двойное слепое рецензирование (рецензент не знает авторов рукописи, авторы рукописи не знаю рецензентов).

Заимствования и плагиат. Редакционная коллегия журнала при рассмотрении статьи проводит проверку материала с помощью системы «Антиплагиат». В случае обнаружения многочисленных заимствований редакция действует в соответствии с правилами COPE.

Подписка. Журнал зарегистрирован в Федеральном агентстве по средствам массовой информации и охраны культурного наследия Российской Федерации. Индекс в общероссийском каталоге РОСПЕЧАТЬ − 18076.

По вопросам подписки на международный научный журнал “International Journal for Computational Civil and Structural Engineering (Международный журнал по расчету гражданских и строительных конструкций)” обращайтесь в Агентство «Роспечать» (Официальный сайт в сети Интернет: http://www.rosp.ru/) или в издательство Ассоциации строительных вузов (АСВ) в соответствии со следующими контактными данными:

ООО «Издательство АСВ»

Юридический адрес: 129337, Россия, г. Москва, Ярославское ш., д. 26, офис 705;

Фактический адрес: 129337, Россия, г. Москва, Ярославское ш., д. 19, корп. 1, 5 этаж, офис 12 (ТЦ Соле Молл);

Телефоны: +7 (925) 084-74-24, +7 (926) 010-91-33;

Интернет-сайт: www.iasv.ru. Адрес электронной почты: iasv@iasv.ru.

Контактная информация. По всем вопросам работы редакции, рецензирования, согласования правки текстов и публикации статей следует обращаться к главному редактору журнала члену-корреспонденту РААСН *Сидорову Владимиру Николаевичу* (адреса электронной почты: sidorov.vladimir@gmail.com, sidorov@iasv.ru, iasv@iasv.ru, sidorov@raasn.ru) или к техническому редактору журнала советнику РААСН *Кайтукову Таймуразу Батразовичу* (адреса электронной почты: tkaytukov@gmail.com; kaytukov@raasn.ru). Кроме того, по указанным вопросам, а также по вопросам размещения в журнале рекламных материалов можно обращаться к генеральному директору ООО «Издательство АСВ» *Никитиной Надежде Сергеевне* (адреса электронной почты: iasv@iasv.ru, nsnikitina@mail.ru, ijccse@iasv.ru).

Журнал становится технологичнее. Издательство АСВ с сентября 2016 года является членом Международной ассоциации издателей научной литературы (Publishers International Linking Association (PILA)), осуществляющей свою деятельность на платформе CrossRef. Оригинальным статьям, публикуемым в журнале, будут присваиваться уникальные номера (индексы DOI – Digital Object Identifier), что значительно облегчит поиск метаданных и местонахождение полнотекстового произведения. DOI – это система определения научного контента в сети Интернет.

С октября 2016 года стал возможен прием статей на рассмотрение и рецензирование через онлайн систему приема статей Open Journal Systems на сайте журнала (электронная редакция): http://ijccse.iasv.ru/index.php/IJCCSE.

Автор имеет возможность следить за продвижением статьи в редакции журнала в личном кабинете Open Journal Systems и получать соответствующие уведомления по электронной почте.

В феврале 2018 года журнал был зарегистрирован в Directory of open access journals (DOAJ) (это один из самых известных поисковых сервисов в мире, который предоставляет открытый доступ к материалам и индексирует не только заголовки журналов, но и научные статьи), в сентябре 2018 года включен в продукты EBSCO Publishing.

International Journal for
Computational Civil and Structural Engineering
(Международный журнал по расчету гражданских и строительных конструкций)
Volume 16, Issue 2 ***2020***
Scientific coordination is carried out by the Russian Academy of Architecture and Construction Sciences (RAACS)

CONTENTS

International Journal for
Computational Civil and Structural Engineering
(Международный журнал по расчету гражданских и строительных конструкций)
Volume 16, Issue 2 ***2020***
Scientific coordination is carried out by the Russian Academy of Architecture and Construction Sciences (RAACS)

СОДЕРЖАНИЕ

DOI:10.22337/2587-9618-2020-16-2-14-25

EXAMPLE OF GRAGUAL TRANSFORMATION OF STIFFNESS MATRIX AND MAIN SET OF EQUATIONS AT ADDITIONAL FINITE ELEMENT METHOD

Anna V. Ermakova
South Ural State University, Chelyabinsk, RUSSIA

Abstract: The paper considers the example of gradual transformation of the stiffness matrix and the main set of equations at Additional Finite Element Method (AFEM). It is corresponded to the increase of load and the ideal failure model of structure. AFEM uses the additional design diagrams and additional finite elements (AFE) for this operation. This process is illustrated by the transformation of design diagram of bended concrete console from the beginning of its loading to the collapse. The structure reveals four physical nonlinear properties before the ultimate limit state. Every nonlinear property appears under the action of corresponded load. The stiffness matrix and the set of equations are changed under influence of the value of load and the presence of observed nonlinear properties at this moment.

Keywords: Additional finite element method, Finite element method, Stiffness matrix, Set of equations, Additional design diagram, Additional finite element, Ideal failure model

ПРИМЕР ПОСТЕПЕННОГО ПРЕОБРАЗОВАНИЯ МАТРИЦЫ ЖЕСТКОСТИ И ОСНОВНОЙ СИСТЕМЫ УРАВНЕНИЙ МЕТОДА ДОПОЛНИТЕЛЬНЫХ КОНЕЧНЫХ ЭЛЕМЕНТОВ

А.В. Ермакова
Южно-Уральский государственный университет, Челябинск, РОССИЯ

Аннотация: В статье рассматривается пример постепенного преобразования матрицы жесткости и основной системы уравнений метода дополнительных конечных элементов (МДКЭ). Это преобразование происходит в соответствии с ростом нагрузки и идеальной моделью разрушения конструкции. Для выполнения этой операции МДКЭ использует дополнительные расчетные схемы из дополнительных конечных элементов (ДКЭ). Для иллюстрации этого процесса рассмотрено изменение расчетной схемы изгибаемой бетонной консоли от начала нагружения до разрушения. Эта конструкция проявляет четыре физически нелинейных свойства к моменту достижения ею предельного состояния. Каждое нелинейное свойство появляется при действии соответствующей нагрузки. Матрица жесткости и система уравнений меняются в зависимости от величины нагрузки и наличия тех нелинейных свойств, которые наблюдаются в этот момент.

Ключевые слова: метод дополнительных конечных элементов, метод конечных элементов, матрица жесткости, система уравнений, дополнительная расчетная схема, дополнительный конечный элемент, идеальная модель разрушения

INTRODUCTION

Some characteristics are necessary when Additional Finite Element Method (AFEM) is used for analysis at limit states of structures with several physical nonlinear properties:

1) The number of all nonlinear properties;
2) The sequence of its appearance before ultimate limit state;
3) The way of taking into account for each nonlinear property;
4) The stress-strain state when each nonlinear property is appeared.

These factors act at the initial design diagram, the stiffness matrix and the main set of algebraic equations. Also they determine of the way of nonlinear analysis. Thus, the problem of mathematic description of this process is appeared. This description must correspond to the logic of AFEM and FEM, the character of observed nonlinear properties and the requirement of limit state analysis. The developed AFEM is destined for decision of this problem. The examples are necessary for verification and realization of its algorithms.

1. GENERAL INFORMATION OF AFEM

Additional Finite Element Method (AFEM) [1] is suggested by author as the variant of the development of Finite Element Method (FEM) [2, 3]. It is destined for analysis of structures with several (n) nonlinear properties at ultimate limit state (state of ultimate equilibrium). It adds the some elements of the Method of Limit States (Ultimate Equilibrium) [4, 5] and the Method of Elastic Decisions [6, 7] to the usual sequence of solving problems by FEM. AFEM is numerical method for combination and development of three science directions:

1) The mathematic basis for several (n) transformations of main set of equations and extension of possibilities of FEM for solving of n-nonlinear problems;
2) The decision of the problems of structural mechanics for analysis of structures at limit states as n-nonlinear systems;
3) The analysis of real structures at limit states as n-nonlinear systems.

The example is given for application AFEM to nonlinear analysis of plane reinforced concrete structure with four nonlinear properties. It corresponds to normative requirements [8 - 10].

2. PROBLEM AND WAY OF DECISION

The nonlinear analysis at limit state is considered for the bended console.

This structure reaches its limit state under increased load gradually.

It gradually reveals four nonlinear properties:

1) The plasticity;
2) The partial unload due to the redistribution of stresses after the cracking;
3) The presence of the cracking;
4) The ultimate limit state before the collapse.

The realization of nonlinear analysis at limit state demands one linear analysis and four nonlinear ones depending on the number of nonlinear properties at this step of loading. The way of these analyses is:

1) The initial linear analysis without any nonlinear properties;
2) The plastic analysis with one nonlinear property;
3) The analysis with taking into account of two nonlinear properties: the plasticity and the partial unload due to redistribution of stresses after cracking;
4) The analysis with taking into account of three nonlinear properties: the plasticity, the partial unload due to the redistribution of stresses and the presence of the cracking;
5) The analysis with taking into account of four nonlinear properties: the plasticity, the partial unload due to the redistribution of stresses, the cracking and limit state.

3. GROWTH OF LOAD AND FORM OF MAIN SET OF EQUATIONS

The growth of load P and appearance of nonlinear properties are the main factors for realization of analysis of structure at limit state.

These factors influence over transformation of the design diagram, the stiffness matrix of structure and the main set of algebraic equations.

3.1. Growth of load and nonlinear properties

There is the condition of analysis at first limit state for guarantee the bearing capacity of structure:

$$P_{max} \leq P_{lim}. \tag{1}$$

Where P_{max} = maximal value of external static load which is equal to minimal kinematic one. P_{lim} = minimal internal resistance of the structure to this external load.
The external load P changes from 0 to P_{lim} gradually ($P \to P_{lim}$):

$$P_1 = 0 < P_2 = P_3 < P_4 = P_{max} = P_{lim}. \quad (2)$$

Where P_i = the intermediate value of load P when i-th nonlinear property is appeared (i changes from 1 to $n = 4$).
The first nonlinear property is plasticity ($i = 1$). It is observed from load $P = 0$ to load $P = P_{lim}$, i.e. all time of loading. It is only nonlinear property under load $P_1 = 0<P<P_2$. The second nonlinear property is the partial unload ($i = 2$) due to redistribution of stresses after the cracking. It is appeared under load $P=P_2=P_3$ together the crack simultaneously. It is manifested from load $P=P_2=P_3$ to load $P=P_4$, i.e. interval of load $P_2=P_3<P<P_4=P_{lim}$. The third nonlinear property is the existence of crack ($i = 3$). It is observed during interval of load $P_3<P<P_4=P_{lim}$. The last nonlinear property is ultimate limit state ($i = n = 4$). It is occurred under load $P=P_4=P_{max}=P_{lim}$. Thus, the way (2) of the growth of load P is:

$$P_1 = 0 \to P_2 = P_3 \to P_4 = P_{max} = P_{lim}. \quad (3)$$

The condition (3) is the first for the formation of the main set of equations.

3.2. Transformation of design diagram

The condition (3) demands the gradual transformation of the design diagram of structure in the nest sequence:

1) The initial linear design diagram of structure without nonlinear properties ($i = 0$) under load $P = P_1 = 0$;
2) The design diagram of structure with plastic property (i=1) only under load P_1=0<P< P_2;
3) The design diagram of structure with two nonlinear properties under load $P = P_2 = P_3$: plasticity ($i = 1$) and the partial unload (i= 2) due to redistribution of stresses after the cracking;
4) The design diagram of structure with three nonlinear properties under load $P_3 < P < P_4$: plasticity ($i = 1$), the partial unload ($i = 2$) due to redistribution of stresses and the cracking ($i = 3$);
5) The design diagram of structure with four nonlinear properties under load $P = P_4 = P_{max} = P_{lim}$: plasticity ($i = 1$), the partial unload ($i = 2$) due to redistribution of stresses, the existence of crack ($i = 3$) and limit state ($i = 4$).

In nonlinear analysis of structure at limit state the initial design diagram gradually takes the three intermediated forms and fifth at last: 1) → 2) → 3) → 4) → 5). The fifth last form is *ideal failure model* or design diagram of structure at limit state. It is necessary for realization of nonlinear analysis by AFEM [11].
Also, when AFEM is used for nonlinear analysis, all five forms of design diagram must have the identical characteristics, for example the same number of nodes points, view and number of finite elements (FE's). It is necessary for the definition of stiffness matrixes of all forms of design diagram.

3.3. Transformation of stiffness matrix

The fulfillment of the condition (1) requires the definition of minimal value of internal resistance P_{lim}. Usually this minimum corresponds to the minimum stiffness of structure due to negative influence of each i-th nonlinear property. For considered example i changes from 1 to $n = 4$. The stiffness matrix is changed gradually from initial value K to its minimal value K_{min} due to these defects:

$$K \to K_1 \to K_2 \to K_3 \to K_4 = K_{min} = K_{lim}. \quad (4)$$

Where K = stiffness matrix of structure without nonlinear properties ($i = 0$) under the load $P = P_1 = 0$;
K_1 = stiffness matrix of structure with plastic property (i=1) under the load P_1= 0<P<P_2;
K_2 = stiffness matrix of structure with plastic property (i=1) and the partial unload (i=2) due to redistribution of stresses after cracking under the load $P = P_2 = P_3$;

K_3 = stiffness matrix of structure with plastic property (i = 1), the partial unload (i = 2) due to redistribution of stresses and the cracking (i = 3) under the load $P_3<P<P_4$;

K_4 = stiffness matrix of structure with plastic property (i = 1), the partial unload (i = 2) due to redistribution of stresses, the existence of cracking (i = 3) and limit state (i = 4) under the load $P = P_4$;

K_{min} = stiffness matrix of structure with n=4 nonlinear properties at moment of its minimal internal resistance to external load $P=P_4=P_{max}$;

K_{lim} = stiffness matrix of structure at limit state under the load $P=P_4=P_{max}=P_{lim}$, when its design diagram is *ideal failure model.*

The condition (4) is the second for the formation of the main set of equations. All matrices K, K_1, K_2, K_3, K_4 (K_{min}, K_{lim}) must have the equal dimensions and the same filling for computer realization of analysis by AFEM.

3.4. Required transformation of the set of algebraic equations

The main operation of analysis by FEM and AFEM is the solving of the set of equations:

$$K_{nonl}V = P\,. \qquad (5)$$

Where P = matrix of external load;

V = matrix of unknown node displacements;

K_{nonl} = stiffness matrix of structure with nonlinear properties. This matrix is changed in accordance with the degree of its influence. The stiffness matrix K_{nonl} is formed from coefficients of stiffness matrices of the separate finite elements (FE's).

The set of equations (5) solves one time in linear analysis because of matrix $K_{nonl} = K = const$ due to the absence of nonlinear properties.

In nonlinear analysis this set of equation must be solved by iterative process because of $K_{nonl} \neq K \neq const.$ In this process matrix K turns into matrix K_{nonl} gradually. The transformation of the set of equation (5) is connected with difficulties in presence of several (n) of physical nonlinear properties due to its different causes. When n = 4 this transformation must go under the condition (3) for right part and the condition (4) for the left one of the set of equations (5):

Under the load $P = P_1 = 0$ and $i = 0$

$$KV = P\,. \qquad (6)$$

Under the load $P_1 = 0 < P < P_2$ and $i = 1$:

$$K_1V = P. \qquad (7)$$

Under the load $P = P_2 = P_3$ and $i = 2$

$$K_2V = P. \qquad (8)$$

Under the load $P_3 < P < P_4$ and $i = 3$

$$K_3V = P\,. \qquad (9)$$

Under the load $P = P_4 = P_{max} = P_{lim}$ and $i = 4$

$$K_4V = P. \qquad (10)$$

Thus the initial form of the set equations (6) takes the requirement forms (7), (8), (9) and (10) gradually according to the value of load P.

In limit state of structure (see (1)) the set of equations (10) must became

$$K_{lim}V = P_{lim}\,. \qquad (11)$$

This description (11) corresponds to the next view of expression (1)

$$P_{lim} = P_{max}\,. \qquad (12)$$

Method of Limit States guarantees the appearance the equality (12) for formula (1) in one case from million ones (see s. 3.1).

4. SET OF EQUATIONS AT AFEM

The Additional Finite Element Method (AFEM) was suggested by author [1] as the variant of the Finite Element Method (FEM) for analysis of structures with several nonlinear properties at limit states. It is numerical combination of the three effective methods of structural analysis: FEM, Method of Elastic Decisions and Limit State Method. It solves the problem of analysis of structure at limit states according to failure model, when nonlinear properties and defects are revealed due to increase of load. AFEM uses the additional finite elements and additional design diagrams for gradually transformation of main set of equations [12].

4.1. Transformation of design diagram by means of additional design diagrams

The example is illustrated the action of additional design diagrams at the initial design diagram for bending console in plane stress-state (see table 1). The initial design diagram consists of 8 triangular deep beam finite elements with liner properties (p.1 table 1). AFEM uses four additional design diagrams for transformation of the initial design diagram into ideal failure model of console (see s. 3.2):

1) The initial design diagram of structure without nonlinear properties ($i = 0$) under load $P = P_1 = 0$ transforms into the design diagram of structure with first ($i = 1$) nonlinear property (plasticity) by means of the first additional design diagram under load $P_1 = 0 < P < P_2$ (p. 2 table 1);
2) The design diagram of structure with one (i=1) nonlinear property (plasticity) under load $P_1 = 0 < P < P_2$ transforms into the design diagram of structure with two ($i = 2$) nonlinear properties (the plasticity ($i = 1$) and partial unload ($i = 2$) due to redistribution of stresses after cracking) by means of the second additional design diagram under load $P = P_2 = P_3$ (p. 3 table 1);
3) The design diagram of structure with two (i=2) nonlinear properties (the plasticity (i=1) and the partial unload (i=2)) under load $P=P_2=P_3$ transforms into the design diagram of structure with three (i=3) nonlinear properties (the plasticity (i=1), the partial unload (i=2) and the cracking (i=3)) by means of the third additional design diagram under load $P_3<P<P_4$ (p. 4 table 1);
4) The design diagram of structure with three (i=3) nonlinear properties (the plasticity (i=1), the partial (i=2) unload and the cracking (i=3)) under load $P_3 < P < P_4$ transforms into the design diagram of structure with four nonlinear properties ((the plasticity (i=1), the partial (i=2) unload, the cracking (i=3) and limit state (i=4)) or ideal failure model by means of the fourth additional design diagram under load $P = P_4 = P_{max} = P_{lim}$ (p. 5 table 1).

Every additional design diagram may be compared with empty space imbedded in the initial design diagram. It is filled negative stiffness for taking into account of only one nonlinear property. It consists of corresponding additional finite elements (AFE-s) (see s. 4.5). Additional design diagrams are basic for realization of nonlinear analysis at limit state due to fulfillment of conditions (3) and (4).

4.2. Transformation of initial stiffness matrix by means of stiffness matrices of additional design diagrams

The condition (4) is realized due to using of stiffness matrices of additional design diagrams.

Under application of AFEM the next equation is correct at the moment of limit state of structure with four nonlinear properties:

$$K_{lim} = K + \Delta K_1 + \Delta K_2 + \Delta K_3 + \Delta K_4 . \quad (13)$$

Where ΔK_1, ΔK_2, ΔK_3, ΔK_4 = stiffness matrices of the first, the second, the third and the fourth additional design diagrams consisting of additional finite elements (AFE's) for taking into account the first, the second, the third and the fourth nonlinear property respectively.

The stiffness matrices of additional design diagrams are destined for fulfillment of condition (4) and may be defined according to next formulas (see s. 3.3):

$$\Delta K_1 = K_1 - K \ , \quad (14)$$
$$\Delta K_2 = K_2 - K_1 \ , \quad (15)$$
$$\Delta K_3 = K_3 - K_2 \ , \quad (16)$$
$$\Delta K_4 = K_4 - K_3 . \quad (17)$$

The next way is used for the gradual transformation of the stiffness matrix K of initial design diagram of structure without nonlinear properties into stiffness matrix $K_{lim} = K_{min} = K_4$ of ideal of failure model or design diagram of structure at limit state (see table 1):
Under the load $P_1 = 0 < P < P_2$ and $i = 1$

$$K_1 = K + \Delta K_1 . \quad (18)$$

Under the load $P = P_2 = P_3$ and $i = 2$

$$K_2 = K + \Delta K_1 + \Delta K_2 . \quad (19)$$

Under the load $P_3 < P < P_4$ and $i = 3$

$$K_3 = K + \Delta K_1 + \Delta K_2 + \Delta K_3 . \quad (20)$$

Under the load $P = P_4 = P_{max} = P_{lim}$ and $i = 4$

$$K_4 = K + \Delta K_1 + \Delta K_2 + \Delta K_3 + \Delta K_4 . \quad (21)$$

The initial stiffness matrix K transforms gradually according to formulas (18) — (21) by means of stiffness matrices of ΔK_1, ΔK_2, ΔK_3, ΔK_4. The main characteristics of matrices K, K_1, K_2, K_3, K_4, ΔK_1, ΔK_2, ΔK_3 and ΔK_4 are: the same dimensions; the same filling positions; the square; the symmetry; the linearity; the positivity of matrices K, K_1, K_2, K_3, K_4; the negativity of matrices ΔK_1, ΔK_2, ΔK_3, ΔK_4. These characteristics are necessary for application of matrix theory [13]. The fulfillment of the condition (4) demands these characteristics for mathematic realization. Thus steps (18) – (21) are developed on the base of Method Elastic Decisions when the nonlinear stiffness matrix is divided into linear and nonlinear component [14].

4.3. Transformation of the set of algebraic equations

AFEM suggests the using of additional design diagrams consisting of additional finite elements (AFE-s) (see s. 3.4 and s. 4.2). In this case the sets of equations (7) – (10) are formed according to the formulas (18) – (21) under conditions (3) and (4):
Under the load $P_1 < P < P_2$ and $i = 1$

$$(K + \Delta K_1)V = P. \quad (22)$$

Under the load $P_2 = P = P_3$ and $i = 2$

$$(K + \Delta K_1 + \Delta K_2)V = P . \quad (23)$$

Under the load $P_3 < P < P_4$ and $i = 3$

$$(K + \Delta K_1 + \Delta K_2 + \Delta K_3)V = P . \quad (24)$$

Under the load $P = P_4 = P_{max} = P_{lim}$ and $i = 4$

$$(K + \Delta K_1 + \Delta K_2 + \Delta K_3 + \Delta K_4)V = P. \quad (25)$$

Thus, the algebraic equations (22) – (25) are corresponded to requirement forms for numerical realization of analysis at limit state of structure with four nonlinear properties.
Also the Method of Elastic Decision (Method of Additional loads) may used for the solving of these sets of equations. In this case the formulas (22)–(25) are formed according to the next way:
Under the load $P_1 < P < P_2$ and $i = 1$:

$$KV = P - \Delta K_1 V. \quad (26)$$

Under the load $P_2 = P = P_3$ and $i = 2$:

$$KV = P - \Delta K_1 V - \Delta K_2 V. \quad (27)$$

Under $P_3 < P < P_4$ $i = 3$:

$$KV = P - \Delta K_1 V - \Delta K_2 V - \Delta K_3 V . \quad (28)$$

Under $P = P_4 = P_{max} = P_{lim}$ and $i = 4$:

$$KV = P - \Delta K_1 V - \Delta K_2 V - \Delta K_3 V - \Delta K_4 V . \quad (29)$$

In relations (26)–(29) values $(-\Delta K_1 V)$, $(-\Delta K_2 V)$, $(-\Delta K_3 V)$ and $(-\Delta K_4 V)$ determines the influence of the first, the second, the third and the fourth nonlinear property respectively. For example the term $(-\Delta K_1 V)$ of the right-hand part of these equations is the additional load which with the main load P must be applied to linear structure to

reach the displacements corresponding to its displacements with the first nonlinear property under the action of the only external load P.
In nonlinear analysis at limit state the sets of algebraic equations (7) – (10) take the forms (22) – (25) or (26) – (29). These forms provide the taking into account the influence of each of four nonlinear property of structure. This way allows the using of different theoretical data [15 – 17] for nonlinear analysis [18 – 20] according to normative rules [8 – 10].
Thus logic of AFEM is corresponded to FEM.

4.4. Two ways for realization of iterative process at AFEM

Solution of the set of algebraic equations by iterative methods is the main step for nonlinear analysis of structures. AFEM suggests two ways for creation of this process [21]. Both ways are based on the decision of the set (6):

$$V = K^{-1}P \quad , \qquad (30)$$

Where K^{-1}= inverse stiffness matrix K.
Operations connected with obtaining of this inverse matrix $K^{-1}$are the most laborious. They take roughly three quarters of time for solving of the set of equations (1). In the first case iterative process is based on (21)–(25) and (30):
Under the load $P_1 < P < P_2$ and $i = 1$

$$V^{(k)} = (K + \Delta K_1^{(k-1)})^{-1}P \,. \qquad (31)$$

Under $P_2 = P = P_3$ and $i = 2$

$$V^{(k)} = (K + \Delta K_1^{(k-1)} + \Delta K_2^{(k-1)})^{-1}P. \qquad (32)$$

Under $P_3 < P < P_4$ and $i = 3$

$$V^{(k)} = (K + \Delta K_1^{(k-1)} + \Delta K_2^{(k-1)} + \Delta K_3^{(k-1)})^{-1}P \,. \qquad (33)$$

Under the load $P = P_4 = P_{max} = P_{lim}$ and $i = 4$

$$V^{(k)} = (K + \Delta K_1^{(k-1)} + \Delta K_2^{(k-1)} + \Delta K_3^{(k-1)} + \Delta K_4^{(k-1)})^{-1}P. \qquad (34)$$

Where k, $(k-1)$ = moving and previous iterations. This way is very laborious due to the obtaining of inverse matrix K^{-1} at everyone iteration.
The second way for realization of iterative process is based on the next views of the formulas (26) – (29):
Under the load $P_1 < P < P_2$ and $i = 1$

$$KV^{(k)} = P - \Delta K_1^{(k-1)} V^{(k-1)} \,. \qquad (35)$$

Under the load $P_2 = P = P_3$ and $i = 2$

$$KV^{(k)} = P - \Delta K_1^{(k-1)} V^{(k-1)} - \Delta K_2^{(k-1)} V^{(k-1)} \,. \qquad (36)$$

Under the load $P_3 < P < P_4$ and $i = 3$)

$$KV^{(k)} = P - \Delta K_1^{(k-1)} V^{(k-1)} - \Delta K_2^{(k-1)} V^{(k-1)} - \Delta K_3^{(k-1)} V^{(k-1)}. \qquad (37)$$

Under the load $P = P_4 = P_{max} = P_{lim}$ and $i = 4$

$$KV^{(k)} = P - \Delta K_1^{(k-1)} V^{(k-1)} - \Delta K_2^{(k-1)} V^{(k-1)} - \Delta K_3^{(k-1)} V^{(k-1)} - \Delta K_4^{(k-1)} V^{(k-1)}. \qquad (38)$$

The iterative process goes in accordance to formulas (35) – (38) and (30):
Under the load $P_1 < P < P_2$ and $i = 1$

$$V^{(k)} = K^{-1}(P - \Delta K_1^{(k-1)} V^{(k-1)}) \,. \qquad (39)$$

Under the $P_2 = P = P_3$ and $i = 2$:

$$V^{(k)} = K^{-1}(P - \Delta K_1^{(k-1)} V^{(k-1)} - \Delta K_2^{(k-1)} V^{(k-1)}) \,. \qquad (40)$$

Under $P_3 < P < P_4$ and $i = 3$:

$$V^{(k)} = K^{-1}(P - \Delta K_1^{(k-1)} V^{(k-1)} - \Delta K_2^{(k-1)} V^{(k-1)} - \Delta K_3^{(k-1)} V^{(k-1)}) \,. \qquad (41)$$

Under the load $P = P_4 = P_{max} = P_{lim}$ and $i = 4$

$$V^{(k)} = K^{-1}(P - \Delta K_1^{(k-1)} V^{(k-1)} - \Delta K_2^{(k-1)} V^{(k-1)} - \Delta K_3^{(k-1)} V^{(k-1)} - \Delta K_4^{(k-1)} V^{(k-1)}) \,. \qquad (42)$$

The formulas (39) – (42) are the results of solution of the sets of equations (35) – (38). They allow the obtaining of inverse stiffness matrix K^-

[1]at the first iteration only when $k = 1$. This advantage is useful when set of equations is solved by means of Gauss Elimination. The second way for creation of iterative process of AFEM is less laborious then the first one.

4.5. Additional finite elements

The condition (4) requires the fulfillment analogous one for every finite element. Due to nonlinear properties the its stiffness matrix gradually decreases from initial value K_e to its minimal value $K_{e,min}$. Usually this minimum corresponds to limit state, when the carrying capacity of finite element is lost and $K_{e,min}=K_{e,lim}= 0$ or close to 0.

If the number of nonlinear properties i changes from 1 to $n = 4$, the next condition is correct

$$K_e \to K_{e,1} \to K_{e,2} \to K_{e,3} \to K_{e,4} = K_{e,min} = K_{e,lim} = 0 \tag{43}$$

Where K_e = stiffness matrix of finite element without nonlinear properties ($i = 0$);

$K_{e,1}$ = stiffness matrix of finite element with plastic property ($i = 1$);

$K_{e,2}$ = stiffness matrix of finite element with plastic property ($i = 1$) and the partial unload ($i = 2$) due to redistribution of stresses after cracking;

$K_{e,3}$ = stiffness matrix of finite element with plastic property ($i = 1$), the partial unload ($i = 2$) due to redistribution of stresses and the cracking ($i = 3$);

$K_{e,4}$ = stiffness matrix of finite element with plastic property ($i = 1$), the partial unload ($i = 2$) due to redistribution of stresses, the existence of cracking ($i= 3$) and limit state ($i = n = 4$);

$K_{e,min}$ = stiffness matrix of finite element with n=4 nonlinear properties at moment of its minimal value;

$K_{e,lim}$ = stiffness matrix of finite element at limit state, when its value is closed to 0.

Four additional finite elements (AFE-s) are necessary for fulfillment of the condition (43). They transform gradually the initial finite element with linear properties into the same finite element with all nonlinear ones [1].

The stiffness matrix $\Delta K_{e,1}$ of the first additional finite element for taking into account the plastic property ($i = 1$) is equal

$$\Delta K_{e,1} = K_{e,1} - K_e. \tag{44}$$

The value $\Delta K_{e,1}$ depends on the level of stress-strain state under load $P_1 = 0<P< P_4=P_{max}=P_{lim}$. These additional finite elements are formed the first additional design diagram for taking into account the plasticity in formulas (22) – (25).

The stiffness matrix $\Delta K_{e,2}$ of the second additional finite element for taking into account the partial unload ($i = 2$) due to redistribution of stresses after cracking has next formula:

$$\Delta K_{e,2} = K_{e,2} - K_{e,1}. \tag{45}$$

The value $\Delta K_{e,2}$ depends on the stress-strain state under load $P=P_2$ when crack is appeared.

These additional finite elements are formed the second additional design diagram for taking into account the partial unload due to redistribution of stresses after cracking in formulas (23) – (25).

The stiffness matrix $\Delta K_{e,3}$ of the third additional finite element for taking into account the existence of cracking ($i = 3$) is defined

$$\Delta K_{e,3} = K_{e,3} - K_{e,2}\,. \tag{46}$$

The value $\Delta K_{e,3}$ depends on the level of stress-strain state under load $P_3 < P < P_4=P_{max}=P_{lim}$.

These additional finite elements are consisted the third additional design diagram for taking into account the existence of cracking in formulas (24) and (25).

The stiffness matrix $\Delta K_{e,4}$ of the fourth additional finite element for taking into account the limit state ($i = 4$) is equal

$$\Delta K_{e,4} = K_{e,4} - K_{e,3}. \tag{47}$$

The value $\Delta K_{e,4}$ depends on the level of limit stress-strain state under load $P = P_4=P_{max}=P_{lim}$.

Table 1. Transformation of initial design diagram of bended console with four nonlinear properties to its ideal failure model be means of additional design diagrams under gradual growth of load P from starting value $P_0 = 0$ to maximal one $P_{max} = P_{lim}$

N	Number of nonlinear property	Value of load P	Required design diagram: Design diagram	Required design diagram: View and stiffness matrix	Transformation of initial design diagram: Initial linear design diagram	Used additional design diagrams, its stiffness matrices and nonlinear properties: Plasticity $i = 1$	Partial unload $i = 2$	Existence of crack $i = 3$	Limit state $i = n = 4$
1	0	$P_0 = 0$	Initial linear design diagram	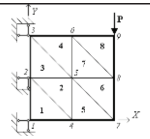 K					
2	1	$P_1=0<P<P_2$	Design diagram with plasticity	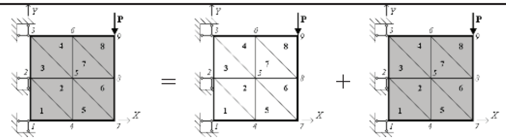 K_1 =	K +	ΔK_1			
3	2	$P=P_2=P_3$	Design diagram with plasticity and partial unload due to cracking	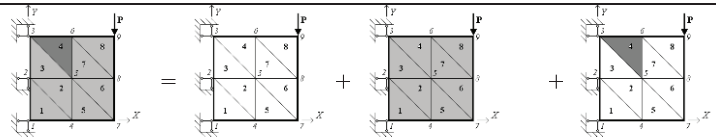 K_2 =	K +	ΔK_1 +	ΔK_2		
4	3	$P_3<P<P_4$	Design diagram with plasticity, partial unload and crack	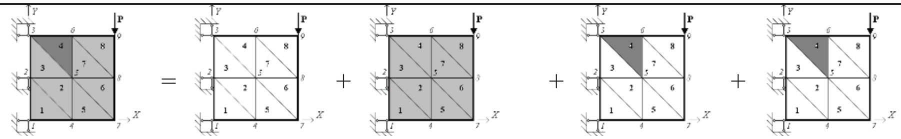 K_3 =	K +	ΔK_1 +	ΔK_2 +	ΔK_3	
5	4	$P=P_4= =P_{max}=P_{lim}$	Design diagram with plasticity, partial unload, crack and limit state, i.e. ideal failure model	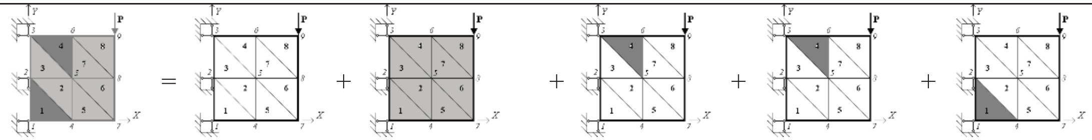 $K_4=K_{min}=K_{lim}$ =	K +	ΔK_1 +	ΔK_2 +	ΔK_3 +	ΔK_4

Comment: 1) Number of nonlinear properties i is changed from 1 to 4. 2) Load P grows from starting value $P_0 = 0$ to maximal one $P_{max} = P_{lim}$. 3) K – stiffness matrix of initial linear design diagram; K_1, K_2, K_3, K_4, – stiffness matrix of design diagram with taking into account of one, two, three and four nonlinear properties respectively; ΔK_1, ΔK_2, ΔK_3, ΔK_4 – stiffness matrix of the first, the second, the third and the fourth additional design diagram consisting of additional finite elements (AFE's) taking into account the first, the second, thee third and the fourth nonlinear property respectively; K_{min} and K_{lim} – stiffness matrix of structure at limit state (ideal failure modal of structure)

If stiffness matrix of finite element at limit state $K_{e,4} = K_{e,min} = K_{e,lim} = 0$ the stiffness matrix of its additional finite element $\Delta K_{e,4} = -K_{e,3}$.

These additional finite elements are consisted the fourth additional design diagram for taking into account the limit state in formula (25).

The initial design diagram of bended console is transformed to its ideal failure model due to four additional finite elements (table 1).

CONCLUSIONS

Considered example proves the possibility of realization the nonlinear analysis at limit state for bended console according to its ideal failure model by means of Additional Finite Element Method (AFEM).

Additional design diagrams and additional finite elements are used for gradual transformation of the stiffness matrix and the main set of equations.

Next conditions are fulfilled for this process:

1) the correspondence to algorithmic logic of nonlinear analysis due to conservation of main mathematic characteristics of stiffness matrix of structure under the numerical variation of its coefficients;
2) the orientation at gradual achievement of criterion of limit state before collapse;
3) the guarantee the allowance for each of four nonlinear properties at stress-strain state;
4) the creation of iterative process for solving of the main set of equations by two ways: usual manner and use the advantages of Method of Elastic Decisions.

REFERENCES

1. **Ermakova A.V.** Metod dopolnitel'nyh konechnyh jelementov dlja rascheta zhelezobetonnyh konstrukcij po predel'nym sostojanijam [Additional finite element method for analysis of reinforced concrete structures at limit states]. Moscow, ASV Publishing House, 2007, 126 pages (in Russian).
2. **Zienkiewicz O.C.** Metod konechnyh jelementov v tehnike [Finite element method in engineering]. Moscow, Mir, 1975, 541 pages (in Russian).
3. **Zienkiewicz O. C., Taylor R.L.** The Finite Element Method. The Fourth Edition, Volume 2, McGraw-Hill, 1989.
4. **Gvozdev A.A.** Raschet nesushhej sposobnosti konstrukcij po metodu predel'nogo ravnovesija. Vyp. 1, Sushhnost' metoda i ego obosnovanie [Analysis of bearing capacity of structures by Limit State Method]. Moscow, Gosstroyisdat, 1949, 280 pages (in Russian).
5. **Oatul A.A.** aschet jelementov zhelezobetonnyh konstrukcij po dvum predel'nym sostojanijam [Analysis of units of reinforced concrete structures at both limit states]. Volume 2. Chelyabinsk, ChPI, 1987, 64 pages (in Russian).
6. **Ilyushin A.A.** Plastichnost' [Plasticity]. Moscow, Gostechisdat, 1948, 376 pages (in Russian).
7. **Ilyushin A.A.** Trudy [Works]. Volume 1, Moscow, Phismathlit, 2003, 350 pages (in Russian).
8. **SP 63.13330.2012.** Betonnye i zhelezobetonnye konstrukcii. Aktualizirovannaja redakcija SNiP 52-01-2003 [Concrete and reinforced concrete structures. Actual version SNiP 52-01-2003]. Moscow, 2013, 152 pages (in Russian).
9. **SNiP 52-01-2003.** Betonnye i zhelezobetonnye konstrukcii [Concrete and reinforced concrete structures]. Moscow, FGUP CPP, 2004, 26 pages (in Russian).
10. 10. **SP 52-102-2004**. Predvaritel'no naprjazhennye zhelezobetonnye konstrukcii [Prestressed Concrete and reinforced concrete structures]. Moscow, FGUP CPP, 2005, 36 pages (in Russian).
11. **Ermakova A.** Ideal Failure Models of Structures for Analysis by FEM and AFEM. // Proceedings ICIE–2017, 2017, Volume 206, pp. 9-15.
12. **Ermakova A.V.** Set of equations of AFEM and properties of additional finite elements.

// International Journal for Computational Civil and Structural Engineering, 2019, Volume 15, Issue 2, pp. 51-64.

13. **Marcus M., Minc H.** Obzor po teorii matric i matrichnyh neravenstv [A survey of matrix theory and matrix inequalities]. The Third Edition. Moscow, Book House “Librocom”, 2009, 232 pages (in Russian).
14. **Postnov V.A.** Chislennye metody rascheta sudovyh konstrukcij [Numerical methods for design of ship structures]. Leningrad, Shipbuilding, 1977, 280 pages (in Russian).
15. **Karpenko N.I.** Obshhie modeli mehaniki zhelezobetona [Construction of Schemes of Reinforced Concrete]. State Administration of Construction, Moscow, 1996, 416 pages (in Russian).
16. **Karpenko N.I., Karpenko S.N., Petpov A.N., Paluvina S.N.** Model' deformirovanija zhelezobetona v prirashhenijah i raschet balok-stenok i izgibaemyh plit s treshhinami [Deformation model of reinforced concrete and analysis of deep beams and bended plates with cracks]. Petrozavodsk, PetrGU, 2013, 156 pages (in Russian).
17. **Shugaev V.V.** Inzhenernye metody v nelinejnoj teorii predel'nogo ravnovesija obolochek [Engineer Methods of Non-Linear Theory of Limit Equilibrium of the Shells]. Moscow, Gotika, 2001, 368 pages (in Russian).
18. **Gorodetsky A.S., Evzerov I.D.** Komp'juternye modeli konstrukcij [Computer models of structures]. Kiev, Fact, 2007, 394 pages (in Russian).
19. **Perelmuter A.V., Slivker V.I.** Raschetnye modeli sooruzhenij i vozmozhnost' ih analiza [Designed models and possibilities of analysis]. Kiev, Steel, 2002, 600 pages (in Russian).
20. **Oatul A.A., Karyakin A.A., Kutin U.F.** Raschet i proektirovanie jelementov zhelezobetonnyh konstrukcij na osnove primenenija JeVM [Computer-aided analysis and construction of reinforced concrete structural elements]. Collected lectures. Part 4. Ed. by Prof. Oatul A.A. Chelyabinsk, Chelyabinsk Polytechnic Institute, 1980, 67 pages (in Russian).
21. **Ermakova A.** Dva sposoba postroenija iteracionnogo processa metoda dopolnitel'nyh konechnyh jelementov [Two ways for realization of iterative process at additional finite element method]. Structural mechanics and analysis of constructions, 2018, No 6. pp. 45-52 (in Russian).

СПИСОК ЛИТЕРАТУРЫ

1. **Ермакова А.В.** Метод дополнительных конечных элементов для расчета железобетонных конструкций по предельным состояниям. – М.: АСВ, 2007. – 126 с.
2. **Зенкевич О. К.** Метод конечных элементов в технике. – М: Мир, 1975 – 541 с.
3. **Zienkiewicz O. C., Taylor R. L.** The Finite Element Method. The Fourth Edition, Volume 2, McGraw-Hill, 1989.
4. **Гвоздев А.А.** Расчет несущей способности конструкций по методу предельного равновесия. Выпуск 1, Сущность метода и его обоснование. – М: Госстройиздат, 1949. – 280 с.
5. **Оатул А.А.** Расчет элементов железобетонных конструкций по двум предельным состояниям. Часть 2. – Челябинск: ЧПИ, 1987. – 64 с.
6. **Ильюшин А.А.** Пластичность. – М.: Гостехиздат, 1948 – 376 с.
7. **Ильюшин А. А.** Труды. Том 1. – М.: Физматлит, 2003. – 350 с.
8. **СП 63.13330.2012.** Бетонные и железобетонные конструкции. Актуализированная редакция СНиП 52-01-2003. – М., 2013. – 152 с.
9. **СНиП 52-01-2003.** Бетонные и железобетонные конструкции. – М.: ФГУП ЦПП, 2004. – 26 с.
10. **СП 52-102-2004**. Предварительно напряженные железобетонные конструкции. – М.: ФГУП ЦПП, 2005. – 36 с.
11. **Ermakova A.** Ideal Failure Models of Structures for Analysis by FEM and AFEM.

// Proceedings ICIE–2017, 2017, Volume 206, pp. 9-15.
12. **Ermakova A.V.** Set of equations of AFEM and properties of additional finite elements. // International Journal for Computational Civil and Structural Engineering, 2019, Volume 15, Issue 2, pp. 51-64.
13. **Маркус М., Минк Х.** Обзор по теории матриц и матричных неравенств. Тртье издание. – М.: Книжный дом «ЛИБРОКОМ», 2009. – 232 с.
14. **Постнов В. А.** Численные методы расчета судовых конструкций. – Л.: Судостроение, 1977. – 280 с.
15. **Карпенко Н.И.** Общие модели механики железобетона. – М.: Стройиздат, 1996. – 416 с.
16. **Карпенко Н. И., Карпенко С. Н., Петров А. Н., Палювина С. Н.** Модель деформирования железобетона в приращениях и расчет балок-стенок и изгибаемых плит с трещинами. – Петрозаводск: Издательство Петрозаводского государственного университета, 2013. – 156 с.
17. **Шугаев В.В.** Инженерные методы в нелинейной теории предельного равновесия оболочек. – М.: Готика, 2001. – 368 с.
18. **Городецкий А.С., Евзеров И.Д.** Компьютерные модели конструкций. – Киев: Факт, 2007. – 394 с.
19. **Перельмутер А. В., Сливкер В. И.** Расчетные модели сооружений и возможность их анализа. – Киев: «Сталь», 2002. – 600 с.
20. **Оатул А.А., Карякин А.А., Кутин Ю.Ф.** Расчет и проектирование элементов железобетонных конструкций на основе применения ЭВМ. Конспект лекций. Часть 4. Под редакцией Оатула А.А. – Челябинск: ЧПИ, 1980. – 67 с.
21. **Ермакова А.В.** Два способа построения итерационного процесса метода дополнительных конечных элементов. // Строительная механика и расчет сооружений, 2018, №6, с. 45-52.

Anna V. Ermakova, Candidate of technical sciences, associate professor, Veteran of South Ural State University, room 306, 76, Lenin Street, Chelyabinsk, 454080, phone 83512679775. 123, 26 Baku's commissars street;
phone 83517226342; e-mail: annaolga11@gmail.com.

Ермакова Анна Витальевна, кандидат технических наук, доцент, ветеран Южно-Уральского государственного университета. 454080, Челябинск, пр. Ленина, 76, ЮУрГУ, к. 306. Т. 83512679775. 454025, Челябинск, ул. 26 Бакинских комиссаров, 123;
тел. 83517226342; e-mail: annaolga11@gmail.com.

DOI:10.22337/2587-9618-2020-16-2-26-38

HIGH-THROUGHPUT DEEP LEARNING ALGORITHM FOR DIAGNOSIS AND DEFECTS CLASSIFICATION OF WATERPROOFING MEMBRANES

Darya Filatova[1,2], Charles El-Nouty[3], Uladzislau Punko[2]
[1]CHArt, EPHE, Paris, FRANCE
[2]Faculty of Computer Systems and Networks Belarusian State University of Informatics and Radioelectronics, Minsk, BELARUS
[3] LAGA, UMR 7539, F-93430, Université Sorbonne Paris Nord, Paris, FRANCE

Abstract: The work is devoted to the development of a high-performance deep learning algorithm related to the diagnosis and classification of defects of water-repellent membranes. The mechanism of constructing visual models of the membrane surface is discussed. This allows to get the representative training data set. The proposed methodology consists in the sequent transformations of pixel-image intensities to find defected fragments on the membrane's surface. The computational algorithm is based on the architecture of convolution neural networks. To assess its effectiveness, the "confidence of confidence" criterion is proposed. The presented computations show that the methodology can be successfully applied in material sciences, for example, to study the properties of building materials, or in forensic science when examining the causes of construction catastrophes.

Keywords: waterproofing membranes, deep learning, machine learning, pathology classification

ВЫСОКОПРОИЗВОДИТЕЛЬНЫЙ АЛГОРИТМ ГЛУБОКОГО ОБУЧЕНИЯ ДЛЯ ДИАГНОСТИКИ И КЛАССИФИКАЦИИ ДЕФЕКТОВ ВОДООТТАЛКИВАЮЩИХ МЕМБРАН

Дарья Филатова[1,2], Шарль Эль-Нути[3], Владислав Пунько
[1] Лаборатория Человеческого и Искусственного Познания
Практическая Школа Высших Исследований, Париж, ФРАНЦИЯ
[2]Факультет Компьютерных Систем и Сетей, Белорусский Государственный Университет Информатики и Радиоэлектроники, Минск, БЕЛАРУСЬ
[3] ЛАГА, СНРС, УМР 7539, Ф-93430, Университет Сорбонна Париж Север, Париж, ФРАНЦИЯ

Аннотация: Работа посвящена разработке высокопроизводительного алгоритма глубокого обучения, связанного с диагностикой и классификации дефектов водоотталкивающих мембран. Обсужден механизм построения визуальных моделей поверхности мембран, позволяющий представить эволюцию различных повреждений. Этот подход позволяет получить тренеровочный набор изображений с известным количеством дефектов. Предложенная методология основана на последовательных преобразованиях интенсивности пиксельных изображений для обнаружения дефектных фрагментов на поверхности мембраны. Вычислительный алгоритм основан на архитектуре сверточных нейронных сетей. Для оценки его эффективности предложен критерий «доверительная область». Представленные вычислителения показывают, что методологияя может быть успешно применена в материаловединии, на пример, для исследования свойств строительных материалов, или в криминологии, на пример, при изучении причин строительных катастроф.

Ключевые слова: гидроизоляционные мембраны, глубокое обучение, машинное обучение, классификация патологий

1. INTRODUCTION

The design of buildings and constructions requires an understanding of the principle of stability, durability, and rigidity of the main constructed structures. Besides, the provision of measures of the building maintenance and monitoring their technical conditions are essential during the design stage. The over-end decade of technological progress acceleration has led to the emergence of new building unique properties materials, which, on the one hand, drove to a simplification of building technologies. On the other hand, it took more stringent requirements on resistance, reliability, durability of structures [1]. The principles of building structures are changing. Virtual modeling has led to an increase in the number of available solutions to the same problems. This fact casts doubt on the authenticity of the standard design principles, thereby facilitating the selection of the right material and the development of the correct structures. Besides, the desire to find the optimal simplification of the structure without reduction of safety mostly through choosing solid materials plays an important role. For example, through chemical reactions, the hydro protective layer mechanically connects to the monolithic reinforced concrete mainstay's surface [2]. This process leads to excellent hydro isolation. Therefore, waterproofing systems perfectly work. However, such a constructive solution loses effectiveness if damage occurs. Numerous works devoted to studying the properties of composite materials often indicate that mechanical damage to the membrane insulation leads to lateral migration of water inside the structure [1–3]. That means the place of soaking does not always match the location of insulation's damage, which unpredictably changes the structure's technical parameters. These papers indicated that the study of the phenomenon of water migration using new technologies and materials requires a new experimental research methodology to identify and classify possible pathologies in waterproofing layers [4, 5]. The solution to this problem will help designers in their subsequent work.

Civil engineering, like all other industries, is gone through the fourth industrial revolution. The main idea of this revolution consists in creating cyber-physical systems. These include physical objects and information models. The physical object is managed at every life cycle stage (from the project concept to the moment of decommissioning) using an information system that analyzes the flows of heterogeneous information using computer systems. Artificial intelligence (AI), as well as machine learning (ML), and deep learning (DL), becomes the leading information technology and not only due to the possibility to work better and faster with large amounts of information. For example, artificial intelligence algorithms simulate the work of the human brain. These last can find and classify a defect or pathology hidden from the human eyes even at an early stage of the corruption process, improving feedback on building information modeling (BIM) and thereby ensuring uninterrupted operation of the entire project.

By analogy with the task of pattern recognition applied to fault detection, this work aims to develop a methodology and an algorithm capable of identifying and classifying the visible defects on the surface of the waterproofing membranes based on available information. To promote defects detection methodology, we will use artificially generated images, imitating real photographs of some waterproofing membranes. We focus our attention on the detailed description of the AI algorithm and its quality performance. The main advantage of this approach is the scenarios' development to investigate defects' propagation on the membrane surface. The same methodology is also useful for concrete's petrographic analysis, biological materials [6].

The rest of this paper is organized in the following manner. In Section 2, we propose a brief description of waterproof membranes and detail a generalized visual model of their surface. Section 3 describes the methodology for the damages detection and classification. Next, in Section 4, we illustrate the methodology by simulation experiments. Finally, in Section 5, we give the concluding remarks concerning the methodology implementation and its further development.

2. PROBLEM FORMULATION

2.1. Conception of waterproof membranes

A waterproofing membrane is a continuous thin layer of waterproof material that is laid on some surface and which does not allow water to pass through it. For example, if a waterproofing membrane is laid on a flat terrace between a structural slab and a finishing tile, water will no longer seep into the structural slab [4]. However, in order for this property to be maintained as long as possible, the structural surface and tile must be correctly installed. Any water that remains as puddles on the tile can leak into the plate over time, provoking corrosion of the hydro-repellent membrane, and then the structural slab. There are two types of the waterproofing membranes. Liquid–applied (see Fig. 1 and Fig. 2) and sheet–based (see Fig. 3) membranes are composed of thin about 2 to 4mm thick layers of waterproof material. Membranes can be used in different elements of a construction, namely for underneath and around basements, over terrace slabs and balconies, over landscaped concrete decks, between the soil and concrete in gutters, and many others.

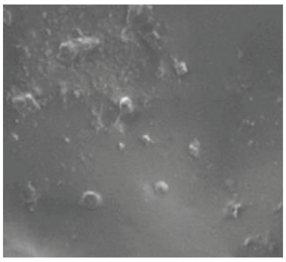

Figure 1. Some corrupted liquid–applied waterproofing membrane: pore deformation and erosive swellings

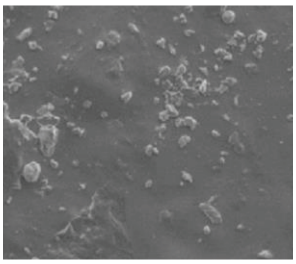

Figure 2. Some corrupted liquid–applied waterproofing membrane: erosive swellings and micro-cracks

UV stability, elongation, breathability, tear and abrasion resistances, chemical stability, geometry play an important role while selecting membrane solutions for the construction. It is impossible not to take into account the influence of the environment in which the structure will be operated. As one can imagine, over time, the desired qualities are lost. Thus, exposure to the sun and precipitation adversely affect breathability. The pores, with which the membrane breathes, over time deform and stop working. In places of deformation there are swellings and cracks. The protective property is lost leading sooner or later to the threat of structural destruction.

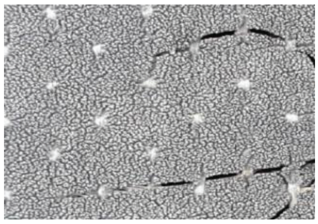

Figure 3. Some corrupted sheet–based waterproofing membrane: pore deformation and macrocracks

2.2. Generalized visual model of surface

We suppose that $n-by-m$ pixels grayscale digital image $\mathcal{I}$ corresponds to the membrane's surface associated with the bounded closed set

$$\mathcal{D}=[0,n-1]\times[0,m-1]\subset\mathbb{R}_+^2. \qquad (1)$$

For the simplicity each pixel correspond to "the smallest unit" of the membrane surface and is denoted as $(x,y)\in\mathcal{D}$. We call this unit "***a region***", that is to say, the membrane consists of the regions. Moreover, each pair $(x,y)\in\mathcal{D}$ is characterized by an intensity

$$f_{(x,y)}\in\mathcal{F},$$

where $\mathcal{F}=\{f_{\min},\dots,f_{\max}\}\subset\mathbb{R}_+$ is an ordered final set. The set $\mathcal{D}$ is discretized as a regular grid such that each vertex (node) has coordinates $(i\,\Delta x, j\,\Delta y)$, where Δx and Δy correspond to the grid spacing, $i\in\{1,..,n_x\}$ and $j\in\{1,..,n_y\}$ with $n_x<<n$ and $n_y<<m$. The

quantity of vertices is $n_x \times n_y$. Let us introduce the set $\mathcal{L} = \{1,..,n_x \times n_y\}$. For the simplicity we denote these coordinates as (x_i, y_j). We assume that at some instant of time t, $t \in [t_0, t_1]$, each pore $-\mathcal{R}_\ell(t)$, $\ell \in \mathcal{L}$ – of the membrane is presented by the disc of center (x_i, y_j), that is

$$\mathcal{R}_\ell(t) = \{(x, y) \in \mathcal{D} \,|\, (x - x_i)^2 + (y - y_j)^2 \le r_\ell^2(t)\}, \tag{2}$$

where $r_\ell(t)$ is the radius of the pore, $r_\ell(t_0) = r_0$. Moreover, we assume that at time t_0 that

$$\forall \ell \in \mathcal{L},\ \forall k \in \mathcal{L},\ \ell \ne k \ \Rightarrow \ \mathcal{R}_\ell(t_0) \cap \mathcal{R}_k(t_0) = \varnothing.$$

We denote the set of the pores by Ω. An example of the possible configuration of the surface of the membrane is illustrated by Fig. 4.

Figure 4. The visual idealized model of the membrane surface: initial state at t_0

The over-time erosion as well as the evolutionary process leading to damage to the pore, and therefore of the membrane surface at the observation time interval $[t_0, t_1]$, is associated with the change in the radius $r_\ell(t)$ of the ℓ^{th} pore, $\ell \in \mathcal{L}$, with the formation of microcracks at its edges, and with cracks propagation on the surface. We can observe these processes only as the changes of the intensities of pixels.

To model these processes we assume that at time t each pore contains $\lambda_\ell(t)$ regions included in $\mathcal{R}_\ell(t)$ and denoted as $\kappa_{\ell i}(t)$, $i \in \{1, 2, ..., \lambda_\ell(t)\}$. Each region is characterized by a state s, which takes one of the two values: s_0 – non-damaged state, s_1 – damaged state. The change of the state corresponds to the change of the intensities of pixels, which make corruption visible on the image. Hence, we can form the time-varying sets of all non-damaged regions

$$\mathcal{S}_{0\ell}(t) = \{\kappa_{\ell i}(t) \in \mathcal{R}_\ell(t) \,|\, s = s_0\} \tag{3}$$

and of all damaged regions

$$\mathcal{S}_{1\ell}(t) = \{\kappa_{\ell i}(t) \in \mathcal{R}_\ell(t) \,|\, s = s_1\}. \tag{4}$$

We obviously have $\mathcal{S}_{0\ell}(t) \cap \mathcal{S}_{1\ell}(t) = \varnothing$, $\mathcal{S}_{0\ell}(t) \cup \mathcal{S}_{1\ell}(t) = \mathcal{R}_\ell(t)$ for any $t \in (t_0, t_1]$. Note, that initially all the regions are in non-damaged state, i.e. $\mathcal{S}_{0\ell}(t) = \mathcal{R}_\ell(t)$. Once the radius of the pore was changed, the state of the ℓ^{th} region can be changed with some probability $p(t)$, $0 \le p(t) \le 1$, namely for $\ell \in \mathcal{L}$

$$\mathbb{P}(s_1 \leftarrow s_0 \,|\, r_\ell(t) > r_0) = p,\ t \in (t_0, t_1]. \tag{5}$$

The damaged regions form the edge-inward micro-cracks on the surface of the pore (see Fig. 5). The visual changes on the pore surface will be displayed in a darker shade of gray than the original. The membrane's surface crack propagation (see Fig. 6a) starts if there exists one pore with damaged area such that

$$\max_{\ell \in \mathcal{L}} card(\mathcal{S}_{1\ell}(t)) \ge \tilde{p}, \tag{6}$$

where $\tilde{p}$ is a critical damage level, which has to be properly chosen. The crack starts from this pore (see Fig. 6b). Here, the visual changes on the membrane's surface will be displayed in a lighter shade of gray than the original. To model the micro-cracks the surface cracks we will use the modified algorithms of Mersenne twister pseudorandom number generator and non-uniform fractals [7]. Finally, to model the non-uniform background of the membrane the fractional Brownian fields [8, 9] with different values of Hurst parameters $H \in (0,1)$ are be used (see Fig. 7).

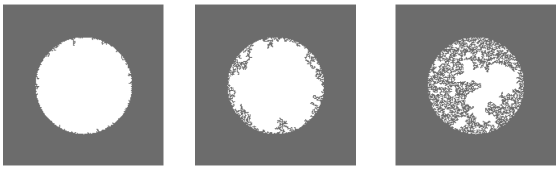

a) $p = 0.12$ *b)* $p = 0.51$ *c)* $p = 0.79$

Figure 5. The pore's over-time erosion

The structure formed in the manner described above we will call as a visual model of the membrane's surface.

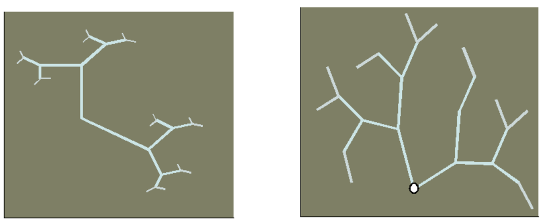

a) *b)*

Figure 6. The propagation of the crack

a) $H = 0.15$ *b)* $H = 0.5$ *c)* $H = 0.95$

Figure 7. The background of the membrane

The research problem of this paper can be formulated as follows:

can we find and classify the damages on the membrane's surface using its visual model and some methods of AI?

As it is possible to notice the responses to the research problem require some specific methodology. In next section, we will focus our attention on it.

3. RESEARCH METHODOLOGY

3.1. Method overview

It is obvious that, visual analysis of the membranes' surface condition requires special equipment that is better than the human eye can determine the place and character of the damage. In addition, in the expertise of the building structure, characterized as large areas, "manual" recognition of the pathologies' localization and classification is extremely time-consuming and often error-prone. Therefore, to solve the above problem, it would be helpful to have both a high-performance embedded device and a computational algorithm capable to complete real-time analysis of visual flow information. In such a manner the human factor can be eliminated for better performance and efficiency. In this study, we concentrate our attention only on the computational aspects.

Being a part of artificial intelligence, machine learning is widely used in image analysis. The advantage is due to the ability to come up with rules based on automated statistical processing of available data called training, that is to say mapping inputs (initial visual information) to associated targets or predictions (detected and classified defects). The remarkable progress made in this area can serve as a ruled defect-type classification by means of deep learning strategy, which includes:

- preprocessing (to speed up the recognition and the classification of the damages by normalizing and removing variations of initial visual information [10]);
- segmentation (to locate pores of the membrane and to detect desired features, i.e. their edges, using simplifications and changes in the representation of the pre-processed visual information avoiding as much as possible the problems initial data artifacts [11]);
- classification (to classify the extracted features into predefined categories by using

suitable methods that compare the image pattern with the predefined etalons [6]);
- post-processing (to correct errors caused by "oversegmentation" and "undersegmentation" and to improve the plausibility of the results [10, 11]);
- evaluation (to estimate the quality of previous steps [12]).

The choice of configuration of the deep learning algorithm depends on many factors associated with the available data, the purpose of their processing, as well as hardware and software.
Let us discuss these aspects in details.

3.2. Dataset

The membrane's surfaces were obtained by the simulation techniques described in subsection 2.2. The major advantage of artificially generated data is the availability of high-quality labeled training datasets for supervised, semi-supervised, and unsupervised deep learning used for object detection and recognition. The image dataset considered in this study is composed of 1000 same-size images. Each image contains 100 pores imitating the corruption processes. The lessons were automatically marked by pre-selection procedure with respect to the critical damage level $\tilde{p}$ and to the critical pore's radius value $\tilde{r} >> r_\ell(t_0)$, $\ell \in \mathcal{L}$, as well as automatically analyzed by the proposed methodology.

3.3. Image recognition: basic technique

3.3.1. Preprocessing. In the general case, the image preprocessing is applied to the original image and consists of the image resizing with further normalization and equalization as well as gamma correction pixels' intensities. Since we have assumed that $\mathcal{I}$ is the digital grayscale image generated as it was described in the subsection 2.2, we can omit the resizing procedure and the gamma-correction which allows the compensation for the non-linear luminance effect of optic devices. In this methodological approach we only need the normalization and the histogram equalization.

Consider the normalization step first. Keep in mind that the normalization is a kind of transformation applied to intensities of each pixel. Recall that the set of intensities of the initial image $\mathcal{I}$ was the set $\mathcal{F}$. The new values of intensities will be elements of the ordered final set $\tilde{\mathcal{F}}$ defined as

$$\tilde{\mathcal{F}} = \left\{ \tilde{f}_{\min}, \ldots, \tilde{f}_{\max} \right\},$$

where

$$\tilde{f}_{(x,y)} = \left(f_{(x,y)} - f_{\min} \right) \frac{\tilde{f}_{\max} - \tilde{f}_{\min}}{f_{\max} - f_{\min}} + \tilde{f}_{\min}. \quad (7)$$

For convenience, $\tilde{\mathcal{F}}$ can be rewritten with respect to the L-leveled gray scale in the following way

$$\tilde{\mathcal{F}} = \left\{ \tilde{f}_{\min} = \tilde{f}_0, \ldots, \tilde{f}_k, \ldots, \tilde{f}_{L-1} = \tilde{f}_{\max} \right\}. \quad (8)$$

Thus, we define a new image $\mathcal{I}$:

$$\tilde{\mathcal{I}} \underset{normalization}{\leftarrow} \mathcal{I}. \quad (9)$$

The goal of (7) is to enhance the contrast by redistributing the intensities toward extreme values. We insist on the fact that the image $\mathcal{I}$ contains also $n \times m$ pixels with the corresponding set of the intensities defined in (8).

Consider the histogram equalization step now. It is completed to normalize the gray color distribution across samples of images (mostly due to illumination, optics of devices etc.), that is to say the transformation of $\tilde{\mathcal{I}}$ into the new image $\tilde{\tilde{\mathcal{I}}}$. Therefore, let us introduce the quantities $\mathbb{T}\left(\tilde{f}_k\right)$, $0 \le k \le L-1$, such that

$$\mathbb{T}\left(\tilde{f}_k\right) = \sum_{\ell=0}^{k} \frac{m_\ell}{nm}, \quad (10)$$

where m_ℓ is the frequency of gray level ℓ. Here, we focus our attention on the frequentist probability. However, the other choice is also possible [10]. Next, we define

$$g\left(\tilde{f}_k\right)=\tilde{f}_{\min}+\left(\tilde{f}_{\max}-\tilde{f}_{\min}\right)\mathbb{T}\left(\tilde{f}_k\right), \quad (11)$$

and, hence, the set of intensities

$$\tilde{\tilde{\mathcal{F}}}=\left\{g\left(\tilde{f}_k\right),\ 0\le k\le L-1\right\}.$$

Thus, we get the new image

$$\tilde{\tilde{\mathcal{I}}} \underset{equalization}{\leftarrow} \tilde{\mathcal{I}}\ . \quad (12)$$

We also insist here, that $\tilde{\tilde{\mathcal{I}}}$ is the $n\times m$-pixels image with the set of intensities being $\tilde{\tilde{\mathcal{F}}}$.

3.3.2. Segmentation. The purpose of this step is to form homogeneous groups of pixels that could serve to assign them to the K specific objects $\bar{\omega}_\tau$, $1\le\tau\le K$ (usually a quantity of $\bar{\omega}_\tau$ are unknown before the segmentation). These elements form a subset $\bar{\Omega}=\left\{\bar{\omega}_\tau, 1\le\tau\le K\right\}$ of $\mathcal{D}$. The segmentation can be done by several techniques, namely: pixel-, edge-, region-, or model-based-techniques as well as the box-counting method. Taking into account the strengths and the weaknesses of these methods [Tosta], we search for the edges of pores by the modified Canny edge detector algorithm [Canny]. The main idea of this algorithm is as follows and consists in four phases.

Let $\mathbf{F}^*$ be a $n\times m$ matrix, such that the element of this matrix $f_{ij}^*\in\tilde{\tilde{\mathcal{F}}}$, $i\in\{1,...,n\}$, $j\in\{1,...,m\}$. The edge of each element of $\bar{\Omega}$ is determined by the transformation and the comparison of the intensities f_{ij}^* of neighboring pixels. In 2D image processing, two spatial variables θ_1 and θ_1 are related to $\mathbf{F}^*$. We denote the non-integer row index by θ_1 and the non-integer column index by θ_2.

Phase 1. Smoothing. The kernel regression filter takes a form

$$g\left(\theta_1,\theta_2\right)=\sum_{i=[\theta_1-3\sigma]}^{i=[\theta_1+3\sigma]}\sum_{j=[\theta_2-3\sigma]}^{j=[\theta_2+3\sigma]}\frac{f_{ij}^*}{2\pi\sigma^2}\exp\left(-\frac{(i-\theta_1)^2+(j-\theta_2)^2}{2\sigma^2}\right),$$

where σ is a smoothing parameter, which can be calculated as a standard deviation of pixel intensities of $\tilde{\tilde{\mathcal{I}}}$ or chosen arbitrary. It is used to avoid false detection and to riddle out the noise). Once applied to the image $\tilde{\tilde{\mathcal{I}}}$ this filter gives

$$\tilde{\tilde{\mathcal{I}}}^* \underset{\substack{\text{kernel}\\ \text{regression}}}{\leftarrow} \tilde{\tilde{\mathcal{I}}}\,. \quad (13)$$

Phase 2. Masking. To detect the black-white boundaries and in a consequence to determine edges of each element of $\bar{\Omega}$, firstly, the Laplacian

$$\mathbb{L}\left(g\left(\theta_1,\theta_2\right)\right)=\frac{\partial^2 g\left(\theta_1,\theta_2\right)}{\partial\theta_1^2}+\frac{\partial^2 g\left(\theta_1,\theta_2\right)}{\partial\theta_2^2} \quad (14)$$

is calculated, and, secondly, the mask $\mathbf{M}$ is the $n\times m$ matrix formed as

$$m_{\theta_1,\theta_2}=\begin{cases}0, & \ell_{\theta_1,\theta_2}<0,\\ 1, & \ell_{\theta_1,\theta_2}\ge 0,\end{cases} \quad (15)$$

where ℓ_{θ_1,θ_2} is the element of $\mathbb{L}\left(g\left(\theta_1,\theta_2\right)\right)$. In other words, zero-crossings in the Laplacian detect the white-black contours of each element of $\bar{\Omega}$.

Phase 3. Hysteresis. The Richardson extrapolation is applied to values of the $n\times m$ matrix $\mathbf{M}$. This permits to finalize the detection of edges of each element of $\bar{\Omega}$ by suppressing all the other edges that are not connected to strong edges.

Phase 4. Morphology and boundary statistics. The application of the Fourier descriptor allows

finding the boundaries as well as calculate the area of each strong edge $\bar{\varpi}$.
To conclude the segmentation step, the set $\bar{\Omega}$ contains K elements $\bar{\varpi}$, each one $\bar{\varpi}$ is defined by two parameters, namely: the contour $\mathcal{C}_{\bar{\varpi}}$ and the area $\mathcal{A}_{\bar{\varpi}}$.

3.3.3. Classification. Once being detected the elements $\bar{\varpi} \in \bar{\Omega}$ can be classified either like corrupted pores (if the radius r exceeds the critical value $\tilde{r}$ and if the surface corruption parameter p exceeds the critical value $\tilde{p}$) or like non-corrupted ones. The sets of corrupted and non-corrupted pores are $\bar{\Omega}_{-1}$ and $\bar{\Omega}_{+1}$, correspondently,

$$\bar{\Omega}_{-1} \cap \bar{\Omega}_{+1} = \varnothing$$

and

$$\bar{\Omega}_{-1} \cup \bar{\Omega}_{+1} = \bar{\Omega}.$$

The patterns of the pores are defined by the formula (2). We denote them by $\omega \in \Omega$, each contour $\mathcal{C}_\omega$ of ω corresponds to the border of $\mathcal{R}_\ell(t_1)$ and $\mathcal{A}_\omega = \pi r_\ell^2(t_1)$, $\ell \in \mathcal{L}$. We also introduce the set of labels $\Xi = \{-1, 1\}$ such that each element $\xi \in \Xi$ is given by

$$\xi_\ell = \begin{cases} -1, & \text{for } r_\ell(t_1) < \tilde{r} \text{ and } p_\ell < \tilde{p}, \\ +1, & \text{for } r_\ell(t_1) \geq \tilde{r} \text{ or } p_\ell \geq \tilde{p}, \end{cases}$$

thus, if $\xi_\ell = -1$, then $\omega_\ell \in \Omega_{-1}$, and if $\xi_\ell = +1$, then $\omega_\ell \in \Omega_{+1}$, moreover, $\Omega_{-1} \cap \Omega_{+1} = \varnothing$ and $\Omega_{-1} \cup \Omega_{+1} = \Omega$.
The classification problem can be formulated as follows:
for a training set of pairs $\{\omega_\ell, \xi_\ell\}_{\ell=1}^{\mathcal{L}}$, where ω_ℓ are input patterns from the set of patterns Ω and $\xi_\ell \in \Xi$ are the corresponding labels, find a classifier $\eta(\bar{\varpi})$ such that to get as few errors as possible.
Let us introduce the classifier

$$\eta(\omega_\ell, \bar{\varpi}) = \sum_{\ell \in \mathcal{L}} \alpha_\ell \xi_\ell \mathrm{K}(\omega_\ell, \bar{\varpi}) + b, \quad (15)$$

where K is a kernel, $b \in \mathbb{R}$ is a shift, the parameters $\alpha_\ell \in \mathbb{R}$ form a weight vector $\boldsymbol{\alpha}$ of the training element ω_ℓ. We put

$$\|\boldsymbol{\alpha}\|_0 = \sum_{\ell \in \mathcal{L}} \mathbf{1}_{\{\alpha_\ell \neq 0\}} \quad (16a)$$

and

$$\|\boldsymbol{\alpha}\|_1 = \sum_{\ell \in \mathcal{L}} |\alpha_\ell|. \quad (16b)$$

Therefore, the goal is to solve the non-convex discontinuous optimization problem

$$\arg\min_{\boldsymbol{\alpha}} \left\{ \|\boldsymbol{\alpha}\|_0 + C \sum_{\ell \in \mathcal{L}} \phi\left(\xi_\ell \eta(\omega_\ell, \bar{\varpi})\right) \right\} \quad (17)$$

$$\text{s.t. } 0 \leq \|\boldsymbol{\alpha}\|_1 \leq C, \quad (18)$$

where C is a hyperparameter and

$$\phi(z) = \begin{cases} 1 - z, & z \leq 1, \\ 0, & z > 1 \end{cases} \quad (19)$$

is the hinge loss. Here, we admit that the solution of the problem (17) - (19) can be found by standard procedure included to ALADIN Optimization ToolBox MatLab [14].

Post-processing. To evaluate the segmentation and classification stages we use the following idea. We suppose that a reference image contains k_1 regions (it can be generated by the procedure described in section 2.2 such that $k_1 = n_x \times n_y$) and k_2 regions detected by the segmentation or by the classification procedures. Let A_i be the i^{th} region on a reference image demarcated by a specialist and B_j be the j^{th} corresponding segmented image ($i \in \{1,2,...,k_1\}$, $j \in \{1,2,...,k_2\}$). It is clear that in both cases regions contain pixels, therefore we treat any region as a set. In an ideal situation $k_1 = k_2$ and $A_i = B_i$ for any $i \in \{1,2,...,k_1\}$. This situation is extremely rare. In practice the following situations are possible:

- $k_1 = k_2$ – the algorithm found the same number of regions, the sets A_i and B_i cover approximately the same domain for any $i \in \{1,2,...,k_1\}$ (see Fig. 8);
- $k_1 > k_2$ – the algorithm found fewer regions than it was marked, for any $i \in \{1,2,...,k_2\}$ the sets A_i and B_i cover approximately the same domain and for any $j \in \{k_2+1,...,k_1\}$ $B_j = \varnothing$;
- $k_1 < k_2$ – the algorithm found more regions than it was marked, for any $i \in \{1,2,...,k_1\}$ the sets A_i and B_i cover approximately the same domain and for $i \in \{k_1+1,...,k_2\}$ $A_i = \varnothing$.

When two the sets A and B cover approximately the same domain, it implies that the sets A and B are not disjoint and than A is a strict subset of $A \bigcup B$. Based on this remark, we can propose the following evaluation criteria (called by us "the domain of confidence criteria" - DoC), defined as follows

$$DoC := \sum_{i=1}^{min\{k_1,k_2\}} \frac{\mathbb{P}(A_i \bigcap B_i)}{\mathbb{P}(A_i)}, \tag{20}$$

$$DoC \geq \beta \frac{\min\{k_1,k_2\}}{\max\{k_1,k_2\}}, \tag{21}$$

where $\beta \in (0,1)$ is a resemblance parameter, which has to be carefully chosen (or estimated). The notation $\mathbb{P}$ denotes once the area of the set, which is used for the segmentation procedure, and once the number of pixels, defined by the classification procedure.

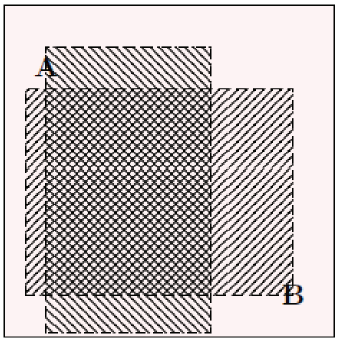

Figure 8. Relation between region A identified by an expert and region B identified by computational techniques.

4. RESULTS AND DISCUSSION

To detect and to classify the damages on the membrane surface, five categories of membrane surface were defined mainly due to differentiation of their backgrounds. The backgrounds were simulated as fractional Brownian fields with five different values of Hurst parameter

$$H \in \{0.05, 0.25, 0.50, 0.75, 0.95\}.$$

Each category contained 200 gray-scale images. The gray scale used 256 different intensities. Each 120×120-pixels-image was full of 100 pores distributed in equidistant–grid nodes. The pixel intensities of each pore's edge were coded by 120, the micro-cracks pixel and crack propagation intensities were coded by 80 and 160 correspondently. The pores evolution was done by 100 steps on the time interval $[0,1]$. The initial radius value for each one pore was $r_\ell(t_0) = 2$, the new radius value was randomly selected from the interval $[2,5]$, the critical value was $\tilde{r} = 4$. The corruption level was increasing by each evolutionary step by randomly selected value from the interval $[0, 0.05]$, the critical damage level was $\tilde{p} = 0.7$. All these images were divided on the training and evolution sets as "3:1". The segmentation and classification procedures were developed using convolutional neural networks (ConvNets, CNNs) included in Deep Learning Toolbox MatLab R2020a. Once the training was done, the image recognition was done for 100 generated surfaces with different values of H. The averaged statistics of the numerical experiments are listed in Tables 1–3, k_1 stands for the number of corrupted pores after the evolution.

Let us comment on the results. Initially, all the objects of interest are homogeneous. However, evolution makes them non-homogeneous. The backgrounds of the membrane's surface, as well as corrupted pores, contain fractional noises, which restrict the effectiveness of segmentation by the intensity-threshold-based method. The influence of a smoothing parameter σ in global senses on the quality of the problem-solution was studied in the first series of experiments (see Table 1). As it was possible to expect, the inhomogeneous backgrounds ($H = 0.05$ and $H = 0.25$) provoke more erroneous detections of corrupted pores then that in the case of $H \geq 0.5$. With increase of σ improves the both statistics (20) and (21). The local smoothing works better then the global one (see Table 2 and Table 3). We can observe the improvement of DoC statistics for highly noisy conditions.

Table 1. Simulation results with the predefined smoothing parameter of kernel regression

H	σ	$\overline{DoC}$	$\lceil \bar{k}_1 \rceil$	$\lceil \bar{k}_2 \rceil$	$\bar{\beta}$
0.05	1	0.5311	51	63	0.4299
0.25	1	0.5492	49	41	0.6563
0.50	1	0.8002	55	57	0.8292
0.75	1	0.6724	56	52	0.7241
0.95	1	0.7310	60	55	0.7975
0.05	2	0.5663	47	56	0.6747
0.25	2	0.5715	52	43	0.6911
0.50	2	0.8533	49	46	0.9090
0.75	2	0.7893	54	49	0.8698
0.95	2	0.8884	52	49	0.9427
0.05	3	0.5718	53	62	0.6689
0.25	3	0.5794	54	47	0.6657
0.50	3	0.8807	48	50	0.8455
0.75	3	0.7956	61	58	0.8368
0.95	3	0.8582	54	51	0.9087

Table 2. Simulation results with the estimated on 5×5 pixel neighborhood smoothing parameter of kernel regression

H	$\overline{DoC}$	$\lceil \bar{k}_1 \rceil$	$\lceil \bar{k}_2 \rceil$	$\bar{\beta}$
0.05	0.6200	56	49	0.7086
0.25	0.6587	48	51	0.6999
0.50	0.8338	58	54	0.8956
0.75	0.8105	57	62	0.8816
0.95	0.8453	61	57	0.9046

However, in all cases, the results still showed incorrect identification of corrupted pores or by their quantity or by their surface. It can be explained by the weak performance of the normalization procedure, which has to be adapted to highly noisy backgrounds and more careful selection of the optimization procedure for the solution of (17)–(18).

Table 3. Simulation results with the estimated on 7×7 pixel neighborhood smoothing parameter of kernel regression

H	$\overline{DoC}$	$\lceil \bar{k}_1 \rceil$	$\lceil \bar{k}_2 \rceil$	$\bar{\beta}$
0.05	0.7225	52	47	0.7993
0.25	0.7199	61	58	0.7571
0.50	0.8401	55	53	0.8718
0.75	0.8539	47	45	0.8156
0.95	0.8600	54	51	0.9105

5. CONCLUSIONS

This study presented the computational strategy for the detection of the membrane's defected recognitions. Its main advantage is due to a multi-agent simulation of the object of interest behavior. Once having values of physical, chemical, or mechanical parameters of water-proofing materials, we can develop different scenarios to predict the material performance. The effective results depend on the careful selection of the parameters of the method's sequential steps. One limitation of the proposed method is the quantity of false detected regions, which is a common phenomenon for highly noisy backgrounds of images [12, 13]. To make this methodology helpful for object detection in different fields of interests such as civil engineering, biology, medicine, or forensic science, we should consider non-Gaussian filters concerning the spatial distribution of image intensities and perform complex analysis of the algorithm.

REFERENCES

1. **Cui H., Li Y., Zhao X., Yin X., Yu J., Ding B.,** Multilevel porous structured polyvinylidene fluoride/polyurethane fibrous membranes for ultrahigh waterproof and breathable application. // Composites Communications, 2017, Volume 6, pp. 63-67.
2. **Lee K., Kim D., Chang S.-H., Choi S.-W., Park B., Lee C.**, Numerical approach to assessing the contact characteristics of a polymer-based waterproof membrane. // Tunnelling and Underground Space Technology, 2018, Volume 79, pp. 242-249.
3. **Rupal A., Sharma S.K., Tyagi G.D.**, Experimental investigation on mechanical properties of polyurethane modified bituminous waterproofing membrane. // Materials Today: Proceedings, 2019.
4. **Walter A., de Brito J., Grandão Lopes J.**, Current flat roof bituminous membranes waterproofing systems – inspection, diagnosis and pathology classification. // Construction and Building Materials, 2005, Volume 19 (3), pp. 233-242.
5. **Yin F., Hu P., Song C., Wang S., Liu H.**, Unveiling the role of gas permeability in air cathodes and performance enhancement by waterproof membrane fabricating method. // Journal of Power Sources, 2020, Volume 449, pp. 227570.
6. **Song Y., Huang Z., Shen Ch., Humphrey Shi, Lange D.A.**, Deep learning-based automated image segmentation for concrete petrographic analysis. // Cement and Concrete Research, 2020, Volume 135, 106118.
7. **Pathan A. K., Monowar M.M., Khan S**. Simulation Technologies in Networking and Communications: Selecting the Best Tool for the Test. CRC Press, 2015
8. **Kroese D. P., Botev Z. I.** Spatial Process Simulation. // Stochastic Geometry, Spatial Statistics and Random Fields Springer International Publishing, 2015, pp. 369-404.
9. **El-Nouty C.**, On approximately stationary Gaussian processes // International Journal for Computational Civil and Structural Engineering, 2015, Volume 11, Issue, pp. 15-26.
10. **Ramírez-Gallego S., Krawczyk B., García S., Woźniak M., Herrera F.** A survey on data preprocessing for data stream mining: Current status and future directions. // Neurocomputing, 2017, Volume 239, pp. 39-57.
11. **Lou Q., Peng J., Wu F., Kong D.** Variational Model for Image Segmentation. In: Bebis G. et al. (eds) Advances in Visual Computing. ISVC 2013. Lecture Notes in Computer Science, Volume 8034, 2013, Springer, Berlin, Heidelberg.
12. **Ma T., Antoniou C., Toledo T**. Hybrid machine learning algorithm and statistical time series model for network-wide traffic forecast. // Transportation Research Part C: Emerging Technologies, 2020, Volume 111, pp. 352-372.
13. **Tosta T., Faria P.R. , Alves Neves L , Zanchetta do Nascimento M.** Computational method for unsupervised segmentation of lymphoma histological images based on fuzzy 3-partition entropy and genetic algorithm. // Expert Systems with Applications, 2017, Volume 81, pp. 223-243.
14. **Engelmann A., Jiang Y., Muhlpfordt T.,**

Houska B., Faulwasser T., Toward distributed OPF using ALADIN. // IEEE Transactions on Power Systems, 2019, Volume 34 (1), pp. 584-594.

СПИСОК ЛИТЕРАТУРЫ

1. **Cui H., Li Y., Zhao X., Yin X., Yu J., Ding B.,** Multilevel porous structured polyvinylidene fluoride/polyurethane fibrous membranes for ultrahigh waterproof and breathable application. // Composites Communications, 2017, Volume 6, pp. 63-67.
2. **Lee K., Kim D., Chang S.-H., Choi S.-W., Park B., Lee C.**, Numerical approach to assessing the contact characteristics of a polymer-based waterproof membrane. // Tunnelling and Underground Space Technology, 2018, Volume 79, pp. 242-249.
3. **Rupal A., Sharma S.K., Tyagi G.D.**, Experimental investigation on mechanical properties of polyurethane modified bituminous waterproofing membrane. // Materials Today: Proceedings, 2019.
4. **Walter A., de Brito J., Grandão Lopes J.**, Current flat roof bituminous membranes waterproofing systems – inspection, diagnosis and pathology classification. // Construction and Building Materials, 2005, Volume 19 (3), pp. 233-242.
5. **Yin F., Hu P., Song C., Wang S., Liu H.**, Unveiling the role of gas permeability in air cathodes and performance enhancement by waterproof membrane fabricating method. // Journal of Power Sources, 2020, Volume 449, pp. 227570.
6. **Song Y., Huang Z., Shen Ch., Humphrey Shi, Lange D.A.**, Deep learning-based automated image segmentation for concrete petrographic analysis. // Cement and Concrete Research, 2020, Volume 135, 106118.
7. **Pathan A. K., Monowar M.M., Khan S**. Simulation Technologies in Networking and Communications: Selecting the Best Tool for the Test. CRC Press, 2015
8. **Kroese D. P., Botev Z. I.** Spatial Process Simulation. // Stochastic Geometry, Spatial Statistics and Random Fields Springer International Publishing, 2015, pp. 369-404.
9. **El-Nouty C.**, On approximately stationary Gaussian processes // International Journal for Computational Civil and Structural Engineering, 2015, Volume 11, Issue, pp. 15-26.
10. **Ramírez-Gallego S., Krawczyk B., García S., Woźniak M., Herrera F.** A survey on data preprocessing for data stream mining: Current status and future directions. // Neurocomputing, 2017, Volume 239, pp. 39-57.
11. **Lou Q., Peng J., Wu F., Kong D.** Variational Model for Image Segmentation. In: Bebis G. et al. (eds) Advances in Visual Computing. ISVC 2013. Lecture Notes in Computer Science, Volume 8034, 2013, Springer, Berlin, Heidelberg.
12. **Ma T., Antoniou C., Toledo T**. Hybrid machine learning algorithm and statistical time series model for network-wide traffic forecast. // Transportation Research Part C: Emerging Technologies, 2020, Volume 111, pp. 352-372.
13. **Tosta T., Faria P.R. , Alves Neves L , Zanchetta do Nascimento M.** Computational method for unsupervised segmentation of lymphoma histological images based on fuzzy 3-partition entropy and genetic algorithm. // Expert Systems with Applications, 2017, Volume 81, pp. 223-243.
14. **Engelmann A., Jiang Y., Muhlpfordt T., Houska B., Faulwasser T.**, Toward distributed OPF using ALADIN. // IEEE Transactions on Power Systems, 2019, Volume 34 (1), pp. 584-594.

Филатова Дарья, профессор, доктор физико-математических наук работает на кафедре информатики факультета Компьютерных систем и сетей Белорусского Государственного Университета Информатики и Радиоэлектроники, Минск, Беларусь и в лаборатории Человеческого и искусственного интеллекта Практическая Школа Высших Исследований , 4–14 ул. Ферруса, 75014 Париж, Франция;

E-mail: filatova@bsuir.by;
orcid.org/0000-0001-9434-7993.

Professor, Dr. hab. Darya Filatova works in Informatics Department, Faculty of Computer Systems and Networks, Belarusian State University of Informatics and Radioelectronics, and CHART EPHE, 4-14 Rue Ferrus, 75014 Paris, France; e-mail: filatova@bsuir.by;
orcid.org/0000-0001-9434-7993.

Шарль Эль-Нути – профессор, доктор физико-математических наук работает в лаборатории ЛАГА, Университет Сорбонна Париж Север; авенью Ж.-Б. Кленанта, д. 99, 94340 Вильтанез, Франция;
E-mail: elnouty@math.univ-paris13.fr,
orcid.org/0000-0002-2321-1041

Professor, Dr. hab. Charles El-Nouty works in LAGA, Université Sorbonne Paris Nord; 99 avenue J-B Clément 93430 Villetaneuse;
E-mail: elnouty@math.univ-paris13.fr;
orcid.org/ /0000-0002-2321-1041

Владислав Валерьевич Пунько является студентом магистрантом кафедре информатики факультета Компьютерных систем и сетей Белорусского Государственного Университета Информатики и Радиоэлектроники, Минск, Беларусь; 220013, Республика Беларусь, г. Минск, ул. Гикало, д. 9;
E-mail: iam.vlad.punko@gmail.com;
orcid.org/0000-0002-2947-3245

Uladzislau Valerevich Punko is a master's student of Informatics Department, Faculty of Computer Systems and Networks, Belarusian State University of Informatics and Radioelectronics, Gikalo 9, 220005 Minsk, Belarus;
E-mail: iam.vlad.punko@gmail.com;
orcid.org/ 0000-0002-2947-3245

DOI:10.22337/2587-9618-2020-16-2-39-49

SIXTH DEGREE OF FREEDOM

Alexander S. Gorodetsky [1], Maryna A. Romashkina [1], Bogdan Yu. Pisarevsky [1,2]
[1] LLC "LIRA CAD", Kiev, UKRAINE
[2] National Aviation University, Kiev, UKRAINE

Abstract: The article describes new types of finite elements that allow you to take into account all six degrees of freedom of the shell. In order to compose the finite elements, the Allman functional with a rotational degree of freedom is used. The use of finite elements is associated with a number of restrictions that are considered in the article.

Keywords: flat shell, method of smoothing deformations, rotational degrees of freedom

ШЕСТАЯ СТЕПЕНЬ СВОБОДЫ

А.С. Городецкий [1], М.А. Ромашкина [1], Б.Ю. Писаревский [1,2]
[1] ООО «ЛИРА САПР», г. Киев, УКРАИНА
[2] Национальный авиационный университет, г. Киев, УКРАИНА

Аннотация: В статье описаны новые типы конечных элементов, которые позволяют учитывать все шесть степени свободы оболочки. Для составления конечных элементов используется функционал Аллмана с вращательной степенью свободы. Применение конечных элементов связано с рядом ограничений, которые рассмотрены в статье.

Ключевые слова: плоская оболочка, метод сглаживания деформаций, вращательная степени свободы

Structural analysis of spatial core systems, as a rule, implies that there are six movements (according to the finite element approach, these are six degrees of freedom) and six corresponding efforts in each node. Each degree of freedom has a physical meaning: linear movements in the direction of the axes X, Y, Z and an angle of rotation UX, UY, UZ relative to the same axes. When calculating plate systems, the physical meaning of the rotation angle UZ (sixth degree of freedom) relative to the axis of the orthogonal plane of the plate (Fig. 1) is an abstraction.

The history of the finite element method contains examples of various exotic degrees of freedom of type

$$\frac{\partial^2 u_z}{\partial x^2};\ \frac{\partial^2 u_z}{\partial x \partial y}$$

etc. However, all of them sooner or later showed their failure. For example, the degree of freedom of the type

$$\frac{\partial^2 u_z}{\partial x^2};\ \frac{\partial^2 u_z}{\partial x \partial y}$$

and other higher derivatives of displacements when changing the orientation of the global coordinate system (a necessary procedure for universal computational complexes) give rise to other types and degrees of freedom.

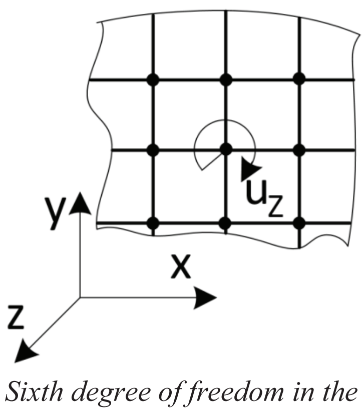

<u>Figure 1.</u> Sixth degree of freedom in the FE shell.

Quadrilateral finite element with a rotating degree of freedom

In various publications, the construction of a stiffness matrix is given. So in [4], the finite element is obtained as a result of combining the approximating Allman functions (moving in the plane of the finite element) and the bilinear normal rotation functions (rotating displacements) [8] (Fig. 2).

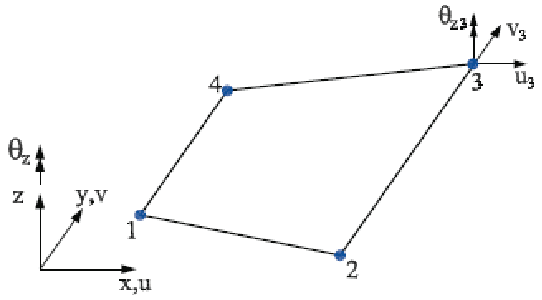

<u>Figure 2.</u> Quadrilateral finite element with a rotating degree of freedom

The field of rotating movements is interpolated as follows:

$$\theta_z = \sum_{i=1}^{4} N_i(\xi,\eta)\theta_{zi},$$

Field of displacements in the plane:

$$\mathrm{u} = \begin{bmatrix} u \\ v \end{bmatrix} = \sum_{i=1}^{4} N_i \begin{bmatrix} u_i \\ v_i \end{bmatrix} + \frac{1}{8}\sum_{k=5}^{8} N_k(\xi,\eta)(\theta_{zj}-\theta_{zi}) \begin{bmatrix} y_{ij} \\ x_{ij} \end{bmatrix},$$

where

$$x_{ij} = x_j - x_i, \quad y_{ij} = y_j - x_i,$$

$$N_i(\xi,\eta) = \frac{1}{4}(1+\xi_i\xi)(1+\eta_i\eta) \qquad i=1,2,3,4$$

$$N_k(\xi,\eta) = \frac{1}{2}(1-\xi^2)(1+\eta_k\eta) \qquad k=5,7$$

$$N_k(\xi,\eta) = \frac{1}{2}(1+\xi_k\xi)(1-\eta^2) \qquad k=6,8.$$

where k, i, j is determined as (5,1,2), (6,2,3), (7,3,4), (8,4,1).

Matrix of deformation ε_m is determined as

$$\varepsilon_m = \sum_{i=1}^{4} B_{mi} u_i,$$

where $\mathrm{u_i} = \begin{bmatrix} u_i & v_i & \theta_i \end{bmatrix}^T$

is nodal displacement vector.

Matrix of derivatives B_{mi} has a form:

$$B_{mi} = \begin{bmatrix} N_{i,x} & 0 & Nx_{i,x} \\ 0 & N_{i,y} & Ny_{i,y} \\ N_{i,y} & N_{i,x} & Nx_{i,x}+Ny_{i,y} \end{bmatrix}.,$$

Where Nx, Ny incompatible form functions defined as:

$$Nx_i = \frac{1}{8}(y_{ij}N_l - y_{ik}N_m),$$

$$Ny_i = \frac{1}{8}(x_{ij}N_l - x_{ik}N_m),$$

Indexes i, j, k, m take values:

i = 1, 2, 3, 4; m = i + 4; l = m – 1 + 4 floor(1/i);
k = mod (m, 4) + 1; j = l – 4;

matrix of deformation (ε_{sk}) is expressed in the form

$$\varepsilon_{sk} = \sum_{i=1}^{4} b_i u_i + \theta_z,$$

where

$$b_i = \begin{bmatrix} -\frac{1}{2}N_{i,y} \\ \frac{1}{2}N_{i,x} \\ \frac{1}{16}(-y_{ij}N_{l,y} + y_{ik}N_{m,y} + x_{ij}N_{l,x} - x_{ik}N_{m,x}) - N_i \end{bmatrix},$$

Indexes i, j, k, m is determined by expression presented above.
The variational formulation of the finite element method proposed in [6] is defined as:

$$\Pi_\gamma(\mathrm{u},\theta_z)=\frac{1}{2}\int_\Omega \varepsilon_m^T D_m \varepsilon_m d\Omega+\frac{1}{2}\gamma\int_\Omega(\varepsilon_{sk}-\theta_z)^2 d\Omega-\int_\Omega \mathrm{u}^\mathrm{T}\mathrm{f}d\Omega,$$

The resulting stiffness matrix is K_{mem} sum of matrix K_m and penalty matrix P_γ.

$$K_{mem}=K_m+P_\gamma=\int_\Omega B_m^T D_m B_m d\Omega+\gamma\int_\Omega b^T b d\Omega.$$

Positive penalty coefficient γ in the equation is problematic issue. However, it is customary to equate the coefficient equal to the shear modulus ($\gamma=G$) [7-8].
Apologists of the sixth degree of freedom usually give the notorious example of an “umbrella” - the task about the slab supported on a single column. In this case the slab is subjected to torsion relative to the vertical axis of the column.
If we simulate the support of the plate on a single point without a sixth degree of freedom in the assembly, then there will be no clamping of the plate in the column, and the plate will rotate relative to the column. We solve this problem taking into account the sixth degree of freedom in the shell.

Example 1 – The use of the sixth degree of freedom in structures of the type "umbrella"
Initial data: square plate a = 6 m, rigidly complied with a column of square cross-section 0.5x0.5 m; length l = 6 m. Plated is under the action of an axial force p = 1t.
Material characteristic: $E = 3x10^6 t/m^2$; $\nu = 0.2$.
Boundary conditions: the column at the base is rigidly clamped. Figure 3 shows calculation scheme of such a construction.

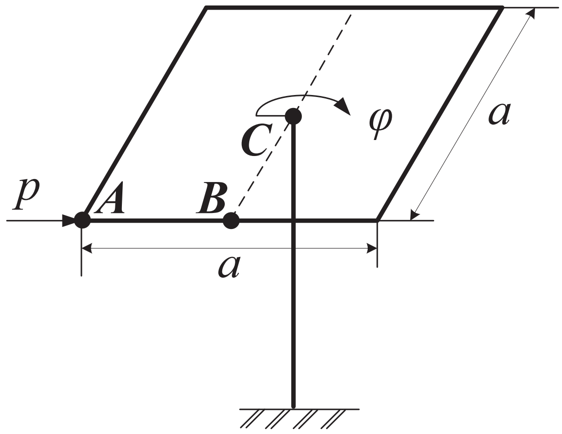

Figure 3. The calculation scheme of the plate supported on a single

Solution:

$$x_{m.B}=x_{m.C}+uz_{m.C}\cdot\frac{a}{2}= \\ =4.608+1.646\cdot10^{-3}\cdot3000=9.546(\text{мм}) \tag{1}$$

Figure 4 and table 1 shows results of structural analysis of structures of the type "umbrella", performed in Lira – CAD Software.
Analyzing the results given in Table 1, we can conclude that the thickening of the grid does not lead to a refinement of the solution, which indicates the incorrectness of the sixth degree of freedom. Similar problems, in a slightly different plane, are considered in [12].
It should be noted that modern modeling techniques include accounting for the "body" of the column. In this case, the interface node of the column and plate is calculated using absolutely rigid bodies (Fig. 5,6) and you can do without the sixth degree. Perfectly rigid body (PRT) - provides a kinematic connection between the movements of the driven nodes and the leading ones. The LIRA-CAD Software allows introducing such rigid bodies automatically. The introduced rigid bodies can simulate the “body” of a column of any configuration (cross, corner, T, etc.). The LIRA-CAD Software allows corresponding between a single master node and an arbitrary number of slave nodes.

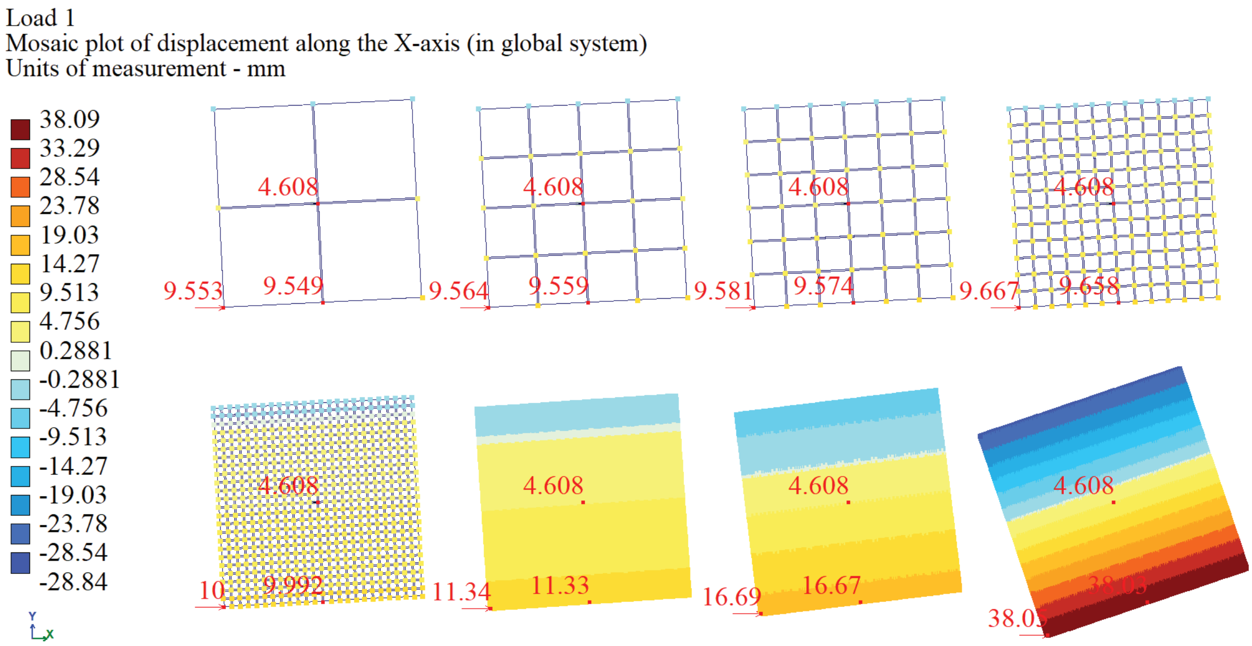

Figure 4. Displacements along the X axis, mm at the control point for various mesh densities (taking into account the sixth degree of freedom in the shell)

Table 1. Results of structural analysis of structures of the type "umbrella"

Mesh of FE	Displacements in the point B along the axis x, mm (an analytical solution)	Displacements in the point B along the axis x, mm (Lira – CAD Software)	Error, %
2x2	9.546	9.549	0.031
4x4	9.546	9.559	0.136
6x6	9.546	9.574	0.292
12x12	9.546	9.658	1.160
24x24	9.546	9.992	4.464
48x48	9.546	11.33	15.746
96x96	9.546	16.67	42.735
192x192	9.546	38.03	74.899

This modeling method, on the one hand, solves the problem of accounting for the "body" of the column, i.e. "Cut-offs" of the peak of moments arising when modeling the support on the column as a point support. On the other hand, it provides the perception of the column of twisting deformations. In most cases, when there are at least two columns, this is not required, because in this case, the torque from deformations in the plane of the plate will be perceived by pairs of transverse forces in the columns, and the torques will be negligibly small and their presence can simply be ignored (the effect of neglecting the moments in the constructed rigid nodes of the trusses when the hinged nodes were taken into account) [1].

This modeling method, on the one hand, solves the problem of accounting for the "body" of the column, i.e. "Cut-offs" of the peak of moments arising when modeling the support on the column as a point support. On the other hand, it provides the perception of the column of twisting deformations.

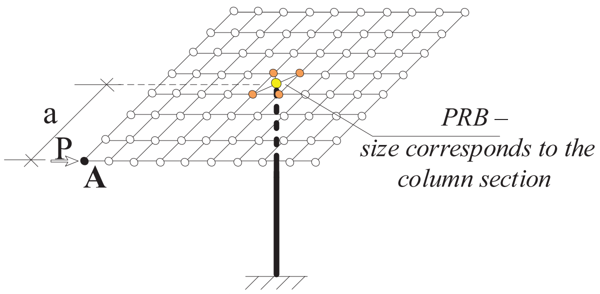

Figure 5. Modeling of a plate supported on a single point using PRB

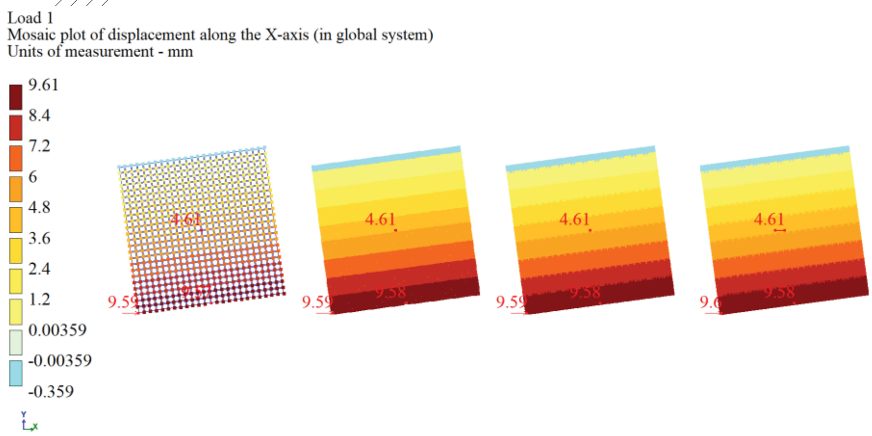

Figure 6. Displacements along the X axis, mm at the control point for different mesh densities (the node linking column and plate calculated using PRB)

In most cases, when there are at least two columns, this is not required, because in this case, the torque from deformations in the plane of the plate will be perceived by pairs of transverse forces in the columns, and the torques will be negligibly small and their presence can simply be ignored (the effect of neglecting the moments in the constructed rigid nodes of the trusses when the hinged nodes were taken into account) [1].

Example 2 – The use of the sixth degree of freedom in structures such as "folded shell"
Somebodies call various spatial plate systems as a reason to apply the sixth degree of freedom (Fig. 7).
Each node of a spatial structure of this type has six degrees of freedom (three linear and three angular displacements). As a rule, the node of the finite element of a flat plate has five degrees of freedom. This causes the appearance of linearly dependent equations in the canonical system, i.e. division by zero in the process of eliminating unknowns.

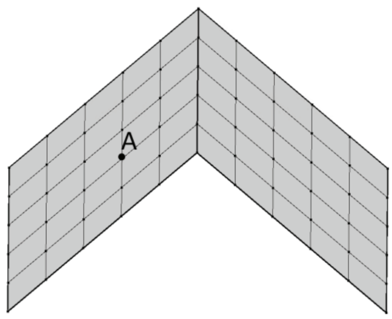

Figure 7. Using the sixth degree of freedom in a node when modeling spatial plate systems

Using the sixth degree of freedom, in some cases, solves this problem. Although advanced software systems have a procedure that circumvents this problem [2]. If during the process of elimination 0 appears in the diagonal canonical equations, then a connection is imposed in this direction at the absence of load in this direction. This simple procedure can be useful in many other cases [2, 10].
Nevertheless, in some cases, the sixth degree in the hands of inexperienced users can lead to incorrect results.

Example 3 – Connection of the frame rod with the diaphragm

Figure 8 shows an example of modeling the girder clamped in a wall. Here the difficulties are due to the fact that the finite elements of the beam-walls (plane stress state) do not have nodal unknowns corresponding to the angle of rotation about an axis orthogonal to the plane of the diaphragm. Therefore, the node at point A (Fig. 8) without any additional measures will be hinged for the rod.

Modeling clamping with the sixth degree of freedom leads to incorrect results. When the mesh thickens, the moment in clamping decreases, i.e. the result substantially depends on the finite element grid, which is wrong.

Consider following example. We study the bending moment in the beam under the action of a concentrated vertical force p = 1t at different mesh densities. Figure 8 shows such a calculation scheme. Figure 9 and Table 2 present the calculation results obtained in LIRA-CAD Software.

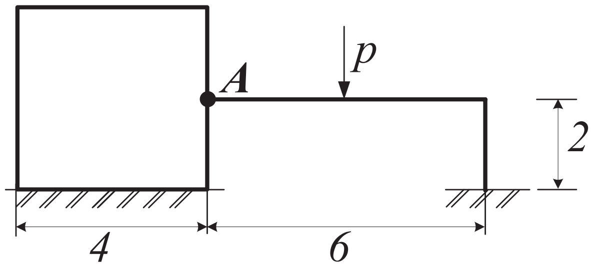

Figure 8. The design scheme of the frame (clamping of the girder in the wall)

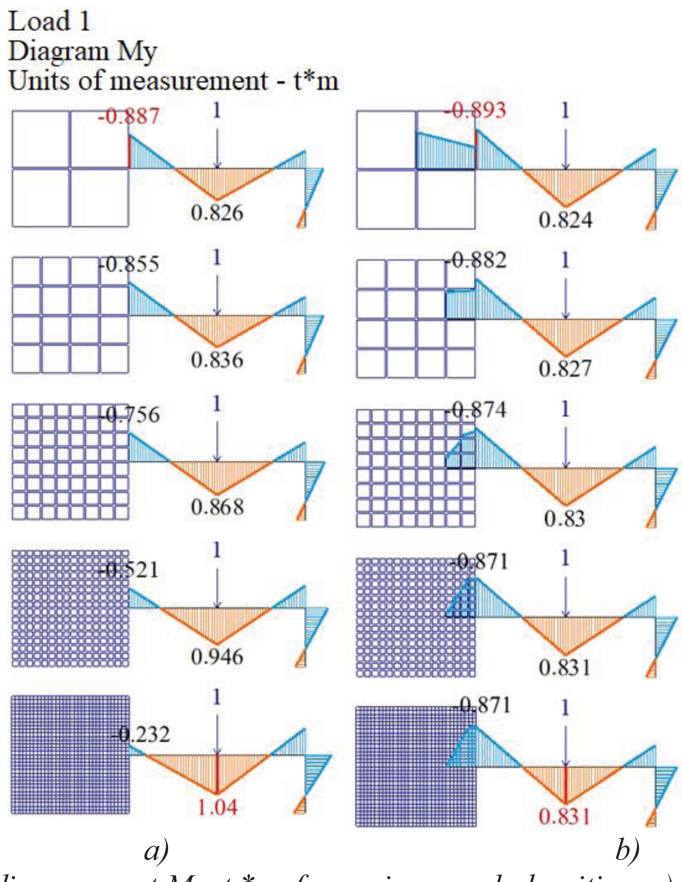

*Figure 9. Bending moment My, t * m for various mesh densities: a) six degrees of freedom in the FE of the shell; b) the girder is inserted into the body of the wall*

*Table 2. Bending moment My, t * m at various mesh densities*

Finite element mesh	My, t * m (six degrees of freedom in the FE of the shell)	My, t * m (the girder is inserted into the body of the wall)
2x2	-0.887	-0.893
4x4	-0.855	-0.882
8x8	-0.756	-0.874
16x16	-0.521	-0.871
32x32	-0.232	-0.884

In this case, clamping must be modeled in other ways (introducing PRB, introducing a girder into the wall body, etc.) [5]. In order to provide clamping of the frame rod in the diaphragm body, it is possible to recommend the introduction of an additional rod between nodes A and B (Fig. 9 b, 10). On the one hand, the extention of such a rod will introduce some local perturbations, but, on the other hand, in a number of cases it will simulate the constructive solution of the assembly (installation of reinforcement of an adjacent rod for the purpose of anchoring) [1].

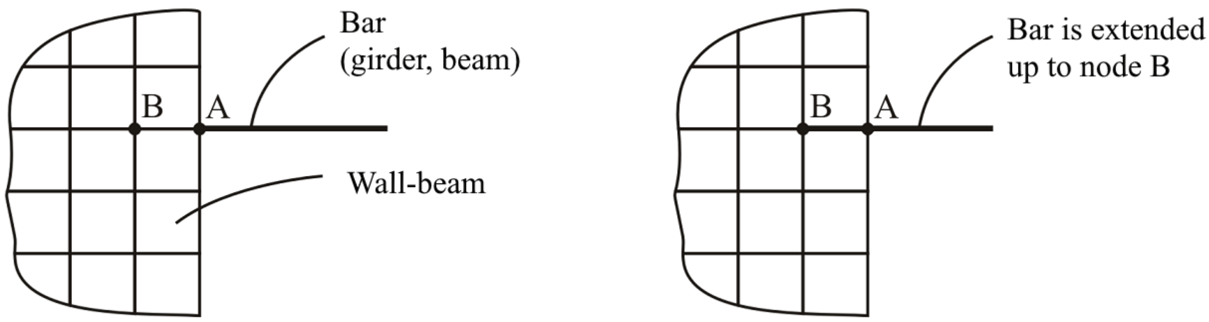

Figure 10. Simulation of the connection of the frame rod with the diaphragm (the girder is inserted into the body of the wall)

An another way is to introduce the Perfectly Rigid Body (PBR) at the point where the beam adjoins the diaphragm (the height of the PRB should be equal to the height of the beam, the leading unit is located at the center of gravity of the beam section) (Fig. 11). This will provide a kinematic connection between the nodes of the diaphragm and the beam [11].

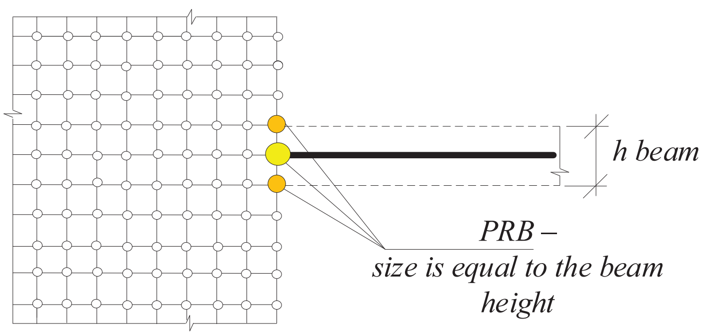

Figure 11. Simulation of the connection of the frame rod with the diaphragm using PRB

As a rule, the number of degrees of freedom exceeds the accuracy of the solution. With the sixth degree of freedom, the situation is somewhat different.

Example 3 - a rectangular beam-wall, rigidly suspended on the sides, under the action of a uniformly distributed load located on the upper side.

Consider the problem (Fig. 12), which has an exact solution [3].

Initial data:

Load: uniformly distributed load acting in the plane of the beam-wall along the Z axis: p = 500 N / m. Dimensions: h = 0.1 m; b = 1.6 m; a = 1.6 m. Material characteristic: E = 2.65 x 106 Pa; ν = 0.15. Boundary conditions: rigidly suspended on the sides. Fig. 12 shows the design scheme of the beam-wall.

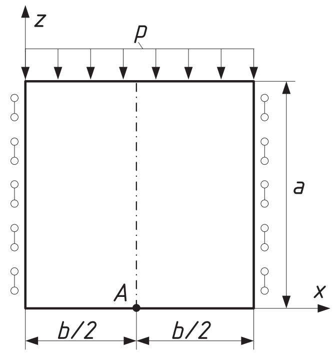

Figure 12. The design scheme of the beam-wall

The task:

Determine the displacements in node A along the Z axis for the finite elements of the beam-wall at different mesh densities and compare with the exact solution (Table 3).

Table 3. Comparison of the results of the calculation of the beam-wall, in the LIRA-CAD Software and analytical calculation

Type of FE	FE mesh	displacements in node A along the Z axis, $m*10^{-3}$			A number of unknown parameters
		Analytical solution	Numerical solution (Lira-CAD Software)	Error, %	
1) FE21 (2 freedom degree per node)	2x4	-0.95	-0.786	17.26	20
	4x8	-0.95	-0.905	4.74	72
	8x16	-0.95	-0.939	1.16	272
	16x32	-0.95	-0.947	0.32	1056
2) FE28- with intermediate nodes on the sides	2x4	-0.95	-0.947	0.32	56
	4x8	-0.95	-0.95	0.00	208
	8x16	-0.95	-0.95	0.00	800
	16x32	-0.95	-0.95	0.00	3136
3) FE21(3 freedom degree per node)	2x4	-0.95	-0.687	27.68	35
	4x8	-0.95	-0.854	10.11	117
	8x16	-0.95	-0.921	3.05	425
	16x32	-0.95	-0.942	0.84	1617

The Table 3 shows the value of the displacement along the Z axis per node A for different FE cells with different types of finite elements of the plane problem: 1) FE 21 with two degrees of freedom per node (X, Z); 2) KE 28 - a rectangular KE of a flat task (beam-wall) with intermediate nodes on the sides, with two degrees of freedom per node (X, Z); 3) KE 21 with three degrees of freedom per node (X, Z and the presence of the sixth degree of freedom UY).

Analyzing the results given in Table 3, it can be noted that the introduction of the sixth degree of freedom does not improve the accuracy of the solution, although the number of degrees of freedom increases. It should also be borne in mind that with an increase in the total number of unknowns L, the conditionality of the matrix K deteriorates, and this can lead to the inability to achieve a given accuracy, although the approximation order for the types of elements used can determine this accuracy. The conditional criterion for matrix K can be the spectral condition number a (K). The greater a (K) corresponds to the worse the conditioning. The work [9] gives an estimate of a (K), which has the form at a uniform grid:

$$a(K) = h^{-2m}, \qquad (2)$$

where m is the order of the system of equations; h is the maximum size of the finite elements.

It can be seen from estimate (2) that in concrete calculations of large problems it is better to avoid excessively dense computational grids, and to achieve the specified accuracy due to a higher approximation order.

CONCLUSIONS

1. In some cases (Fig. 3, 7) the introduction of the sixth degree of freedom makes some sense. Although in this case, the introduction of certain methods of adequate modeling avoids the need to use the sixth degree of freedom.

2. When modeling structural solutions of слампинг (Fig. 8), the application of the sixth degree of freedom leads to incorrect results.

3. The use of the sixth degree of freedom to improve the accuracy of solving the problem (Fig. 12) leads to the opposite results: the total number of degrees of freedom increases, and the accuracy deteriorates.

REFERENCES

1. **Gorodetsky A., Barabash M., Sidorov V.** Komp'juternoe modelirovanie v zadachah stroitel'noj mehaniki [Computer simulation in problems of structural mechanics]. Moscow, ASV Publishing House, 2016, 338 pages (in Russian).
2. **Gorodetsky A.S, Evzerov I.D.** Komp'juternye modeli konstrukcij [Computer models of the structures]. The Second Edition. Kiev, “FAKT”, 2007, 394 pages (in Russian).
3. **Kalmanok A.S.** Raschet plastinok [Analysis of wall-beams]. Moscow, Gosstrojizdat, 1959, 212 pages (in Russian).
4. **Allman D.J.** A compatible triangular element including vertex rotations for plane elasticity analysis. // Computers and Structures, 1984, Volume 19, pp. 1-8.
5. **Gorodetsky A.S., Batrak L.G., Gorodetsky D.A., Laznuk M.V., Yusipenko S.V.** Raschet i proektirovanie konstrukcij vysotnyh zdanij iz monolitnogo zhelezobetona: problemy, opyt, vozmozhnye reshenija i rekomendacii, komp'juternye modeli, informacionnye tehnologii [Analysis and design of high-rise buildings from monolithic RC: difficulties, experience, possible solutions and recommendations, computer models, information technologies]. Kiev, FAKT, 2004, 106 pages (in Russian).
6. **Hughes T.J.R., Brezzi F.** On drilling degrees of freedom. // Computer Methods in Applied Mechanics and Engineering, 1989, Volume 72, pp. 105-121.

7. **Hughes T.J.R., Brezzi F., Masud A., Harari I.** Finite element with drilling degrees of freedom: Theory and numerical evaluations. // Proceedings of the fifth international symposium on numerical methods in engineering. Computational mechanics publications, Ashurst, U.K., 1989, pp. 3-17.
8. **Ibrahimbegovic A., Taylor R.L., Wilson E.L.** (1990): A robust quadrilateral membrane finite element with drilling degrees of freedom. International Journal for Numerical Methods in Engineering, vol. 30, pp. 445–457.
9. **Rozin L.A.** Metod konechnyh jelementov v primenenii k uprugim sistemam [Finite element method applied to elastic systems]. Moscow, Stroyizdat, 1977, 129 pages (in Russian).
10. **Barabash M.S.** Komp'juternoe modelirovanie processov zhiznennogo cikla objektov stroitel'stva [Computer simulation of life cycle for the building objects]. Kiev, Steel, 2014, 301 pages (in Russian).
11. **Kirjyazjev P., Genzersky Y., Romashkina M.** Komp'juternye modeli uzlov primykanija k diafragme [Computer models for joints of slab-to-diaphragm connection]. // Scientific and technical collection: Issues of urban development. Kiev, NAU, 2014, No. 2 (12), pp. 236-246 (in Ukrainian).
12. **Perelmuter A.V., Slivker V.I.** Raschetnye modeli sooruzhenij i vozmozhnost' ih analiza [Design models of structures and the possibility of their analysis]. Kiev, Steel, 2002, 600 pages (in Russian).

СПИСОК ЛИТЕРАТУРЫ

1. **Городецкий А.С., Барабаш М.С., Сидоров В.Н.** Компьютерное моделирование в задачах строительной механики. – М.: АСВ, 2016. – 338 с.
2. **Городецкий А.С., Евзеров И.Д.** Компьютерные модели конструкций. – Киев: Факт, 2007. – 394 с.
3. **Калманок А.С.** Расчет пластинок. – М.: Госстройиздат, 1959. – 212 с.
4. **Allman D.J.** A compatible triangular element including vertex rotations for plane elasticity analysis. // Computers and Structures, 1984, Volume 19, pp. 1-8.
5. **Городецкий А.С., Батрак Л.Г., Городецкий Д.А., Лазнюк М.В., Юсипенко С.В.** Расчет и проектирование конструкций высотных зданий из монолитного железобетона: проблемы, опыт, возможные решения и рекомендации, компьютерные модели, информационные технологии. – Киев: Факт, 2004. – 106 с.
6. **Hughes T.J.R., Brezzi F.** On drilling degrees of freedom. // Computer Methods in Applied Mechanics and Engineering, 1989, Volume 72, pp. 105-121.
7. **Hughes T.J.R., Brezzi F., Masud A., Harari I.** Finite element with drilling degrees of freedom: Theory and numerical evaluations. // Proceedings of the fifth international symposium on numerical methods in engineering. Computational mechanics publications, Ashurst, U.K., 1989, pp. 3-17.
8. **Ibrahimbegovic A., Taylor R.L., Wilson E.L.** A robust quadrilateral membrane finite element with drilling degrees of freedom. // International Journal for Numerical Methods in Engineering, 1990, Volume 30, pp. 445–457.
9. **Розин Л.А.** Метод конечных элементов в применении к упругим системам. – М.: Стройиздат, 1977. – 129 с.
10. **Барабаш М.С.** Компьютерное моделирование процессов жизненного цикла объектов строительства. – Киев: Сталь, 2014. – 301 с.
11. **Кирьязев П., Гензерский Ю., Ромашкина М.** Компьютерные модели узлов примыкания к диафрагме. // Проблеми розвитку міського середовища, 2014, Вип. 2, с. 236-246.
12. **Перельмутер А.В., Сливкер В.И.** Расчетные модели сооружений и

возможность их анализа. – Киев: Сталь, 2002. – 600 с.

Городецкий Александр Сергеевич – академик Российской академии архитектуры и строительных наук, доктор технических наук, профессор, заместитель директора по научной работе ООО «ЛИРА САПР», Украина, 04053 Киев, Кияновский переулок 7-а; тел.: +38 (050) 351 96 61;
E-mail: info@liraland.com.ua, http: www.liraland.ru

Ромашкина Марина Андреевна – кандидат технических наук, инженер группы сопровождения ООО «ЛИРА САПР», Украина, 04053 Киев, Кияновский переулок 7-а, phone: +38 (095) 931-52-50;
e-mail: romashkina.liraland@gmail.com,
http: www.liraland.ru
ORCID ID: 0000-0002-7158-4037

Писаревский Богдан Юрьевич – аспирант кафедры компьютерные технологии строительства, Национального авиационного университета, инженер-программист компании ООО «ЛИРА САПР», 04053, Украина, Киев, пер. Кияновский, д.7-а ,
тел.: +38 (044) 590 58 85,
E-mail: mikst1234@gmail.com
ORCID ID: 0000-0002-1001-2879

Alexander S. Gorodetsky – Academician of Russian Academy of Architecture and Construction Sciences, DSc, Professor, Deputy Director for Science of «LIRA SAPR» Ltd, 7a, Kiyanovsky side street (pereulok), Kiev, 04053, Ukraine; phone: +38 (050) 351 96 61;
E-mail: info@liraland.com.ua, http: www.liraland.ru

Maryna A. Romashkina – PhD, Support Engineer of «LIRA SAPR» Ltd, 7a, Kiyanovsky side street (pereulok), Kiev, 04053, Ukraine; phone: +38 (095) 931-52-50;
E-mail: romashkina.liraland@gmail.com,
http: www.liraland.ru
ORCID ID: 0000-0002-7158-4037

Bogdan Y. Pysarevskiy – Postgraduate student; Department of Computer Technology Building, National Aviation University,software engineer «LIRA SAPR» Ltd, 7a, Kiyanovsky side street (pereulok), Kiev, 04053, Ukraine; phone +38 (044) 590 58 85,
E-mail: mikst1234@gmail.com
ORCID ID: 0000-0002-1001-2879

DOI:10.22337/2587-9618-2020-16-2-50-62

"CHARACTERISTIC LOAD" PRINCIPLE

Alexander S. Gorodetsky[1], Maria S. Barabash[1,2], Maryna A. Romashkina[1], Andrii V. Tomashevsky[1,2]

[1] "LIRA SAPR" Ltd, Kiev, UKRAINE

[2] National Aviation University, Kiev, UKRAINE

Abstract: The article discusses examples of the application of the principle of "characteristic load" (calculations taking into account engineering non-linearity; the designation of subgrade reaction moduli; the designation of the sizes of shelves for beam grillage). The principle of "characteristic load" on the one hand implements the consideration of various factors that are not available when calculating in a linear formulation, on the other hand, it preserves the traditional calculation technology.

Keywords: characteristic load, engineering nonlinearity, moduli of subgrade reaction, beam grillage, ribbed floor

ПРИНЦИП «ОПРЕДЕЛЯЮЩЕЕ НАГРУЖЕНИЕ»

А.С. Городецкий[1], М.С. Барабаш[1,2], М.А. Ромашкина[1], А.В. Томашевский[1,2]

[1] ООО «ЛИРА САПР, г. Киев, УКРАИНА

[2] Национальный авиационный университет, г. Киев, УКРАИНА

Аннотация: В статье рассматривается примеры применения принципа «определяющее нагружение» (расчеты с учетом инженерной нелинейности; назначении коэффициентов постели; назначении размеров полок для балочного ростверка). Принцип «определяющее нагружение» с одной стороны реализует учет различных факторов, недоступных при расчете в линейной постановке, с другой стороны сохраняет традиционную технологию расчета.

Ключевые слова: определяющее нагружение, инженерная нелинейность, коэффициентов постели, балочный ростверк, ребристое перекрытие

Modern software systems allow computer modeling of the life cycle of structures - loading processes, erection processes, dynamic impact processes, various force majeure situations, etc.

Figure 1 shows the structural methodological scheme for modeling a building object, taking into account all the processes of changing the stress-strain state (SSS) of structures at each stage.

Assemblage stages correspond to the sequence of construction, each of which "stores" the loading history. The stages are successively replaced by each other, respectively, the constructed structure at each stage has a modified. The last ASk stage corresponds SSS to the erected structure, and its SSS "stores" all the information of the erection sequence associated with changes in the structural scheme, addition and removal of mounting loads, etc.

The ASk stage is the starting stage for calculating operational loads. The SSS at the operational stages is determined by the calculation for various combinations of loads (DCL1 - operational static loads; DCL2 - payloads taking into account the pulsating wind component, DCL2 - payloads taking into account seismic effects, etc.). Some operational stages, in turn, are the starting ones for modeling force majeure situations that may arise with some probability Pj [1, 5-6].

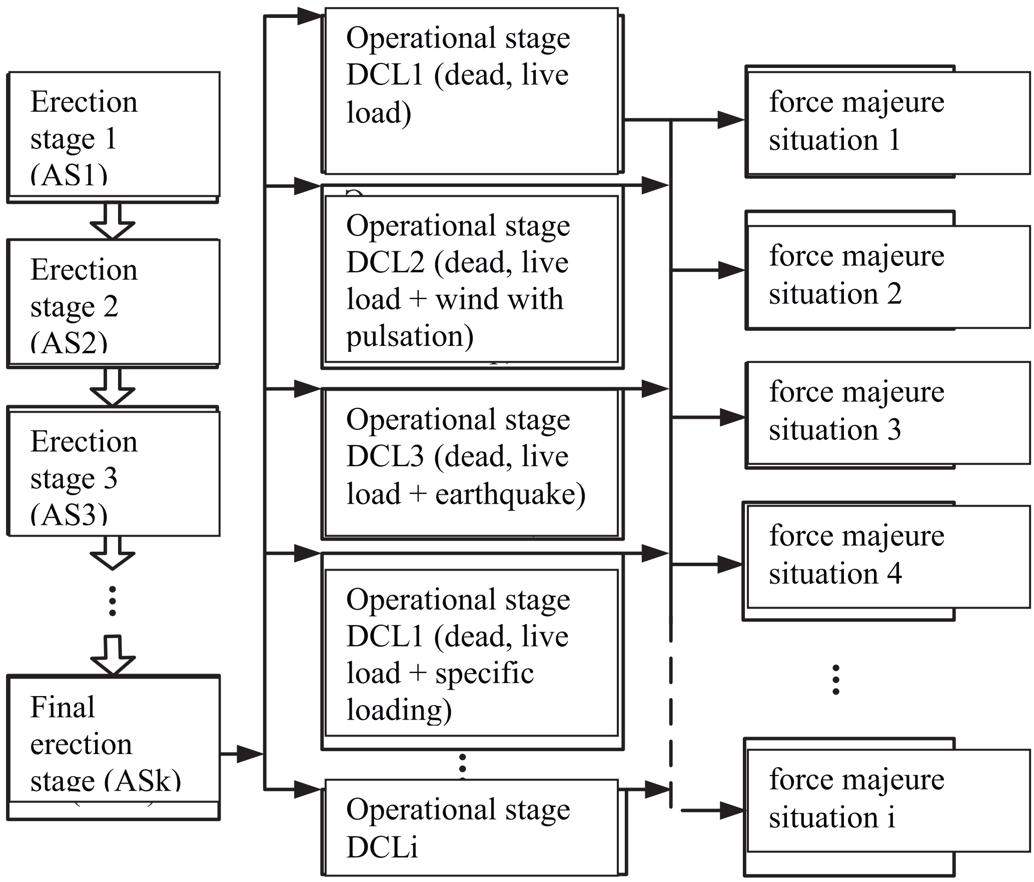

Figure 1. A possible design scheme of structures taking into account the stages of the life cycle of a building object.

Of course, such a simulation, even taking into account the increasing capabilities of modern computers, is cumbersome in addition to a large number of calculations of various structural schemes, each of them, as a rule, must be carried out taking into account geometric, physical, constructive, genetic nonlinearity. This is especially true for force majeure situations, when it is necessary to determine additional reserves of the structural bearing capacity in order to prevent progressive collapse with minimal additional material costs. In addition, the determination of the stress-strain state of costruction at operational stages should take into account temporary changes in the rheological properties of the material (shrinkage, creep, etc.), which also necessitates the calculation in a nonlinear formulation [4].

Carrying out such a calculation is nevertheless rather cumbersome and is currently used only when designing unique objects that have no analogues. As a rule, the vast majority of calculations are carried out according to the traditional scheme (Figure. 2).

The linear static analysis does not take into account a number of important factors, for example, the physical nonlinearity of reinforced concrete.

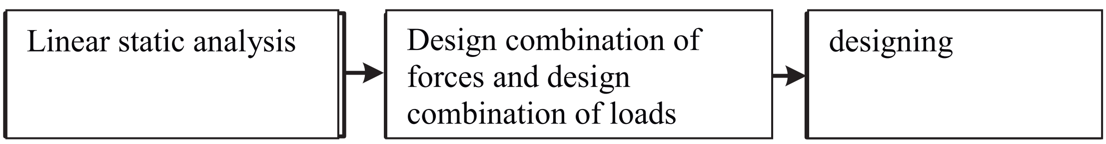

Figure 2. The traditional design scheme.

This factor determines not only a significant increase in displacements (by a factor of 2 – 3 compared with the calculation in a linear formulation), but also a redistribution of forces, which adequately reflects the actual work of the structures.
The principle of “characteristic load” on the one hand implements the consideration of various factors that are not available when calculating in a linear formulation, on the other hand, it preserves the traditional calculation technology (Fig. 2).

An example of the principle of "Characteristic loading" in the methodology "Engineering non-linearity"
Creep, cracks, and other specific features of reinforced concrete cause a change in the stiffness characteristics of elements already in the early stages of loading, including the operational stage. This leads to a redistribution of forces, a significant increase in displacements compared with linear-elastic analysis. Regulatory documents orient the engineer to account for these factors. So Eurocode and the Russian Federation standards recommend to carry out the calculation taking into account physical non-linearity. The LIRA-SAPR software package provides an opportunity for an engineer to perform such calculations. However, the design calculation taking into account physical nonlinearity [2, 7, 8] in the strict mathematical understanding of this process when used in mass engineering calculations has several disadvantages:

• such a calculation can only be performed for one load and cannot be used in DCF or DCL;
• such a calculation requires large resource costs since the step-type method makes it necessary to repeatedly solve systems of linearized equations;
• such a calculation requires specifying the reinforcement (diameters and location) in each section of the bar or plate element.

On the other hand, the standards of the Russian Federation SP 52-103-2007, to take these factors into account in engineering calculations, suggest simply introducing decreasing stiffness coefficients for bent elements 0.3 and compressed 0.6. Of course, such a crude assumption does not take into account that the decrease in stiffness depends on the magnitude and nature of the stress-strain state of the cross section. Nothing is said at all about reducing the stiffness of the stretched elements.
This approach roughly estimates the actual situation. This can be demonstrated by the example of an elementary beam clamped on the both edges (Figure 3).

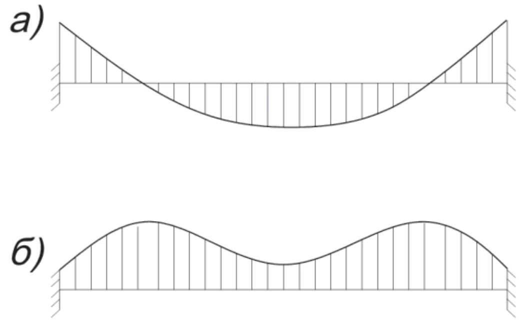

Figure 3. Stress-strain state of the clamped beam: a) diagram of moments, b) corresponding diagram of stiffness.

In real calculations, the situation is even more complicated: the columns often experience significant normal forces: the beams subjected to significant bending force; in plastic elements, as a rule, commensurate membrane and bending forces arise.
The Engineering Nonlinearity method (an iterative calculation method for determining load) is aimed at some elimination of this discrepancy (some ideas in this direction were proposed earlier [3]) and this method should be positioned as a method of improved differentiated accounting for the reduction of the stiffness characteristics of reinforced concrete elements.

The method conception
The Engineering Nonlinearity Method consists in the following:
1. A “characteristic load” is set, which, according to the engineer, mainly determines

the stress-strain state of the structure (crack development, plastic deformation of concrete and reinforcement) throughout the life cycle of the structure. "Characteristic load" can be compiled on the basis of a set of loads (dead weight, payloads, etc.), which are set by the engineer for the subsequent traditional calculation or appointed by the engineer on the basis of other assumptions.

2. The calculation is made for "characteristic load" in a physically non-linear formulation with the simultaneous selection of reinforcement. The calculation is performed by the iterative method and the selection of reinforcement is performed.
3. As a result of an iterative calculation based on the stress-strain state of each section of the rod and the FE of the plate structure, the stiffness characteristics are determined.
4. A traditional structural analysis is performed. The elements of structure have stiffness characteristics determined as a result of an iterative calculation. The traditional calculation involves the calculation in a linear-elastic setting for the entire set of loads (dead weight, live load, earthquake, etc.), compiling the DCF or DCL, selecting or checking the cross-sections of the rods of reinforced concrete and steel elements, designing.

The most responsible and difficult in the formulation and implementation is the stage of determining the stiffness characteristics of the cross sections of the rod and plate element [9, 11].

Determination of the stiffness characteristics of the cross section of the rod

Figure 4 shows an arbitrary section of the rod, on which two moments Mx and My and the normal force N act. The moments act relative to the principal axes of the section x and y. Normal force is applied at point C — the intersection of the geometrical axis of the rod with the section plane. Required: to determine the stiffness characteristics of the section corresponding to the secant modulus of deformation of concrete and reinforcement.

Figure 4 shows the sigma – eps dependence for concrete and Figure 5 shows the same dependence for reinforcement.

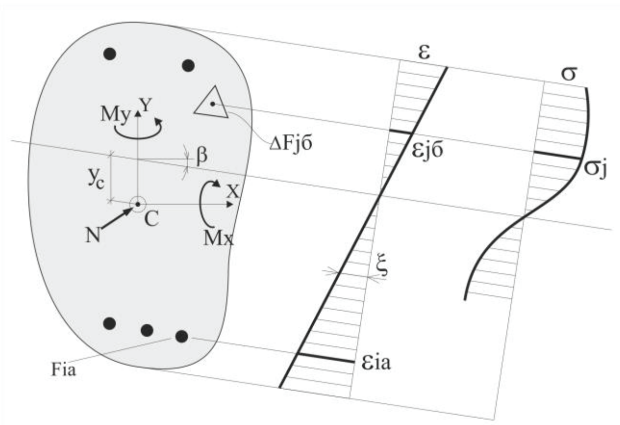

Figure 4. Stress-strain state of rod cross section

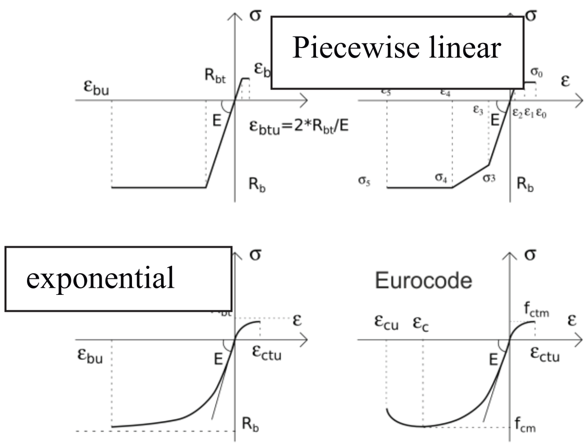

Figure 5. The stress-strain dependence for concrete

In order to determine the cross section stress-strain state, it is necessary to find the position of the neutral axis, which is characterized by two values of Yc, β and the curvature of the section ξ (Figure 4):

Yc is the offset of the neutral axis;

β is the angle of rotation of the neutral axis;

ξ is the curvature of the section.

The solution to the problem is performed by a numerical method. As a result of the iterative process, three unknowns Yc, β, ξ are determined, which are found from three equilibrium equations:

∑z=0, ∑Mx=0, ∑My=0.

$$\sum z = \sum_{j=1}^{n} \Delta F_{jб} \cdot \sigma_{jб}(y_c, \beta, \xi) +$$

$$+ \sum_{i=1}^{m} f_{ia} \sigma_{ia}(y_c, \beta, \xi) + N = 0$$

$$\sum M_x = \sum_{j=1}^{n} \Delta F_{jб} \cdot \sigma_{jб}(y_c, \beta, \xi) y_j(y_c, \beta, \xi) +$$

$$+ \sum_{i=1}^{m} f_{ia} \sigma_{ia}(y_c, \beta, \xi) y_{ia}(y_c, \beta, \xi) + M_x + Ne_x = 0$$

$$\sum M_y = \sum_{j=1}^{n} \Delta F_{jб} \cdot \sigma_{jб}(y_c, \beta, \xi) \cdot x_j(y_c, \beta, \xi) +$$

$$+ \sum_{i=1}^{m} f_{ia} \sigma_{ia}(y_c, \beta, \xi) \cdot x_{ia}(y_c, \beta, \xi) + M_y + Ne_y = 0$$

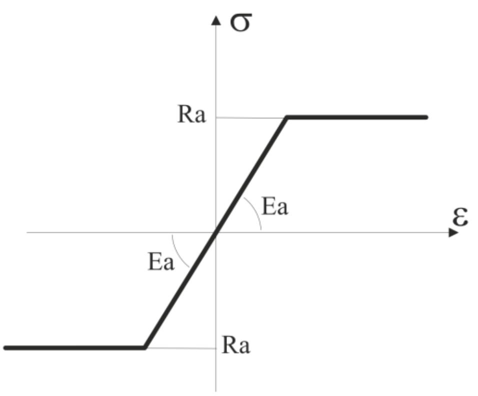

Figure 6. The stress-strain dependence for reinforcement

The stiffness characteristics of $E_{ob}F$, $E_{ob}I_x$, $E_{ob}I_y$ are determined based on the σ–ε dependences for concrete and reinforcement (Fig. 5, 6). For concrete, the definition includes only the compressed part of concrete with cross-sectional secant deformation models. For each reinforcing bar, the corresponding deformation modulus is also used.

$$E_{об}F = \sum_{j=1}^{n} E_{секj\,б} \Delta F_{jб} + \sum_{i=1}^{m} E_{секіa} f_{ia}$$

$$E_{об}I_x = \sum_{j=1}^{n} E_{секj\,б} \Delta F_{jб} y_{jб}^2 + \sum_{i=1}^{m} E_{секіa} f_{ia} y_{ia}^2$$

$$E_{об}I_y = \sum_{j=1}^{n} E_{секj\,б} \Delta F_{jб} x_{jб}^2 + \sum_{i=1}^{m} E_{секіa} f_{ia} x_{ia}^2$$

Here $\Delta F_{jб}$, f_{ia} are elementary sections into which the concrete section and the area of individual reinforcement bars are divided; n is the number of concrete sections; m is the number of reinforcing bars; $E_{секj\,б}$, $E_{секіa}$ – secant deformation modules of concrete and reinforcement, which are determined on the basis of dependencies σ–ε (Figures 4,5); $x_{jб}$, $y_{jб}$, x_{ia}, y_{ia} – the distance of the center of gravity of the j-th concrete section and the i-th section of the reinforcing bar to the main axes, the position of which (Yc, β) is determined as a result of iterative calculation.

For concrete, the definition of stiffness includes only the compressed part of concrete with a cross-sectional secant deformation modulus. For each reinforcing bar, the corresponding secant deformation modulus is also used.

The stiffness matrix of a rod having variable-length secant stiffness characteristics (Fig. 3) is also constructed numerically (each rod is considered as a kind of super element).

Application examples

Below are the results of calculating the frame based on engineering non-linearity 1 (Figure 7). The load q = 15 t / l.m was adopted as the determining load. in fig. Figure 8 shows the corresponding stiffnesses for the crossbar b - c and the columns a - b. Analyzing the diagrams of stiffness characteristics, we can conclude that the recommended decrease in stiffness characteristics for columns by a decreasing factor of 0.6 (in this case, the diagram for columns would look constant and equal to 0.6x2500 = 1500 tm2) and for crossbars 0.3 (in this If the plot would look constant and equal to 0.3x5900 = 1770 tm2) it looks like a rather rough approximation.

Table 1 shows the results of linear-elastic calculation of the frame for the load q = 20 t / l.m. taking into account the differentiated distribution of stiffnesses for all elements obtained on the basis of the Engineering Nonlinearity 1 mode.

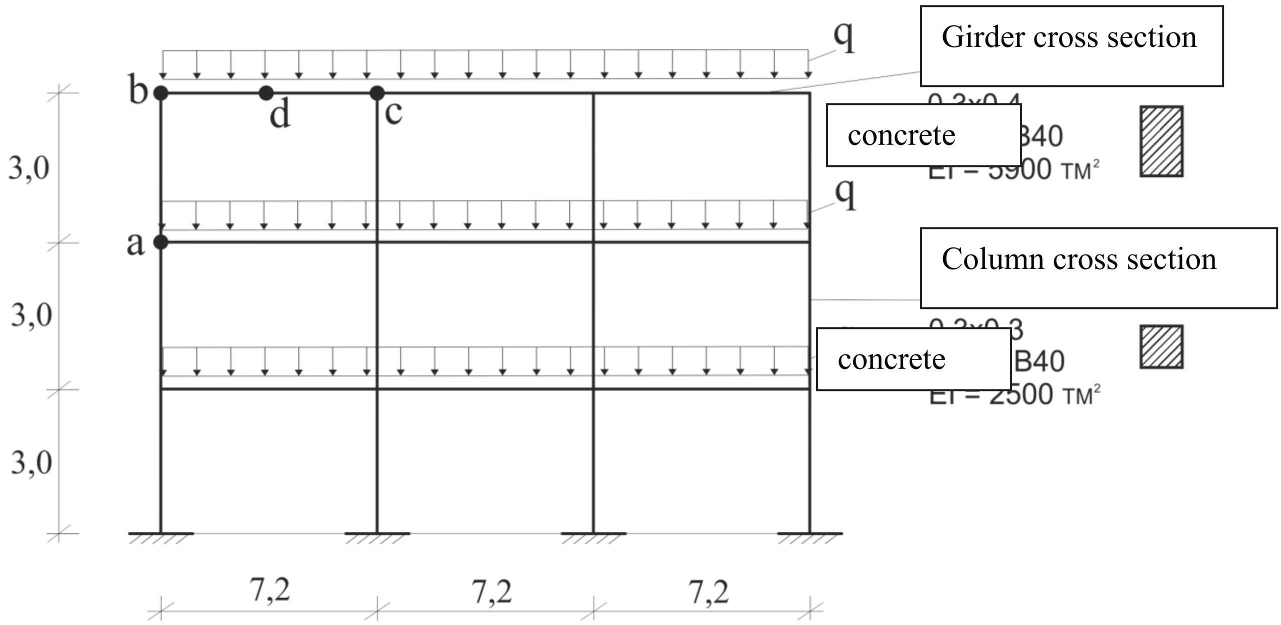

Figure 7. The design scheme of the investigated structure.

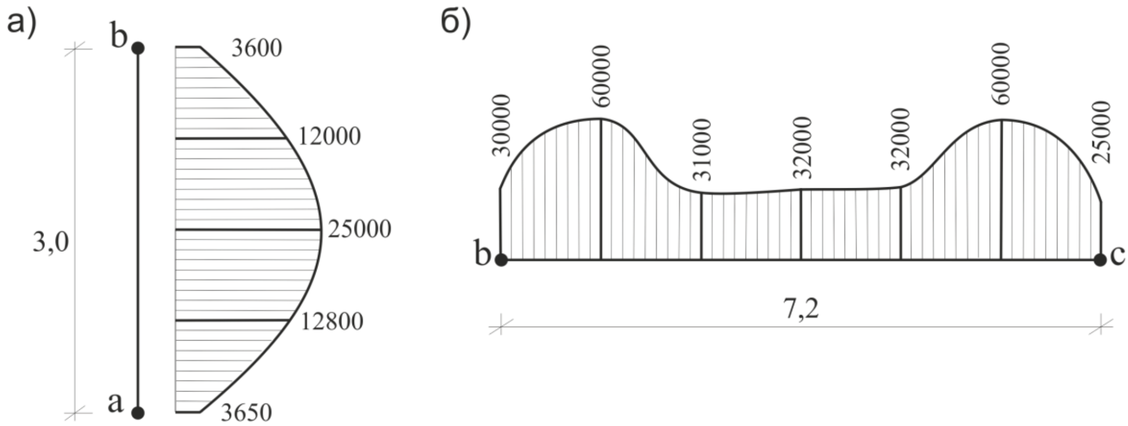

Figure 8. Plots of stiffness EI tm2 obtained on the basis of calculation by the method "Engineering nonlinearity": a) for the column, b) for the crossbar.

Table 1. Linear-elastic analysis results for the frame.

Value of stress-strain state parameters / Type of analysis	Static analysis			Dynamic analysis	
	The moment in the crossbar “b-c” in the node “b” in the tm	The moment in the crossbar “b-c” in the node “d” in the tm	Displacement of the node ‘d’,в mm	Frequency ω Hz	Period T sec.
Linear elastic analysis with initial stiffness	-25.3	28.3	-21.65	0.187	5.51
Linear elastic analysis with stiffness by “Engineering Nonlinearity 1”	-28.6	25.5	-32.84	0.162	6.32
Linear elastic analysis with stiffness by SP 52-103-2007	-31	25.7	-58.86	0.144	6.95

Analyzing the calculation results given in table. 1, we can draw the following conclusions:

- some redistribution of efforts was obtained - in a less loaded cross-section "b" of the girder, the moment increased, in a more loaded cross-section "d" of the crossbar the moment decreased;
- the movement of the node "d" increased by more than 2 times;
- the frequency of natural vibrations (first form) decreased, and the period increased.

In LIRA-SAPR, a second version of engineering non-linearity was also developed, (Engineering non-linearity 2 is a step-by-step calculation method for determining load), which has its own characteristics (Table 2):

Table 2. Comparison of techniques Engineering nonlinearity 1 and 2.

Concepts	Engineering Nonlinearity 1	Engineering Nonlinearity 2
Characteristic load	can include arbitrary loads	real permanent loads are included
Calculation for characteristic load	iterative	Step-type
Reinforcement set up	reinforcement is selected during the iterative calculation	Reinforcement is accepted
Calculation by traditional scheme	the calculation is performed for all loads based on secant deformation moduli	calculation for temporary loads is performed on the basis of the tangent deformation modulus corresponding to the last step of the step calculation
Account of physical non linearity in assemblage	is absent	available
Account of nonlinear behavior of nodes	is absent	available

An example of the application of the principle of "Characteristic load" when assigning subgrade reaction moduli

The values of the subgrade reaction moduli depend on the depth of the compressible stratum, which in turn depends on the load. Thus, this leads to a nonlinear formulation of the problem.

An example of the principle of "Characteristic loading" allows you to carry out the calculation according to the following scheme:

1. First, we assign a uniform stress under the sole of the footing by dividing the mass of the building by the area of the footing (step 1, Fig. 9). We get variable subgrade reaction moduli according to the footing area from uniform stress under the sole. We apply soil rebuff from the selected characteristic load (step 2-4, Figure 9).
2. We determine the subgrade reaction moduli for each finite element of the foundation structure from uneven stress under the bottom of the foundation (step 5, Figure 9).
3. Calculation according to the traditional scheme for all loads, taking into account those found in section 2 subgrade reaction moduli.

When modeling pile foundations in LIRA-SAPR software, it is possible to specify the loads on the pile heads to recalculate the stiffnesses (the stiffnesses change taking into account the mutual influence of sediments in the pile group, since the loads on the heads of the neighboring piles have changed). Starting with the LIRA-SAPR 2019 version, a tool has been implemented to automate iterative calculations (without user intervention) (Figure 10).

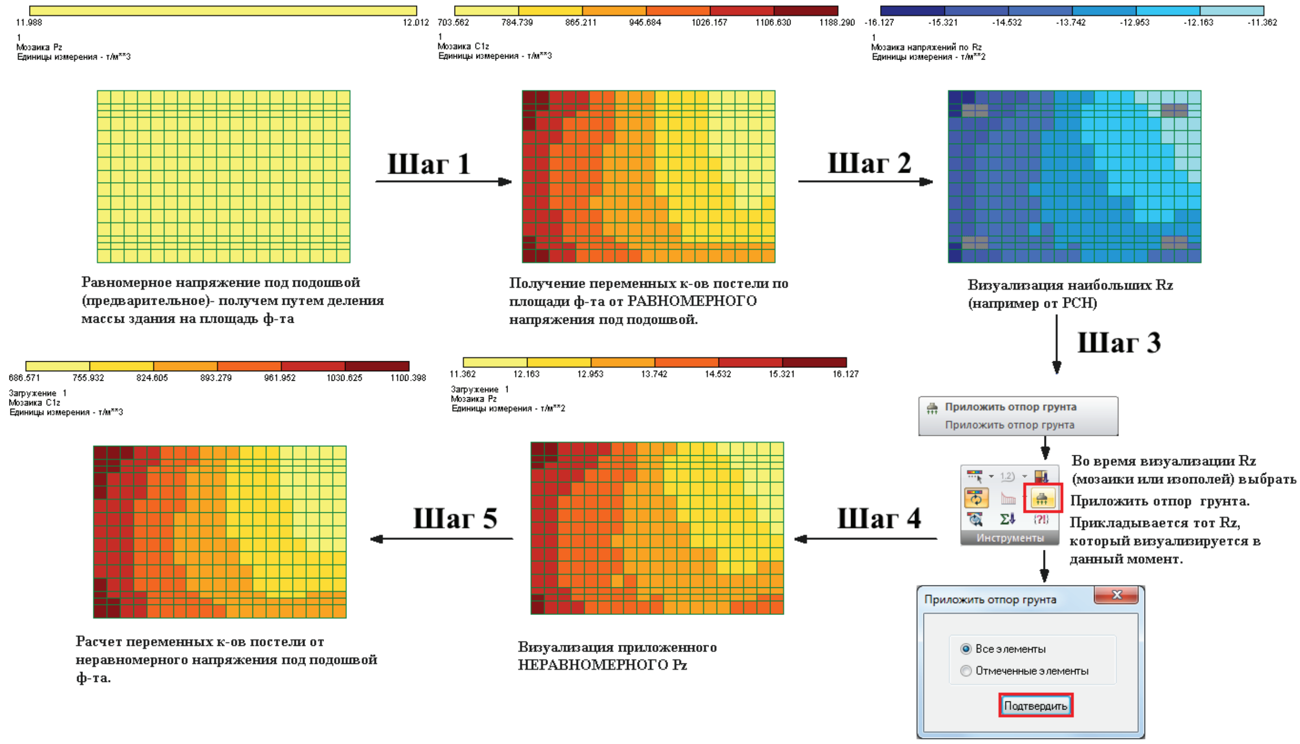

Figure 9. Algorithm for determining the magnitude of bed coefficients for each finite element of the foundation structure.

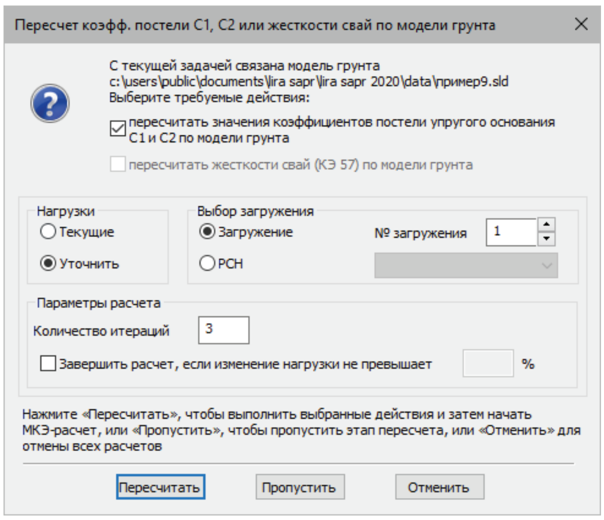

Figure 10. Dialog window calculating subgrade reaction modulus C1, C2 or stiffness of piles according to soil model.

Application of the principle of "Characteristic load" in the determination of the sizes of shelves for beam grillage

Reinforcement of slabs with beams is often found in modern housing construction. The arrangement of beams, as a rule, is irregular, there is no clearly defined system of main and secondary beams, the beams can have a small height, and here loads are often transferred to the supports due to the operation of both the slab itself and the beams.

In this case, the experience of calculating and designing ribbed floors (these examples are available in each textbook on reinforced concrete structures, where it is recommended to collect the load from the slab on the secondary beams, considering the support of the slab on them rigid, then calculate the secondary beams, considering their bearing on the main beams rigid and etc.) is unsuitable and may have only antique value.

On the other hand, from the point of view of the finite element method, it would seem that there should be no problems: a finite element grid of the slab is introduced with base points on the lines of the beams, a load is applied on the top of the slab, etc. But there are many problems associated with linking of elements of different dimensions in a finite element model. The main

problem here is how to assign the rigidity of the beam.
If we introduce rods with the hc x bc cross-section into the finite element model of the slab, the grid nodes of which lie on the middle surface, then the system with the mutual arrangement of the slab and the beam shown in Fig. 11b. Of course, such a model does not stand up to criticism. You can enter a T-section of the beam. The mutual arrangement of the slab and the beam in this case is shown in Fig. 11, c. However, the question arises of how to assign the width of the shelf. Different textbooks give different recommendations - from 6 to 15 plate thicknesses. In addition, according to this scheme, the work of the plate is taken into account twice. However, this is quite acceptable, since the finite elements of the plate simulate a bending force group, and part of the plate as part of the beam shelf models the membrane force group, which causes small stresses in the plate compared to stresses from the bending group. The model proposed in [10] is quite adequate, where the interaction of the slab and the beam is shown in Fig. 11, d.
In this case, the rods with hc x bc section are suspended using absolutely rigid inserts to the nodes of the finite element model of the plate lying in its middle surface. Here (in contrast to the models in Fig. 11b and Fig. 11c, where in the finite elements of the plate and rods only a bending group of forces arises, and each node of the finite element circuit has three nodal unknowns - vertical movement and two rotation angles), each node of finite element model has five nodal unknowns - three linear displacements and two rotation angles, and the finite elements of the plate subjected a membrane force group as well as the bending group, and in the rod element, in addition to the bending moment (Ms) and the transverse force, a normal force (Nc) also appears .

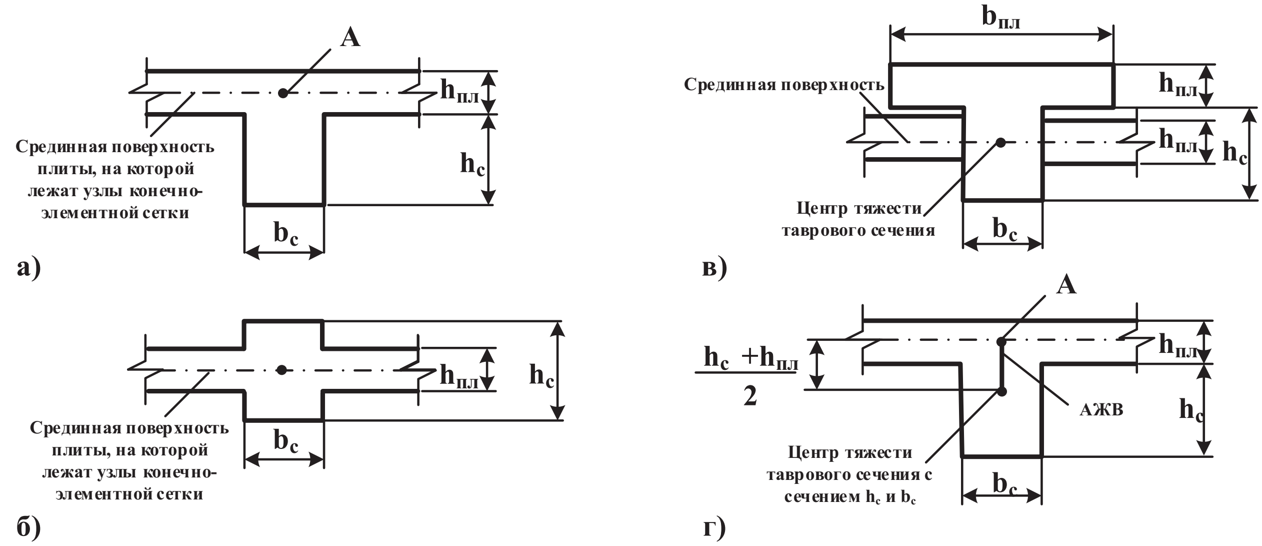

Figure 11. Modeling slab reinforced beams.

Although the latter model most fully reflects the actual work of the structure, and removes the question of the appointment of the width of the shelves in the T-beam, however, difficulties arise at the last stages of beam design. Of course, you can simply calculate the cross section of the rod hc x bc on the basis of the efforts Mc, and Nc. However, as a rule, the value of Nc is large, and the cross section will be designed as an eccentrically stretched element, and the selected reinforcement in it will be distributed around the entire perimeter, while according to the rules for constructing beam grillages, the reinforcement should be located at the lower and upper faces. Thus, for designing, it is desirable to consider the T-section of the beam subject to bending, however, it is unclear what bending moment acts on the beam and what section of the beam must be calculated. In this case, the following engineering approach can be considered, based on the hypothesis that the resultant membrane forces of the plate, balancing the normal force in the suspended rod (Nc) applied in the center of the plate (point A of Fig . 12a). Then we can assume that the bending moment acting on the beam of the T-section is equal to Mb = Ms + Nx0.5 (hs + hn). It remains only to determine the width of the shelf of the T-beam. Here, with some exaggeration, the above hypothesis can be used: if the center of gravity of the membrane forces is applied in the center of the plate part (point A), then the shelf should be uniformly compressed. Since the reinforcement will be calculated under assumptions about the ultimate state of the section, the stresses in the shelf will be Rb. Therefore, the width of the shelf bn = Nc / (hn × Rb).

The shear force in the beam is defined as the first derivative (finite-difference approach is used in numerical calculations) of the moments Mb (x). Since the diagrams Mc and Nc in the rod have a stepped form, ie, in each section there are two values of the moment and normal force, they should either be averaged or their values should be taken in the middle of the segments. Of course, the assumptions that the stresses in the shelf for determining Mb are assumed to be constant, and when determining bn, are equal to Rb, in some cases may not be successful enough, therefore, a slightly different approach based on the hypothesis of flat sections is given below (Fig. 12b). The deformation of the cross section is determined on the basis of the diagram of stresses in the cross section of the rod:

$$\sigma_{\max} = +N_c / F_c + M_c / W_c;$$
$$\sigma_{\min} = +N_c / F_c - M_c / W_c;$$
$$F_c = h_c \times b_c;$$
$$W_c = b_c \cdot h_c^2 / 6.$$

Further, the slope of the cross-section is extended into the plate region and determined from geometric ratios $\sigma_n, y, z, R_{сж} = R_{раст}$.

After that, the definition of Mb and bn seems to be a matter of technique:

$$M_б = R_{раст} \times z;$$
$$b_h = R_{сж} / (0.5\sigma_n \times y).$$

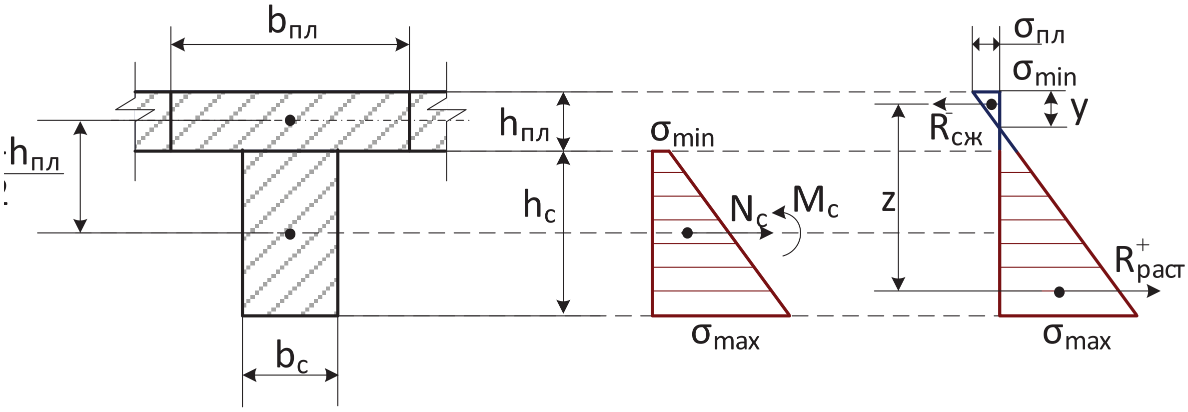

a) b)

Figure 12. Determining the width of the shelf of the T-beam.

In this case, the principle of "characteristic load" allows the calculation according to the following scheme.

1. Set up of the characteristic load.
2. Determination of the width of the shelf according to the above method for each section of the beam grillage.

3. Calculation of the beam grillage for all loads with the dimensions of shelves designated according to section 2.

CONCLUSIONS

Examples of the application of the principle of "characteristic load" are considered, apparently it does not exhaust all areas of its application. Engineering practice will prompt these areas, which will be implemented in the LIRA-SAPR Software.

REFERENCES

1. **Barabash M.S.** Vlijanie processa vozvedenija na prostranstvennuju rabotu nesushhih sistem zdanij [Influence of the erection process on the spatial work of load-bearing systems of buildings]. // Construction, materials science, mechanical engineering. Scientific Proceedings. Dnepropetrovsk, PGASA, 2012, No. 65, pp. 29-34 (in Russian).
2. **Barabash M.S.** Komp'juternoe modelirovanie processov zhiznennogo cikla objektov stroitel'stva [Computer simulation of the life cycle of construction projects]. Kiev, Stal, 2014, 301 pages (in Russian).
3. **Bondarenko V.M.** Inzhenernye metody nelinejnoj teorii zhelezobetona [Engineering methods of the nonlinear theory of reinforced concrete]. Moscow, Stroyizdat, 1982, 287 pages (in Russian).
4. **Gorodetsky A.S., Evzerov I.D.** Komp'juternye modeli konstrukcij [Computer models of structures]. The Second Edition. Kiev, FACT, 2007, 394 pages (in Russian).
5. **Gorodetsky A.S., Barabash M.S.** Komp'juternoe modelirovanie processa vozvedenija stroitel'nyh konstrukcij [Computer simulation of the process of erection of building structures]. // Structural mechanics and calculation of structures, 2014, Issue 5(256), pp. 28-33 (in Russian).
6. **Gorodetsky A.S., Barabash M.S., Sidorov V.N.** Komp'juternoe modelirovanie v zadachah stroitel'noj mehaniki [Computer modeling in the problems of structural mechanics]. Moscow, ASV Publishing House, 2016, 338 pages (in Russian).
7. **Gorodetsky A.S., Zdorenko V.S.** K raschetu fizicheski nelinejnyh ploskih ramnyh system [To the calculation of physically nonlinear planar frame systems] Structural mechanics and calculation of structures, 1969, No. 4, pp. 61-68 (in Russian).
8. **Gorodetsky A.S.** Komp'juternoe modelirovanie processa nagruzhenija zhelezobetonnyh konstrukcij [Computer simulation of the process of loading reinforced concrete structures]. // Collection of scientific works of the Lugansk National University, a series of “Technical Sciences”, No. N49 / 52, Lugansk, “LNAU” Publishing House, 2004, pp. 3-10 (in Russian).
9. **Gorodetsky A.S., Barabash M.S.** Uchet nelinejnoj raboty zhelezobetonnyh konstrukcij v prakticheskih raschetah [Accounting for the nonlinear work of reinforced concrete structures in practical calculations]. // Construction, materials science, mechanical engineering. Scientific Proceedings. Dnepropetrovsk, PGASA, 2014, Issue 77, pp. 54-59 (in Russian).
10. **Gorodetsky A.S., Evzerov I.D., Strelets-Streletsky E.B.** and others. Metod konechnyh jelementov: teorija i chislennaja realizacija [The finite element method: theory and numerical implementation]. Kiev, FACT, 1997, 138 pages (LIRA-Windows software package) (in Russian).
11. **Pikul A.V., Gorodetsky A.S.** Opredelenie zhestkostnyh harakteristik sechenija zhelezobetonnogo sterzhnja s uchetom nelinejnyh svojstv materiala

[Determination of the stiffness characteristics of the cross section of a reinforced concrete rod taking into account the nonlinear properties of the material]. // Actual problems of computer modeling of structures and structures: abstracts of the IV International Symposium. Chelyabinsk, Publishing Center of SUSU, 2012, p. 228 (in Russian).

СПИСОК ЛИТЕРАТУРЫ

1. **Барабаш М.С.** Влияние процесса возведения на пространственную работу несущих систем зданий. // Строительство, материаловедение, машиностроение // Сб. научных трудов. – Днепропетровск, ПГАСА, 2012, №65, с. 29-34.
2. **Барабаш М.С.** Компьютерное моделирование процессов жизненного цикла объектов строительства. – Киев: Сталь, 2014. – 301 с.
3. **Бондаренко В.М.** Инженерные методы нелинейной теории железобетона. – М.: Стройиздат, 1982. – 287 с.
4. **Городецкий А.С., Евзеров И.Д.** Компьютерные модели конструкций. – Киев: ФАКТ, 2007. – 394 с.
5. **Городецкий А. С., Барабаш М. С.** Компьютерное моделирование процесса возведения строительных конструкций. // Строительная механика и расчет сооружений, 2014, Выпуск 5(256), с. 28-33.
6. **Городецкий А.С., Барабаш М.С., Сидоров В.Н.** Компьютерное моделирование в задачах строительной механики. – М.: АСВ, 2016. – 338 с.
7. **Городецкий А. С., Здоренко В.С.** К расчету физически нелинейных плоских рамных систем. // Строительная механика и расчет сооружений, 1969, №4, с. 61-68.
8. **Городецкий А. С**. Компьютерное моделирование процесса нагружения железобетонных конструкций. // Сборник научных трудов Луганского национального университета, серия «Технические науки», №49/52. – Луганск: Из-во «ЛНАУ», 2004, с. 3-10.
9. **Городецкий А.С., Барабаш М.С.** Учет нелинейной работы железобетонных конструкций в практических расчетах. // Строительство, материаловедение, машиностроение. Сборник научных трудов. – Днепропетровск: ПГАСА, 2014, Выпуск 77, с. 54–59.
10. **Городецкий А.С., Евзеров И.Д., Стрелец-Стрелецкий Е.Б.** и др. Метод конечных элементов: теория и численная реализация. – Киев: ФАКТ, 1997. – 138 с. (программный комплекс ЛИРА-Windows).
11. **Пикуль А.В., Городецкий А.С.**. Определение жесткостных характеристик сечения железобетонного стержня с учетом нелинейных свойств материала. // Актуальные проблемы компьютерного моделирования конструкций и сооружений: тезисы докладов IV Международного симпозиума. – Челябинск.: Издательский центр ЮУрГУ, 2012, с. 228.

Alexander S. Gorodetsky, Foreign Member of the Russian Academy of Architecture and Construction Sciences (RAACS), Professor, DSc; Deputy Director for Science of “LIRA SAPR” Ltd; 7a, Kiyanovsky side street (pereulok), Kiev, 04053, Ukraine,
phone: +38 (050) 351 96 61;
E-mail: info@liraland.com.ua, http: www.liraland.ru.

Maria S. Barabash, Academician of the Academy of Construction of Ukraine, DSc (Eng.); Director of “LIRA SAPR” Ltd; Associate Professor, Professor of Department of Computer Technology Building, Educational and Scientific Institute of Airports, National Aviation University; 1, Kosmonavta Komarova, 03058, Kiev, Ukraine; phone: +38 (095) 286-39-90;
E-mail: bmari@ukr.net, http: www.liraland.ru;
https://orcid.org/0000-0003-2157-521X;
Researcher ID: R-9181-2016.

Maryna A. Romashkina, PhD, Support Engineer of "LIRA SAPR" Ltd, 7a, Kiyanovsky side street (pereulok), Kiev, 04053, Ukraine; phone: +38 (095) 931-52-50;
E-mail: romashkina.liraland@gmail.com;
http: www.liraland.ru;
ORCID ID: 0000-0002-7158-4037.

Andrii V. Tomashevskyi, postgraduate student, Computer Technologies of Construction Department, National Aviation University; software engineer "LIRA SAPR" Ltd, 7a, Kiyanovsky side street (pereulok), Kiev, 04053, Ukraine; phone: +38 (096) 225 38 42;
E-mail: tomashevsky.a.v@gmail.com;
ORCID ID: 0000-0001-5960-2100.

Городецкий Александр Сергеевич, иностранный член Российской академии архитектуры и строительных наук (РААСН), профессор, доктор технических наук; заместитель директора по научной работе, ООО «ЛИРА САПР»; 04053, Украина, г. Киев, Кияновский переулок 7-а; тел.: +38 (050) 351 96 61;
E-mail: info@liraland.com.ua, http: www.liraland.ru.

Барабаш Мария Сергеевна, академик Академии строительства Украины, доктор технических наук; директор ООО «ЛИРА САПР», профессор кафедры компьютерных технологий строительства Учебно-научного института Аэропортов, Национального авиационного университета; 03058, Украина, г. Киев, проспект Космонавта Комарова, д. 1;
тел: +38 (095) 286-39-90;
E-mail: bmari@ukr.net, http: www.liraland.ru
ORCID ID: 0000-0003-2157-521X;
Researcher ID: R-9181-2016.

Ромашкина Марина Андреевна, кандидат технических наук; инженер группы сопровождения, ООО «ЛИРА САПР»; 04053, Украина, г. Киев, Кияновский переулок 7-а, тел. +38 (095) 931-52-50;
E-mail: romashkina.liraland@gmail.com,
http: www.liraland.ru,
ORCID ID: 0000-0002-7158-4037.

Томашевский Андрей Владимирович, аспирант кафедры компьютерных технологий строительства Национального авиационного университета; инженер-программист ООО «ЛИРА САПР»; 04053, Украина, г. Киев, пер. Кияновский, д.7-а;
тел.: +38 (096) 225 38 42;
E-mail: tomashevsky.a.v@gmail.com;
ORCID ID: 0000-0001-5960-2100.

DOI:10.22337/2587-9618-2020-16-2-63-70

EQUATION DECOMPOSITION METHOD FOR SOLVING OF PROBLEMS OF STATICS, VIBRATIONS AND STABILITY OF THIN-WALLED CONSTRUCTIONS

Elena B. Koreneva [1], Valery R. Grosman [2]

[1] Moscow Higher Combined-Arms Command Academy, Moscow, RUSSIA

[2] Moscow State Academy for River Transport, Moscow, RUSSIA

Abstract: The work suggests the effective equation decomposition method (EDM) for solving of statics, vibrations and stability problems of thin-walled constructions. This method is based on the partition of the initial problem on the consideration of more simple auxiliary problems. The additional unknown functions are introduced for definition of the sought solutions. The paper shows the method's advantages on the examples of the boundary value problems for rectangular areas. The problem of anisotropic plate resting on an elastic subgrade and subjected to an action of expanding forces acting in the middle surface and to transverse loads is under study. The plate's edges are elastically supported. Also free vibrations of the rectangular plates of variable thickness with different boundary conditions were under consideration. The approximate analytical solutions with high exactness are obtained.

Key words: equation decomposition method, boundary value problems, approximate analytical solutions.

МЕТОД ДЕКОМПОЗИЦИИ УРАВНЕНИЙ ДЛЯ РЕШЕНИЯ ЗАДАЧ СТАТИКИ, КОЛЕБАНИЙ И УСТОЙЧИВОСТИ ТОНКОСТЕННЫХ КОНСТРУКЦИЙ

Е.Б. Коренева[1], В.Р. Гросман[2]

[1] Московское высшее общевойсковое командное орденов Жукова, Ленина и Октябрьской Революции Краснознаменное училище, г. Москва, РОССИЯ

[2] Московская государственная академия водного транспорта, г. Москва, РОССИЯ

Аннотация: Для решения задач статики, колебаний и устойчивости тонкостенных конструкций в работе предлагается эффективный приближенный аналитический метод декомпозиции уравнений (МДУ). Этот метод основан на расчленении исходной краевой задачи на ряд более простых вспомогательных задач. В этих задачах вводятся подлежащие определению дополнительные искомые функции, позволяющие определить решение. В работе достоинства метода показаны на примерах рассмотрения следующих краевых задач для прямоугольных областей. Решается задача о пластине, сделанной из анизотропного материала, лежащей на упругом основании и находящейся под действием растягивающих сил, действующих в срединной плоскости, и поперечной нагрузки. Контур пластины упруго оперт. Изучаются также свободные колебания прямоугольной пластины переменной толщины с различными условиями закрепления. Получены приближенные аналитические решения, обладающие высокой точностью.

Ключевые слова: метод декомпозиции уравнений, краевая задача, приближенные аналитические решения.

1. INTRODUCTION

The equation decomposition method (EDM) was for the first time suggested and justified in the works [1], [2]. Linear and nonlinear statics, vibrations and stability problems of thin-walled constructions computation can be solved by means of EDM. At the first time this method was applied for solving of problems, containing variable parameters for rectangular areas in the works [3], [4]. This method is based on the fact that the stated problem is replaced by the consideration of more simple auxiliary problems containing additional unknown functions. The EDM has considerably high exactness. The present work suggests the solutions of urgent problems of thin-walled constructions computation, obtained by means of EDM.

2. SOLVING OF BENDING PROBLEM OF THE RECTANGULAR ORTHOTROPIC PLATE, RESTING ON AN ELASTIC SUBGRADE AND SUBJECTED TO AN ACTION OF EXPANDING FORCES

Let us consider the bending problem of the rectangular orthotropic plate, resting on an elastic subgrade, which properties are described by Winkler's model. The plate is subjected to an action of expanding forces effective in its middle surface and by transverse loads. The plate's boundary is elastically supported (Fig.1). The relevant resolving equation is:

$$D_1 \frac{\partial^4 w}{\partial x^4} + 2D_3 \frac{\partial^4 w}{\partial x^2 \partial y^2} + D_2 \frac{\partial^4 w}{\partial x^2 \partial y^2} + cw - - p\left(\frac{\partial^2 w}{\partial x^2} + \frac{\partial^2 w}{\partial y^2} \right) = q, \qquad (1)$$

where c is the modulus of subgrade.
We have in the generally accepted notations [4]:

$$D_1 = \frac{E_x' h^3}{12}, \; D_2 = \frac{E_y' h^3}{12}, \; D_3 = (E'' + 2G)\frac{h^3}{12}.$$

For isotropic plate we have:

$$E_x' = E_y' = \frac{E}{1-\sigma^2}, \; E'' = \frac{\sigma E}{1-\sigma^2}, \; G = \frac{E}{2(1+\sigma)}.$$

The boundary conditions for the problem under examination have the following form:

$$x = \pm a, \; w = 0, \; M_x = \pm r_1 \frac{\partial w}{\partial x}, \qquad (2)$$

$$x = \pm b, \; w = 0, \; M_y = \pm r_2 \frac{\partial w}{\partial y},$$

where r_1, r_2 are the coefficients of the contour's elasticity.

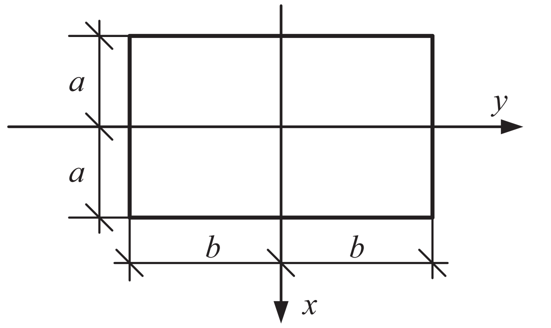

Fig.1. Rectangular plate with elastic contour

Taking into account the dimensionless elasticity coefficients:

$$k_1 = \frac{D}{D + r_1 a}, \; k_2 = \frac{D}{D + r_2 b}. \qquad (3)$$

The conditions (2) can be represented in the following form:

when $x = \pm a$

$$w = k_1 a \frac{\partial^2 w}{\partial x^2} \pm (1 - k_1)\frac{\partial w}{\partial x} = 0; \qquad (4)$$

when $x = \pm b$

$$w = k_2 b \frac{\partial^2 w}{\partial y^2} \pm (1 - k_2)\frac{\partial w}{\partial y} = 0. \qquad (5)$$

It was taken into account that in the formulae (4), (5) the second terms in the expressions for M_x and M_y [4] on the contour, where $w = 0$, are equal to zero. The values of r_1 and r_2 are positive or equal to zero. Therefore, according to the expressions (3), the coefficients k_1 and k_2 can change in the following way: $0 \le k_1 \le 1$, $0 \le k_2 \le 1$. The limiting values 0 and 1 correspond to the cases of rigid and simply supporting of the plate's boundary.

We will solve the boundary value problem (1), (4), (5) by means of the equation decomposition method (EDM). For this aim three auxiliary problems are introduced.

The first auxiliary problem (boundary) is to solve the differential equation

$$D_1 \frac{\partial^4 w_1}{\partial x^4} - p \frac{\partial^2 w_1}{\partial x^2} = f_1(x, y) \tag{6}$$

with the boundary conditions (4) when $w = w_1$.

The second auxiliary problem (boundary) is to solve the differential equation

$$D_2 \frac{\partial^4 w_2}{\partial y^4} - p \frac{\partial^2 w_2}{\partial y^2} = f_2(x, y) \tag{7}$$

with the boundary conditions (5) when $w = w_2$.

The third auxiliary problem is to solve the following differential equation:

$$\begin{gathered} \Phi(x, y) = 2D_3 \frac{\partial^4 w_3}{\partial x^2 \partial y^2} + c w_3 + f^{(1)}(x, y) + \\ + f^{(2)}(x, y) - q = 0. \end{gathered} \tag{8}$$

The solution of the initial problem (3), (4), (5) will coincide with the solutions of the auxiliary problems when the following equality will fulfilled:

$$w = w_1 = w_2 = w_3. \tag{9}$$

The mentioned conditions allow to determine the functions $f^{(1)}(x, y)$ and $f^{(2)}(x, y)$. We solve the posed task approximately. Let us present the sought functions $f^{(1)}(x, y)$ and $f^{(2)}(x, y)$ in the form of power series. The calculations and comparision of the received results for the deflections and the bending moments with the existing for certain boundary conditions exact solution show that we can retain two terms in these expansions:

$$\begin{gathered} f^{(1)}(x, y) = f_0^{(1)}(y) + x^2 f_2^{(1)}(y); \\ f^{(2)}(x, y) = f_0^{(2)}(x) + y^2 f_2^{(2)}(x). \end{gathered} \tag{10}$$

Let us receive the solutions of the first and the second boundary value problems using the conditions (10). We obtain the following:

$$\begin{gathered} w^{(1)} = w^{(2)} = C_1 \psi_1(x) \psi_2(y) + \\ + C_2 \psi_1(x) \psi_4(y) + C_3 \psi_3(x) \psi_2(y) + \\ + C_4 \psi_3(x) \psi_4(y), \end{gathered} \tag{11}$$

where $\psi_1(x) = \varphi_1(x, a, \lambda_1, k_1)$,
$\psi_2(y) = \varphi_1(y, b, \lambda_2, k_2)$,
$\psi_3(x) = \varphi_2(x, a, \lambda_1, k_1, D_1)$,
$\psi_4(y) = \varphi_2(y, b, \lambda_2, k_2, D_2)$,

$$\varphi_1(z, d, \lambda, k) = \frac{1}{p} \left\{ \frac{d\left(sh\sqrt{\lambda} z - sh\sqrt{\lambda} d\right)}{\lambda \left[kd\, sh\sqrt{\lambda} d + (1-k) \dfrac{ch\sqrt{\lambda} d}{\sqrt{\lambda}} \right]} + \frac{d^2}{2} - \frac{z^2}{2} \right\},$$

$$\varphi_2(z, d, \lambda, k, D) = \frac{1}{D\lambda^2} \times$$

$$\times \left\{ \frac{1}{\lambda} \frac{\left[kd\left(d^2 \lambda + 2\right) + (1-k)\left[\dfrac{d^3}{3} \lambda + 2d \right] \right]}{kd\, sh\sqrt{\lambda} d + (1-k) \dfrac{1}{\sqrt{\lambda}} ch\sqrt{\lambda} d} \left(sh\sqrt{\lambda} z - sh\sqrt{\lambda} d \right) + \left[\frac{d^4}{12} \lambda + d^2 \right] - \left[\frac{z^4}{12} \lambda + z^2 \right] \right\};$$

here $\lambda_1 = \dfrac{p}{D_1}$, $\lambda_2 = \dfrac{p}{D_2}$, C_1, C_2, C_3, C_4 - are the arbitrary constants.

The expression (11) is the approximate solution of the initial problem with the exactness up to four constants. Taking into account (11) and (9) we can determine these constants from the condition of the approximate solution of the differential equation (8) which takes the following form:

$$\begin{gathered}\Phi(x,y) = C_1[\psi_1(x) + \psi_2(y) + \\ + c\psi_1(x)\psi_2(y) + 2D_3\psi_1''(x)\psi_2''(y)] + \\ + C_2\left[y^2\psi_1(x) + \psi_4(y) + c\psi_1(x)\psi_4(y) + \right. \\ + 2D_3\psi_1''(x)\psi_4''(y)] + C_3[\psi_3(x) + \\ + x^2\psi_2(y) + c\psi_3(x)\psi_2(y) + \\ + 2D_3\psi_3''(x)\psi_2''(y)] + C_4\left[y^2\psi_3(x) + \right. \\ + x^2\psi_4(y) + c\psi_3(x)\psi_4(y) + \\ + 2D_3\psi_3''(x)\psi_4''(y)] - q = 0.\end{gathered} \tag{12}$$

For receiving of the (12) approximate solution the following conditions are used when $x = y = 0$:

$$\Phi = \frac{\partial^2\Phi}{\partial x^2} = \frac{\partial^2\Phi}{\partial y^2} = \frac{\partial^4\Phi}{\partial x^2\partial y^2} = 0. \tag{13}$$

Thus the constants $C_i (i = 1,2,3,4)$ are determined from the solution of the system of four equations in four unknowns. Then we can write the solution of the formulated problem by use (11).

The example for the square plate when $a = b$ was fulfilled. It was assumed that $k_1 = k_2 = 1$ that is the all the edges are simply supported and $c = 0$. The solution received by the help of EDM was compared with the existing for this case exact solution. It was shown that the values of the maximum deflection and bending moment in the plate's center which were received by the help of EDM differ from the exact solution respectively with 1,33% and 1,09%.

3. VIBRATIONS OF RECTANGULAR PLATES OF VARIABLE THICKNESS

Natural vibrations of the rectangular plate (Fig.2) with the rigidity varying along one direction according to the exponential law

$$D = D_0 e^{by}, \tag{14}$$

where D_0, b are the constants, are under consideration.

The resolving differential equation has the form:

$$\begin{gathered}D\left\{\nabla^2\nabla^2 W + 2b_1\frac{\partial}{\partial y}\nabla^2 W + b_1^2\nabla^2 W - \right. \\ \left. - b_1^2(1-\sigma)\frac{\partial^2 W}{\partial x^2}\right\} + \frac{\gamma h}{gD}\frac{\partial^2 W}{\partial t^2} = q,\end{gathered} \tag{15}$$

where $\dfrac{\gamma}{g}$ is the mass of the unit volume, h is the plate's thickness.

After the separation of variables first we shall examine the case of the simply supporting of all the plate's edges (Fig.2).

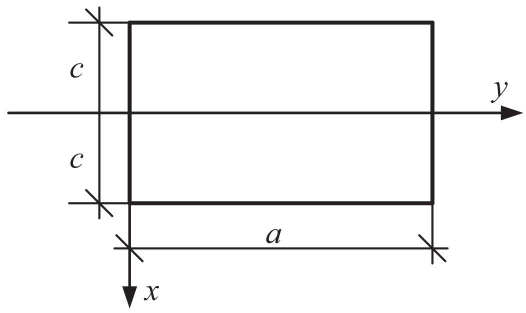

Fig.2. Rectangular plate of variable thickness

$$x = \pm c, \ \ w = \frac{\partial^2 w}{\partial x^2} = 0; \tag{16}$$

$$y = 0, a, \ \ w = \frac{\partial^2 w}{\partial y^2} = 0. \tag{17}$$

Using the substitution (14) we obtain the equation:

$$D_0 e^{b_1 y}\left(\nabla^2\nabla^2 w + 2b_1\frac{\partial}{\partial y}\nabla^2 w + b_1^2\nabla^2 w - \right. \\ \left. - b_1^2(1-\sigma)\frac{\partial^2 w}{\partial x^2\partial y^2}\right) - \lambda_s w = q, \tag{18}$$

where $\lambda_s = \dfrac{\gamma h w^2}{gD}$.

Boundary value problem (16)-(18) will be solved by use of the EDM. For this aim the three auxiliary problems are introduced.

The first auxiliary problem (boundary): to receive the solution of the differential equation

$$\frac{\partial^4 w_1}{\partial x^4} + b^2\sigma\frac{\partial^2 w_1}{\partial x^2} = f^{(1)}(x,y), \tag{19}$$

satisfying the boundary conditions (16) when $w = w_1$.

The second auxiliary problem (boundary): to obtain the solution of the differential equation

$$D_0 e^{by}\left[\frac{\partial^4 w_2}{\partial x^4} + 2b\frac{\partial^3 w_2}{\partial y^3} + b^2\frac{\partial^2 w_2}{\partial y^2}\right] = \\ = f^{(2)}(x,y), \tag{20}$$

satisfying the boundary conditions (17) when $w = w_2$.

The third auxiliary problem: to receive the solution of the following differential equation:

$$\Phi(x,y) = D_0 e^{b_1 y}\left[2\left(\frac{\partial^4 w_3}{\partial x^2\partial y^2} + b\frac{\partial^3 w_3}{\partial x^2\partial y}\right) + \right. \\ \left. + f^{(1)}(x,y)\right] + f^{(2)}(x,y) - \lambda_s w_3 - q = 0. \tag{21}$$

The solution of the posed problem (16)-(18) will coincide with the solution of the auxiliary problems when the conditions of their equality (9) are fulfilled. These conditions allow to determine the auxiliary functions $f^{(1)}(x,y)$ and $f^{(2)}(x,y)$.

As well as in the previous example we solve the formulated problem approximately. We represent the functions $f^{(1)}(x,y)$ and $f^{(2)}(x,y)$ in the form of power series. The calculations showed that retaining of two members of power series is unsufficiently. For the mentioned case the comparision of the maximum values of the bending moments and the deflections received by the such way with the existing exact solution shows the deviations are respectively with 7,59% and 10,10%. It was defined that for obtaining of the solution possessing high exactness we must accept the following expansions, taking into account the symmetry on the coordinate x:

$$f^{(1)}(x,y) = f_0^{(1)}(y) + x^2 f_2^{(1)}(y); \tag{22}$$

$$f^{(2)}(x,y) = f_0^{(2)}(x) + y f_1^{(2)}(x) + \\ + y^2 f_2^{(2)}(x). \tag{23}$$

Solving the first boundary value problem (19) and (16) we receive:

$$w_1 = \psi_1(x) f_0^{(1)}(y) + \psi_2(x) f_2^{(1)}(y), \tag{24}$$

where

$$\psi_1(x) = \frac{1}{\gamma_1^2}\left\{\frac{\cos\gamma_1 x}{\gamma_1^2\cos\gamma_1 c} - \left[\frac{1}{\gamma_1^2} + \frac{c^2}{2}\right] + \frac{x^2}{2}\right\}, \\ \psi_2(x) = \frac{1}{\gamma_2^2}\left\{\frac{\cos\gamma_1 x}{\gamma_1^2\cos\gamma_1 c}\left[c - \frac{2}{\gamma_1^2}\right] - \right. \\ \left. - \left[\frac{c^4}{12} - \frac{2}{\gamma_1^4}\right] + \left[\frac{x^4}{12} - \frac{x^2}{\gamma_1^2}\right]\right\}, \\ \gamma_1 = b_1\sqrt{\sigma}. \tag{25}$$

Solving the second boundary value problem (20) and (17) we obtain:

$$w_2 = \psi_3(y) f_0^{(2)}(x) + \psi_4(y) f_1^{(2)}(x) + \\ + \psi_5(y) f_2^{(2)}(x), \tag{26}$$

where

$$\psi_3(y)=\frac{A}{b_1^3}\left\{-\frac{a}{2}\left(b_1e^{-b_1y}+2e^{-b_1y}\right)-\left[e^{-ab_1}\left(1+\frac{3}{ab_1}\right)+\left(1-\frac{3}{ab_1}\right)\right]y+\left(a-\frac{3}{b_1}\right)y+\right.$$
$$\left.+\frac{e^{-b_1y}b_1}{2}\left(y^2+\frac{4y}{b_1}+\frac{6}{b_1^2}\right)\right\},$$
$$\psi_4(y)=\frac{A}{6b_1^3}\left\{-a^2\left(b_1e^{-b_1y}y+2e^{-b_1y}\right)-y\left[2e^{-ab_1}\left(2+\frac{9}{b_1}+\frac{12}{ab_1^2}\right)+\frac{2}{a}\left(a^2-\frac{12}{b_1^2}\right)\right]+\right.$$
$$\left.+2\left(a^2-\frac{12}{b_1^2}\right)+e^{-b_1y}b_1\left(y^3+\frac{6y^2}{b_1}+\frac{18y}{b_1^2}+\frac{24}{b_1^3}\right)\right\},\tag{27}$$
$$\psi_5(y)=\frac{A}{12b_1^3}\left\{-a^3\left(b_1e^{-b_1y}+2e^{-b_1y}\right)-\frac{12}{a}\left[\frac{e^{-b_1a}}{2}\left(a^3+\frac{6a^2}{b_1}+\frac{16a}{b_1^2}+\frac{20}{b_1^3}\right)+\left(\frac{a^3}{6}-\frac{10}{b_1^3}\right)\right]y+\right.$$
$$\left.+2\left(a^3-\frac{60}{b_1^3}\right)+e^{-b_1y}b_1\left(y^4+\frac{8y^3}{b_1}+\frac{36y^2}{b_1^2}+\frac{96y}{b_1^3}+\frac{120}{b_1^4}\right)\right\},$$
$$A=\frac{1}{D_0}.$$

Further using the equality (9) we receive:

$$\begin{aligned}w_1=w_2&=C_1\psi_1(x)\psi_3(y)+C_2\psi_1(x)\psi_4(y)+\\&+C_3\psi_1(x)\psi_5(y)+C_4\psi_2(x)\psi_3(y)+\\&+C_5\psi_2(x)\psi_4(y)+C_6\psi_2(x)\psi_6(y),\end{aligned}\tag{28}$$

where $C_i(i=1,...,6)$ are the arbitrary constants.

The expression (27) is the approximate solution of the posed problem up to the exactness of six constants. We can find these constants, taking into account the equality (9), by means of approximate solution of the differential equation (21), which takes the form:

$$\begin{aligned}\Phi(x,y)&=C_1\{D_0e^{b_1y}\{2\psi_1''(x)[\psi_3''(y)+b_1\psi_3'(y)]+\psi_3(y)\}+\psi_1(x)[1-\lambda_s\psi_3(y)]\}+\\&+C_2\{D_0e^{b_1y}\{2\psi_1''(x)[\psi_4''(y)+b_1\psi_4'(y)]+\psi_4(y)\}+\psi_1(x)[y-\lambda_s\psi_4(y)]\}+\\&+C_3\{D_0e^{b_1y}\{2\psi_1''(x)[\psi_5''(y)+b_1\psi_5'(y)]+\psi_5(y)\}+\psi_1(x)[y^2-\lambda_s\psi_5(y)]\}+\\&+C_4\{D_0e^{b_1y}\{2\psi_2''(x)[\psi_3''(y)+b_1\psi_3'(y)]+x^2\psi_3(y)\}+\psi_2(x)[1-\lambda_s\psi_3(y)]\}+\\&+C_5\{D_0e^{b_1y}\{2\psi_2''(x)[\psi_4''(y)+b_1\psi_4'(y)]+x^2\psi_4(y)\}+\psi_2(x)[y-\lambda_s\psi_4(y)]\}+\\&+C_6\{D_0e^{b_1y}\{2\psi_2''(x)[\psi_5''(y)+b_1\psi_5'(y)]+x^2\psi_5(y)\}+\psi_2(x)[y^2-\lambda_s\psi_5(y)]\}-q=0.\end{aligned}\tag{29}$$

For the estimation of the coefficients $C_i(i=1,...,6)$ the Bubnov-Galerkin's method may be used. Below the another effective method which was applied in the previous example will be used. Let us call $\Phi(x,y)$ as the residual function. This function is equal to zero in the exact solution. We minimize the residual function in the plate's midpoint when $x=0$, $y=a/2$ for the determination of the constants $C_i(i=1,...,6)$. Evidently that the residual function in this section significantly affects on the approximate solution exactness. Therefore we will write the conditions of the equality to zero of the function $\Phi(x,y)$ and a few of its lower derivatives with respect to the arguments x and y when $x=0$ and $y=a/2$:

$$\Phi = \frac{\partial^2\Phi}{\partial x^2} = \frac{\partial\Phi}{\partial y} = \frac{\partial^2\Phi}{\partial y^2} = \frac{\partial^4\Phi}{\partial x^4} = \frac{\partial^3\Phi}{\partial x^2\partial y} = 0. \quad (30)$$

It is taken into account that because of symmetry with respect to the argument x the odd derivatives on x are equal to zero. Further the system of the six equations with six unknown values is under consideration for the aim of the constants C_i determination. Then the deflections and the stresses are defined.

Let us examine the bending of the rectangular plate with the rigidity (14) with another boundary conditions; the edges

$$y = 0, a$$

are simply supported and the edges

$$x = \pm a$$

are clamped, that is we have:

$$x = \pm c, \ w = \frac{\partial w}{\partial x} = 0. \quad (31)$$

Then the solution of the first boundary value problem is to solve the differential equation (19) with the boundary conditions (31). As a result we obtain the following relations for the functions $\psi_1(x)$ and $\psi_2(x)$:

$$\psi_1(x) = \frac{c}{\gamma_1^2}\left\{\frac{\cos\gamma_1 x}{\gamma_1 \sin\gamma_1 c} - \left[\frac{ctg\gamma_1 c}{\gamma_1} + \frac{c}{2}\right] + \frac{x^2}{2c}\right\},$$

$$\psi_2(x) = \frac{c}{\gamma_1^2}\left\{\frac{\cos\gamma_1 x}{\gamma_1^2 \sin\gamma_1 c}\left(\frac{c^2}{3} - \frac{2}{\gamma_1^2}\right) - \right.$$
$$-\left[\frac{1}{\gamma_1}ctg\gamma_1 c\left(\frac{c^2}{3} - \frac{2}{\gamma_1^2}\right) + c\left(\frac{c^2}{12} - \frac{1}{\gamma_1^2}\right)\right] + \quad (32)$$
$$\left. + \frac{1}{c}\left(\frac{x^4}{12} - \frac{x^2}{\gamma_1^2}\right)\right\},$$
$$\gamma_1 = b_1\sqrt{\sigma}.$$

The solution of the second boundary value problem remains unvariable and is represented by the expression (24) where the functions $\psi_3(y)$, $\psi_4(y)$, $\psi_5(y)$ are defined by the relations (25). Then the deflections and the stresses are determined in the same way as it was described above.

6. CONCLUSION

The work stated the equation decomposition method intended for solving of boundary value problems of thin-walled structures computation. This method is based on the fact that the consideration of the original problem is replaced by the examination of the auxiliary problems including boundary value ones. For the consideration of the mentioned problems the auxiliary functions are introduced. The approximate analytical solutions possessing high exactness are obtained.

REFERENCES

1. **Pshenichnov G.I.** Metod Dekompozitsii Uravnenij i Kraevyh Zadach. [Equation Decomposition Method for Solving of Equations and Boundary Value Problems] // Doklady AN SSSR. 1985, t.282, №4, pp. 792-794 (in Russian).
2. **Pshenichnov G.I.** A Theory of Latticed Plates and Shells. World Scientific. Singapore, New Jersey, London, Hong Kong, 1993, 309 pages.
3. **Koreneva E.B., Pshenichnov G.I.** Primenenie Metoda Dekompozitsii Uravnenij k Resheniju Zadach Teorii Izgiba Plastin Peremennoj Tolshiny [Equation Decomposition Method Application for Solving of Bending Problems of Plates of Variable Thickness] // Zhurnal Vychislitelnoj Matematiki i Matematicheskoj Phyziki. 1997. №3, pp. 553-558 (in Russian).
4. **Koreneva E.B.** Analiticheskie Metody Rascheta Plastin Peremennoj Tolschiny i ih Prakticheskije Prilozhenija [Analylical Methods for Calculation of Plates with Vary-

ing Thickness and Their Practical Application]. Moscow, ASV, 2009, 238 p. (in Russian).

СПИСОК ЛИТЕРАТУРЫ

1. **Пшеничнов Г.И.** Метод декомпозиции решения уравнений и краевых задач. // Доклады А.Н. СССР, 1985, том 282, №4, с. 792-794.
2. **Pshenichnov G.I.** A Theory of Latticed Plates and Shells. World Scientific. Singapore, New Jersey, London, Hong Kong, 1993, 309 pages.
3. **Коренева Е.Б., Пшеничнов Г.И.** Применение метода декомпозиции уравнений к решению задач теории изгиба пластин переменной толщины. // Журнал вычислительной математики и математической физики, 1997, №3, с. 553-558.
4. **Коренева Е.Б.** Аналитические методы расчета пластин переменной толщины и их практические приложения. – М.: АСВ, 2009. – 238 с.

Elena B. Koreneva, Dr.Sc., Professor, Dr.Sc., Moscow Higher Combined-Arms Command Academy; 2, ul. Golovacheva, Moscow, 109380, Russia,
tel.: +7(499)175-82-45;
E-mail: elena.koreneva2010@yandex.ru.

Valery R. Grosman, Associate Professor, Moscow State Academy for River Transport; 2, k. 1, Novodanilovskaya nab., Moscow, 117105, Russia; phone: +7(499)618-52-56;
E-mail: elena.koreneva2010@yandex.ru.

Коренева Елена Борисовна, доктор технических наук, профессор, Московское высшее общевойсковое командное орденов Жукова, Ленина и Октябрьской Революции Краснознаменное училище; 109380, Россия, г. Москва, ул. Головачева, д.2;
тел.: +7(499)175-82-45;
E-mail: elena.koreneva2010@yandex.ru.

Гросман Валерий Романович, старший преподаватель, МГАВТ – филиал ФГБОУ ВО «ГУМРФ имени адмирала С.О. Макарова»; 117105, Россия, г. Москва, Новоданиловская наб., д. 2, корп. 1;
тел.: +7(499)618-52-56;
E-mail: elena.koreneva2010@yandex.ru.

DOI:10.22337/2587-9618-2020-16-2-71-82

ASSESSMENT OF THE PROXIMITY OF DESIGN TO MINIMUM MATERIAL CAPACITY SOLUTION OF PROBLEM OF OPTIMIZATION OF THE FLANGE WIDTH OF I-SHAPED CROSS-SECTION RODS WITH ALLOWANCE FOR STABILITY CONSTRAINTS OR CONSTRAINTS FOR THE VALUE OF THE FIRST NATIONAL FREQUENCY AND STRENGTH REQUIREMENTS

Leonid S. Lyakhovich [1], ***Pavel A. Akimov*** [1, 2, 3], ***Boris A. Tukhfatullin*** [1]
[1] Tomsk State University of Architecture and Civil Engineering, Tomsk, RUSSIA
[2] National Research Moscow State University of Civil Engineering, Moscow, RUSSIA
[3] Peoples' Friendship University of Russia, Moscow, RUSSIA

Abstract: There are known methods for optimizing the flange width of I-shaped cross-section rods with stability constraints or the constraints for the value of the first natural frequency. Corresponding objective function has the form of the volume of the flange material for the case when only the flange width varies and the cross-section height, wall thickness and flange thickness are specified. Special criterion for assessment of proximity of corresponding an optimal solution to the design of minimal material capacity was formulated for the considering problem. In this case, the resulting solution may not meet some other unaccounted constraints, for example, strength requirements. Modification of solution in order to meet previously unaccounted constraints does not allow researcher to consider such design as optimal. In the distinctive paper allowance for strength requirements, stability constraints or constraints for the value of the first natural frequency are proposed within considering problem of optimization. Special approach is formulated, which proposes to assess proximity to the design of minimum of material capacity obtained as a result of optimization. Increment of the objective function and criteria corresponding to constrains and restrictions are under consideration within computational process.

Keywords: criterion, optimization, limitations, strength conditions, minimum material capacity, stability, frequency, critical force, forms of stability loss, forms of natural vibrations, reduced stresses

ОЦЕНКА БЛИЗОСТИ К ПРОЕКТУ МИНИМАЛЬНОЙ МАТЕРИАЛОЕМКОСТИ РЕШЕНИЯ ОБ ОПТИМИЗАЦИИ ШИРИНЫ ПОЛОК СТЕРЖНЕЙ ДВУТАВРОВОГО СЕЧЕНИЯ ПРИ ОГРАНИЧЕНИЯХ ПО УСТОЙЧИВОСТИ ИЛИ ВЕЛИЧИНЫ ПЕРВОЙ ЧАСТОТЫ СОБСТВЕННЫХ КОЛЕБАНИЙ С УЧЁТОМ ТРЕБОВАНИЙ ПРОЧНОСТИ.

Л.С. Ляхович [1], ***П.А. Акимов*** [1, 2, 3], ***Б.А. Тухфатуллин*** [1]
[1] Томский государственный архитектурно-строительный университет, г. Томск, РОССИЯ
[2] Национальный исследовательский Московский государственный строительный университет, г. Москва, РОССИЯ
[3] Российский университет дружбы народов, г. Москва, РОССИЯ

Аннотация: Известны методы оптимизации ширины полок стержней двутаврового поперечного сечения при ограничениях по устойчивости или величине первой частоты собственных колебаний, функции цели в виде объема материала полок, для случая, когда варьируется только ширина полок, а высота сечения, толщина стенки и толщина полки заданы. Для этого варианта постановки задачи был сформулирован критерий оценки близости такого оптимального решения к проекту минимальной материалоемкости.

При этом в полученном решении могут не выполняться некоторые другие неучтённые ограничения, например, по прочности. Изменение полученного решения с целью удовлетворения неучтённым ранее ограничениям не позволяет считать такой проект оптимальным. В данной статье предлагается в рассматриваемой задаче учитывать в процессе оптимизации при ограничениях по устойчивости или величине первой частоты собственных колебаний ещё и условии прочности. Формулируется подход, в котором предлагается для оценки близости к проекту минимальной материалоемкости решения, полученного в результате оптимизации, наряду с анализом в процессе вычислений изменений величины приращения функции цели, использовать ещё и критерии, характеризующие каждое из принятых ограничений.

Ключевые слова: критерий, оптимизация, ограничения, условия прочности, минимальная материалоемкость, устойчивость, частота; критическая сила, формы потери устойчивости, формы собственных колебаний, приведенные напряжения

Earlier [1], the problem of the optimal outline of the flange width of the I-shaped cross-section rod [2], [3] was considered with allowance for stability constraints or constraints for the value of the first natural frequency. Corresponding objective function was the volume of the material of the flanges for the case when only the flange width varies and the section height, wall thickness and flange thickness are specified. Besides, special criterion was formulated for the proximity of such a solution to the minimal material capacity solution [1]. Criteria of assessment of proximity of the optimized design to corresponding minimum material capacity solution have also been formulated in many papers dealing with structural design [6, 9] and strengthening of structures [4, 5, 7, 8]. Some specific theoretical problems dealing with formulation of the criteria [10, 11, 12, 13] were also considered. At the same time, other constraints (for example, strength conditions) were not taken into account normally. Therefore, solutions obtained in such cases might not satisfy these constraints. However, if the obtained design (project) is modified so that restrictions not previously considered are fulfilled, then the modified design (project) cannot be considered as optimal. In the distinctive paper allowance for strength requirements, stability constraints or constraints for the value of the first natural frequency are proposed within considering problem of optimization of the flange width of I-shaped cross-section rods.

As is known, analysis of changes in the increments of the objective function is normally used within optimization methods [14]. However, there are cases when the objective function changes slightly at the computational stages but the optimal solution has not yet been obtained and the corresponding design (project) is noticeably different from the minimum material capacity solution.

We recommend application of criteria corresponding to considering constraints and analysis of changes in the increments of the objective function within optimization process for assessment of proximity of design to minimum material capacity solution.

Thus, the I-shaped cross-section rod is under consideration. The cross-section height b_1, wall thickness δ_{st} and flange thickness δ_p are specified. Flange width along the length of the rod (x axis) $b_2(x)$ or $b_2[i]$ within discrete model of the rod varies (Figure 1).

It is necessary to find a function $b_2(x)$ that, together with the given parameters ($b_1, \delta_{st}, \delta_p$), determines a rod that satisfies the stability constraints or constraints for the value of the first natural frequency (as well as the strength requirements and structural constraints) and at the same time provide a minimum volume of material of flanges.

The objective function within considering formulation of the problem has the form

$$V_0 = 2\int_0^l b_2(x)\delta_p dx . \quad (1)$$

For discrete model including n sections we have

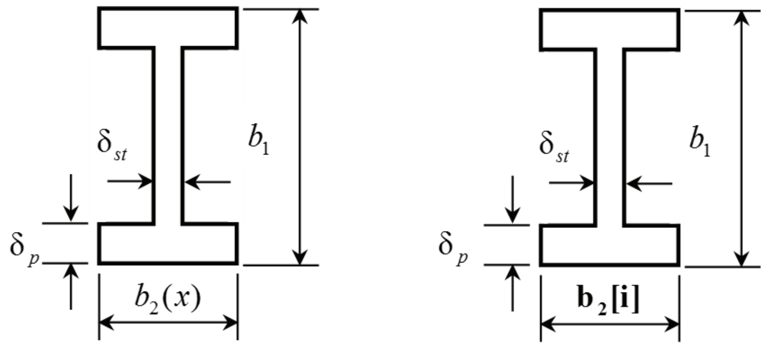

Figure 1. *Considering cross-section of rods.*

$$\bar{\sigma}_{1\omega t}(x) = \sqrt{\sigma_{1\omega}^2(x)\cdot\frac{b_1}{2\cdot\delta_p} - \sigma_{1\omega t}^2(x)\cdot(\frac{b_1}{2\cdot\delta_p} - 1) - 3\cdot E\cdot(\omega_0)^2\cdot v_\omega^2(x)\cdot\rho} = \text{const}, \tag{7}$$

$$V_0 = 2\frac{l}{n}\sum_1^n b_2[i]\delta_p \ , \tag{2}$$

where V_0 is the volume of material of flanges; l is the length of the rod.

Stability constraints have the form

$$P \le P_{kp}, \tag{3}$$

where P is the acting force, P_{kp} is the corresponding critical force.

Constraint for the value of the first natural frequency has the form

$$\omega_0 \le \omega 1 \ , \tag{4}$$

where ω_0 is the given value, $\omega 1$ is the value of the first natural frequency of the system.

Special criterion for assessments of results of optimization of flange width with allowance for stability constraints or constraints for the value of the first natural frequency is also formulated by the authors for the case when the flange width varies continuously along the length of the rod. This criterion can be presented in the form of three variants (versions, options):

$$\bar{\sigma}_{1\omega t}^2(x) = \sigma_{1\omega}^2(x)b_1 - \sigma_{1\omega t}^2(x)(b_1 - 2\delta_p) - \\ - 3E(\omega_0)^2\rho\cdot 2\delta_p v_\omega^2(x) = \text{const}; \tag{5}$$

$$\bar{\sigma}_{1\omega t}^2(x) = \sigma_{1\omega}^2(x)\frac{b_1}{2\delta_p} - \sigma_{1\omega t}^2(x)(\frac{b_1}{2\delta_p} - 1) - \\ - 3\cdot E\cdot(\omega_0)^2\cdot v_\omega^2(x)\cdot\rho = \text{const}; \tag{6}$$

where $\sigma_{1\omega}(x)$ and $\sigma_{1\omega t}(x)$ are respectively normal stresses in the extreme fibers of the I-shaped cross-section and in the fibers at the boundary of the wall and the flange, created by bending moments arising from loss of stability or natural vibrations; $v_\omega(x)$ are the coordinates of the form of loss of stability or natural vibrations.

The variant (7) of the formulation of criterion was introduced only in order to emphasize its association with the previously formulated criteria. Application of this variant of the criterion with allowance for constraints for the value of the lowest natural frequency can lead to negative values of sub-root expressions and to corresponding problems dealing with computational process at the initial stages of optimization.

In this connection one of the equivalent variants (5) or (6) will be used in the distinctive paper. Criteria (5), (6), (7) can be used in combination with stability constraints or constraints for the value of the first natural frequency. In case of stability constraints we should assume that $\omega_0 = 0$ in the expressions of the criterion.

Three strength conditions must be fulfilled for rods of I-shape cross-section [14].

Strength condition for normal stresses in extreme fibers has the following form:

$$\sigma(x) \le R, \tag{8}$$

where σ is normal stresses from the load in the extreme fibers of the rod; R is design strength of the material of construction.

The condition for the fourth theory of strength at the junction of the flange with the wall has the following form:

$$\sigma_{eq}(x) = \sqrt{\sigma_p^2(x) + 3\tau_p^2(x)} \le R, \tag{9}$$

where $\sigma_{eq}(x)$, $\sigma_p(x)$, $\tau_p(x)$ are respectively equivalent, normal, and shear stresses from the load at the junction of the flange with the wall.

The condition for the fourth theory of strength at the center of gravity of the section has the following form:

$$\sigma_{экв}(x) = \sqrt{\sigma_0^2(x) + 3\tau_0^2(x)} \le R, \tag{10}$$

where $\sigma_{eq}(x)$, $\sigma_0(x)$, $\tau_0(x)$ are respectively equivalent, normal, and shear stresses from the load at the center of gravity of the cross section.

Let us rewrite expressions (8), (9) and (10) in expanded form, reflecting in them the internal forces of the rod and the parameters of its cross section. Besides, let us introduce the following notation system: $M(x)$, $Q(x)$, $N(x)$ are respectively, bending moments, transverse and longitudinal forces in the corresponding cross-sections of the rod.

Condition (8) will take the following form:

$$\sigma(x) = \frac{N(x)}{b_1 \cdot b_2(x) - (b_1 - 2\delta_p)\cdot(b_2(x) - \delta_{st})} + \\ + \frac{6M(x)\cdot b_1}{b_2(x)\cdot b_1^3 - (b_2(x) - \delta_{st})(b_1 - 2\delta_p)^3} \le R \tag{11}$$

Condition (9) will take the form:

$$\sigma_{eq}(x) = \\ = \left\{ \left[\begin{array}{l} \dfrac{N(x)}{b_1 \cdot b_2(x) - (b_1 - 2\delta_p)\cdot(b_2(x) - \delta_{st})} + \\ + \dfrac{12M(x)}{b_2(x)\cdot b_1^3 - (b_2(x) - \delta_{st})(b_1 - 2\delta_p)^3} \times \\ \times \left(\dfrac{b_1}{2} - \delta_p\right) \end{array} \right]^2 + \right. \\ \left. + 3\cdot\left[\frac{6\cdot Qb_2(x)\delta_p(b_1 - \delta_p)}{(b_2(x)b_1^3 - (b_2(x) - \delta_{st})(b_1 - 2\delta_p)^3)\delta_{st}}\right]^2 \right\}^{\frac{1}{2}} \le R \tag{12}$$

Condition (10) will take the form:

$$\sigma_{eq} = \left\{ \left[\frac{N(x)}{b_1 b_2 - (b_1 - 2\delta_p)(b_2 - \delta_{st})} \right]^2 + \right. \\ \left. + 3\cdot\left[\frac{Q(x)\cdot\left[\begin{array}{l} \dfrac{3b_2(x)b_1^2}{2} - \\ - 6(b_2(x) - \delta_{st})\left(\dfrac{b_1}{2} - \delta_p\right)^2 \end{array} \right]}{[b_2(x)b_1^3 - (b_2(x) - \delta_{st})(b_1 - 2\delta_p)^3]\delta_{st}} \right]^2 \right\}^{\frac{1}{2}} \le R \tag{13}$$

Design restrictions have the following form:

$$b_2(x) \ge bb, \tag{14}$$

where bb is minimum flange width.

Within a discrete model of the rod, the corresponding coordinates of considering cross-section ((x)) are replaced by the corresponding number of the model section ($[i]$).

In order to ensure uniformity of the use of criteria and restrictions for assessing the proximity of the resultant optimized design (project) to design of minimum of material capacity we should normalize criterion (4) (or (5)) and conditions (8), (9), (10) and (13) so that if performed in the form of equalities, they would take a value equal to unity.

When normalizing criterion (5) (or (6)), bending moments (which, like mode shapes (natural modes) are determined with accuracy to a constant factor) are revealed by the form of loss of stability or the first natural mode. Stresses $\sigma_{1\omega}(x)$, $\sigma_{1\omega t}(x)$ and $\bar{\sigma}^2_{1\omega t}(x)$ are computed in accordance with these moments in cross-sections. Then, the maximum value is selected among $\bar{\sigma}^2_{1\omega t}(x)$ and the values of expression (5) (or (6)) are divided into it. Now, if the design (project) obtained as a result of optimization is the design of minimum material capacity, then the criterion takes the form

$$\bar{\sigma}^2_{1\omega t}(x) = 1. \qquad (15)$$

If constraints (8), (9) and (10) are also used within optimization process, then the criterion (15) must be applied only to those parts of the rod in which dependencies (8), (9) and (10) are fulfilled in the form strict inequalities.

Let us normalize constraint (7).

Dividing both sides of expression (7) by R we obtain

$$R1(x) = \frac{\sigma(x)}{R} \le 1. \qquad (16)$$

We can similarly normalize constraints (8) and (9) and get

$$R2(x) = \frac{\sigma_{экв}(x)}{\mathrm{R}} = \frac{\sqrt{\sigma_p^2(x) + 3\tau_p^2(x)}}{R} \le 1; \qquad (17)$$

$$R3(X) = \frac{\sigma_{экв}(\mathrm{x})}{\mathrm{R}} = \frac{\sqrt{\sigma_0^2(x) + 3\tau_0^2(x)}}{R} \le 1. \qquad (18)$$

In order to normalize the constraint (14), we should divide put both parts of the expression (13) by $b_2(x)$ and rewrite this constraint in the form

$$bb_0(x) = \frac{bb}{b_2(x)} \le 1. \qquad (19)$$

Let us explain that $\bar{\sigma}^2_{1\omega t}(x)$, $R1(x)$, $R2(x)$, $R3(x)$ и $bb_0(x)$ in (15), (16), (17), (18) are indicators of fulfillment of restrictions ((2) or (3)), (8), (9) (10) and (14).

Now, after normalizing all the restrictions used, the proximity to the design (project) of minimum material capacity of the design (project), obtained as a result of optimization with allowance for stability constraints (or constraints for the value of the first natural frequency), strength and structural constraints is determined by the proximity of at least one of indicators (15), (16), (17), (18) and (19) to unity in each cross-section.

Let us give an illustration of the assessment of the proximity of the solution of the considering problem to the project of minimal material consumption by an example.

Sample.

A rigidly restrained rod of an I-shape cross-section is under consideration (Figure 2). The span of the rod is equal to $l = 12m$. The height of the cross-section of the rod is equal to $b_1 = 0.16m$. Wall thickness is equal to $bst = 0.01m$. Flange thickness is equal to $b_p = 0.014\,m$. Flange width is equal to $b_2 = 0.12m$. Besides, flange width is constant along the entire length of the rod. The modulus of elasticity of the material of the rod is equal to $E = 2060000000\ 00\,N/m^2$. Its specific gravity is equal to $7850\,kg/m^3$. Volumetric weight is equal to $77008.5\,N/m^3$. Design strength is equal to $R = 240000000\ N/m^2$.

The rod carries a uniformly distributed mass of intensity $m = 400kg/m$. The same mass is an external load with intensity $q = 3924N/m$.

Own weight of the rod are taken into account in optimization process with allowance for strength conditions.

The critical force (ultimate load) of the rod (without taking into account possible vibrational effects) is equal to $Pcr = 1118457N$.

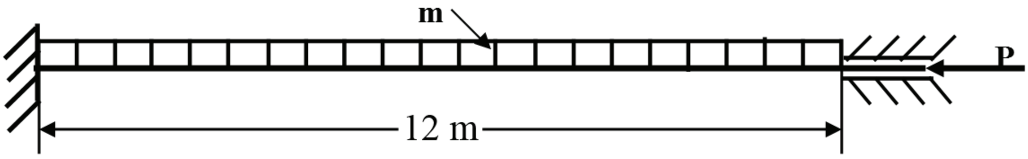

Figure 1. Considering sample.

The first natural frequency (without taking into account the influence of the longitudinal force on the frequency) is equal to $\omega = 18.5773\,\sec^{-1}$. Let the compressive force be $P = 300000\ N$. The flange width is equal to $b_2 = 0.12m$ (it is the same along its entire length of the rod). The first natural frequency of the rod with allowance for the influence of the longitudinal force on the frequency is equal to $\omega = 12.9291\,\sec^{-1}$. It should be noted that strength conditions were not considered within determination of the critical force and frequency.

Thus, in the considering sample it is required to optimize the shape of the width of the flanges of the considering rod loaded by $P = 300000\ N$, provide special value of the first natural frequency ($\omega 1 \geq \omega_0 = 13\,\sec^{-1}$) and minimum volume of the material of the flanges. Constraints for the value of the first natural frequency (4), strength constraints (8), (9), (10) and structural constraints (10) must be taken into account within optimization process. Let $bb = 0.01m$ be the smallest possible flange width.

Discrete model of the rod including 30 sections (elements) is used for corresponding analysis. Evenly distributed mass and load are reduced to nodes. Besides, we have nodal masses ($m[i] = 160kg$) and loads ($\mathrm{q[i]} = 1569.6N$) within this discrete model. The mass and weight of the structure are taken into account within the optimization process.

Generally optimization can be performed by one of the well-known methods (various modifications of method of descent, random search method and so on) [16, 17]. The random search method is used in the considering sample.

After completion of the optimization process, we will evaluate the proximity of the obtained solution to the corresponding minimal material capacity solution.

First of all, in order to compare the design of minimum material consumption with other possible solutions, several options should be considered.

The first variant. Conventional solution is considered in which the minimum value for the flange width (b_2) is determined, provided that it is the same along the entire length of the rod, but restrictions (4), (8), (9), (10) and (14) are accepted.

Table 1. Results of analysis.

1	Flange width $b_2[i]$			$\overline{\sigma}^2_{\omega}[i]$
i	2	3	4	5
1	0.2070	0.1649	0.2070	0.9967
2	0.1800	0.1421	0.1800	0.9970
3	0.1515	0.1196	0.1514	0.9969
4	0.1215	0.0975	0.1215	0.9969
5	0.0903	0.0755	0.0903	0.9969
6	0.0582	0.0534	0.0582	0.9976
7	0.0300	0.0300	0.0254	1.0000
8	0.0100	0.0100	0.0100	0.0339
9	0.0279	0.0279	0.0131	0.9911
10	0.0460	0.0460	0.0403	0.9968
11	0.0633	0.0599	0.0633	0.9971
12	0.0818	0.0707	0.0818	0.9972
13	0.0958	0.0785	0.0958	0.9965
14	0.1052	0.0837	0.1052	0.9966
15	0.1098	0.0863	0.1098	0.9972
16	0.1098	0.0863	0.1098	0.9972
17	0.1052	0.0837	0.1052	0.9966
18	0.0958	0.0785	0.0958	0.9965
19	0.0818	0.0707	0.0818	0.9972
20	0.0633	0.0599	0.0633	0.9971
21	0.0460	0.0460	0.0403	0.9968
22	0.0279	0.0279	0.0131	0.9911
23	0.0100	0.0100	0.0100	0.0339
24	0.0300	0.0300	0.0254	1.0000
25	0.0584	0.0534	0.0582	0.9976
26	0.0903	0.0755	0.0903	0.9969

i	2	3	4	5
27	0.1215	0.0975	0.1215	0.9969
28	0.1515	0.1196	0.1514	0.9969
29	0.1800	0.1421	0.1800	0.9970
30	0.2070	0.1649	0.2070	0.9967

This solution implements the flange width, which is equal to $b_2 = 0.1542m$. Moreover, restriction (7) in sections 1 and 30 is fulfilled in the form of an equality, and in all other sections it is fulfilled in the form of inequalities. Constraints (9), (10) and (14) in all sections of the rod are fulfilled in the form of inequalities. Constraint (3) is fulfilled in the form of inequality as well.

In this connection the first natural frequency of the rod is equal to $\omega 1 = 14.89\,\text{sec}^{-1} \geq 13\,\text{sec}^{-1}$.

Thus, the minimum value of flange width $b_2 = 0.1542m$ (it is constant along the entire length of the rod) is determined by the active fulfillment of the strength constraint (8) for sections 1 and 30 and the passive fulfillment of all other constraints. The volume of material of the flanges in the considering variant is equal to $V_0 = 0.05181\ m^3$.

The second variant. Let us optimize the values $b_2[i]\ (i = 1, 2, ..., 30)$, that vary in each section, but without taking into account the strength constraints (i.e. constraints (4) and (14)). The results of this optimization are shown in the fourth column of Table 1. The volume of material of the flanges in the considering variant is equal to $V_0 = 0.030309\ m^3$. The fifth column shows the indicators (15) of the fulfillment of the constraint (4). In all sections except section number 8 and section number 23, they differ only by a fraction of a percent from unity. In section number 8 and section number 23 we have $b_2[i] = 0.01m$. Therefor in these sections the restriction (14) is fulfilled in the form of equality and corresponding indicators are equal to $bb_0[8] = 1$, $bb[23] = 1$. Thus, in all sections of the rod we have indicator, which is fairly close to unity. This circumstance allows researcher to consider the resultant design quite close to the design of minimum material capacity but only with allowance for corresponding constraints. Otherwise, with the constraints taken into account, the objective function is minimal within the limits of errors and the proximity of the indicators $\bar{\sigma}^2_{\omega}[i]$ to unity.

The third variant. In order to verify the fulfillment of the strength conditions for the design obtained in the second variant with the values $b_2[i]$ bending moments and shear forces were determined in accordance with the deformed pattern taking into account applied load $q = 3924N/m$, dead weight and the influence of the longitudinal force $P = 300000\ N$.

Then, using formulas (11), (12), (13), a value of $b_2[i]$ was determined for each section under which one of the conditions (11), (12), (13) is satisfied as equality, and remaining as inequalities. They determine the minimum permissible flange width ($b_2[i]$), satisfying the strength conditions. These values of $b_2[i]$ are shown in the third column of Table 1. Comparison of the values of $b_2[i]$ in the third column with the corresponding values in the fourth column 4 shows that strengths constraints are not fulfilled in sections with the following numbers: 7, 9, 10, 21, 22, 24. If in these sections the dimensions of the flange width are increased to the minimum permissible dimensions under the strength conditions, leaving the dimensions in the remaining sections unchanged, then we get the design presented in the second column of Table 1. The objective function for this design is equal to $V_0 = 0.030874\ m^3$, the value of the first natural frequency is equal to $\omega = 13.1103\,\text{sec}^{-1}$ (constraint (4) is fulfilled in the form of an inequality). In this connection, the subsequent fulfillment of constraints not taken into account within optimization process does not allow researcher to consider the solution as a design of minimal material capacity.

The fourth variant. Let us now optimize the values $b_2[i] (i = 1, 2, .., 30)$ with allowance for constraints (4), (8), (9), (10) and (14) (including strength constraints). The results of this analysis are presented in Table 2.

Table 2. Results of analysis.

i	$b_2[i]$	$\bar{\sigma}^2_{\omega}[i]$	$R1[i]$	$R2[i]$	$R3[i]$	$bb_0[i]$
1	0.1995	0.9986	0.8276	0.7238	0.2218	0,050
2	0.1727	0.9994	0.8249	0.7247	0.2387	0,058
3	0.1444	0.9991	0.8308	0.7340	0.2635	0,069
4	0.1147	0.9992	0.8500	0.7564	0.3012	0,087
5	0.0837	0.9992	0.8905	0.8000	0.3614	0,119
6	0.0518	1.0000	0.9701	0.8834	0.4668	0,193
7	0.0254	0.7037	1.0000	0.9351	0.6276	0,394
8	0.0100	-0.0239	0.9243	0.9002	0.7920	1
9	0.0321	0.4443	1.0000	0.9256	0.5726	0,312
10	0.0498	0.8364	1.0000	0.9074	0.4679	0,201
11	0.0675	0.9999	0.9571	0.8592	0.3948	0,148
12	0.0859	0.9993	0.8933	0.7967	0.3391	0,116
13	0.0998	0.9993	0.8560	0.7599	0.3058	0,100
14	0.1091	0.9993	0.8349	0.7390	0.2865	0,092
15	0.1138	0.9991	0.8251	0.7293	0.2775	0,088
16	0.1138	0.9991	0.8251	0.7293	0.2775	0,088
17	0.1091	0.9993	0.8349	0.7390	0.2865	0,092
18	0.0998	0.9993	0.8560	0.7599	0.3058	0,100
19	0.0859	0.9993	0.8933	0.7967	0.3391	0,116
20	0.0675	0.9999	0.9571	0.8592	0.3948	0,148
21	0.0498	0.8364	1.0000	0.9074	0.4679	0,201
22	0.0321	0.4443	1.0000	0.9256	0.5726	0,312
23	0.0100	-0.0239	0.9243	0.9002	0.7920	1
24	0.0254	0.7037	1.0000	0.9351	0.6276	0,394
25	0.0518	1.0000	0.9701	0.8834	0.4668	0,193
26	0.0837	0.9992	0.8905	0.8000	0.3614	0,119
27	0.1147	0.9992	0.8500	0.7564	0.3012	0,087
28	0.1444	0.9991	0.8308	0.7340	0.2635	0,069
29	0.1727	0.9994	0.8249	0.7247	0.2387	0,058
30	0.1995	0.9986	0.8276	0.7238	0.2218	0,050

The second column shows the values of the flange width $b_2[i]$ within optimization process with allowance for considering constraints. The third column contains indicators (15) of the fulfillment of the constraint (4). In all sections (except sections with the following numbers: 7, 8, 9, 10, 21, 22, 23, 24) they differ only by a small fraction of a percent from unity. In sections with numbers 7 and 23 we have $b_2[8] = 0.01m$ (i.e. in these sections, constraint (13) is fulfilled in the form of equality and indicators (15) are equal to $bb_0[8] = 1$ and $bb_0[23] = 1$. In sections with numbers 7, 9, 10, 21, 22, 24, indicators (16) of constraint (7) are equal to unity up to rounding. The remaining indicators (16) and (17) of strength constraints (9) and (10) are fulfilled in the form of inequalities (the sixth column and the seventh column). So, in each section, we revealed indicator which is quite close to unity in terms of the adopted set of constraints. This circumstance allows to consider resultant design (after corresponding optimization process with allowance for constraints for the value of the first natural frequency, strength constraints and structural constraints) as close, within the accepted errors, to the design of minimum material capacity (the second column of Table 2.

Table 3. Comparison of variants.

	Variants			
Number	1	2	3	4
V_0, m^3	**0.05181**	**0.030309**	**0.030874**	**0.030468**
%%	0	41.50	40.41	41.20
$\omega 1, \sec^{-1}$	**14.89**	13	**13.1103**	13

In this variant the objective function is equal to $V_0 = 0.030468\ m^3$.

A decrease in the value of the objective function is performed in comparison with the first variant. In the first and third variants, the constraint $\omega 1 = 13 \sec^{-1}$ is not reached, while the values of the objective function are greater than in the fourth variant, in which all constraints are fulfilled. In the second variant the objective function is less than in the fourth variant, but strength conditions are not fulfilled. A comparison of the variants confirms the feasibility of taking into account all the necessary constraints within optimization process (the fourth variant), and not after its completion (the third variant).

The solution closest to the design of minimal material capacity can be used in real design practice. We should note that normally it is impossible to formalize the full set of various constraints of the problem within the design of optimal systems. These are, for example, constraints dealing with technological requirements in the manufacture, transportation, installation, operation and disposal of an object, as well as many others.

An optimal design can perform various functions in real design practice. For example, a design of minimal material capacity can be considered as an idealized object. This function of such a design makes it possible to evaluate a real design solution by the criterion of its proximity to the limit (for example, by material capacity).

In addition, the optimal design can be used as a guideline for real design. Within this approach real design is considered as a phased process of moving away from an ideal object in order to fulfill the requirements (constraints) not considered in the optimal design.

In the distinctive paper we propose to use special criteria for assessment proximity of resultant design after optimization process (computing flange with of I-shape cross-section of rod) with allowance for stability constraints, constraints for the value of the first natural frequency and structural constraints.

ACKNOWLEDGEMENTS

The distinctive research work was carried out at the expense of the State program of the Russian Federation “Scientific and technological development of the Russian Federation” and the Program for Fundamental Research of State Academies of Science for 2013–2020, as part of the Plan for Fundamental Scientific Research of the Ministry of Construction and Housing and Communal Services of the Russian Federation and the Russian Academy of Architecture and Construction Sciences for 2020, within science topic “Research and development of fundamental theoretical foundations of the synthesis of optimal structures as methods for designing structures with predetermined properties”.

REFERENCES

1. **Lyakhovich L.S.** Osobye Svojstva Optimal'nyh Sistem i Osnovnye Napravlenija ih Realizacii v Metodah Rascheta Sooruzhenij [Special Properties of Optimal Systems and the Main Directions of Their Implementation in the Methods of Calculation of Structures]. Tomsk, Tomsk State University of Architecture and Construction, 2009, 372 pages (in Russian).
2. **Li D., Paradowska A., Uy B., Wang J., Khan M.** Residual stresses of box and I-shaped columns fabricated from S960 ultra-

high-strength steel. // Journal of Constructional Steel Research, 2020, Volume 166, article 105904.

3. **Xiao Y., Bie X.-M., Song X., Zhang J., Du G.** Performance of composite L-shaped CFST columns with inner I-shaped steel under axial compression. // Journal of Constructional Steel Research, 2020, Volume 170, article 106138.
4. **Ljahovich L.S, Malinovskij A.P.** Kriterij minimal'noj materialoemkosti pri usilenii sterzhnej dvutavrovogo poperechnogo sechenija i ogranichenijah na velichinu kriticheskoj sily ili pervoj sobstvennoj chastoty [Criterion of minimum material consumption with reinforcement of I-beam cross-section and restrictions on the value of the critical force or the first natural frequency]. // Vestnik TGASU, 2015, No. 5, pp. 41-50 (in Russian).
5. **Ljahovich L.S., Tuhfatullin B.A., Puteeva L.E., Grigor'ev A.I.** Ispol'zovanie metodov optimizacii v zadachah usilenija konstrukcij [Using optimization methods in problems of strengthening structures]. // Vestnik TGASU, 2015, No. 6, pp. 51-70 (in Russian).
6. **Ляхович Л.С., Тухфатуллин Б.А. Ljahovich L.S., Tuhfatullin B.A.** Proektirovanie sterzhnej postojannogo poperechnogo sechenija, minimal'noj materialoemkosti pri ogranichenijah po prochnosti na szhatie i na velichinu pervoj chastoty sobstvennyh kolebanij // «Aktual'nye problemy chislennogo modelirovanija zdanij, sooruzhenij i kompleksov». Tom 2. K 25-letiju Nauchno-issledovatel'skogo centra StaDiO [Design of rods of constant cross-section, minimum material consumption under constraints on compressive strength and on the value of the first frequency of natural vibrations]. // "Actual problems of numerical modeling of buildings, structures and complexes", Volume 2. To the 25th anniversary of the Research Center StaDyO. Moscow, ASV Publishing House, 2016, pp. 438-443 (in Russian).
7. **Lyakhovich L.S., Malinovsky A.P., Tukhfatullin B.A.** Criteria for Optimal Strengthening of Bar Flange with I-type Cross-section with Stability Constraints on the Value of the First Natural Frequency. // Procedia Engineering, 2016, Volume 153, pp. 427-433.
8. **Ljahovich L.S., Malinovskij A.P., Tuhfatullin B.A.** Kriterii optimal'nogo usilenija stenki sterzhnej dvutavrovogo poperechnogo sechenija pri ogranichenijah po ustojchivosti ili na velichinu pervoj sobstvennoj chastity [Criteria for the optimal reinforcement of the wall of the I-beam cross-section under constraints on stability or by the value of the first natural frequency]. // International Journal for Computational Civil and Structural Engineering, 2016, Volume 12, Issue 2, pp. 118-125 (in Russian).
9. **Ljahovich L.S., Akimov P.A., Tuhfatullin B.A.** Kriterii minimal'noj materialoemkosti sterzhnej prjamougol'nogo poperechnogo sechenija pri ogranichenijah po ustojchivosti ili na velichinu pervoj sobstvennoj chastoty [Criteria for the minimum material consumption of rods of rectangular cross-section with restrictions on stability or on the value of the first natural frequency]. // International Journal for Computational Civil and Structural Engineering, 2017, Volume 13, Issue 1, pp. 9-22 (in Russian).
10. **Ljahovich L.S., Akimov P.A., Tuhfatullin B.A.** O zadachah poiska minimuma i maksimuma v stroitel'noj mehanike [On the problems of finding the minimum and maximum in structural mechanics]. // International Journal for Computational Civil and Structural Engineering, 2017, Volume 13, Issue 2, pp. 103-124 (in Russian).
11. **Lyakhovich L.S., Tukhfatullin B.A., Akimov P.A.** About the solution of a structural class optimization problems. Part 1: Formulation of theoretical foundations problems of the solution procedure. // IOP Conf. Series: Materials Science and Engineering, 2018, Volume 456, 012005.
12. **Lyakhovich L.S., Tukhfatullin B.A., Akimov P.A.** The solution of structural class optimization problems. Part 2: Numerical

examples. IOP Conf. Series: Materials Science and Engineering, 2018, Volume 456, 012006.

13. **Lyakhovich L.S., Malinovsky A.P., Akimov P.A.** Using the Criterion of the Minimum Material Capacity of Rods Under Stability Restrictions for the Case of Multiple Critical Load. // International Journal for Computational Civil and Structural Engineering, 2019, Volume 15, Issue 1, pp. 78-89.
14. **Takezawa A., Yamamoto T., Zhang X., Yamakawa K., Nakano S., Kitamura M.** An objective function for the topology optimization of sound-absorbing materials. // Journal of Sound and Vibration, 2019, Volume 443, pp. 804-819.
15. Svod pravil SP 16.13330.2017 «Stal'nye konstrukcii» (aktualizirovannaja redakcija SNiP II-23-81*) [Code of rules SP 16.13330.2017 "Steel structures" (updated edition of SNiP II-23-81 *)]. Moscow, Minstroj Rossii, 2017, 140 pages (in Russian).
16. **Hedli Dzh.** Nelinejnoe i dinamicheskoe programmirovanie [Non-linear and dynamic programming]. Moscow, Mir, 1967, 507 pages (in Russian).
17. **Хог Э., Арора Я.** Hog Je., Arora Ja. Prikladnoe optimal'noe proektirovanie. Mehanicheskie sistemy i konstrukcii [Applied Optimal Design. Mechanical systems and structures]. Moscow, Mir, 1983, 479 pages (in Russian).

СПИСОК ЛИТЕРАТУРЫ

1. **Лахович Л.С.** Особые свойства оптимальных систем и основные направления их реализации в методах расчета сооружений. – Томск, ТГАСУ, 2009. – 372 с.
2. **Li D., Paradowska A., Uy B., Wang J., Khan M.** Residual stresses of box and I-shaped columns fabricated from S960 ultra-high-strength steel. // Journal of Constructional Steel Research, 2020, Volume 166, article 105904.
3. **Xiao Y., Bie X.-M., Song X., Zhang J., Du G.** Performance of composite L-shaped CFST columns with inner I-shaped steel under axial compression. // Journal of Constructional Steel Research, 2020, Volume 170, article 106138.
4. **Ляхович Л.С, Малиновский А.П.** Критерий минимальной материалоемкости при усилении стержней двутаврового поперечного сечения и ограничениях на величину критической силы или первой собственной частоты. // Вестник ТГАСУ, 2015, №5, с. 41–50.
5. **Ляхович Л.С., Тухфатуллин Б.А., Путеева Л.Е., Григорьев А.И.** Использование методов оптимизации в задачах усиления конструкций. // Вестник ТГАСУ, 2015, №6, с. 51-70.
6. **Ляхович Л.С., Тухфатуллин Б.А.** Проектирование стержней постоянного поперечного сечения, минимальной материалоемкости при ограничениях по прочности на сжатие и на величину первой частоты собственных колебаний // «Актуальные проблемы численного моделирования зданий, сооружений и комплексов». Том 2. К 25-летию Научно-исследовательского центра СтаДиО. – М.: АСВ, 2016, с. 438–443.
7. **Lyakhovich L.S., Malinovsky A.P., Tukhfatullin B.A.** Criteria for Optimal Strengthening of Bar Flange with I-type Cross-section with Stability Constraints on the Value of the First Natural Frequency. // Procedia Engineering, 2016, Volume 153, pp. 427-433.
8. **Ляхович Л.С., Малиновский А.П., Тухфатуллин Б.А.** Критерии оптимального усиления стенки стержней двутаврового поперечного сечения при ограничениях по устойчивости или на величину первой собственной частоты. // International Journal for Computational Civil and Structural Engineering, 2016, Volume 12, Issue 2, pp. 118-125.
9. **Ляхович Л.С., Акимов П.А., Тухфатуллин Б.А.** Критерии минимальной материалоемкости стержней прямоугольного поперечного сечения при ограничениях по устойчивости или на величину

первой собственной частоты. // International Journal for Computational Civil and Structural Engineering, 2017, Volume 13, Issue 1, pp. 9-22.
10. **Ляхович Л.С., Акимов П.А., Тухфатуллин Б.А.** О задачах поиска минимума и максимума в строительной механике. // International Journal for Computational Civil and Structural Engineering, 2017, Volume 13, Issue 2, pp. 103-124.
11. **Lyakhovich L.S., Tukhfatullin B.A., Akimov P.A.** About the solution of a structural class optimization problems. Part 1: Formulation of theoretical foundations problems of the solution procedure //IOP Conf. Series: Materials Science and Engineering. 456 (2018).
12. **Lyakhovich L.S., Tukhfatullin B.A., Akimov P.A.** About the solution of a structural class optimization problems. Part 1: Formulation of theoretical foundations problems of the solution procedure. // IOP Conf. Series: Materials Science and Engineering, 2018, Volume 456, 012005.
13. **Lyakhovich L.S., Tukhfatullin B.A., Akimov P.A.** The solution of structural class optimization problems. Part 2: Numerical examples. IOP Conf. Series: Materials Science and Engineering, 2018, Volume 456, 012006.
14. **Takezawa A., Yamamoto T., Zhang X., Yamakawa K., Nakano S., Kitamura M.** An objective function for the topology optimization of sound-absorbing materials. // Journal of Sound and Vibration, 2019, Volume 443, pp. 804-819.
15. Свод правил СП 16.13330.2017 «Стальные конструкции» (актуализированная редакция СНиП II-23-81*). – М.: Минстрой России, 2017. – 140 с.
16. **Хедли Дж.** Нелинейное и динамическое программирование. – М.: Мир, 1967. – 507 с.
17. **Хог Э., Арора Я.** Прикладное оптимальное проектирование. Механические системы и конструкции. – М.: Мир, 1983. – 479 с.

Ляхович Леонид Семенович, академик РААСН, профессор, доктор технических наук, профессор кафедры строительной механики, Томский государственный архитектурно-строительный университет; 634003, Россия, г. Томск, Соляная пл. 2;
E-mail: lls@tsuab.ru

Акимов Павел Алексеевич, академик РААСН, профессор, доктор технических наук; временно исполняющий обязанности ректора Национального исследовательского Московского государственного строительного университета; профессор Департамента архитектуры и строительства Российского университета дружбы народов; профессор кафедры строительной механики Томского государственного архитектурно-строительного университета; 107031, г. Москва, ул. Большая Дмитровка, д. 24, стр. 1;
тел. +7(495) 625-71-63; факс +7 (495) 650-27-31;
Email: akimov@raasn.ru, pavel.akimov@gmail.com.

Тухфатуллин Борис Ахатович, доцент, кандидат технических наук, доцент кафедры строительной механики, Томский государственный архитектурно-строительный университет; 634003, Россия, г. Томск, Соляная пл. 2; e-mail: bat9203@gmail.com.

Leonid S. Lyakhovich, Full Member of the Russian Academy of Architecture and Construction Sciences, Professor, DSc, Head of Department of Structural Mechanics, Tomsk State University of Architecture and Building; 634003, Russia, Tomsk, Solyanaya St., 2;
E-mail: lls@tsuab.ru

Pavel A. Akimov, Full Member of the Russian Academy of Architecture and Construction Sciences, Professor, Dr.Sc.; Acting Rector of National Research Moscow State University of Civil Engineering; Professor of Department of Architecture and Construction, Peoples' Friendship University of Russia; Professor of Department of Structural Mechanics, Tomsk State University of Architecture and Building; 24, Ul. Bolshaya Dmitrovka, 107031, Moscow, Russia; phone +7(495) 625-71-63;
Fax: +7 (495) 650-27-31;
E-mail: akimov@raasn.ru, pavel.akimov@gmail.com.

Boris A. Tukhfatullin, Associate Professor, Ph.D, Associate Professor of Department of Structural Mechanics, Tomsk State University of Architecture and Building; 634003, Russia, Tomsk, Solyanaya St., 2;
E-mail: bat9203@gmail.com.

DOI:10.22337/2587-9618-2020-16-2-83-93

INFLUENCE OF BUCKLING FORMS INTERACTION ON STIFFENED PLATE BEARING CAPACITY

Gaik A. Manuylov, Sergey B. Kosytsyn, Irina E. Grudtsyna
Russian University of Transport (MIIT), Moscow, RUSSIA

Abstract: The work is devoted to studying the influence of initial geometric imperfections on a value of the peak load for the compressed stiffened plate with the two-fold buckling load. The finite-element set MSC PATRAN – NASTRAN was used for solving the set tasks. When modelling the stiffened plate, flat four-unit elements were used. Geometric non-linearity was assumed for calculations. The plate material was regarded as perfectly elastic. Buckling forces of stiffened plate at the two-fold buckling load were calculated (simultaneous buckling failure on the form of the plate total bending and on the local form of wave formation in stiffened ribs). Equilibrium state curves, peak load decline curves depending on initial imperfection values and the bifurcation surface were plotted.

Key words stability, stiffened plate, bifurcation, initial geometric imperfections, buckling force

ВЛИЯНИЕ ВЗАИМОДЕЙСТВИЯ ФОРМ ВЫПУЧИВАНИЯ НА НЕСУЩУЮ СПОСОБНОСТЬ ПОДКРЕПЛЕННОЙ ПЛАСТИНЫ

Г.А. Мануйлов, С.Б. Косицын, И.Е. Грудцына
Российский университет транспорта (РУТ (МИИТ)), г. Москва, РОССИЯ

Аннотация: В работе исследовано влияния начальных геометрических несовершенств на величину максимальной нагрузки для сжатой подкрепленной пластины с двукратной критической нагрузкой. Для решения поставленных задач использовался конечноэлементный комплекс MSC PATRAN - NASTRAN. При моделировании подкрепленной пластины использованы плоские четырехузловые элементы. Расчеты выполнялись с учетом геометрической нелинейности. Материал пластины считался абсолютно упругим. Рассчитаны критические силы подкрепленной пластины при двукратной критической нагрузке (одновременная потеря устойчивости по форме общего изгиба пластины и по локальной форме волнообразования в подкрепляющих ребрах). Построены кривые равновесных состояний, кривые падения максимальных нагрузок в зависимости от величины начальных несовершенств, а также бифуркационная поверхность.

Ключевые слова: устойчивость, подкрепленная пластина, бифуркация, начальные геометрические несовершенства, критическая сила

1. INTRODUCTION

Stiffened plates are quite a widespread element of construction, machine-building, aviation and ship structures. Interaction of forms of buckling failure is an important factor at evaluation of post-critical equilibrium of thin-walled stiffened plates. Such interaction is manifested either in form of interinfluence of the plate total deflection as Eulerian rod and the local buckling failure of the lining (wave formation in the plate), or as interinfluence of the abovementioned total deflection and wave formation at buckling failure of compressed ribs. Especially interesting in buckling problems are stiffened plates with two-fold buckling loads corresponding to the simultaneous buckling failure both on the shape of total bending of the plate and on the form of local bending in form of wave formation of ribs for plates possessing open profile rib stiffeners; this interinfluence considerably decreases the buckling load A. Van Der Neut, M. Tvergaard, W. Fok, J. Rhodes, A. Walker, G. Hunt, M.T. Thompson, A.I. Manevich, et al. devoted their efforts to studying of the effect of forms interaction whereat bearing capacity of stiffened plates and shells would decline. In his doctor's thesis [19] A.I. Manevich described interaction effects of buckling failure forms for thin-walled stiffened structures using the non-linear stability approach. His results occurred to be of great interest: the wave formation of ribs decreased the buckling load of stiffened plates from 40% to 60%; this paper also demonstrates necessity to use the plate-like pattern of a rib. In this paper, the authors explored the phenomenon of influence of non-linear interinfluence of forms and initial geometrical imperfections on the buckling load. To plot equilibrium state lines in vicinity of the two-fold semi-symmetric critical point, conceptions of the modern bifurcation theory and catastrophe theory were used. Earlier, on the base of V.Tvergaard's solution for the wide integrally stiffened plate under compression, G. Hunt plotted a bifurcation surface for a homeoclinal point of hyperbolic umbilic bifurcation. This surface is determined with the three parameters (the load parameter, and two imperfections parameters, that is, relative amplitudes of buckling failure partial forms). The mentioned two-fold semi-symmetric critical point (homeoclinal point of bifurcation) is realized when the critical force for the general form of buckling failure as of Eulerian rod is near or coincident in its value to the buckling load of wave formation local point [2]. It is related to the development direction of the stiffened plate general deflection toward ribs. At such deflection, a deflecting moment is generated which additionally loads the plate (shell) and unloads the ribs. However, if the general deflection develops in opposite direction, ribs under compression will be additionally loaded, while the plate (shell), on the contrary, will be unloaded in terms of compression. In the case of total or near-coincidence of buckling loads of the buckling and wave formation general form in the ribs, the near-critical equilibriums shall be described by another semi-symmetric two-fold bifurcation point, that is, by the anticlinal one [2] corresponding to the elliptical umbilic catastrophe. In the paper [2] G. Hunt, while analyzing the paper [1], pointed out the possibility of occurring of the bifurcation anticlinal point, if the general deflection causes additional compression of ribs. We note here that studying of the stiffened plate behaviour near an unstable two-fold bifurcation point was dictated by the consideration that it was there where the ultimate sensitivity to initial imperfections was observed for majority of elastic systems.

2. PROBLEM FORMULATION

The stability problem for the stiffened plate was solved by the finite elements' method in geometrically non-linear formulation. The plate had the following geometric parameters:

- Plate length: 86 cm,
- Plate width: 36 cm,
- $\delta = 0.155$ cm, $e = 0.342$ cm,
- $J = 3.136$ cm^4,
- $b_p = 0.1$ cm, $h_p = 1.2$ cm,

where δ – plate thickness, e – position of the cross section main central axis, J – moment of inertia in respect to the main central axis,
b_p – rib thickness, h_p – rib height.
The accepted boundary conditions: hinge support along short sides, with free longitudinal edges. The stiffened plate cross section is shown in figure 1. The finite-element model is built within the MSC PATRAN – NASTRAN calculation complex, with use of finite elements of shell type (4002 elements) (figure 2). The material was regarded perfectly elastic ($E=2\cdot10^6$ kg/cm^2, $\mu = 0.3$).
The compressing load (four forces) has been applied in points of intersection of ribs symmetry axes and the cross section main central axis.

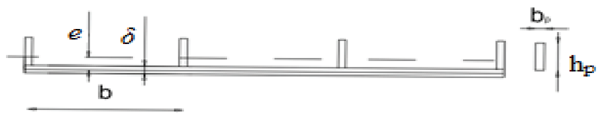

Figure 1. The plate cross section.

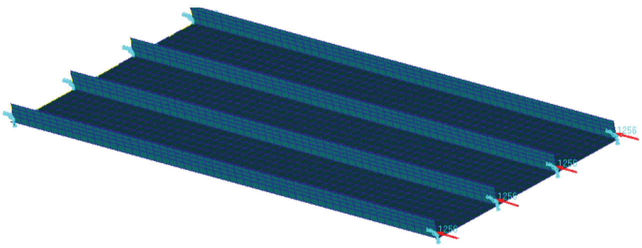

Figure 2. Finite-element model.

3. STUDYING OF POST-CRITICAL EQUILIBRIUM OF A STIFFENED PLATE WITH TWO-FOLD BUCKLING LOAD

This paper is devoted to studying of the problem of interaction of buckling failure forms between the shape of the plate general bending and the local shape of ribs wave formation. In practice, such a situation can occur, e.g., in bridges with continuous carriageways in form of a compressed stiffened plate. The linear computation of stability showed that the buckling load corresponding to the shape of plate buckling in form of Eulerian rod ($P_{эл}$ = 7708 kg) is sufficiently close to the buckling load corresponding to the form of wave formation of ribs ($P_{в.р.}$ = 7818 kg). The under-critical and initial post-critical equilibrium was studied in the geometrically non-linear formulation; the following results were obtained:

- as the compression load increases, the plate total deflection would develop downwards (i.e. in such a way that the ribs occur on the plate concave side and would receive additional compression).
- buckling failure occurs at the maximum buckling load Pcr = 6797 kg in the wave formation symmetric bifurcation point in the two middle ribs (the point of sharp inflection to curves of general deflection development. This load is 11.81% less than the buckling load obtained from the linear calculation);
- upon passing of the peak value, deflections will rise at the lowering load (figure 3). The secondary bifurcation (wave formation in the plate extreme ribs) will occur at the second buckling load Pbif. = 5880 kg.

Figure 4 shows the deformed state of a stiffened plate. It is obvious that the increasing deflection makes the bending moment bigger in the middle part, and we see not only the developing wave formation in the ribs but also the forced wave formation of the plate itself, which provokes considerable decrease of the bending rigidity.

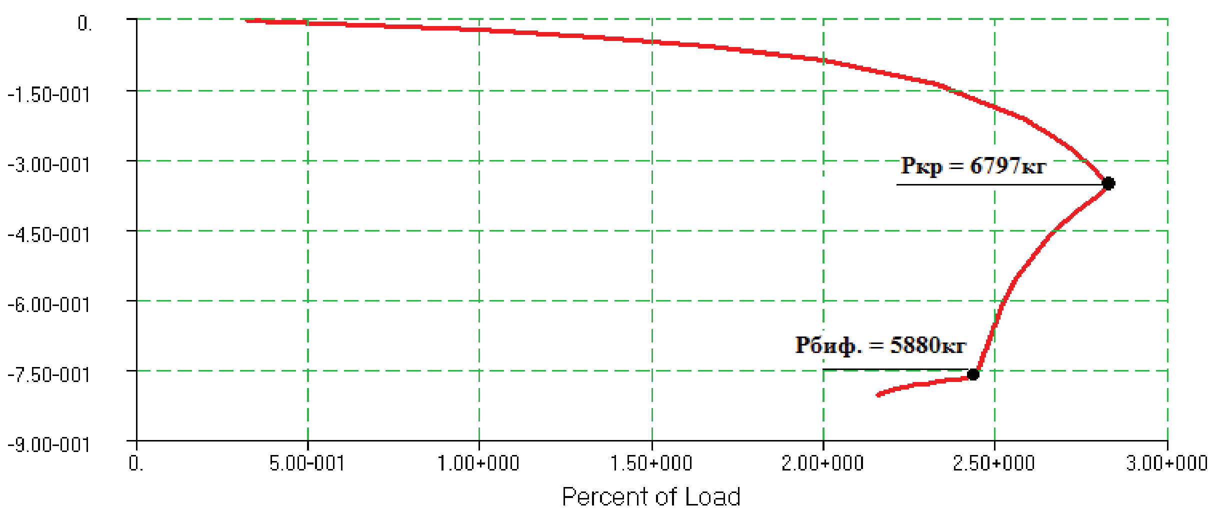

Figure 3. Graph of dependency “deflections vs compressing loads”.

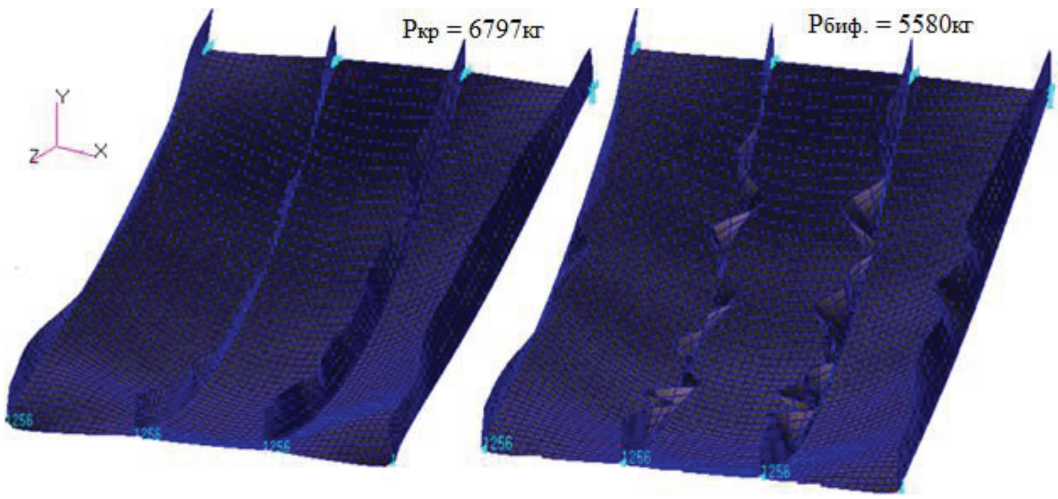

Figure 4. Deformable state of stiffened plate δ = 0.155 cm thick.

4. TWO-FOLD BIFURCATION POINT

The semi-symmetric two-fold bifurcation point is a special critical point. At an odd number of waves, the symmetry of post-bifurcation paths will remain for wave formation shape of ribs only.

Initial post-bifurcation paths (there may be one or three of them) are plotted in the three-dimensional space on two coordinates q_1, q_2, and load parameter λ.

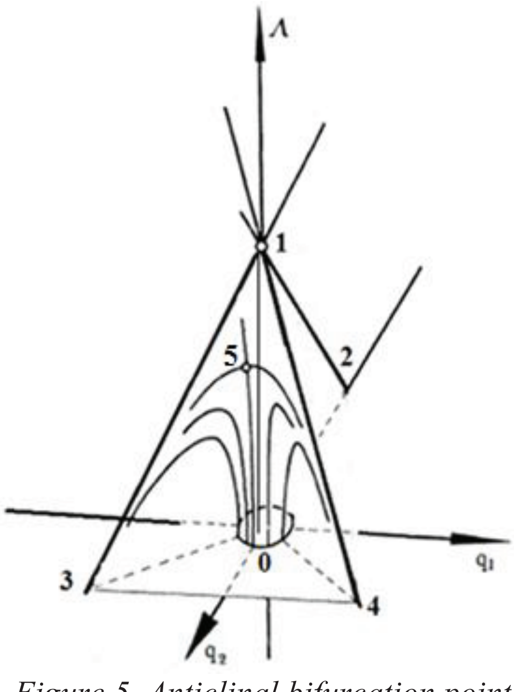

Figure 5. Anticlinal bifurcation point

In figure 5 we use the following notation:

q_1 – coordinate corresponding to relative amplitudes of wave formation in ribs;

q_2 – coordinate corresponding to relative amplitudes of the plate buckling as a Eulerian rod;

λ – load parameter ($\lambda = P - P_{cr}$)

Point 1 – semi-symmetric two-fold bifurcation point;

Right line 0 – 1 describes the pure compression pre-critical equilibrium;

Right line 1 – 2 is the line of incoherent equilibriums corresponding to the relative amplitude on the form of the stiffened plate buckling a Eulerian rod;

Right lines 1– 3 and 1– 4 are the lines coherent equilibriums coordinates whereof depend both on Eulerian deflection and on amplitude of wave formation in ribs [2];

Consequently, at the two-fold buckling load, the ribs (or plate) buckling failure cannot arise in form of a separate (partial) buckling form (i.e. wave formation at the zero general deflection).

Point 5 is the point of symmetric unstable bifurcation on the Eulerian general deflection curve which occurs at intersection of the “triangle” plane of coherent equilibriums 1 – 3 – 4 by this curve. This point corresponds to the bifurcation point at the peak load $P_{cr} = 6797$ kg (figure 3).

The catastrophe germ of the elliptic umbilic (the first two terms in expression (1) is generated from uniform cubes for two variables with taking into account the symmetry on the first coordinate and absence of symmetry on the second one. In total, the cubic potential for umbilic catastrophes can be presented as follows:

$$V(q_1, q_2, \varepsilon_j) = \frac{1}{6}V^{\text{кр}}_{222}q_2^3 + \frac{1}{2}V^{\text{кр}}_{112}q_1^2 q_2 + \frac{1}{2}\lambda\left(V^{\text{кр}}_{11\lambda}q_1^2 + V^{\text{кр}}_{22\lambda}q_2^2\right) + V_1^{1\text{кр}}\varepsilon_1 q_1 + V_2^{2\text{кр}}\varepsilon_2 q_2; \quad (1)$$

The lower indexes designate differentiation on appropriate coordinates and on the load parameters. All derivatives are calculated in the bifurcation point (the upper index “кр”).

For an ideal system, at $\varepsilon_1 = \varepsilon_2 = 0$, equilibrium equations are obtained by setting equal to zero of derivatives of potential (1) on each coordinate:

$$V^{\text{кр}}_{112}q_1 q_2 + \lambda V^{\text{кр}}_{11\lambda}q_1 = 0; \quad (2)$$

$$\frac{1}{2}V^{\text{кр}}{}_{222}q_2^2 + \frac{1}{2}V^{\text{кр}}{}_{112}q_1^2 + \lambda V^{\text{кр}}_{22\lambda}q_2 = 0 \quad (3)$$

Let’s show that initial post-bifurcation paths of equilibriums are straight lines.

Equilibrium equations (2), (3) may be solved in three variants:

- $q_1 = q_2 = 0$ – initial equilibrium of a non-bent stiffened plate;
- the solution at $q_1 = 0$, $q_2 \neq 0$ corresponds to the general bending of the plate as a Eulerian rod. Then, from the equilibrium equation (3), taking $q_1=0$, we obtain the equation of non-coherent post-bifurcation straight line of general deflection 1 – 2 (figure 5):

$$q_2 = \frac{-2\lambda V^{\text{кр}}_{22\lambda}}{V^{\text{кр}}{}_{222}} \quad \text{or} \quad \frac{\lambda}{q_2} = \frac{V^{\text{кр}}{}_{222}}{2V^{\text{кр}}_{22\lambda}}. \quad (4)$$

- $q_2 \neq 0$, $q_1 \neq 0$. Then, expressing λ from Equation (2):

$$\lambda = \frac{-V^{\text{кр}}_{112}q_2}{V^{\text{кр}}_{11\lambda}}, \quad (5)$$

and substituting it into Equation (3), we obtain:

$$\frac{1}{2}V^{\text{кр}}{}_{222}q_2^2 + \frac{1}{2}V^{\text{кр}}{}_{112} - \frac{V^{\text{кр}}_{112}V^{\text{кр}}_{22\lambda}{q_2}^2}{V^{\text{кр}}_{11\lambda}} = 0 \quad (6)$$

$$\frac{q_1}{q_2} = \pm\left(\frac{2V^{\text{кр}}_{22\lambda}}{V^{\text{кр}}_{11\lambda}} - \frac{V^{\text{кр}}{}_{222}}{V^{\text{кр}}{}_{112}}\right)^{\frac{1}{2}}. \quad (7)$$

Thus, it is demonstrated that all post-bifurcation equilibrium paths are straight lines. Earlier, similar computations for the homeoclinal bifurcation point were presented in the authors’ paper [16], when analyzing interaction of wave formation shape in the plate and general deflection of the plate as a Eulerian rod.

Ratio signs of derivatives under the root sign in Formula (7) are important for determining the type of bifurcation umbilic point. The first ration is always positive here. If ratios $\frac{V^{\text{кр}}_{22\lambda}}{V^{\text{кр}}_{11\lambda}}$ and $\frac{2V^{\text{кр}}{}_{222}}{V^{\text{кр}}{}_{112}}$ possess opposite signs, straight lines of coherent equilibriums 1-3 and 1-4 “fall” in the direction opposite to that of “falling” of the non-coherent post-bifurcation straight line of general deflection 1 - 2, and we obtain the anticlinal bifurcation point corresponding to the elliptic umbilic catastrophe. For a stiffened plate, such two-fold bifurcation point may be realized only when deflection of this plate develops in such a way that ribs and additionally loaded with compression stresses from the bending moment arisen.

5. STUDYING OF INFLUENCE OF INITIAL GEOMETRIC IMPERFECTIONS ON BUCKLING LOAD

To explore the influence of initial imperfections, the authors used eigenforms of buckling failure obtained by means of liner computations. Geometric imperfections were set on the forms of:

- initial wave formation in ribs (wave formation of two extreme ribs, two middle ribs, simultaneous wave formation in four ribs), ε_1;
- buckling of the plate as a Eulerian rod, ε_2;
- imperfection on two forms $\varepsilon_1+\varepsilon_2$ and $\sqrt{3}\varepsilon_1+\varepsilon_2$.

Relative amplitudes of imperfections were set in fractions of the plate thickness (0.1δ,0.2δ, 0.5δ,1δ,2δ). It is obvious that the provoking factor of wave formation in ribs was the bending moment developing under action of compressive forces in the stiffened plate middle part. Upon excluding the initial deflection and using only the shape of wave formation of ribs as the initial imperfection, we obtained the following results:

- buckling failure occurred in the limit point of equilibrium curves of wave formation in ribs;
- initial imperfection in form of wave formation in extreme ribs only provoked local buckling of the plate, and thereafter the secondary bifurcation of wave formation in middle ribs took place; the same effect was observed at setting of imperfections for two middle ribs only;
- it was found that wave formation in middle ribs only decreased bearing capacity of a stiffened plate to a higher extent, as compared to influence of the similar imperfections in extreme ribs.

Table 1 presents values of buckling loads of imperfect plates.

Table 1. Values of buckling loads for a plate with imperfection on the shape of wave formation of ribs

Imperfection value on the shape of wave formation of ribs (wave formation of two middle ribs)					
0	0.1δ	0.2δ	0.5δ	1 δ	2 δ
Buckling load, kg					
6797	6327	6009	5469	4874	4656
Imperfection value on the shape of wave formation of ribs (wave formation of two extreme ribs)					
0	0.1δ	0.2δ	0.5δ	1δ	2δ
Buckling load, kg					
6797	6644	6508	6238	5812	5130

The decrease of the stiffened plate-buckling load from imperfection on the shape of wave formation of ribs (wave formation of two extreme ribs) was 24.52%, and that from imperfection of wave formation of two middle ribs was 31.5%. In figure 6 we can see curves of decrease of critical values for a plate with imperfection on the shape of wave formation of ribs.

The next step in the research is aimed at studying of curves of equilibrium states of imperfect stiffened plates and at plotting of the bifurcation surface.

In figure 7, we can see curves of equilibrium states of the plate with various imperfection amplitudes on buckling form as Eulerian rod.

The initial deflection direction was chosen in such a way that the ribs would occur in the compressed zone (with convex section downward). Buckling failure occurred in the limit point of the curve of equilibrium on deflections.

Depending on the initial imperfection amplitude, bifurcation of wave formation of ribs arose either later than the limit point (in case of small amplitudes 0.1δ, 0.2δ, 05δ), or in the limit point (when imperfection amplitude is equal to 1δ), or preceded to it, as in the case of setting of the imperfection with amplitude 2δ (inflection on the curve of equilibrium states, figure 7).

The decrease of the buckling load in case of setting the initial imperfection on the general deflection shape and amplitude 2δ was equal to 32.78%. Turning to the bifurcation diagram (figure 5) one can state that all post-bifurcation paths of imperfect equilibriums achieve their peak loads in limit points; further on, they become instable and asymptotically approach coherent equilibriums 1-2 straight line.

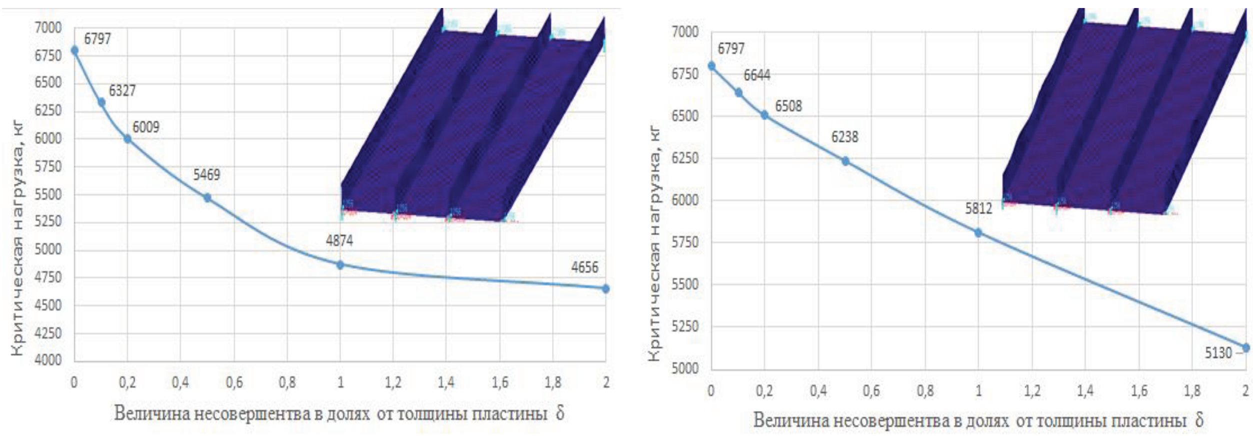

Figure 6. Curves of decrease of stiffened plate buckling loads from imperfection of wave formation of ribs (0.1δ, 0.2δ, 0.5δ, 1δ, 2δ).

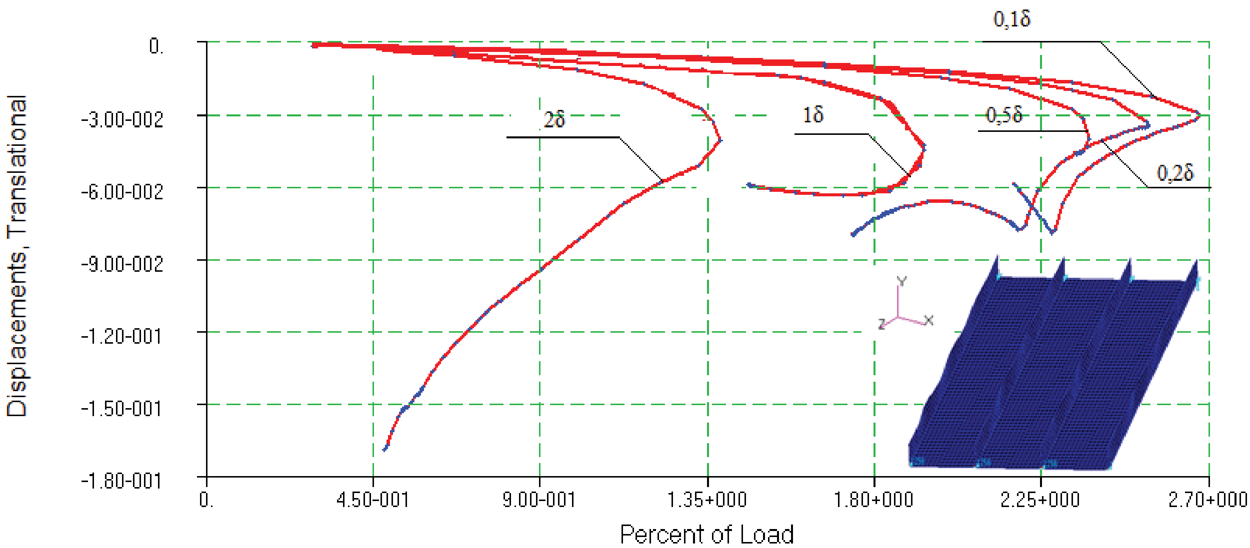

Figure 7. Curves of equilibrium states of stiffened plate with imperfection on buckling form as Eulerian rod (0.1δ, 0.2δ, 0.5δ, 1δ, 2δ).

In figure 8 we can see curves equilibrium states of a stiffened plate with imperfection on the form of wave formation in ribs (simultaneous wave formation in four ribs).

Analysis of results showed that buckling failure occurs in limit points of the curves of ribs wave formation. The maximum decrease of the buckling load from imperfection on this shape with amplitude 2δ was equal to 51%. All post-bifurcation paths of imperfect equilibriums achieved their limit points and further on they asymptotically approached straight lines of coherent equilibriums 1-3 and 1-4 (figure 5).

Basing on the obtained results, the bifurcation surface "front part" was plotted close in the shape to a relevant part of the elliptical umbilic bifurcation surface demonstrated in the monograph by B. Gilmour, page 277 [15]. Table 2 presents values of buckling loads for stiffened plates with various types and amplitudes of initial imperfections.

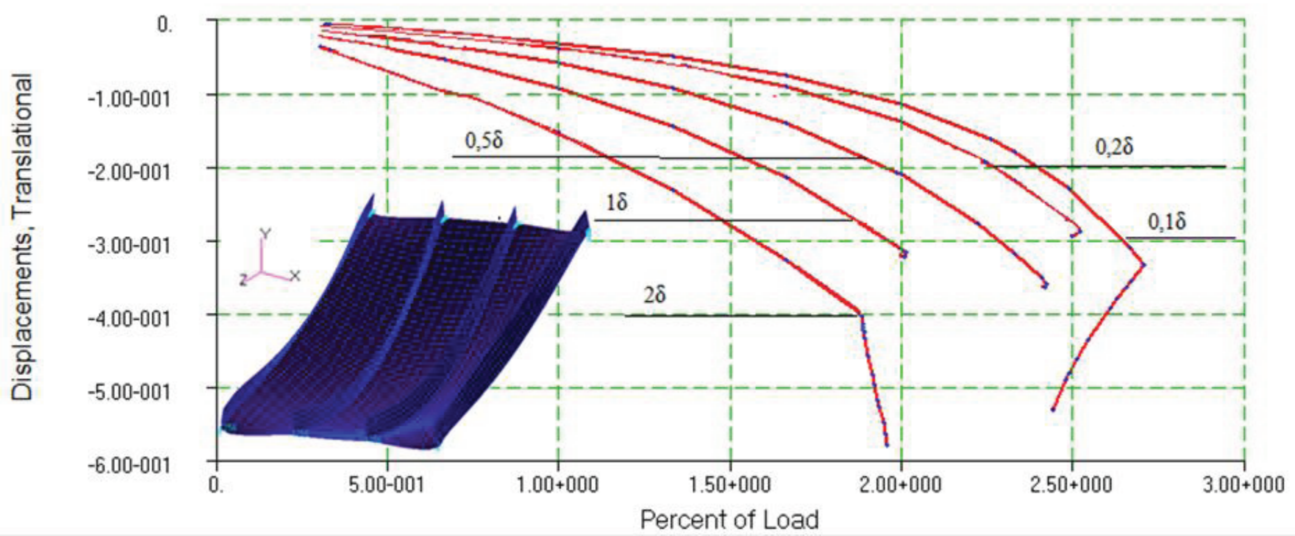

Figure 8. Curves of equilibrium states of stiffened plate with imperfection on the form of simultaneous wave formation in four ribs (amplitudes 0.1δ, 0.2δ, 0.5δ, 1δ, 2δ).

Table 2. Data for plotting of bifurcation surface

	Pcr, kg										
ε_1 / ε_2	0	0.1δ	√3*0.1δ	0.2δ	√3*0.2δ	0.5δ	√3*0.5δ	1δ	√3*1δ	2δ	√3*2δ
0	6797	6421	-	6096	-	5660	-	4640	-	3329	-
0.1δ	6495	5954	5934	-	-	5559	-	-	-	-	-
0.2δ	6440	-	-	5720	5616	-	-	4454	-	-	-
0.5δ	6317	5359	-	-	-	5072	4428	-	-	3027	-
1δ	4842	-	-	4814	-	-	-	3897	3304	-	-
2δ	4569	-	-	-	-	3972	-	-	-	2557	2128

6. CONCLUSIONS

It is demonstrated that the peak decrease of the buckling load of a stiffened plate was recorded at setting of the joint imperfection on two forms $\sqrt{3}\varepsilon_1+\varepsilon_2$ with amplitude 2δ + √3*2δ and was equal to 68.7%. Setting of the joint imperfection on two forms $\varepsilon_1+\varepsilon_2$ with amplitude 2δ decreased the bearing capacity by 62%. The obtained results of the study of initial imperfections influence confirm D. Ho's theorems ([14], 1974), according whereto, for two-fold bifurcation points with cubic potential, the buckling load peak decrease is caused by imperfections possessing the shape of the most steeply falling post-bifurcation equilibriums. Within this task, most steeply falling are straight lines of coherent equilibriums 1 – 2 and 1 – 3 (figure 5).

Let's note also that our results confirm certain conclusions of A.I. Manevich [12] about strong response of buckling loads to initial imperfections in the plate ribs. It was found that the provoking factor of wave formation in ribs was additional compression generated by the bending moment in the stiffened plate middle part, due to development of general deflection in a certain direction.

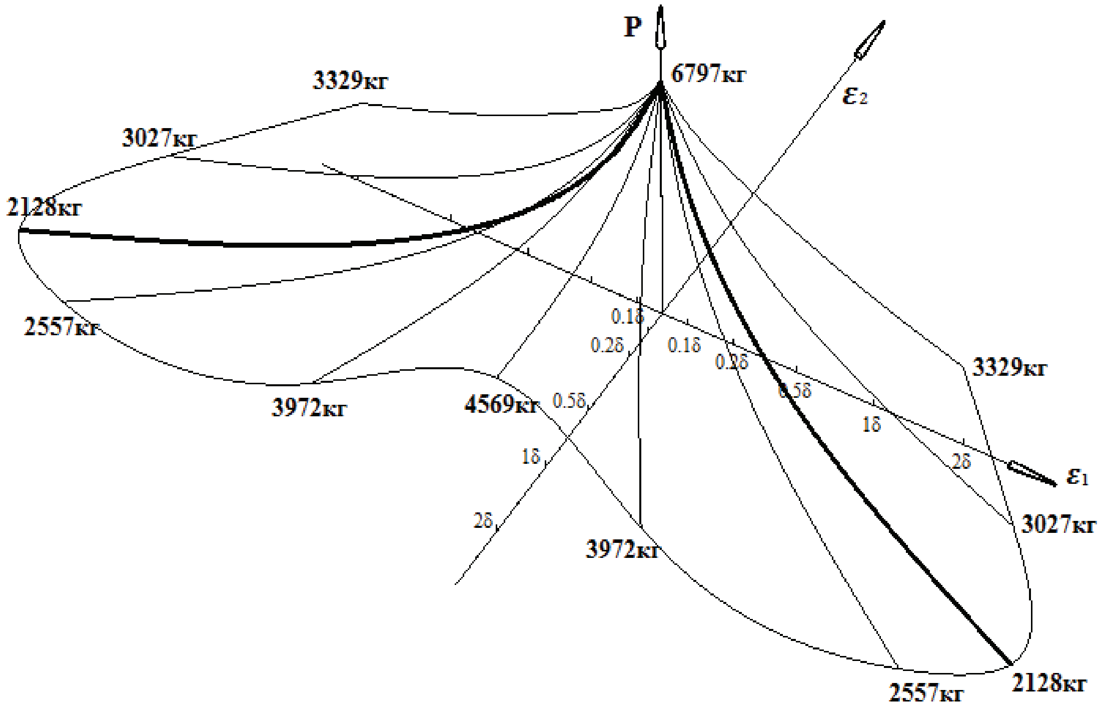

Figure 9. *Bifurcation surface.*

REFERENCES

1. **Fok W.C., Rhodes J., Walker A.C.** Local buckling of outstands in stiffened plates. // Aeronaut Q 27, 1976, pp. 277-291.
2. **Hunt G.W.** Imperfections and near-coincidence for semi-symmetric bifurcations. // New York in Conference on Bifurcation Theory and Applications in Scientific Disciplines Ann. N.Y. Academy of Science 316, 1977, pp. 572-589.
3. **Hunt G.W.** An algorithm for the nonlinear analysis of compound bifurcation. London Phil. Trans. R. Soc. Lond. A 1981, 1981, 300 pages.
4. **Hunt G.W.** Imperfection-sensitivity of semi-symmetric branching (Proc. R. Soc. Lond. A 1977, 1977, Volume 357, pp. 193-211.
5. **Koiter W.T., Pignataro M.A.** General Theory for the interaction between Local and Overall Buckling of Stiffened Panels. Delft WTHD Report 83, 1976, pp. 179-222.
6. **Maquoi R., Massonnet C.** Interaction between local plate buckling and overall buckling in thin-walled compression members. // New York Harvard University Theories and experiments in Proceedings of the IUTAM International Symposium on Buckling of Structures, 1976, pp. 365-382.
7. **Roorda J.** The buckling behavior of imperfect structural systems. London Department of Civil Engineering, University College, 1965, pp. 267-280.
8. **Thompson J.M.T., Tan J.K.Y., Lim K.C.** On the Topological Classification of Post-buckling Phenomena (Journal of Structural Mechanics Volume, 1978, Volume 64, pp. 383-414.
9. **Thompson J.M.T., Gaspar Z.** A buckling model for the set of umbilic catastrophes. // Mathematical Proceedings of the Cambridge Philosophical Society, 1977, Volume 82, Issue 03, pp. 497-507.
10. **Tvergaard V** Imperfection sensitivity of a wide integrally stiffened panel under compression. // Int. J. Solids Sructures, 1973, Volume 9, pp. 177-192.
11. **Van Der Neut A.** The interaction of local buckling and column failure of imperfect thin-walled compression members. Delft

Technological University Report VTH 149, 1968, pp. 391-398.
12. **Van Der Neut A.** Mode interaction with a stiffened panel. // Harvard Proc. IUTAM Symp., Buckling of structures, 1974, pp. 117-132.
13. **Van Der Neut A., Majer J.** The interaction of local buckling and column failure of imperfect thin-walled compression members. Delf University of Technology, Department of Aeronautic engineering Report VTH - 160, 1970, pp. 6-18.
14. **Ho D.** Buckling load of non-linear systems with multiple eigenvalues. // Int. J. Solids Structures, Pergamon Press. Printed in Gt. Britain, 1974, pp. 1315-1330.
15. **Gilmour B.** Prikladnaja teorija katastrof [Applicable theory of catastrophes]. Volume 1. Moscow, MIR, 1984, pp. 268-277 (in Russian)
16. **Manuylov G.A., Kositsyn S.B., Grudtsyna I.E.** Chislennyj analiz kriticheskogo ravnovesija gibkoj podkreplennoj plastiny s uchetom vlijanija nachal'nyh geometricheskih nesovershenstv [Numerical Analysis Critical Equilibrium Of Flexible Supported Plate With Allowance For Influence Initial Geometrical Imperfections]. // Structural Mechanics And Analysis Of Constructions, 2020, No. 1, pp. 30-36 (in Russian).
17. **Manevich A.I.** K teorii svjazannoj poteri ustojchivosti podkreplen-nyh tonkostennyh konstrukcij [On the theory of coupled loss of stability in stiffened thin-walled structures]. // Applicable mathematics and mechanics, 1982, No. 2, pp. 337-345 (in Russian).
18. **Manevich A.I.** Vzaimodejstvie form poteri ustojchivosti szhatoj podkreplennoj paneli [Interaction of forms of buckling failure of compressed stiffened panel]. // Structural Mechanics And Analysis Of Constructions, 1981, No. 5, pp. 24-29 (in Russian).
19. **Manevich A.I.** Nelinejnaja teorija ustojchivosti podkreplennyh plastin i obolochek s uchetom vzaimodejstvija form vypuchivanija [Nonlinear theory of stability of stiffened plates and shells, with taking into account of buckling forms interaction]. Dissertation abstract for procuring of the academic degree of Doctor of Engineering, Leningrad, 1988, 33 pages (in Russian).
20. **Thompson J.M.T.** Neustojchivosti i katastrofy v nauke i tehnike [Buckling and catastrophes in science and engineering]. Moscow, MIR, 1985, pp. 21-37 (in Russian).

СПИСОК ЛИТЕРАТУРЫ

1. **Fok W.C., Rhodes J., Walker A.C.** Local buckling of outstands in stiffened plates. // Aeronaut Q 27, 1976, pp. 277-291.
2. **Hunt G.W.** Imperfections and near-coincidence for semi-symmetric bifurcations. // New York in Conference on Bifurcation Theory and Applications in Scientific Disciplines Ann. N.Y. Academy of Science 316, 1977, pp. 572-589.
3. **Hunt G.W.** An algorithm for the nonlinear analysis of compound bifurcation. London Phil. Trans. R. Soc. Lond. A 1981, 1981, 300 pages.
4. **Hunt G.W.** Imperfection-sensitivity of semi-symmetric branching (Proc. R. Soc. Lond. A 1977, 1977, Volume 357, pp. 193-211.
5. **Koiter W.T., Pignataro M.A.** General Theory for the interaction between Local and Overall Buckling of Stiffened Panels. Delft WTHD Report 83, 1976, pp. 179-222.
6. **Maquoi R., Massonnet C.** Interaction between local plate buckling and overall buckling in thin-walled compression members. // New York Harvard University Theories and experiments in Proceedings of the IUTAM International Symposium on Buckling of Structures, 1976, pp. 365-382.
7. **Roorda J.** The buckling behavior of imperfect structural systems. London Department of Civil Engineering, University College, 1965, pp. 267-280.
8. **Thompson J.M.T., Tan J.K.Y., Lim K.C.** On the Topological Classification of Post-buckling Phenomena (Journal of Structural Mechanics Volume, 1978, Volume 64, pp. 383-414.

9. **Thompson J.M.T., Gaspar Z.** A buckling model for the set of umbilic catastrophes. // Mathematical Proceedings of the Cambridge Philosophical Society, 1977, Volume 82, Issue 03, pp. 497-507.
10. **Tvergaard V** Imperfection sensitivity of a wide integrally stiffened panel under compression. // Int. J. Solids Sructures, 1973, Volume 9, pp. 177-192.
11. **Van Der Neut A.** The interaction of local buckling and column failure of imperfect thin-walled compression members. Delft Technological University Report VTH 149, 1968, pp. 391-398.
12. **Van Der Neut A.** Mode interaction with a stiffened panel. // Harvard Proc. IUTAM Symp., Buckling of structures, 1974, pp. 117-132.
13. **Van Der Neut A., Majer J.** The interaction of local buckling and column failure of imperfect thin-walled compression members. Delf University of Technology, Department of Aeronautic engineering Report VTH - 160, 1970, pp. 6-18.
14. **Ho D.** Buckling load of non-linear systems with multiple eigenvalues. // Int. J. Solids Structures, Pergamon Press. Printed in Gt. Britain, 1974, pp. 1315-1330.
15. **Гилмор Р.** Прикладная теория катастроф. Том 1. – М.: Мир, 1984, с. 268-277.
16. **Мануйлов Г.А., Косицын С.Б., Грудцына И.Е.** Численный анализ критического равновесия гибкой подкрепленной пластины с учетом влияния начальных геометрических несовершенств. // Строительная механика и расчет сооружений, 2020, №1, с. 30-36.
17. **Маневич А.И.** К теории связанной потери устойчивости подкрепленных тонкостенных конструкций. // Прикладная математика и механика, 1982, №2, с. 337-345.
18. **Маневич А.И.** Взаимодействие форм потери устойчивости сжатой подкрепленной панели. // Строительная механика и расчет сооружений, 1981, №5, с. 24-29.
19. **Маневич А.И.** Нелинейная теория устойчивости подкрепленных пластин и оболочек с учетом взаимодействия форм выпучивания. Автореферат диссертации на соискание ученой степени доктора технических наук по специальности 01.02.04 – «Механика деформируемого твердого тела». – Л.: Ленинградский политехнический институт имени М.И. Калинина, 1988. – 33 с.
20. **Томпсон Дж.М.Т.** Неустойчивости и катастрофы в науке и технике. – М.: Мир, 1985, с. 21-37.

Gaik A. Manuylov, Ph.D.; Associate Professor, Department of Structural Mechanics, Moscow State University of Railway Engineering (MIIT); 127994, Russia, Moscow, 9b9 Obrazcova Street; phone/fax +7(499)972-49-81.

Sergey B. Kosytsyn, Advisor of the Russian Academy of Architecture and Construction Sciences (RAACS), Professor, Dr.Sc.; Head of Department of Theoretical Mechanics, Russian University of Transport (MIIT); 9b9, Obrazcova Street, Moscow, 127994, Russia;
phone/fax: +7(499) 978-16-73;
E-mail: kositsyn-s@yandex.ru, kositsyn-s@mail.ru.

Irina E. Grudtsyna, PhD student of Department of Theoretical Mechanics, Russian University of Transport (MIIT); 9b9, Obrazcova Street, Moscow, 127994, Russia;
Phone/fax: +7(915) 351-95-09;
E-mail: Grudtsyna_ira90@mail.ru.

Мануйлов Гайк Александрович, кандидат технических наук, доцент, доцент кафедры «Строительная механика» Российского Университета Транспорта (РУТ (МИИТ)); 127994, г. Москва, ул. Образцова, 9;
тел./факс +7(499) 972-49-81.

Косицын Сергей Борисович, доктор технических наук, профессор, заведующий кафедрой «Теоретическая механика» Российского Университета Транспорта (РУТ (МИИТ)); 127994, Россия, г. Москва, ул. Образцова, 9;
тел./факс +7(499) 978-16-73;
E-mail: kositsyn-s@yandex.ru, kositsyn-s@mail.ru.

Грудцына Ирина Евгеньевна, ассистент кафедры «Теоретическая механика» Российского Университета Транспорта (РУТ (МИИТ)); 127994, Россия, г. Москва, ул. Образцова, 15; тел./факс +7(915) 351-95-09;
E-mail: Grudtsyna_ira90@mail.ru.

DOI:10.22337/2587-9618-2020-16-2-94-100

ANALYSIS OF RHEOLOGICAL MODELS OF PROCESS OF SELF-FORMING OF GLUED WOODEN

Vladislav S. Ponomarev, Galina G. Kashevarova
[1]Perm National Research Polytechnic Universities, Perm, RUSSIA

Abstract: The article considers a promising technology for self-shaping glued wooden elements of curved forms. This method is based on rheological processes occurring in wood, such as dehumidification and swelling of wood and its anisotropic properties. To predict the final curved shape of the wooden structure, the authors analyzed existing rheological models of wood and concluded that the rheological model proposed by European researchers includes the most complete list of factors that affect the process of deformation of wood: elastic and plastic deformation, drying and swelling of wood, deformation of viscous-elastic creep and mechanical sorption deformation. Based on the results of experimental studies and numerical modeling of the change in the curvature of glued wooden elements, which were made by European researchers, it was found that the proposed rheological model of wood needs to be clarified, namely, the correction of hygro-expansion coefficients depending on the moisture content of wood. A further direction of the authors' research will be aimed at conducting model experiments to determine the hygro-expansion coefficients of different grades of wood depending on the thickness of the wooden elements and the orientation of the layers in the glued structure.

Keywords: method of self-shaping of glued wooden structures, rheological model, deformation.

АНАЛИЗ РЕОЛОГИЧЕСКИХ МОДЕЛЕЙ ПРОЦЕССА САМО-ФОРМООБРАЗОВАНИЯ КЛЕЁНЫХ ДЕРЕВЯННЫХ КОНСТРУКЦИЙ

В.С. Пономарев, Г.Г. Кашеварова
Пермский национальный исследовательский политехнический университет, г. Пермь, РОССИЯ

Аннотация: В статье рассмотрена перспективная технология само-формообразования клеёных деревянных элементов конструкций изогнутой формы. Данный метод основан на реологических процессах, происходящих в древесине, таких как деформации усушки и набухания древесины и ее анизотропных свойствах. Для прогнозирования конечной изогнутой формы деревянной конструкции, авторы проанализировали существующие реологические модели древесины и пришли к выводу о том, что в настоящее время реологическая модель, предложенная Европейскими исследователями, включает в себя наиболее полный перечень факторов, которые влияют на процесс деформации древесины: упругая и пластическая деформация, усушка и набухание древесины, деформация вязко-упругой ползучести и механо-сорбционная деформация. На основании результатов экспериментальных исследований и численного моделирования изменения кривизны клеёных деревянных элементов, которые были выполнены Европейскими исследователями, было установлено, что предложенная реологическая модель древесины нуждается в уточнении, а именно в корректировке коэффициентов гидрорасширения в зависимости от влажности древесины. Дальнейшее направление исследования авторов будет направлено на проведение натурных экспериментов по определению коэффициентов гидрорасширения различных сортов древесины в зависимости от толщины деревянных элементов и ориентации слоев в клееной конструкции.

Ключевые слова: метод само-формообразования клеёных деревянных конструкций, реологическая модель, деформация

1. INTRODUCTION

In modern construction practice, the use of wooden structures is widespread. Over the past ten years, unique wood facilities have been built in Western Europe, such as “Las Setas de Sevilla”, also known as the “Metropol Parasol” in Seville (Figure 1), the viewing tower on Pyramidenkogel in Austria (Figure 2), apartment building in London “The Cube” etc.

Figure 1. Las Setas de Sevilla.

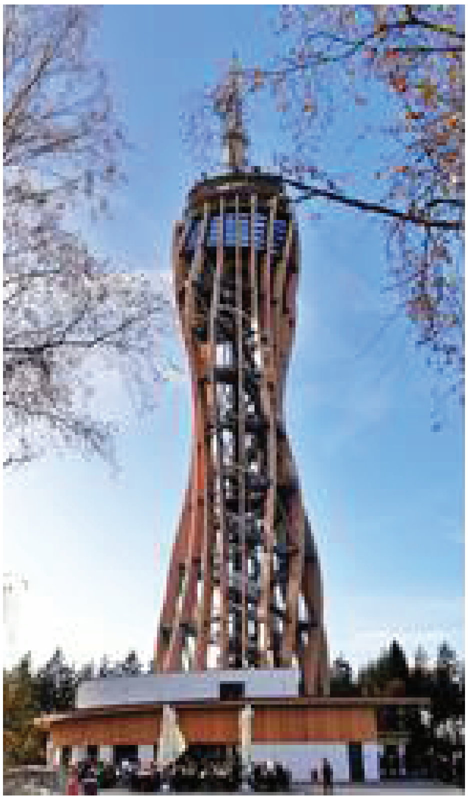

Figure 2. The viewing tower on Pyramidenkogel.

The world practice of using wooden structures pushes scientists to study the natural structure of wood for its effective use as a building material. The variety of wood products requires the development of methods for calculating structures from this material. A great deal of knowledge and experience in wood design is now being developed, but there are a number of issues that remain unresolved [1-4].

Wood – natural anisotropic material. A distinctive feature of its structure is the specific orientation of various tissues in it. Their directional arrangement forms a fibrous structure. In addition, and concentrically arranged annual rings give the wood a layered structure [5].

The unique structure of wood gives the wood exceptional advantages: relatively low density, high specific tensile strength along the fibers, resistance to salt aggression and other chemically active substances, high aesthetic and acoustic properties, etc. At the same time, wood defects, such as knot cluster, spiral grain, porosity, bultswell, reduce the quality of products and structures. Low fire resistance, decay and damages by bugs require additional protection measures for wooden structures. Anisotropy and change in physical and mechanical properties significantly limit the field of application of wood. But at the beginning of the second decade, based on the scientific works of S.P. Tymoshenko [6], several researchers from Switzerland and Germany [7] proposed a technology for using these shortcomings of wood to produce glued wooden structures of complex architectural shape. They called their method "self-shaping glued wooden structures".

2. METHOD OF SELF-SHAPING OF GLUED WOODEN STRUCTURES

Self-shaping method used for the production of glued wooden structures of curved shape. This method is based on the processes of drying and swelling of wood, as well as on its anisotropy. To give a curved shape, two layers are distinguished in a glued wooden structure: active and passive (Figure 3).

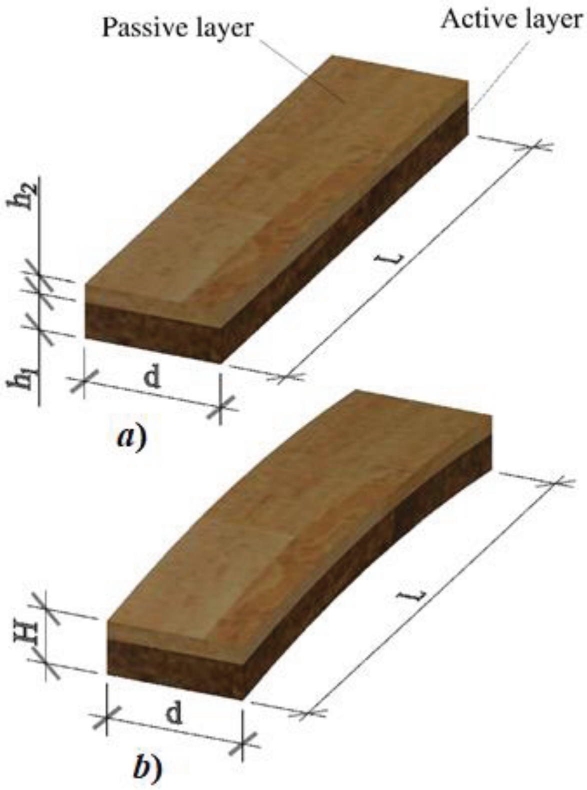

Figure. 3. (a) - wood element before drying; (b) - wood element after drying: L - length, d - width, H - general thickness, h_1 - thickness of the active layer, h_2 - thickness of a passive layer.

The main idea of the self-shaping method is that when the active layer is moistened to a certain value before gluing the layers of wood, the layer swells and increases in size. After that, the active and passive layers are glued together.

During drying of the glued wooden structure, moisture from the wood of the active layer is removed, and it decreases in size. The passive layer resists deformation of the active layer, as a result of which the glued wooden structure acquires a curved shape. The curvature of the structure depends on several factors, such as mechanical properties of the wood (modulus of elasticity, modulus of shear, Poisson's coefficient), humidity and thickness of the active and passive layers, orientation of the layers.

3. DESCRIPTION OF RHEOLOGICAL WOOD MODELS

The application of the self-shaping method of glued wooden structures requires the most complete and accurate rheological model of wood to predict the final shape of the structures. To date, scientists from around the world are conducting research to refine or develop a new rheological model of wood.

For example, E. M. Tyuleneva [8] proposed her rheological model of wood, in which the complete relative deformation of wood is defined as

$$\varepsilon = \frac{\sigma}{E_1} + \frac{\sigma}{E_2} + \frac{\sigma}{E_3}\left(1 - e^{-\frac{E_2}{\eta_2}t}\right), \qquad (1)$$

where σ - stress in wood, E_1 - instant module of elasticity, E_2 - elastic modulus of the second kind, E_3 - plastic module of deformation, η_2 - elasticity coefficient, t - loading time of wooden specimen.

A group of researchers Vasilenko A. S. and Yudin R. V. conducted studies to determine the deformation of wood in the manufacture of sleepers. The authors of article [9] proposed a mathematical model in which the total relative deformation of wood is defined as

$$\varepsilon = \frac{\sigma}{E_M} + \frac{\sigma}{E_M}\left(\frac{E_M}{E_g} - 1\right)\left(1 - e^{-\left(\frac{E_g}{E_M}\right)\left(\frac{t}{n}\right)\alpha}\right), \quad (2)$$

where σ - stress in wooden element, E_M - instant elastic modulus, E_g - long modulus of elasticity, which characterizes the final elastically elastic state of wood, t - loading time, n - relaxation time, $\alpha \le 1$ - rheological coefficient.

Foreign researchers Hassani M. M. and others from Germany and Switzerland, who proposed the method of self-shaping, developed their own rheological model of wood [10]. It defines the total relative deformation of wood as the sum of five components (Figure 4):

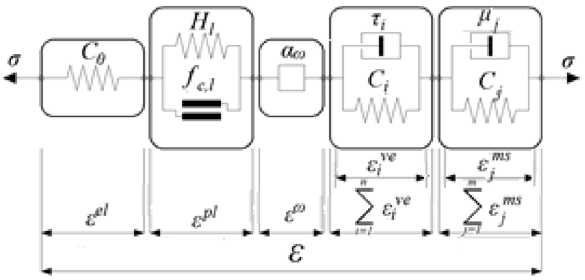

Figure. 4. Schematic illustration of the rheological model of wood [7].

– elastic deformation ε^{el};
– irrecoverable plastic deformation ε^{pl};
– deformation of drying or swelling caused by change in moisture content of wood ε^{ω};
– deformation of viscous-elastic creep ε_i^{ve};
– deformation of mechano-sorption creep ε_j^{ms}.

As a result, the tensor of complete relative deformation of wood consists of five components:

$$\varepsilon = \varepsilon^{el} + \varepsilon^{pl} + \varepsilon^{\omega} + \sum_{i=1}^{n} \varepsilon_i^{ve} + \sum_{j=1}^{m} \varepsilon_j^{ms}. \qquad (4)$$

The key feature of this model is the determination of the deformation of drying and swelling of wood, since it is it that plays an important role in the method of self-shaping of glued wooden structures. When drying wood, moisture inside the wood moves to the surface, and moisture evaporates from the surface of the material into the environment. With a decrease or increase in moisture, wood shrinks or swells.

To describe deformation in these processes, the authors [10] proposed to use an approach similar to the thermal expansion of the material. Change of linear dimensions of wood in different anatomical directions directly proportional to increase of wood humidity [10]:

$$\varepsilon^{\omega} = \alpha_{\omega}\left(Min\left(\omega, \omega_{FS}\right) - \omega_0\right), \qquad (5)$$

where ω - current humidity of material, ω_{FS} - moisture content of wooden specimen, at the value of which shrinkage or swelling does not occur (for a number of sources this value varies from 28 to 30 percent [11]), ω_0 - final humidity of wood. The vector α_{ω} consists of hydraulic expansion coefficients and in the coordinate system RTL (R, T, L - the anatomical direction of wood growth: radial, tangential longitudinal) is defined as

$$\alpha_{\omega} = \left\{\alpha_R, \alpha_T, \alpha_L; 0, 0, 0\right\}. \qquad (6)$$

The authors [10] assume that the coefficients are α_R, α_T, α_L constant for each type of wood and do not depend on the level of humidity. Coefficient values are given in [10]

Analyzing the presented rheological models of wood behavior, we can say that the rheological model proposed by foreign authors takes into account more factors affecting wood deformation. For the practical application of the self-forming method of glued laminated wooden structures, accounting for the deformation of drying and swelling of wood is the most important factor for predicting the final curved shape of the wooden structure.

4. VERIFICATION OF THE RHEOLOGICAL MODEL OF WOOD

Based on the above-described rheological model of wood (4) and the method of self-shaping of glued wooden structures, a numerical simulation of the deformation process of wooden beams was carried out in order to verify the rheological model with natural experimental studies (Figure 5) [7].

As the material of the initial samples, two varieties of wood were used *European beech* and *Norwegian spruce.* A total of three types of specimens 600 mm length, 100 mm wide and 15, 30 and 45 mm thick, specimen number 1, 2 and 3 respectively, were tested. The ratio of the thickness of the active layer of the passive layer was 1:2.

The passive layer was made of a solid board 600 mm long and 100 mm wide, and the active layer was made of a board 250 mm long and 100 mm wide.

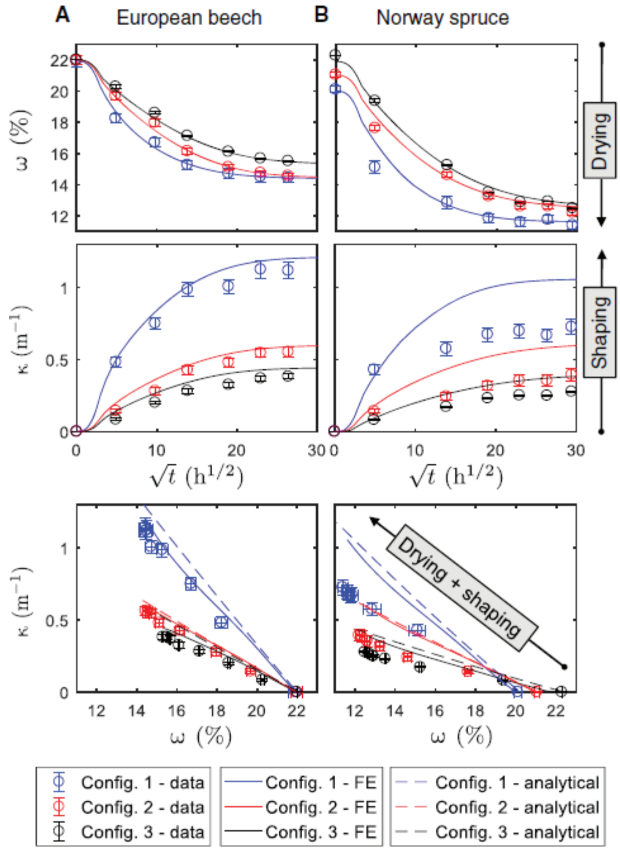

Figure. 5. Results of reshaping samples after drying. Bilayer samples (configurations 1-3) made of European beech (A) and Norwegian spruce (B). Moisture change of wood (ω) modeled by finite element method and measured on experimental samples. Curvatures (k) versus square root of time, and curvatures versus moisture contents with comparison to model predictions [7].

A polymer adhesive composition was used to glue the active and passive layers. In addition, the researchers conducted an analytical and numerical calculation of the deformation of glued wooden structures made by method of self-shaping.

Analyzing the obtained values of deformations of glued wooden beams, obtained from the results of full-scale experiments, numerical modeling and analytical calculation, we can conclude that:

– in the process of drying both wood grades, the humidity and time changes obtained during the full-scale experiment and as a result of numerical modeling are close to each other;

– for *European beech*, the dependencies of the change in curvature (shape change) of the sample on the time and moisture of wood, obtained during the full-scale experiment and as a result of numerical modeling, are also close to each other, but for *Norwegian spruce*, similar dependencies differ: the beam curvature according to the results of numerical modeling is greater than the curvature obtained during the full-scale experiment.

5. CONCLUSION

The method of self-shaping of glued wooden structures is a promising technology for designing and producing building structures of unique architectural forms from wood. This method is based on rheological processes occurring in anisotropic material, drying and swelling of wood. Studying the change in the mechanical characteristics of various types of wood due to an increase or decrease in its humidity will allow you to more accurately predict the final form of wooden structures made by self-forming.

Currently, the rheological model (4), describing the complete relative deformation of wood as the sum of five components: elastic and plastic deformation, drying or swelling of wood, deformation of viscous-elastic creep and mechanical-sorption deformation, needs to be clarified. This was shown by the results of field experiments and numerical modeling. According to the authors, these discrepancies can be caused by not taking into account the influence of thickness and orientation of the active layers in determining the factors of hygro-expansion coefficients of wood (6) [10].

Further research on the mechanical behavior of wood by the authors will focus on refining the mathematical model of the processes of drying and swelling of wood and conducting full-scale experiments to determine the hygro-expansion coefficients at different thicknesses and arrangement of wooden elements.

REFERENCES

1. **Kalugin A.V.** Dereviannye konstruktsii: ucheb. posobie [Wooden construction: educational book]. Moscow, ASV Publishing House, 2008, 288 pages (in Russian).
2. **Sobolev Iu.S.** Drevesina kak konstruktsionnyi material [Wood as a construction material]. Moscow, Lesnaia promishlennost, 1979, 248 pages (in Russian).
3. **Piatikrestovskii K.P.** Nelineinye metody mekhaniki v proektirovanii sovremennykh dereviannykh konstruktsii [Nonlinear methods of mechanics in the design of modern wooden structures]. Moscow, MISI-MGSU Publishing House, 2017, 320 pages (in Russian).
4. **Filimonov Je.L** at el. Konstrukcii iz dereva i plastmass [Structures made of wood and plastics: Tutorial]. Moscow, ASV Publishing House, 2010, 440 pages (in Russian).
5. **Chudinov B.S.** Voda v drevesine [The water in the wood]. Novosibirsk, Nauka, 1984, 270 pages (in Russian).
6. **Timoshenko S.P., Lessel's Dzh.** Prikladnaja teorija uprugosti [Applied theory of elasticity]. Leningrad, Gosudarstvennoe tehnicheskoe izdatel'stvo, 1931, 394 pages (in Russian).
7. **Grönquist P., Wood D., Hassani M.M., Wittel F.K., Menges A., Rüggeberg M.** Analysis of hygroscopic self-shaping wood at large scale for curved mass timber structures. // Science Advances, 2019, Volume 5, Number 9.
8. **Tiuleva E.M.** Utochnenie reologicheskoi modeli drevesiny [Clarification of the rheological wood model]. // Khvoinye boreal'noi zony, 2008, Volume 1-2, pp. 179-183 (in Russian).
9. **Iudin R.V., Vasilenko A.S.** Matematicheskaia model' reologicheskikh iavlenii deformirovaniia drevesiny dlia izgotovleniia shpal [Mathematical model of rheological phenomena of wood deformation for the production of sleepers]. // Aktual'nye napravleniia nauchnykh issledovanii XXI veka: teoriia i praktika (Current directions of scientific research of the XXI century: theory and practice).Voronezh, 2017, pp. 301-306.
10. **Hassani M.M., Wittel F.K., Hering S., Herrmann H.J.** Rheological model for wood. // Comput. Methods Appl. Mech. Engrg, 2014, Volume 283, pp. 1032-1060.
11. **Peich N.N., Tsarev B.S.** Sushka drevesiny [Wood drying]. Moscow, Vysshaia shkola, 1971, 220 pages (in Russian).

СПИСОК ЛИТЕРАТУРЫ

1. **Калугин А.В.** Деревянные конструкции. – М.: АСВ, 2008. – 288 с.
2. **Соболев Ю.С.** Древесина как конструкционный материал. – М.: Лесная промышленность 1979. – 248 с.
3. **Пятикрестовский К.П.** Нелинейные методы механики в проектировании современных деревянных конструкций. – М.: Изд-во МИСИ-МГСУ, 2017. – 320 с.
4. **Филимонов Э.В. и др.** Конструкции из дерева и пластмасс. – М.: АСВ, 2010. – 440 с.
5. **Чудинов Б. С.** Вода в древесине. – Новосибирск: Наука, 1984. – 270 с.
6. **Тимошенко С.П., Лессельс Дж.** Прикладная теория упругости. – Л.: Государственное техническое издательство, 1931. – 394 с.
7. **Grönquist P., Wood D., Hassani M.M., Wittel F.K., Menges A., Rüggeberg M.** Analysis of hygroscopic self-shaping wood at large scale for curved mass timber structures. // Science Advances, 2019, Volume 5, Number 9.
8. **Тюлева Е.М.** Уточнение реологической модели древесины. // Хвойные бореальной зоны, 2008, №1-2, с. 179-183.
9. **Юдин Р.В., Василенко А.С.** Математическая модель реологических явлений

деформирования древесины для изготовления шпал. // Актуальные направления научных исследований XXI века: теория и практика. Воронеж, 2017, с. 301-306.
10. **Hassani M.M., Wittel F.K., Hering S., Herrmann H.J.** Rheological model for wood. // Comput. Methods Appl. Mech. Engrg, 2014, Volume 283, pp. 1032-1060.
11. **Пейч Н.Н., Царев Б.С.** Сушка древесины. – М.: Высшая школа, 1971. – 220 с.

Vladislav S. Ponomarev, post-graduate student of department "Building constructions and computational mechanics", Perm National Research Polytechnic University; 109, ul. Kuibyshev, Perm, 614010, Russia;
Phone +7 (342) 219-83-61;
Ee-mail: vlad59russia@mail.ru.

Galina G. Kashevarova, Corresponding Member of Russian Academy of Architecture and Construction Sciences, Professor, Dr.Sc., Head of department "Building constructions and computational mechanics", Perm National Research Polytechnic University; 109, ul. Kuibyshev, Perm, 614010, Russia; phone +7 (342) 219-83-61;
E-mail: ggkash@mail.ru.

Пономарев Владислав Семенович, аспирант кафедры «Строительные конструкции и вычислительная механика» Пермского национального исследовательского политехнического университета; 614010, Россия, г. Пермь, ул. Куйбышева, 109; тел. +7(342) 219-83-61;
e-mail: vlad59russia@mail.ru.

Кашеварова Галина Геннадьевна, член-корреспондент Российской академии архитектуры и строительных наук (РААСН), доктор технических наук, профессор, заведующая кафедрой «Строительные конструкции и вычислительная механика» Пермского национального исследовательского политехнического университета; Россия 614010, г. Пермь, ул. Куйбышева, 109;
тел. +7(342) 219-83-61;
E-mail: ggkash@mail.ru.

DOI:10.22337/2587-9618-2020-16-2-101-112

NUMERICAL MODELING AND FULL-SCALE EXPERIMENTS OF GLUED WOODEN STRUCTURES JOINT DESTRUCTION ON CARBON-FIBER DOWEL PINS

***Mikhail A. Vodiannikov*[1], *Galina G. Kashevarova*[2], *Danil I. Starobogatov*[3]**
[1] Perm National Research Polytechnic University, JSC "VNII Galurgii"; Perm, RUSSIA;
[2] Perm National Research Polytechnic University, Perm, RUSSIA;
[3] Durham College, Ontario, CANADA

Abstract: This paper presents the results of numerical modeling and full-scale experiments of the failure process of a glued laminated timber beam with rigid joint in the middle. All the connecting parts are made of carbon fiber. The structural analysis is done with the finite element method (ANSYS software). The nonlinear problem was solved. The contact interaction of the structural elements in the process of deformation and fracture, as well as orthotropy of the wood, the transversely isotropic properties of the plates, and the real diagrams of the deformation of carbon fiber dowel pins were taken into account. The influence of the structural parameters of the joint on the position of the most loaded dowel pin in the joint and the bearing capacity of the general structure are investigated. To verify the structural analysis results, field tests were carried out before destruction by a stepwise increasing load on a personally designed stand. The destruction of the structure occurred according to the forecast of the numerical model as a result of the mutual slip of the glued wood layers and the destruction of the polymer matrix of the glued dowel pins with the beginning of the formation of plastic joints and the formation of cracks in the wood at the junction.

Keywords: wood, carbon fiber, computer model, ANSYS, finite element analysis, composite material, contact

ЧИСЛЕННОЕ МОДЕЛИРОВАНИЕ И НАТУРНЫЕ ЭКСПЕРИМЕНТЫ РАЗРУШЕНИЯ СТЫКОВ КЛЕЕНЫХ ДЕРЕВЯННЫХ КОНСТРУКЦИЙ НА УГЛЕПЛАСТИКОВЫХ НАГЕЛЯХ

***Водянников М.А.*[1,2], *Кашеварова Г.Г.*[1], *Старобогатов Д.И.*[3]**
[1] Пермский национальный исследовательский политехнический университет, г. Пермь, РОССИЯ
[2] АО «ВНИИ Галургии», г. Пермь, РОССИЯ
[3] Durham College, г. Онтарио, КАНАДА

Аннотация: В данной работе представлены результаты численного моделирования и натурных экспериментов процесса разрушения конструкции балки из клееной древесины с нагельным стыком, соединительные элементы которого изготовлены из углепластика. Расчеты проводились методом конечных элементов в программном комплексе ANSYS. Решалась нелинейная задача. Учитывалось контактное взаимодействие составляющих элементов конструкции в процессе деформирования и разрушения, а также ортотропия древесины, трансверсально-изотропные свойства пластин, реальные диаграммы деформирования углепластиковых нагелей. Исследовано влияние конструктивных параметров стыка на положение наиболее нагруженного стержня в соединении и несущую способность конструкции балки. Для верификации результатов расчета проводились натурные испытания балок до разрушения пошагово возрастающей нагрузкой на специально запроектированном стенде. Разрушение конструкции произошло согласно прогнозу численной модели в результате взаимного проскальзывания слоев клееной древесины и разрушения полимерной матрицы вклеиваемых стержней с началом образования пластических шарниров под пятками траверсы и образованием трещин в древесине в месте стыка.

Ключевые слова: древесина, углепластик, компьютерная модель, ANSYS, конечноэлементное моделирование, композитный материал, контакт

1. INTRODUCTION

Joints of solid and glued timber structures are the most responsible and extremely labor-intensive design section in the construction of long-span architectural forms. Numerous studies of wooden structures joints were carried out by such institutions as VIAM, TSNIISK, TsAGI, MISI, LISI, VIA and researchers: G. G. Carlsen, I. P. Kulibin, V. G. Shukhov, V. M. Kochenov; Gestesi, Earl, Schnidtman and others.

S. A. Andreev [1], V. N. Maslov [2], V. F. Ivanov [3], B. L. Nikolai [4], A. V. Lenyashin [5], V. G Donchenko [6], Yu. V. Slitskoukhov [7]) considered a dowel as a beam on an elastic base.

G. G. Carlsen was the first to propose a method for calculating joints by permissible stresses. V. M. Kochenov [8] proposed a methodology for calculating nugget joints taking into account the elastic-plastic work of wood in the nest for collapse and the plastic work of rods for bending.

The authors S. B. Turkovskii and A. A. Pogoreltsev [10-13] proposed a universal joint on glued rods (“TsNIISK system”) using steel pins and overlays (Figure 1), which made it possible to create a large number of unique large-span wood structures.

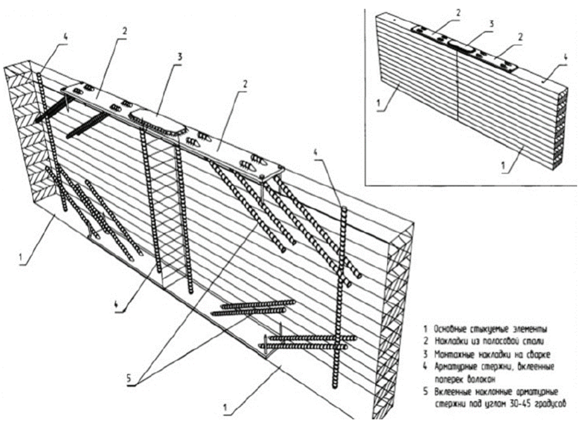

<u>Figure 1.</u> Universal joint “TsNIISK system”.

Despite the multipurpose of such compounds, their practical use in load-bearing structures in some cases (chemically aggressive environment, high humidity, etc.) is not reliable, since there is a risk of premature failure of the structure due to corrosion of steel parts. The restoration of the anticorrosion layer is often impossible without stopping the operation of the facility. The high-temperature effect when using steel parts at the joints of the weld joint (patch pads, reinforcing bars) leads to stress concentrators associated with the destruction of the wood structure in these areas. A significant difference in the linear thermal expansion coefficients α*106 (1/0C) of steel (13.0) and wood parallel to the fibers (3.7) leads to a limitation of the joining of large-assembled large-span elements under conditions of a large annual temperature difference. The fire resistance of a massive wooden section treated with flame retardant allows structures to withstand up to 60 minutes without collapse, while the transition of steel connecting parts to a plastic state in a fire will occur 5-12 times less (depending on temperature).

In [14, 15], it was shown that it is mainly possible to use composite materials (carbon fiber, basalt, fiberglass) instead of steel to create equal strength joints of wooden structures [16]. But the widespread use of composites today is hindered by the lack of a full regulatory framework, a relatively high cost, a small number of industries and limited application experience.

The issue of improving the connections of solid and glued wood structures using glued rods and pads made of composite materials (including carbon fiber reinforced plastics) is relevant and expands the possibilities of using renewable natural materials.

The existing methodology for calculating the connections of the “TsNIISK system” is reduced to comparing the minimum bearing capacity of a rod from the condition of crushing a wood point or bending, the most loaded of rods. However, methods for determining the forces in the pins to find the most loaded rod in the normative documents are not given [17].

The study of the processes of deformation and fracture of a structure under complex stress conditions requires the use of adequate mathematical models of the mechanical behavior of materials and a high degree of detail of structural elements. The use of numerical methods, the capabilities of modern software systems and computers allows us to describe with high accuracy the behavior of the elements of the joint structure in a complex stress state. To analyze the stress-strain state of the structure, the finite element method in the form of the displacement method and "ANSYS" program complex [18], verified at the Russian Academy of Architecture and Building Sciences, was used.

The purpose of this study is to determine the stress-strain state of the elements of the rigid joint of glued wooden structures using composite parts with numerical modeling and a full-scale experiment. To show the fundamental possibility of using composite parts and rods as an alternative to steel elements when creating equal strength assemblies.

To achieve this goal, the following tasks were solved:

1. Creating a design model for the construction of a wooden beam with a joint node, taking into account the orthotropy of glued wood and the contact of the elements of the joint.
2. Structural analysis of the stress-strain state of the structure with different configuration options using four-point bending.
3. To determine the places of the most possible destruction of the structure depending on the parameters of the joint design.
4. To verify the results obtained, conduct full-scale experiments and a comparative analysis with the engineering calculation method.

2. METHODS

In this study, a calculated finite-element model of a layered wooden beam with a joint in the middle of the span was created. It was tested using the four-point bending technique (Figure 2*a*). The model was built in AutoCAD and exported to ANSYS using macros written in the parametric programming language APDL. The joint overview is shown in Figure 2*b*.

The main feature of the considered structure is the contact interaction of bodies [19], the inclusion of which allows to simulate the behavior of its constituent elements in the process of deformation and fracture.

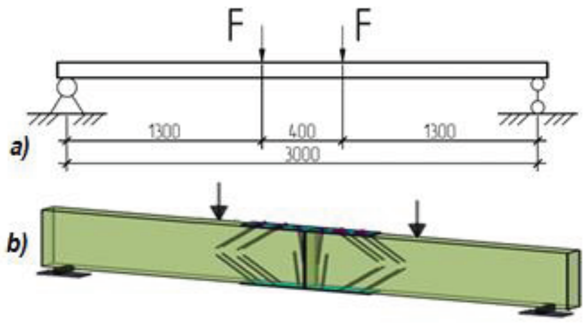

Figure 2. The design scheme of the beam and joint overview.

The stress state in the contact zones is extremely diverse. Surfaces can come in and out of contact all of a sudden. The stress state is significantly affected by friction, and it must be taken into account.

At the joint boundaries of the contacting elements, distributed surface forces arise. Normal t_n and tangent t_t components of the distributed contact force acting on any element have the form:

$$t_n = t \cdot n \leq 0 \quad (1)$$

$$t_t = t \cdot \tau, \quad (2)$$

where n - external normal to the contact surface of the body, τ - tangent vector to the contact surface of the body.

In equation (1), non-strict inequality turns into equality when the bodies exit the contact and into strict inequality when they are in contact. Tangent contact forces can take any value. The application of the tangential stress in the contact does not lead to slippage, provided that the bodies in the contact area are glued to each other or the friction coefficient tends to infinity. In this case, the tangential contact forces are independent of normal contact forces, but are not equal to zero.

The contacting bodies are motionless relative to each other, i.e. tangential forces obey Coulomb's law as long as the inequality holds:

$$|t_t| \leq \mu_s |t_n|, \tag{3}$$

where $\mu_s > 0$ – static coefficient of friction.
If inequality (1) is violated, the bodies begin to move relative to each other. Then the tangential contact forces obey the following equality:

$$|t_t| = \mu_d |t_n|, \tag{4}$$

where μ_d – dynamic coefficient of friction, $\mu_d \leq \mu_s$.
The movement will continue until inequality is fulfilled and will not start again until inequality is violated again (3).

$$|t_t| < \mu_d |t_n|, \tag{5}$$

When friction in the contact zones is taken into account, the solution of the problem substantially depends on the sequence of application of external loads, and complex loading programs are implemented at the points entering and leaving the contact [20 - 22].
The development trend of leading software systems (PCs) is the implementation of a set of mathematical models in them to describe different physical processes. The user connects the necessary models at the stage of setting the problem, setting the corresponding boundary conditions and other required input data.
The ANSYS Workbench software module contains a large set of contact technology tools integrated into the finite element method for developing various contact options [7, 8]. Two interacting surfaces are distinguished in a contact – a contact pair. One of the surfaces is conventionally called “contact” and the second – “target”. The choice of contact model is the most important issue in solving contact problems.
In this task the contact area can change and in the general case it contains both adhesion and sliding sections that occur when the module exceeds the tangential force of the limit value of the friction force (rest friction). To model contact interaction and sliding between three-dimensional surfaces, the Frictional model and contact elements CONTA174 and TARGE170 were used. The friction coefficient depends on the materials, and is adopted for a pair of wood-carbon fiber – 0.25, and for a pair of wood-wood – 0.33.
The following finite elements were used to create the calculated finite element model of the model: the beam body was modeled with 8-node SOLID185 elements, the rods with 3-node BEAM188 elements, and the pads with 8-node SHELL281 elements. Different mesh options were considered. From the point of view of convergence and calculation speed, a mesh with grinding in the contact zone is preferable. The size and type of mesh significantly affects the analysis results.
The load in the form of two concentrated forces F=1,25 kN (Figure 2a) was adopted in accordance with the recommendations of the National Standart “Wooden Structures”.
The joint was made in the middle of the span.
The design is a composite. Wood is defined as an orthotropic material with the following characteristics: elastic modulus along the x axis, $E_x = 1.1\times10^{10}$ Pa; elastic modulus $E_y = E_z = 4.5\times 10^8$ Pa; Poisson's ratios $\nu_{xy} = 0.45$, $\nu_{yz} = \nu_{xz} = 0.018$; shear modulus $G_x = G_y = G_z = 6 \times 10^8$ Pa.
The glued rods are carbon fiber on a polymer matrix [23] with the following characteristics: tensile strength at break $\sigma_t = 2.248 \times 10^6$ Pa; elastic modulus $E = 117 \times 10^9$ Pa; Poisson's ratio $\nu_{xy} = \nu_{yx} = 0.31$.
The overlays are defined as a transversally isotropic bidirectional carbon fiber reinforced plastic with a direction of reinforcing layers of ±45 degrees with the following characteristics: tensile strength at break $\sigma_t = 7.65 \times 10^6$ Pa; elastic moduli $Ex = Ey = 87.2 \times 10^9$ Pa, $Ez = 65.4 \times 10^9$ Pa; Poisson's ratios $\nu_{xy} = \nu_{yx} = 0.268$; $\nu_{xz} = 0.018$.
Numerical implementation of nonlinear problems of determining the stress-strain state of a structure was carried out by a step-by-step method by replacing the entire load with a series of its small increments. Within each loading step, the load can be further divided into several solution steps to ensure gradual application of the load. At each step of the solution, to obtain

convergence, equilibrium iterations were performed using the Newton-Raphson method. The convergence check for forces and displacements was carried out using the Euclidean norm for all degrees of freedom.

3. RESULTS AND DISCUSSION

The results of calculating a variant of a beam with arrangement at the junction of eight pins on each side at an angle of 45 ° to a line running along the long edge of the beam are shown. Figures 3 and 4 show the isofield of the distribution of equivalent stresses in wood and connecting parts (pads and rods).

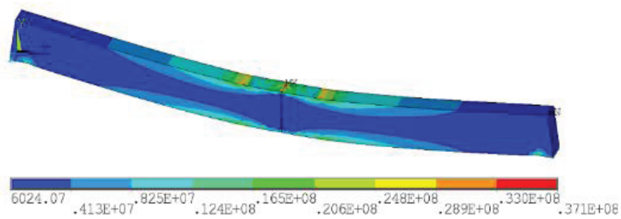

Figure 3. Isofields of stress distribution in the body of wood (Pa).

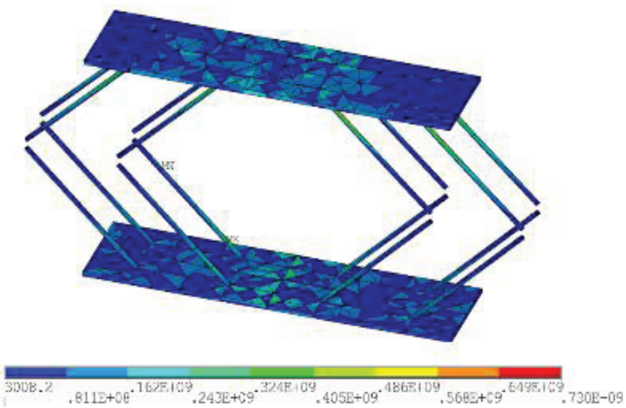

Figure 4. Isofields of the stress distribution in connecting parts (Pa).

The contact interaction status of structural elements is shown in Figure 5 (orange color indicates slippage of wood layers relative to each other ("SLIDING" in ANSYS terminology), as well as slippage of rods in landing slots at the moment of sample destruction).

Plastic deformations in a specimen with a rigid joint begin to form under the supports of the beam in the zone of maximum bending moment at a load of 15.4 kN. A diagram with the locations of the resulting plastic hinges is shown in Figure 6. The failure of the joint occurs at a load of 25.6 kN. In this case, the opening of the joint zone and the separation of the connecting strips, as well as the rods at the contact points.

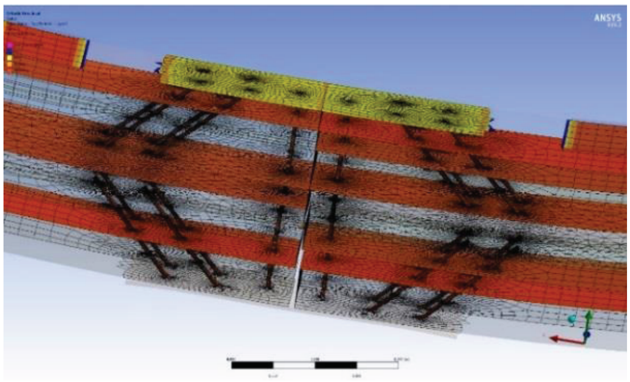

Figure 5. Contact interaction of the rods, pads and layers of wood at the time of destruction.

The maximum equivalent stresses in the glued rods forming a rigid joint were 600.7 MPa. The voltage distribution fields in the connecting parts are shown in Figure 6.

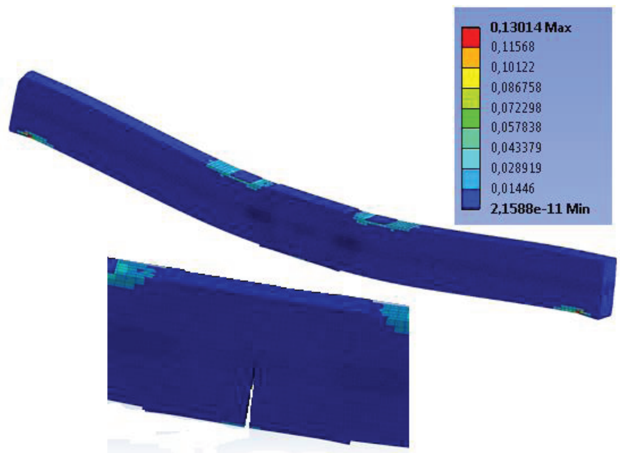

Figure 6. Plots at the beginning of the formation of plastic hinges under the supports of the beam.

At the moment of sample destruction, the maximum displacements of the middle of the beam span (at the junction) according to the results of numerical simulation were equal to 9.75 mm.

The maximum equivalent stresses in the glued rods forming a rigid joint were 600.7 MPa. The voltage distribution fields in the connecting parts are shown in Figure 7.

The most responsible (bottleneck) is the area of glued rods located between the plate and the wood - in this place the greatest bending stresses arise. In Figure 7, these areas are painted in light blue. When designing the joint, it is advisable to use conical-shaped rods with a thickening at the junction of the parts to be joined.

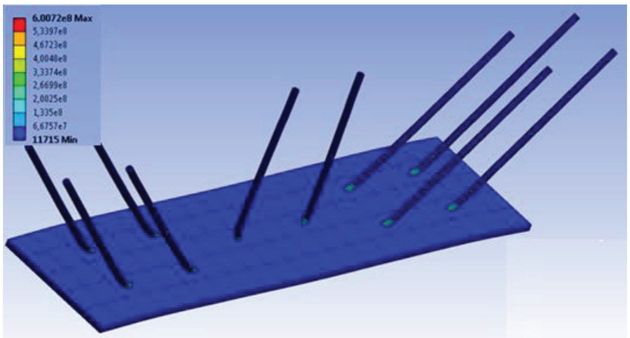

Figure 7. Isofields and stresses in the rods on a stretched pad.

In order to assess the influence of the parameters of structural elements on the bearing capacity of the joint and to determine the most loaded rod in the joint, a multivariate computational experiment was conducted. The following parameters were taken as variable: position (gluing angle) φ=15, 30, 45, 60° (Figure 8); the number of pins in the connection N = 4, 8, or 12 pcs.

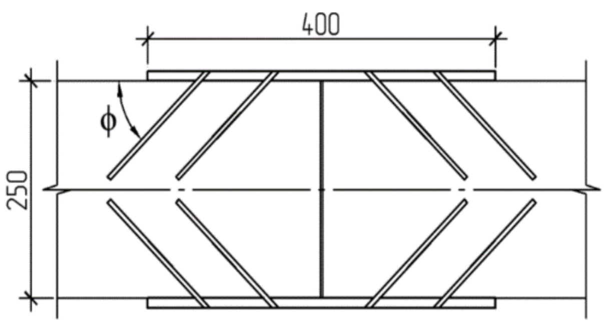

Figure 8. The angle of gluing rods.

The rods are installed in two longitudinal rows, the location of the rods is taken in accordance with the requirements of paragraphs 7.18, 7.19 [9].

The following are taken as controlled design parameters: maximum equivalent stresses before failure for all joints: in wood, in rods, in overlays and maximum beam deflection in the vertical plane.

The following are taken as controlled design parameters: maximum equivalent stresses before failure for all joints: in wood, in rods, in overlays and maximum beam deflection in the vertical plane.

The results obtained during the computational experiments are shown in Figures 9-12.

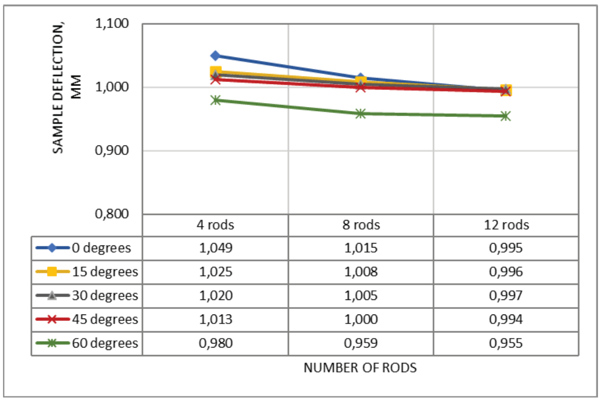

	4 rods	8 rods	12 rods
0 degrees	1,049	1,015	0,995
15 degrees	1,025	1,008	0,996
30 degrees	1,020	1,005	0,997
45 degrees	1,013	1,000	0,994
60 degrees	0,980	0,959	0,955

Figure 9. Deflection of the beam in the vertical plane.

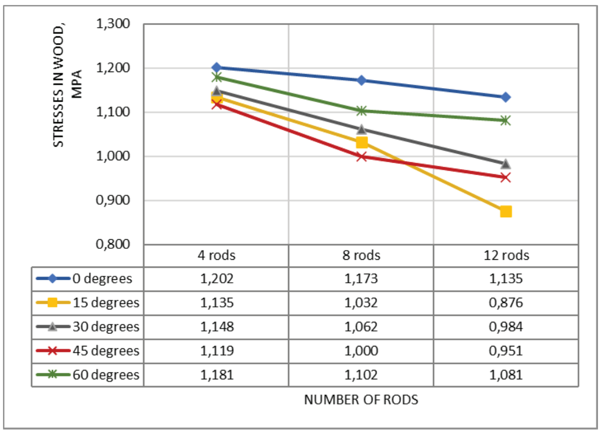

	4 rods	8 rods	12 rods
0 degrees	1,202	1,173	1,135
15 degrees	1,135	1,032	0,876
30 degrees	1,148	1,062	0,984
45 degrees	1,119	1,000	0,951
60 degrees	1,181	1,102	1,081

Figure 10. Maximum equivalent stresses in wood.

It can be seen from the graphs that the beam deflection decreases with an increase in the angle of inclination of the rod (logically, the rods become more parallel to the boards and create longitudinal reinforcement). Stresses in wood and CFRP vary insignificantly, and the stresses in the rods and pads are greater, the smaller the rods.

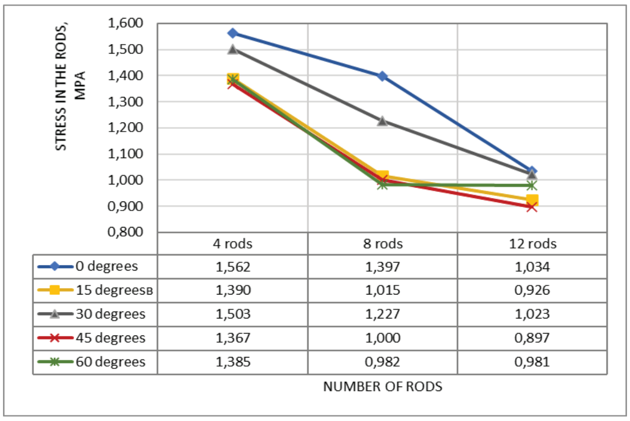

Figure 11. Maximum equivalent stresses in the rods.

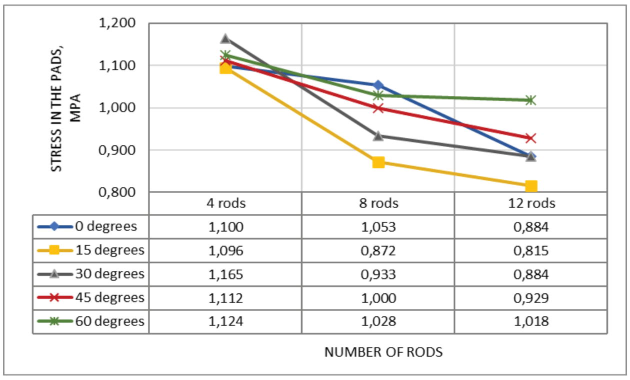

Figure 12. Maximum equivalent stresses in pads.

4. FULL-SCALE EXPERIMENTS

The scheme of full-scale testing of the samples corresponded to the design scheme shown in Figure 2. The joint was made in the middle of the span. The beam body is glued wood of the second grade with a section of 100×225×3000 mm. The glued rods are carbon fiber with a diameter of 5 mm, obtained by pultrusion. The overlays on the top and bottom of the beam – bidirectional carbon fiber on the matrix of the synthetic polymer binder are anchored (fixed) into the body of the wood using glued rod.

The tests were carried out until the destruction of the sample stepwise increasing load on a individually designed bench. The pressure on the beam was transmitted by means of a hydraulic jack DU50P250 through a traverse with two articulated supports. The load value was taken from an electronic pressure gauge connected to the oil station via high pressure hoses. The value of the breaking load was taken at the moment at which an increase in displacements was observed with the jack support pressure drop. To measure the displacements, inductive linear displacement sensors DPL-100 were used, connected to the TEREM-4.1 recording unit.
A general view of the beam on the bench is shown in Figure 13. The sample after the destruction of the joint, is shown in Figure 14.

Figure 13. General view of the beam on the bench.

Figure 14. The sample after the destruction of the joint.

The tests were carried out until the sample was destroyed by a stepwise increasing load on a specially designed bench. The breaking load is set at 25.4 kN, the displacement in the middle of the span was 7.2 mm. The compressed (upper) edge of the beam at the junction closely approached the opposite part of the beam, forming a frontal stop. The maximum width of the opening of the lower edge at the junction was noted with an indicator value of 5.7 mm, with an initial gap value of 1 mm before the test.

Figure 15 shows the graphs of the dependence of the maximum displacements of the beam on the load obtained in computational and field experiments. Sensors "1" and "3" are installed under the support heels of the beam, transmitting the force directly to the beam. Sensor "2" is installed in the middle of the beam span (at the junction).

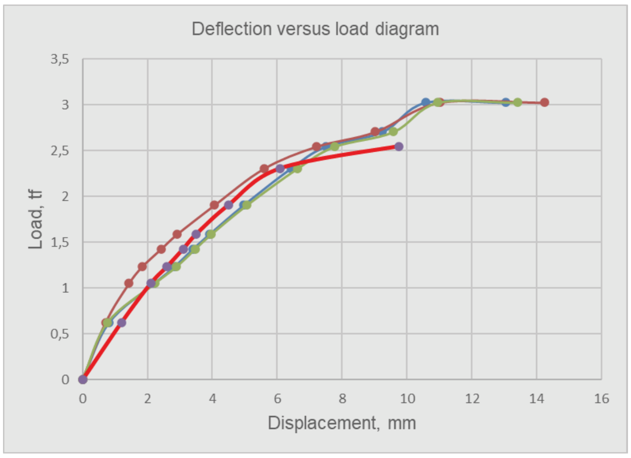

Figure 15. Graphs of the dependence of displacements on load for experimental and theoretical data.

The experiments were carried out until the collapse of the beam and the joint with the occurrence of mutual displacements of the layers of wood and pulling out individual rods. After destruction, the beam did not return to its original state.

The nature of the damage in full-scale tests corresponds to the forecast of the numerical model. The structure is destroyed as a result of the mutual slip of the glued wood layers, the destruction of the polymer matrix of the glued rods, the formation of plastic joints under the heels of the beam and the formation of cracks in the wood at the junction.

After the first rod was turned off from work, the structure continued to work elastically for some time, but with an increase in load and a sharp destruction of the remaining rods, the joint of the structure completely destroyed. This information is confirmed by the spasmodic behavior of the curve on the load-displacement graph, followed by an increase in deformations when the load drops.

5. CONCLUSION

The creation of a correct design model for the construction of a wooden beam with a nodal joint, taking into account the orthotropy of glued wood and the contact interaction of the joints, the use of numerical methods and modern software systems, allows us to understand the nature of the destruction of the composite structure, the distribution of stresses and displacements that occur inside the joint, hidden for registration during experimental research.

The places of the most probable destruction of the structure are determined depending on the parameters of the joint design.

The principal possibility of replacing metal parts with carbon fiber to create equal strength joints of wooden structures is shown. When comparing the results of experiments of a beam with a joint on glued rods with a similar continuous beam, the reinforcing effect of the rods is noted, since the glued joint rods prevent mutual displacement of the layers.

Short-term tests as a whole showed viable solutions when designing joints on glued rods [24], however, to complete the picture of the operation of such parts, it is necessary to conduct long-time based experiments, including fire tests and vibration load tests. It is necessary to take into account the aging of composites. Also, a long-time experiment is designed to show the joint work of the composite and wood, because, for example, steel rods form an oxide corrosion shell over time and after several years of operation cease to provide the initial joint work in the wood nests. It is assumed that composite solutions for joints of glued wooden structures will be free from such drawbacks.

REFERENCES

1. **Andreev S.A.** Primenenie sterzhnevyh soedinenij v derevyannyh konstrukciyah [The use of rod joints in wooden structures]. // Strojindustriya, 1930, No. 7 (in Russian).
2. **Maslov V.N.** Raschet boltovogo, rabotayushchego na razryv styka derevyannoj fermy kak uprugoj sistemy [Calculation of the bolted working on the gap of the wooden truss as an elastic system]. // Collection of works of the Moscow Institute of Engineering Transport, 1926, No. 2, pp. 119-114 (in Russian).
3. **Ivanov V.F., Maltsev L.I.** Issledovanie raboty nagel'nyh soedinenij v predelah uprugosti [The study of the work of joint compounds in the range of elasticity]. // Proceedings of the Leningrad Institute of Engineering and Public Construction, 1939, pp. 167-175 (in Russian).
4. **Nikolai B.A.** Teoriya rascheta nagel'nogo sopryazheniya v derevyannyh konstrukciyah [Theory of the calculation of the brass mates in wooden structures]. Moscow, NDTVCH, 1935, 164 pages (in Russian).
5. **Lenyashin A.V.** Issledovanie sopryazhenij na nagelyah: nauchno-tekhnicheskij otchet laboratorii derevyannyh konstrukcij CNIIPS [Conjugation of mates on pins: scientific and technical report of the laboratory of wooden structures TsNIIPS]. Moscow, 1935, No. 4412-5100 (in Russian).
6. **Donchenko V.G.,** Nagel'nye soedineniya v avtodorozhnyh mostah [Fuse connections in road bridges]. Moscow, Dorizdat, 1952, 255 pages (in Russian).
7. **Slitkoukhov Y.V.** Issledovanie raboty simmetrichnyh sopryazhenij elementov derevyannyh konstrukcij na nagelyah iz krugloj stali [The study of the symmetric mating elements of wooden structures on the dowel of round steel]. PhD Thesis, 1956, 12 pages (in Russian).
8. **Kochenov V.M.** Nesushchaya sposobnost' elementov i soedinenij derevyannyh konstrukcij [Bearing capacity of elements and connections of wooden structures]. Moscow, Gosstroiizdat, 1953, 320 pages (in Russian).
9. SP 64.13330.2017. Derevyannye konstrukcii. Aktualizirovannaya redakciya SNiP II-25-80 [Wooden structures. Updated edition]. Moscow, TSNIISK, 2017, 87 pages (in Russian).
10. **Turkovskij S.B., Sayapin V.V.** Issledovanie montazhnyh uzlovyh soedinenij kleyonyh derevyannyh konstrukcij [Investigation of assembly nodal joints of glued wooden structures]. // Bearing wooden structures: Collection of scientific papers. Moscow, TSNIISK, 1981, pp. 92-105 (in Russian).
11. **Turkovskij S.B., Lomakin A.D.** Pogorel'cev A.A., Zavisimost' sostoyaniya kleenyh derevyannyh konstrukcij ot vlazhnosti okruzhayushchego vozduha [Dependence of the state of glued wooden structures on the humidity of the surrounding air]. // Industrial and Civil Engineering. Institute Proceedings, Moscow, TSNIISK, 2012, No. 3, pp. 30-32 (in Russian).
12. **Turkovskij S.B., Pogorel'cev A.A.** Sozdanie derevyannyh konstrukcij sistemy TSNIISK na osnove naklonno vkleennyh sterzhnej [Creation of wooden structures of the TSNIISK system based on inclined glued rods]. // Industrial and Civil Engineering. Institute Proceedings. Moscow, TSNIISK, 2007, No. 3, pp. 6-8 (in Russian).
13. **Turkovskij S.B., Pogorel'cev A.A.** Preobrazhenskaya I.P. Kleenye derevyannye konstrukcii s uzlami na vkleennyh sterzhnyah v sovremennom stroitel'stve (sistema CNIISK) [Glued wooden structures with knots on the glued

rods in modern construction (TSNIISK system)]. Moscow, Strojmaterial,. 2013, 308 pages (in Russian).

14. **Kashevarova G. G., Vodiannikov M.A.** Chislennoe i eksperimental'noe modelirovanie zhestkogo styka sloistyh derevyannyh konstrukcij [Numerical and experimental modeling of hard joints of laminated wooden structures]. // International Journal for Computational Civil and Structural Engineering, 2017, Volume 13, Issue 2, pp. 84-92 (in Russian).
15. **Vodiannikov M., Kashevarova G.** Analysis of Wood Structure Connections Using Cylindrical Steel and Carbon Fiber Dowel Pins. // IOP Conference Series: Materials Science and Engineering, 2017, Volume 205.
16. **Gugutsidze G., Draskovic F.** Reinforcement of Timber Beams with Carbon Fiber Reinforced Plastics. // Slovak Journal of Civil Engineering, 2010, No. 2, pp. 1-6.
17. **Mett'yuz F., Rolings R.** Kompozitnye materialy. Mekhanika i tekhnologiya [Composite materials. Mechanics and technology]. Moscow, Tehnosfera, 2004, 408 pages (in Russian).
18. **Kaplun A. B.** ANSYS v rukah inzhenera. Prakticheskoe rukovodstvo [ANSYS in the hands of an engineer. Practical guide]. Moscow, Librokom, 2015, 272 pages (in Russian).
19. **Stankevich I. V., Yakovlev M. E., Si Tu Htet.** Matematicheskoe modelirovanie kontaktnogo vzaimodejstviya uprugoplasticheskih sred [Mathematical modeling of the contact interaction of elastoplastic media]. Moscow, NEIKON, 2012 (in Russian).
20. **Mashkov Y.K.** Tribofizika metallov i polimerov [Tribophysics of metals and polymers]. Omsk, OMGTU Publishing, 2013, 240 pages (in Russian).
21. **Popov V.L.** Mekhanika kontaktnogo vzaimodejstviya i fizika treniya. Ot nanotribologii do dinamiki zemletryasenij [Mechanics of contact interaction and physics of friction. From nanotribology to earthquake dynamics]. Moscow, Fizmatlit, 2013, 352 pages (in Russian).
22. **Podgornyj A.N., Gontarovskij P.P.** and others. Zadachi kontaktnogo vzaimodejstviya elementov konstrukcij. Monografiya [Tasks of contact interaction of structural elements]. Kiev, Nauk Dumka, 1989, 232 pages (in Russian).
23. **Perepelkin K.E.** Himicheskie volokna: razvitie proizvodstva, metody polucheniya, svojstva, perspektivy [Chemical fibers: production development, production methods, properties, prospects]. Saint-Petersburg,. SPGUTD Publishing, 2008, 354 pages (in Russian).
24. **Vodiannikov M., Kashevarova G.** Composite Solutions for Glulam Joints. // Key Engineering Materials, 2019, Volume 801.

СПИСОК ЛИТЕРАТУРЫ

1. **Андреев, С.А.** Применение стержневых соединений в деревянных конструкциях. // Стройиндустрия, 1930, №7.
2. **Маслов В.Н.** Расчет болтового, работающего на разрыв стыка деревянной фермы как упругой системы. // Сборник трудов Московского института инженеров транспорта, 1926, Выпуск 2, с. 114-119.
3. **Иванов В.Ф., Мальцев Л.И.** Исследование работы нагельных соединений в пределах упругости. // Труды Ленинградского института инженеров коммунального строительства, 1939, с. 167-175.
4. **Николаи Б.А.** Теория расчета нагельного сопряжения в деревянных конструкциях. – М.: НДТВЧ, 1935. – 164с.
5. **Леняшин А.В.** Исследование сопряжений на нагелях: научно-технический отчет лаборатории деревянных конструкций ЦНИИПС. Москва, 1935, №4412-5100.
6. **Донченко В. Г.** Нагельные соединения в автодорожных мостах. – М.: Дориздат, 1952. – 255 с.

7. **Слицкоухов Ю.В.** Исследование работы симметричных сопряжений элементов деревянных конструкций на нагелях из круглой стали. Автореферат диссертации на соискание ученой степени кандидата технических наук. – М., 1956. – 12 с.
8. **Коченов В.М.** Несущая способность элементов и соединений деревянных конструкций. – М.: Госстройиздат, 1953. – 320 с.
9. СП 64.13330.2017. Деревянные конструкции. Актуализированная редакция СНиП II-25-80. ЦНИИСК им. В.А. Кучеренко – институт ОАО «НИЦ «Строительство». – М., 2011. – 87 с.
10. **Турковский С.Б., Саяпин В.В.** Исследование монтажных узловых соединений клеёных деревянных конструкций. // Несущие деревянные конструкции: Сборник научных трудов. – М.: ЦНИИСК им. Кучеренко, 1981, с. 92-105.
11. **Турковский С.Б., Ломакин А.Д. Погорельцев А.А.** Зависимость состояния клееных деревянных конструкций от влажности окружающего воздуха. // Промышленное и гражданское строительство. Труды института. – М.: ЦНИИСК им. В.А. Кучеренко, 2012, №3, с. 30-32.
12. **Турковский С.Б., Погорельцев А.А.** Создание деревянных конструкций системы ЦНИИСК на основе наклонно вклеенных стержней. // Промышленное и гражданское строительство. Труды института. – М.: ЦНИИСК им. В.А. Кучеренко, 2007, №3, с. 6-8.
13. **Турковский С.Б., Погорельцев А.А.** Преображенская И.П. Клееные деревянные конструкции с узлами на вклеенных стержнях в современном строительстве (система ЦНИИСК). – М.: РИФ «Стройматериалы», 2013. – 308 с.
14. **Кашеварова Г. Г., Водянников М.А.** Численное и экспериментальное моделирование жесткого стыка слоистых деревянных конструкций // International Journal for Computational Civil and Structural Engineering, 2017, Volume 13, Issue 2, pp. 84-92.
15. **Vodiannikov M., Kashevarova G.** Analysis of Wood Structure Connections Using Cylindrical Steel and Carbon Fiber Dowel Pins // IOP Conference Series: Materials Science and Engineering, 2017, Volume 205.
16. **Gugutsidze G., Draskovic F.** Reinforcement of Timber Beams With Carbon Fiber Reinforced Plastics. // Slovak Journal of Civil Engineering, 2010, No. 2, pp. 1-6.
17. **Мэттьюз Ф., Ролингс Р.** Композитные материалы. Механика и технология. – М: Техносфера, 2004. – 408 с.
18. **Каплун, А.Б., Морозов Е.М., Олферьева М.А.** ANSYS в руках инженера. Практическое руководство. – М.: Либроком, 2015. – 272 с.
19. **Станкевич И. В., Яковлев М. Е., Си Ту Хтет.** Математическое моделирование контактного взаимодействия упругопластических сред. – М.: НП «Неикон», 2012.
20. **Машков Ю.К.** Трибофизика металлов и полимеров: монография. – Омск: Издательство ОмГТУ, 2013. - 240 с.
21. **Попов В.Л.** Механика контактного взаимодействия и физика трения. От нанотрибологии до динамики землетрясений. – М.: ФИЗМАТЛИТ, 2013. – 352 с.
22. **Подгорный А.Н., Гонтаровский П.П. и др.** Задачи контактного взаимодействия элементов конструкций. – Киев: Наукова Думка, 1989. – 232 с.
23. **Перепелкин К. Е.** Химические волокна: развитие производства, методы получения, свойства, перспективы – СПб.: Издание СПГУТД, 2008. – 354 с.
24. **Vodiannikov M., Kashevarova G.** Composite Solutions for Glulam Joints. // Key Engineering Materials, 2019, Volume 801.

Mikhail A. Vodiannikov, Engineer of the department for survey and monitoring of building structures of JSC “VNII Galurgii”; Graduate Student, Department of Building Constructions and Computational Mechanics, Perm National

Research Polytechnic University; 29, Komsomolsky prospect, Perm, 614990, Russian Federation;
email: vodyannikov@mail.ru.

Galina G. Kashevarova, Corresponding Member of Russian Academy of Architecture and Construction Sciences (RAACS), Professor, Dr.Sc., Head of department "Building constructions and computational mechanics", Perm National Research Polytechnic University; Russia, 614010, Perm, ul. Kuibyshev, 109;
phone +7 (342) 219-83-61;
E-mail: ggkash@mail.ru.

Danil I. Starobogatov, Part-time professor at Durham College, Ontario, Canada; 1610 Champlain Avenue Whitby, ON, Canada L1N 6A7;
E-mail: dstarobogatov@gmail.com.

Водянников Михаил Алексеевич, аспирант кафедры «Строительные конструкции и вычислительная механика» Пермского национального исследовательского политехнического университета; Инженер отдела обследования и мониторинга строительных конструкций АО «ВНИИ Галургии»; 614990, Россия, г. Пермь, Комсомольский проспект, д. 29;
тел./факс: +7 (342) 2-198-361;
E-mail: vodyannikov@mail.ru.

Кашеварова Галина Геннадьевна, член-корреспондент Российской академии архитектуры и строительных наук (РААСН), доктор технических наук, профессор, заведующая кафедрой «Строительные конструкции и вычислительная механика» Пермского национального исследовательского политехнического университета; 614010, Россия, г. Пермь, ул. Куйбышева, 109;
тел. +7(342) 219-83-61; e-mail: ggkash@mail.ru.

Старобогатов Данил И., профессор Durham College, Ontario, Canada; 1610 Champlain Avenue Whitby, ON, Canada L1N 6A7; e-mail: dstarobogatov@gmail.com.

DOI:10.22337/2587-9618-2020-16-2-113-129

ANALYSIS OF NONLINEAR FORCED VIBRATIONS OF FRACTIONALLY DAMPED SUSPENSION BRIDGES SUBJECTED TO THE ONE-TO-ONE INTERNAL RESONANCE

Marina V. Shitikova[1,2], Aleks L. Katembo[1]
[1]Voronezh State Technical University, Voronezh, RUSSIA
[2] Research Institute of Structural Physics of the Russian Academy of Architecture and Construction Sciences, Moscow, RUSSIA

Abstract: Nonlinear force driven coupled vertical and torsional vibrations of suspension bridges, when the frequency of an external force is approaching one of the natural frequencies of the suspension system, which, in its turn, undergoes the conditions of the one-to-one internal resonance, are investigated. The method of multiple time scales is used as the method of solution. The damping features are described by the fractional derivative, which is interpreted as the fractional power of the differentiation operator. The influence of the fractional parameters (orders of fractional derivatives) on the motion of the suspension bridge is investigated.

Keywords: suspension bridge, nonlinear force driven vibrations, fractional damping, generalized method of multiple time scales

АНАЛИЗ ВЫНУЖДЕННЫХ НЕЛИНЕЙНЫХ КОЛЕБАНИЙ ВИСЯЧИХ МОСТОВ ПРИ НАЛИЧИИ ВНУТРЕННЕГО РЕЗОНАНСА ОДИН-К-ОДНОМУ С ПОМОЩЬЮ ПРОИЗВОДНЫХ ДРОБНОГО ПОРЯДКА

М.В. Шитикова[1,2], А.Л. Катембо[1]
[1] Воронежский государственный технический университет, г. Воронеж, РОССИЯ
[2] Научно-исследовательский институт строительной физики
Российской академии архитектуры и строительных наук, г. Москва, РОССИЯ

Аннотация: Исследуются нелинейные вынужденные изгибно-крутильные колебания висячего моста при наличии внутреннего резонанса один-к-одному в случае, когда частота возмущающей силы близка одной из собственных частот колебаний. В качестве метода решения используется обобщенный метод многих временных масштабов. Силы демпфирования описываются при помощи производной дробного порядка, которая интерпретируется как дробная степень оператора дифференцирования. Проанализировано влияние париметра дробности на колебания висячего моста.

Ключевые слова: висячий мост, нелинейные вынужденные колебания, демпфирование с помощью дробной производной, обобщенный метод многих временных масштабов

1. INTRODUCTION

The suspension bridges are unique building structures, as they allow one not only to cover large spans, but also are economically viable. Compared to other types of bridges, suspension bridges have a number of technical and aesthetic advantages, that is why they are so widely used in the modern world. The history of suspension bridges met with the largest catastrophe in bridge construction - the collapse of the bridge over the Tacoma River (USA) in 1940 (Tacoma Narrows Bridge). In flexible suspension bridges under the action of various dynamic loads, such as moving load or wind, strong bending-torsional vibrations could occur, sometimes resulting in extremely large amplitudes complicating the normal operation of the bridge, and sometimes causing its destruction. Due to the low damping ability of the suspension bridges, the oscillations could be accompanied by the transfer of energy between different modes of vibrations for a long time even after unloading, which was the cause of their occurrence. This is explained by the phenomenon of internal resonance, when one of the frequencies of free bending vibrations is close in value to one of the natural frequencies of torsional vibrations, which in practice can occur quite often due to the density of the spectrum of the natural frequencies of suspension bridges, which largely depend on the geometric parameters of the bridge.

To analyze the phenomena of the internal resonance during dynamic response of suspension bridges, different mathematical models have been utilized. Thus, the continuous model proposed in [1] has been used in [2-6] to solve the system of nonlinear differential equations describing the dynamics of suspension bridges under one-to-one [2-6] and two-to-one [3-5] internal resonances by means of the multiple time scales perturbation technique [7]. The state-of-the-art survey of the internal phenomena in suspension bridges was made by Shitikova and Rossikhin [8] in their plenary lecture at the 5th European Conference of Civil Engineering held in Florence, Italy in 2014. During this report, the authors passed aloud their opinion that the reason of failure of the Tacoma Narrows Bridge was connected with the internal resonance between vertical and torsional vibrations.

This idea was repeated a year later, in 2015, by Arioli and Gazzola [9], who trying to explain why did torsional oscillations suddenly appears before the Tacoma Narrows collapse found out that vertical oscillations had become large enough and switched to torsional ones. The four-degree-of-freedom model accounting for both the flexural-torsional motion of the bridge deck and for the transversal motion of a pair of hangers has been considered in [10], and the internal resonance between the modes of deck and hangers vibrations has been studied. Stability of dynamic response of suspension bridges with due account for the phenomenon of the internal resonance has been considered in [11]. The generation of the force induced internal resonance was recorded during repairs connected with the retrofit of suspension bridges in the U.S.A. [12].

Thus, the potential occurrence of internal resonance phenomena has been identified as the potential cause of critical dynamic states in long-span suspension bridges. Therefore, the task of studying the internal resonance in suspension bridges is very relevant and important.

The first field observations of the vibrations of the Golden Gate suspension bridge were made in the period from 1933 to 1942, when seismological instruments were installed on the piers, towers and cables to measure any vibration that might occur [13]. After the failure of the Tacoma Narrows Bridge in 1940, it was decided to install ten instruments for measuring the vertical movement of the bridge, which worked continuously until 1954. Vincent [14-16] analyzed these recordings of observations of the Golden Gate Bridge vibrations, and the field observations of this bridge were further continued to [17-20]. Thus, the experimental data obtained in [20] showed that different vibrational modes feature different amplitude damping coefficients, and the order of smallness of these coefficients tells about low damping capacity of suspension combined systems, resulting in prolonged energy transfer from one partial subsystem to another. However, the analytical model described in [2] with its further extension in [3,4] allows one to analyze only free undamped vibrations of suspension bridges.

Nonlinear free damped vibrations of suspension bridges in the cases of the one-to-one internal resonance, when the natural frequency of a certain mode of vertical vibrations is close to the natural frequency of a certain mode of torsional vibrations, and the two-to-one internal resonance, when one natural frequency is nearly twice as large as another natural frequency, have been examined in [5] when damping features of the system are prescribed by the first derivative of the displacement with respect to time. It has been shown that for the both types of the internal resonance the damping coefficient does not depend on the natural frequency of vibrations, but this result is in conflict with the experimental data presented in [20] and [21].

To lead the theoretical investigations in line with the experiment, fractional derivatives were introduced in [22] for describing the processes of internal friction occurring in suspension combined systems at nonlinear free vibrations. The nonlinear suspension bridge model put forward allows one to obtain the damping coefficient dependent on the natural frequency of vibrations.

The overview of the existing research of the internal resonance in suspension bridges could be found in [23,24].

In the present paper, the model proposed in [22] for the analysis of free damped vibrations is generalized to the case of nonlinear forced vibrations of suspension bridges, when the frequency of the external force is close to one of the natural frequencies of the vertical vibrations of the suspension combined system, which is subjected to the condition of the one-to-one internal resonance.

2. PROBLEM FORMULATION

To analyze the forced damped vibrations of suspension bridges we will use its classical scheme involving a bisymmetrical thin-walled stiffening girder connected with two suspended cables by virtue of vertical suspensions [25]. The cables are thrown over the pilons and are tensioned by anchor mechanisms. The suspensions are considered as inextensible and uniformly distributed along the stiffening girder. The cables are parabolic, and the contour of the girder's cross-section is underformable. It is assumed that the girder's contour translates as a rigid body vertically (in the y-axis direction) on the value of $\eta(z,t)$ and rotates with respect to the girder's axis (the z-axis) through the angle of $\varphi(z,t)$ (Fig. 1). The origin of the frame of references is in the center of gravity of the cross section.

It is known for suspension bridges [2-4] that some natural modes belonging to different types of vibrations could be coupled with each other, i.e., the excitation of one natural mode gives rise to another one. Two modes interact more often that not, although the possibility for interaction of a greater number of modes is not ruled out.

Below it would be considered the case when only two modes predominate in the vibrational process, namely: the vertical n-th mode with linear natural frequency ω_{0n}, and the torsional m-th mode with the natural frequency Ω_{0m}.

Under such an assumption the functions $\eta(z,t)$ and $\varphi(z,t)$ could be approximately defined as (using the eigenbase of the associated linear undamped unforced problem)

$$\begin{aligned}\eta(z,t) &\sim v_n(z)x_{1n}(t),\\ \varphi(z,t) &\sim \Theta_m(z)x_{2m}(t),\end{aligned} \tag{1}$$

where $x_{1n}(t)$ and $x_{2m}(t)$ are the generalized displacements, and $v_n(z)$ and $\Theta_m(z)$ are natural shapes of the two interacting modes of vibrations.

When the harmonic force $F=\hat{F}\cos(\omega_F t)$ is applied at the center of the suspension bridge, then the equations of its forced vibrations are written in the dimensionless form as (what is the immediate generalization of the approach proposed in [22] by adding the external vertical excitation with amplitude $\hat{F}=const$ and frequency ω_F)

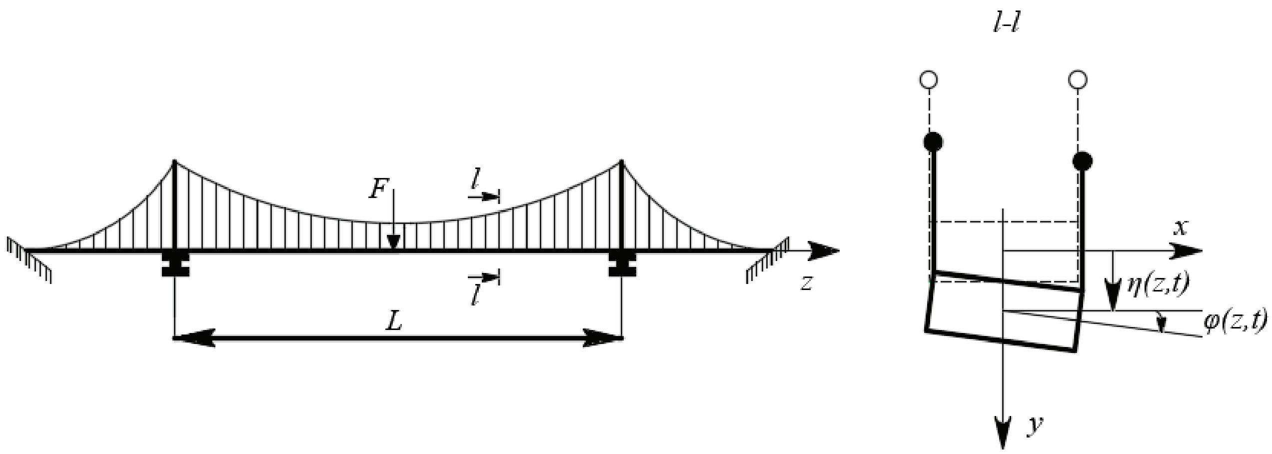

Figure 1. Scheme of a suspension bridge.

$$\ddot{x}_{1n} + \omega_{0n}^2 x_{1n} + \beta D_{0+}^{\gamma} x_{1n} + a_{11}^{n} x_{1n}^2 + a_{22}^{nm} x_{2m}^2 + (b_{11}^{n} x_{1n}^2 + b_{22}^{nm} x_{2m}^2) x_{1n} = \hat{F}\cos(\omega_F t), \tag{2a}$$

$$\ddot{x}_{2m} + \Omega_{0m}^2 x_{2m} + \beta D_{0+}^{\gamma} x_{2m} + a_{12}^{nm} x_{1n} x_{2m} + (c_{11}^{nm} x_{1n}^2 + c_{22}^{m} x_{2m}^2) x_{2m} = 0, \tag{2b}$$

where a_{ij}, b_{ii}, and c_{ii} ($i=1,2$, $j=2$) are certain dimensionless coefficients which are defined in [2,22] (subsequently the indices n and m are omitted for ease of presentation), dots denote differentiation with respect to time, the terms $\beta D_{0+}^{\gamma_1} x_1$ and $\beta D_{0+}^{\gamma_2} x_2$ characterize inelastic reaction of the system, β is the viscosity coefficient, the fractional derivative $D_{0+}^{\gamma} x$ ($\gamma = \gamma_1$ or γ_2) is defined as follows [26]

$$D_{0+}^{\gamma} x = \frac{d}{dt}\int_0^t \frac{x(t-t')dt'}{\Gamma(1-\gamma)t'^{\gamma}} \quad (0<\gamma\le 1), \tag{3}$$

γ is the order of the fractional derivative (fractional parameter), and $\Gamma(1-\gamma)$ is the Gamma-function.

Let us consider the case of the one-to-one internal resonance, as well as suppose that the frequency of the external force is close to the natural frequency of the interacting modes, i.e.,

$$\omega_0 \approx \Omega_0 \approx \omega_F. \tag{4}$$

Note that the influence of the detuning parameter characterizing the small difference in magnitudes of the natural frequencies ω_0 and Ω_0 has been investigated in [4,6,24].

Since for finding the solution of equations (2) we will use the method of multiple time scales, where the functions $e^{\pm i\omega t}$ are utilized as the main harmonic functions, then in order to carry out the calculations the following formulas will be utilized [27]

$$D_{0+}^{\gamma} e^{\pm i\omega t} = D_{+}^{\gamma} e^{\pm i\omega t} + \frac{\sin \pi\gamma}{\pi}\int_0^{\infty} \frac{u^{\gamma} e^{-ut} du}{u \pm i\omega}, \tag{5}$$

$$D_{+}^{\gamma} e^{\pm i\omega t} = (\pm i\omega)^{\gamma} e^{\pm i\omega t}, \tag{6}$$

where D_{+}^{γ} is obtained from (3) changing the low limit to $-\infty$.

It has been shown in [28] and [29] that the second term in formula (5) does not produce secular terms in the method of multiple time scales under the limitation of the zero- and first-order approximations. In other words, this term could be neglected in further consideration, and it is possible to use the approximate formula

$$D_{0+}^{\gamma} e^{\pm i\omega t} \approx D_{+}^{\gamma} e^{\pm i\omega t}. \tag{7}$$

If we take into account formula (5.82) from [26]

$$D_{+}^{\gamma}e^{\pm i\omega t}=\left(\frac{d}{dt}\right)^{\gamma}e^{\pm i\omega t}, \tag{8}$$

then from the combination of (7) and (8) it follows the relationship

$$D_{0+}^{\gamma}e^{\pm i\omega t}\approx\left(\frac{d}{dt}\right)^{\gamma}e^{\pm i\omega t}, \tag{9}$$

which will be used in further calculations.

3. METHOD OF SOLUTION

We will seek the solution for two cases:

(1) $\beta=\varepsilon\mu$ and that $\hat{F}=\varepsilon^2 f$,

and

(2) $\beta=\varepsilon^2\mu$ and that $\hat{F}=\varepsilon^3 f$,

where a small parameter ε is introduced as a bookkeeping device to indicate the smallness of terms [7].

In these cases, an approximate solution of equations (2) for small amplitudes weakly varying with time can be represented by an expansion in terms of different time scales

$$\begin{aligned}
x_1(t)&=\varepsilon x_{11}(T_0,T_1,T_2)+\varepsilon^2 x_{12}(T_0,T_1,T_2)+\\
&+\varepsilon^3 x_{13}(T_0,T_1,T_2)+\ldots,\\
x_2(t)&=\varepsilon x_{21}(T_0,T_1,T_2)+\varepsilon^2 x_{22}(T_0,T_1,T_2)+\\
&+\varepsilon^3 x_{23}(T_0,T_1,T_2)+\ldots,
\end{aligned} \tag{10}$$

where

$$T_n=\varepsilon^n t \ (n=0,1,2)$$

are new independent variables, ε is a small parameter which is of the same order of magnitude as the amplitudes, and μ and f are finite values. Here, $T_0=t$ is a fast scale, characterizing motions with the natural frequencies ω_0 and Ω_0, while

$$T_1=\varepsilon t \ \text{ and } \ T_2=\varepsilon^2 t$$

are slow scales, characterizing the modulations of the amplitudes and phases.

Considering that [7]

$$\begin{aligned}
d/dt&=D_0+\varepsilon D_1+\varepsilon^2 D_2,\\
d^2/dt^2&=D_0^2+2\varepsilon D_0D_1+\varepsilon^2(D_1^2+2D_0D_2),
\end{aligned} \tag{11}$$

as well as applying the expansion of the fractional derivative as it was suggested in Rossikhina and Shitikova [22]

$$\begin{aligned}
(d/dt)^{\gamma}&=(D_0+\varepsilon D_1+\varepsilon^2 D_2+\ldots)^{\gamma}=\\
&=D_{+}^{\gamma}+\varepsilon\gamma D_{+}^{\gamma-1}D_1+\frac{1}{2}\varepsilon^2\gamma(\gamma-1)D_{+}^{\gamma-2}D_1^2\ldots
\end{aligned} \tag{12}$$

where $D_n=\partial/\partial T_n$,

$$D_{+}^{\gamma-n}x=\frac{d}{dt}\int_{-\infty}^{t}\frac{x(t-t')dt'}{\Gamma(1-\gamma+n)t'^{\gamma-n}} \quad (n=0,1,2)$$

substituting (10) into (2), and equating the coefficients at like powers of ε to zero, we obtain

to order ε:

$$\begin{aligned}
D_0^2x_{11}+\omega_0^2x_{11}&=0,\\
D_0^2x_{21}+\Omega_0^2x_{21}&=0;
\end{aligned} \tag{13}$$

to order ε^2:

$$\begin{aligned}
D_0^2x_{12}+\omega_0^2x_{12}&=-2D_0D_1x_{11}-\mu(2-k)D_{+}^{\gamma}x_{11}-\\
&-a_{11}x_{11}^2-a_{22}x_{21}^2+(2-k)f\cos(\omega_0T_0),
\end{aligned} \tag{14}$$

$$\begin{aligned}
D_0^2x_{22}+\Omega_0^2x_{22}&=-2D_0D_1x_{21}-\mu(2-k)D_{+}^{\gamma}x_{21}-\\
&-a_{12}x_{11}x_{21};
\end{aligned}$$

to order ε^3:

$$
\begin{aligned}
&D_0^2 x_{13} + \omega_0^2 x_{13} = -2D_0 D_1 x_{12} - (D_1^2 + 2D_0 D_2) x_{11} - \\
&-\mu(2-k) D_+^\gamma x_{12} - \mu(2-k)\gamma D_+^{\gamma-1} D_1 x_{11} - \\
&-\mu(k-1) D_+^\gamma x_{11} - 2a_{11} x_{11} x_{12} - 2a_{22} x_{21} x_{22} - \\
&-b_{11} x_{11}^3 - b_{22} x_{21}^2 x_{11} + (k-1) f \cos(\omega_0 T_0), \qquad (15)\\
&D_0^2 x_{23} + \Omega_0^2 x_{23} = -2D_0 D_1 x_{22} - (D_1^2 + 2D_0 D_2) x_{21} - \\
&-\mu(2-k) D_+^\gamma x_{22} - \mu(2-k)\gamma D_+^{\gamma-1} D_1 x_{21} - \\
&-\mu(k-1) D_+^\gamma x_{21} - a_{12}(x_{11} x_{22} + x_{12} x_{21}) - \\
&-c_{11} x_{11}^2 x_{21} - c_{22} x_{21}^3.
\end{aligned}
$$

At $k=1$ and $k=2$, we obtain governing equations for the first and second cases, respectively.
Integrating equations (13) yields

$$
\begin{aligned}
x_{11} &= A_1(T_1, T_2) e^{i\omega_0 T_0} + \bar{A}_1(T_1, T_2) e^{-i\omega_0 T}, \\
x_{21} &= A_2(T_1, T_2) e^{i\Omega_0 T_0} + \bar{A}_2(T_1, T_2) e^{-i\Omega_0 T_0},
\end{aligned} \qquad (16)
$$

where A_1 and A_2 are unknown complex functions, and $\bar{A}_1$ and $\bar{A}_2$ are the complex conjugates of A_1 and A_2, respectively.
In order to integrate the sets of equations (14) and (15), it is necessary to consider each case separately.

3.1.The case $k=1$

Substituting (19) in equations (18) and integrating, we obtain the expressions for x_{12} and x_{22}. Then substituting found x_{12} and x_{22} in equations (15) and using the standard procedure for eliminating the secular terms, we have

$$
\begin{aligned}
&D_2 a_1 + \left[\frac{1}{8} \mu^2 (i\omega_0)^{2\gamma-3} (1-2\gamma) + \right. \\
&\left. + \frac{1}{4} i \frac{f^2 (a_{11}^2 - 3b_{11})}{\mu^2 \omega_0^{2\gamma+1}} e^{-2\pi i \gamma} \right] a_1 = 0,
\end{aligned} \qquad (20)
$$

$$
\begin{aligned}
&D_2 a_2 + \left[\frac{1}{8} \mu^2 (i\omega_0)^{2\gamma-3} (1-2\gamma) + \right. \\
&\left. + \frac{1}{4} i \frac{f^2 (a_{11} a_{12} - 2c_{11} - \frac{1}{3} a_{12}^2 \omega_0^{-2})}{\mu^2 \omega_0^{2\gamma+1}} e^{-2\pi i \gamma} \right] a_2 = 0.
\end{aligned}
$$

Now let us substitute (16) into the right-hand sides of equations (14) putting there $k=1$, then gather all terms standing at $e^{i\omega_0 T_0}$ and $e^{-i\omega_0 T_0}$ with due account for (4) and vanish them in order to exclude secular terms. As a result we obtain

$$
\begin{aligned}
&D_1 A_1 + \frac{1}{2} \mu (i\omega_0)^{\gamma-1} A_1 - \frac{f}{4i\omega_0} = 0, \\
&D_1 A_2 + \frac{1}{2} \mu (i\omega_0)^{\gamma-1} A_2 = 0,
\end{aligned} \qquad (17)
$$

$$
\begin{aligned}
&D_0^2 x_{12} + \omega_0^2 x_{12} = -\left(a_{11} A_1^2 + a_{22} A_2^2 \right) e^{2i\omega_0 T_0} - \\
&-a_{11} A_1 \bar{A}_1 - a_{22} A_2 \bar{A}_2 + cc, \\
&D_0^2 x_{22} + \omega_0^2 x_{22} = -a_{12} A_1 A_2 e^{2i\omega_0 T_0} - \\
&-a_{12} A_1 \bar{A}_2 + cc,
\end{aligned} \qquad (18)
$$

where cc is the complex conjugate part to the preceding terms.
Integrating equations (17), we find

$$
A_1(T_1, T_2) = a_1(T_2) \exp\left[-\frac{1}{2} \mu (i\omega_0)^{\gamma-1} T_1 \right] + \frac{f}{2\mu (i\omega_0)^\gamma}, \qquad (19a)
$$

$$
A_2(T_1, T_2) = a_2(T_2) \exp\left[-\frac{1}{2} \mu (i\omega_0)^{\gamma-1} T_1 \right]. \qquad (19b)
$$

Integrating equations (20) yields

$$a_1 = a_1^0 \exp\left\{T_2\left[-\frac{1}{8}\mu^2(1-2\gamma)(i\omega_0)^{2\gamma-2} - -\frac{1}{4}\frac{f^2(a_{11}^2-3b_{11})}{\mu^2\omega_0^{2\gamma+1}}(i\cos 2\pi\gamma+\sin 2\pi\gamma)\right]\right\}, \quad (21a)$$

$$a_2 = a_2^0 \exp\left\{T_2\left[-\frac{1}{8}\mu^2(1-2\gamma)(i\omega_0)^{2\gamma-3} - -\frac{1}{4}\frac{f^2\left(a_{11}a_{12}-2c_{11}-\frac{1}{3}a_{12}^2\omega_0^{-2}\right)}{\mu^2\omega_0^{2\gamma+1}}\times \times\left(i\cos 2\pi\gamma+\sin 2\pi\gamma\right)\right]\right\}, \quad (21b)$$

where a_1^0 and a_2^0 are arbitrary constants.

Considering formulas (10), (16), (19), and (21), we finally obtain

$$x_1 = \varepsilon\left[2a_1^0 e^{-\alpha_1 t}\cos\Omega_1 t + +\frac{f}{\mu\omega_0^\gamma}\cos\left(\omega_0 t - \frac{\pi}{2}\gamma\right)\right] + O(\varepsilon^2), \quad (22a)$$

$$x_2 = \varepsilon 2a_2^0 e^{-\alpha_2 t}\cos\Omega_2 t + O(\varepsilon^2), \quad (22b)$$

where

$$\alpha_1 = \frac{1}{2}\varepsilon\mu\omega_0^{\gamma-1}\sin\left(\frac{\pi\gamma}{2}\right)\times \times\left[1+\frac{1}{2}\varepsilon\mu(2\gamma-1)\omega_0^{\gamma-2}\cos\left(\frac{\pi\gamma}{2}\right)\right] - -\frac{1}{4}\varepsilon^2\frac{f^2(a_{11}^2-3b_{11})}{\mu^2\omega_0^{2\gamma+1}}\sin(2\pi\gamma),$$

$$\Omega_1 = \omega_0\left[1+\frac{1}{2}\varepsilon\mu\omega_0^{\gamma-2}\cos\left(\frac{\pi\gamma}{2}\right)+ +\frac{1}{8}\varepsilon^2\mu^2(2\gamma-1)\omega_0^{2(\gamma-2)}\cos(\pi\gamma) - -\frac{1}{4}\varepsilon^2\frac{f^2(a_{11}^2-3b_{11})}{\mu^2\omega_0^{2(\gamma+1)}}\cos(2\pi\gamma)\right],$$

$$\alpha_2 = \frac{1}{2}\varepsilon\mu\omega_0^{\gamma-1}\sin\left(\frac{\pi\gamma}{2}\right)\times \times\left[1+\frac{1}{2}\varepsilon\mu(2\gamma-1)\omega_0^{\gamma-2}\cos\left(\frac{\pi\gamma}{2}\right)\right] - -\frac{1}{4}\varepsilon^2\frac{f^2(a_{11}a_{12}-2c_{11}-a_{12}^2\omega_0^{-2}/3)}{\mu^2\omega_0^{2\gamma+1}}\sin(2\pi\gamma),$$

$$\Omega_2 = \omega_0\left[1+\frac{1}{2}\varepsilon\mu\omega_0^{\gamma-2}\cos\left(\frac{\pi\gamma}{2}\right)+ +\frac{1}{8}\varepsilon^2\mu^2(2\gamma-1)\omega_0^{2(\gamma-2)}\cos(\pi\gamma) - -\frac{1}{4}\varepsilon^2\frac{f^2(a_{11}a_{12}-2c_{11}-a_{12}^2\omega_0^{-2}/3)}{\mu^2\omega_0^{2(\gamma+1)}}\cos(2\pi\gamma)\right].$$

Reference to the found analytical solution (22) shows that it involves two parts: the first corresponds to the damping vibrations with damping coefficients and nonlinear frequencies dependent on the fractional parameters and describes the transient process, while the second one is nondamping in character and describes forced vibrations with the frequency of the exciting force and with the phase difference depending on the fractional parameter.

3.2.The case $k=2$

Let us substitute relations (16) in the right-hand parts of equations (14) at $k=2$. Eliminating secular terms and integrating the equations obtained, we have

$$D_1A_1 = D_1A_2 = 0, \quad (23)$$

$$x_{12} = \frac{a_{11}}{3\omega_0^2}A_1^2e^{2i\omega_0T_0} + \frac{a_{22}}{3\omega_0^2}A_2^2e^{2i\omega_0T_0} - -\left(a_{11}A_1\bar{A}_1 + a_{22}A_2\bar{A}_2\right)\omega_0^2 + cc, \quad (24a)$$

$$x_{22} = \frac{a_{12}}{3\omega_0^2}A_1A_2e^{2i\omega_0T_0} - \frac{a_{12}}{\omega_0^2}A_1\bar{A}_2 + cc. \quad (24b)$$

From (23) it follows that the functions A_1 and A_2 are T_1-independent.

Substituting then (16) and (24) in equations (15) and utilizing the standard procedure for eliminating secular terms, we obtain

$$-iD_2A_1-\frac{1}{2}\mu\omega_0^{-1}(i\omega_0)^{\gamma}A_1-\lambda_1A_1^2\overline{A}_1- \\ -\lambda_2A_1A_2\overline{A}_2+\frac{1}{4}\Gamma_1\overline{A}_1A_2^2+\frac{1}{4}\frac{f}{\omega_0}=0, \qquad (25a)$$

$$-iD_2A_2-\frac{1}{2}\mu\omega_0^{-1}(i\omega_0)^{\gamma}A_2-\lambda_3A_1\overline{A}_1A_2- \\ -\lambda_4A_2^2\overline{A}_2+\frac{1}{4}\Gamma_2A_1^2\overline{A}_2=0, \qquad (25b)$$

where coefficients λ_i and Γ_j ($i=1,2,3,4$ and $j=1,2$) are presented in [2,4].

Now we multiply (25a) and (25b) by $\overline{A}_1$ and $\overline{A}_2$, respectively, and find their complex conjugates. Adding every pair of the mutually adjoint equations and subtracting one from another, and after all manipulations representing the functions A_1 and A_2 in their polar form, i.e.,

$$A_1(T_2)=a_1(T_2)\exp\left[i\varphi_1(T_2)\right], \\ A_2(T_2)=a_2(T_2)\exp\left[i\varphi_2(T_2)\right],$$

as a result we obtain the modulation equations

$$\dot{a}_1+\frac{1}{2}\mu\omega_0^{\gamma-1}\sin\left(\frac{1}{2}\pi\gamma\right)a_1-\frac{1}{4}\Gamma_1a_1a_2^2\sin\delta+ \\ +\frac{1}{4}f\omega_0^{-1}\sin\varphi_1=0, \qquad (26a)$$

$$\dot{a}_2+\frac{1}{2}\mu\Omega_0^{\gamma-1}\sin\left(\frac{1}{2}\pi\gamma\right)a_2+ \\ +\frac{1}{4}\Gamma_2a_1^2a_2\sin\delta=0, \qquad (26b)$$

$$\dot{\varphi}_1-\frac{1}{2}\mu\omega_0^{\gamma-1}\cos\left(\frac{1}{2}\pi\gamma\right)-\lambda_1a_1^2-\lambda_2a_2^2+ \\ +\frac{1}{4}\Gamma_1a_2^2\cos\delta+\frac{1}{4}f\omega_0^{-1}a_1^{-1}\cos\varphi_1=0, \qquad (26c)$$

$$\dot{\varphi}_2-\frac{1}{2}\mu\Omega_0^{\gamma-1}\cos\left(\frac{1}{2}\pi\gamma\right)-\lambda_3a_1^2-\lambda_4a_2^2+ \\ +\frac{1}{4}\Gamma_2a_1^2\cos\delta=0, \qquad (26d)$$

where

$$\delta=2(\varphi_2-\varphi_1)$$

is the phase difference, and a dot denotes differentiation with respect to T_2.

The set of differential equations (26) subjected to the initial conditions competely describes the modulations of amplitude and phases of forced damped vibrations. An approximate analytical solution of equations (26) could be found by the method of successive approximations.

As the initial approximation, let us consider the solution of the homogeneous part of equations (26):

$$\dot{a}_1+\frac{1}{2}\mu\omega_0^{\gamma_1-1}\sin\left(\frac{1}{2}\pi\gamma_1\right)a_1=0, \\ \dot{a}_2+\frac{1}{2}\mu\Omega_0^{\gamma_2-1}\sin\left(\frac{1}{2}\pi\gamma_2\right)a_2=0, \\ \dot{\varphi}_1-\frac{1}{2}\mu\omega_0^{\gamma_1-1}\cos\left(\frac{1}{2}\pi\gamma_1\right)-\sigma_1=0, \\ \dot{\varphi}_2-\frac{1}{2}\mu\Omega_0^{\gamma_2-1}\cos\left(\frac{1}{2}\pi\gamma_2\right)-(\sigma_1-\sigma)=0, \qquad (27)$$

which has the form

$$a_1=a_{10}e^{-S_1T_2},\quad a_2=a_{20}e^{-S_2T_2}, \\ \varphi_1=S_3T_2+\varphi_{10},\quad \varphi_2=S_4T_2+\varphi_{20}, \qquad (28)$$

where a_{i0} and φ_{i0} (i=1,2) are, respectively, the initial values of amplitudes and phases to be found from the initial conditions,

$$\delta_0=2(\varphi_{20}-\varphi_{10})$$

is the initial phase difference, and

$$
\begin{aligned}
S_1 &= \frac{1}{2}\mu\omega_0^{\gamma-1}\sin\left(\frac{1}{2}\pi\gamma\right),\\
S_2 &= \frac{1}{2}\mu\Omega_0^{\gamma-1}\sin\left(\frac{1}{2}\pi\gamma\right),\\
S_3 &= \frac{1}{2}\mu\omega_0^{\gamma-1}\cos\left(\frac{1}{2}\pi\gamma\right),\\
S_4 &= \frac{1}{2}\mu\Omega_0^{\gamma-1}\cos\left(\frac{1}{2}\pi\gamma\right).
\end{aligned} \tag{29}
$$

Now substituting (28) in equations (26) yields

$$
\begin{aligned}
&\dot{a}_1 + S_1 a_1 = \frac{1}{4}\Gamma_1 a_{10} e^{-(S_1+2S_2)T_2} a_{20}^2 \sin(\Sigma T_2 + \delta_0) -\\
&-\frac{1}{4}F\omega_0^{-1}\sin(S_3T_2+\varphi_{10}),\\
&\dot{a}_2 + S_2 a_2 = -\frac{1}{4}\Gamma_2 a_{10}^2 e^{-(2S_1+S_2)T_2} a_{20}\sin(\Sigma T_2+\delta_0),\\
&\dot{\varphi}_1 - S_3 = \lambda_1 a_{10}^2 e^{-2S_1T_2} + \lambda_2 a_{20}^2 e^{-2S_2T_2} -\\
&-\frac{1}{4}\Gamma_1 a_{20}^2 e^{-2S_2T_2}\cos(\Sigma T_2+\delta_0) -\\
&-\frac{1}{4}F\omega_0^{-1}a_{10}^{-1}e^{S_1T_2}\cos(S_3T_2+\varphi_{10}),\\
&\dot{\varphi}_2 - S_4 = \lambda_3 a_{10}^2 e^{-2S_1T_2} + \lambda_4 a_{20}^2 e^{-2S_2T_2} -\\
&-\frac{1}{4}\Gamma_2 a_{10}^2 e^{-2S_1T_2}\cos(\Sigma T_2+\delta_0),
\end{aligned} \tag{30}
$$

where $\Sigma = 2(S_4 - S_3)$.

To solve the first two equations in (30), we will use the method of variation of arbitrary functions, and assume the proposed solution in the form

$$
\begin{aligned}
a_1(T_2) &= C_1(T_2)e^{-S_1T_2},\\
a_2(T_2) &= C_2(T_2)e^{-S_2T_2},
\end{aligned} \tag{31}
$$

where $C_1(T_2)$ and $C_2(T_2)$ are arbitrary functions to be found.

Substituting the proposed solution (31) in equations (30) yields

$$
\begin{aligned}
&\dot{C}_1(T_2) = \frac{1}{4}\Gamma_1 a_{10}a_{20}^2 e^{-2S_2T_2}\sin(\Sigma T_2+\delta_0) -\\
&-\frac{1}{4}F\omega_0^{-1}e^{S_1T_2}\sin(S_3T_2+\varphi_{10}),\\
&\dot{C}_2(T_2) = -\frac{1}{4}\Gamma_2 a_{10}^2 a_{20} e^{-2S_1T_2}\sin(\Sigma T_2+\delta_0).
\end{aligned} \tag{32}
$$

Integrating equations (32), we have

$$
\begin{aligned}
&C_1(T_2) = -\frac{1}{4}\Gamma_1 a_{10}a_{20}^2\left[2S_2\sin(\Sigma T_2+\delta_0)+\right.\\
&\left.+\Sigma\cos(\Sigma T_2+\delta_0)\right]\left(4S_2^{\,2}+\Sigma^2\right)^{-1}e^{-2S_2T_2} -\\
&-\frac{F}{4\omega_0}\left[S_1\sin(S_3T_2+\varphi_{10})-\right.\\
&\left.-S_3\cos(S_3T_2+\varphi_{10})\right]\left(S_1^2+S_3^2\right)^{-1}e^{S_1T_2}+C_{10},\\
&C_2(T_2) = \frac{1}{4}\Gamma_2 a_{10}^2 a_{20}\left[2S_1\sin(\Sigma T_2+\delta_0)+\right.\\
&\left.+\Sigma\cos(\Sigma T_2+\delta_0)\right]\left(4S_1^{\,2}+\Sigma^2\right)^{-1}e^{-2S_1T_2}+C_{20},
\end{aligned} \tag{33}
$$

where C_{10} and C_{20} are constants of integration.

Considering relationships (33), the amplitude functions take the form

$$
\begin{aligned}
&a_1 = a_{10}e^{-S_1T_2} - \frac{1}{4}\Gamma_1 a_{10}a_{20}^2\left[2S_2\sin(\Sigma T_2+\delta_0)+\right.\\
&\left.+\Sigma\cos(\Sigma T_2+\delta_0)\right]\left(4S_2^{\,2}+\Sigma^2\right)^{-1}e^{-(S_1+2S_2)T_2} -\\
&-\frac{F}{4\omega_0}\left[S_1\sin(S_3T_2+\varphi_{10})-\right.\\
&\left.-S_3\cos(S_3T_2+\varphi_{10})\right]\left(S_1^2+S_3^2\right)^{-1}e^{S_1T_2}+C_{10}e^{-S_1T_2},\\
&a_2 = a_{20}e^{-S_2T_2} + \frac{1}{4}\Gamma_2 a_{10}^2 a_{20}\left[2S_1\sin(\Sigma T_2+\delta_0)+\right.\\
&\left.+\Sigma\cos(\Sigma T_2+\delta_0)\right]\left(4S_1^{\,2}+\Sigma^2\right)^{-1}e^{-(2S_1+S_2)T_2}+C_{20}e^{-S_2T_2}.
\end{aligned} \tag{34}
$$

Integrating the third and fourth equations in (30), we obtain the T_2-functions of the phases of vibration

$$\varphi_1 = S_3T_2 + \varphi_{10} - \frac{\lambda_1 a_{10}^2}{2S_1} e^{-2S_1T_2} - \frac{\lambda_2 a_{20}^2}{2S_2} e^{-2S_2T_2} +$$
$$+\frac{1}{4}\Gamma_1 a_{20}^2 \frac{2S_2\cos(\Sigma T_2+\delta_0)+\Sigma\sin(\Sigma T_2+\delta_0)}{4S_2^{\ 2}+\Sigma^2} e^{-2S_2T_2} -$$
$$-\frac{1}{4}\frac{Fa_{10}^{-1}}{\omega_0}\frac{S_1\cos(S_3T_2+\varphi_{10})+S_3\sin(S_3T_2+\varphi_{10})}{S_1^2+S_3^2} e^{S_1T_2} +$$
$$+C_{30}, \tag{35}$$
$$\varphi_2 = S_4T_2 + \varphi_{20} - \frac{\lambda_3 a_{10}^2}{2S_1} e^{-2S_1T_2} - \frac{\lambda_4 a_{20}^2}{2S_2} e^{-2S_2T_2} +$$
$$+\frac{1}{4}\Gamma_2 a_{10}^2 \frac{2S_1\cos(\Sigma T_2+\delta_0)+\Sigma\sin(\Sigma T_2+\delta_0)}{4S_1^{\ 2}+\Sigma^2} e^{-2S_1T_2} +$$
$$+C_{40},$$

where C_{30} and C_{40} are constants of integration to be determined from the initial conditions.
Since the general solution of the system under consideration is the sum of the particular solution of the inhomogeneous set of equations and the general solution of the corresponding homogeneous system, then the arbitrary constants could be chosen in such a way that the initial conditions of all successive approximations would be zero. Thus, for the first approximation the constants to be found take the form

$$C_{10} = \frac{1}{4}\Gamma_1 a_{10} a_{20}^2 \frac{2S_2\sin\delta_0+\Sigma\cos\delta_0}{4S_2^{\ 2}+\Sigma^2} +$$
$$+\frac{F}{4\omega_0}\frac{S_1\sin\varphi_{10}-S_3\cos\varphi_{10}}{S_1^2+S_3^2},$$
$$C_{20} = -\frac{1}{4}\Gamma_2 a_{10}^2 a_{20}\frac{2S_1\sin\delta_0+\Sigma\cos\delta_0}{4S_1^{\ 2}+\Sigma^2},$$
$$C_{30} = \frac{\lambda_1 a_{10}^2}{2S_1} + \frac{\lambda_2 a_{20}^2}{2S_2} - \frac{1}{4}\Gamma_1 a_{20}^2 \frac{2S_2\cos\delta_0+\Sigma\sin\delta_0}{4S_2^{\ 2}+\Sigma^2} +$$
$$+\frac{1}{4}\frac{Fa_{10}^{-1}}{\omega_0}\frac{S_1\cos\varphi_{10}+S_3\sin\varphi_{10}}{S_1^2+S_3^2}, \tag{36}$$
$$C_{40} = \frac{\lambda_3 a_{10}^2}{2S_1} + \frac{\lambda_4 a_{20}^2}{2S_2} - \frac{1}{4}\Gamma_2 a_{10}^2 \frac{2S_1\cos\delta_0+\Sigma\sin\delta_0}{4S_1^{\ 2}+\Sigma^2}.$$

Substitution of the found constants of integration (36) in relationships (34) and (35) results in the approximate analytical solution of the formulated problem.

4. NUMERICAL RESULTS

For numerical studies of the influence of the parameters of the fractional derivative viscoelastic model on forced vibrations of suspension bridges, the fourth-order Runge-Kutta method was used in the «GNU Octave» system for numerical mathematics utilizing different values of the fractional parameter.
Envelopes of the amplitudes of nonlinear vibrations of the Golden Gate Bridge in the case of the internal resonance $\omega_{05}^s = \Omega_{03}^s = 2.61$ rad/sec (according to data presented in [2], the natural frequency of the fifth symmetric mode of vertical vibrations is equal to that of the third symmetric mode of the torsional vibrations) are depicted in Figure 2(a) for free vibrations and in Figure 2(b) for forced vibrations at *f*=1 at different magnitudes of the fractional parameter γ= 0, 0.15, and 0.5. Reference to Fig. 2 shows that the increase in the fractional parameter results in a significant decrease in dimensionless amplitudes of nonlinear oscillations. The energy exchange between the interacting modes takes place both in the case of undamped ($\gamma = 0$) and damped ($0 < \gamma \le 1$) vibrations, and the action of the external force does not affect this phenomenon.
Dimensionless displacements of the Golden Gate Bridge for forced vibrations are shown in Fig. 3 for different levels of the external force magnitudes. From Fig. 3 it is evident that the displacement x_1 is more susceptible to a higher vertical force than x_2. This is due to the fact that x_1 and x_2 are responsible for vertical and torsional vibrations, respectively, whence it follows that the x_2 -displacement is weakly sensitive to the increase in the force amplitude *f*.
Figure 4 allows one to trace the influence of the level of the external force magnitude on the dimensionless amplitudes of vertical a_1 and torsional a_2 vibrations. From Figure 4 it could be seen that the magnitudes of the amplitudes of vertical vibrations are very sensitive to the action of the force.

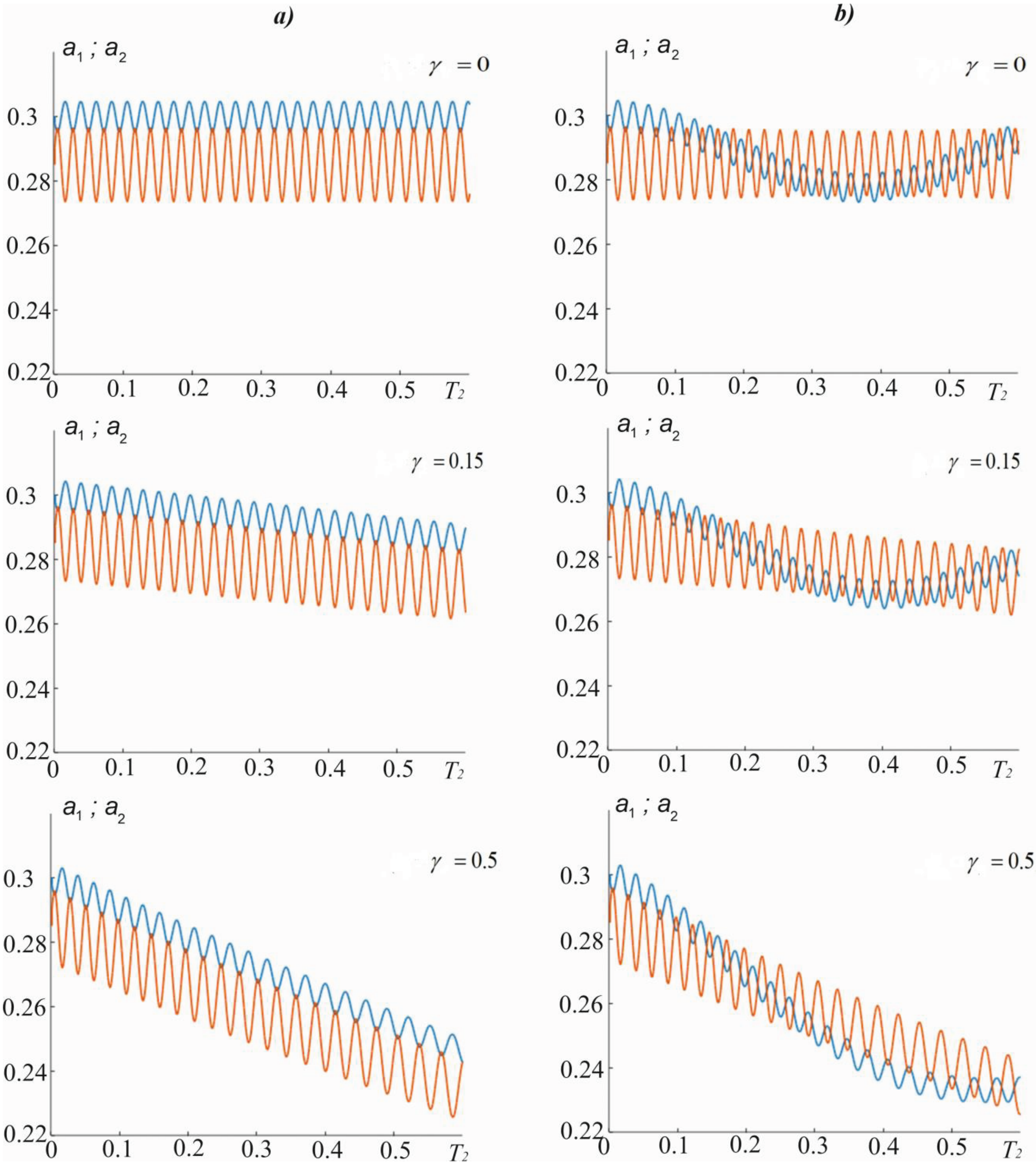

Figure 2. Dimensionless amplitude vs. dimensionless time:
(a) free vibrations, (b) forced vibrations at $f = 1$ with the initial amplitude $a_{i0} = 0.3$,
blue line – a_1, orange line – a_2.

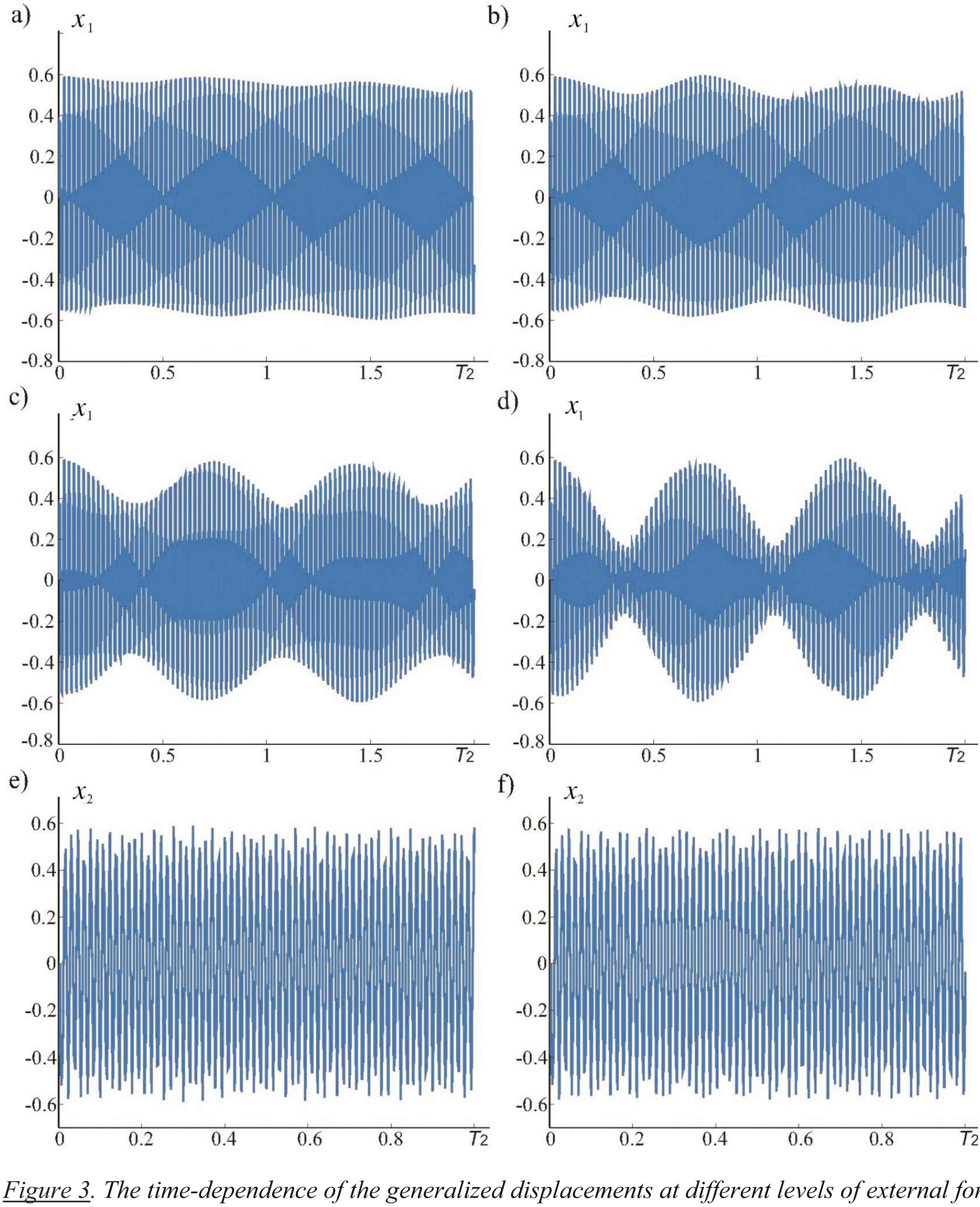

Figure 3. The time-dependence of the generalized displacements at different levels of external force magnitude for $\gamma = 0$.

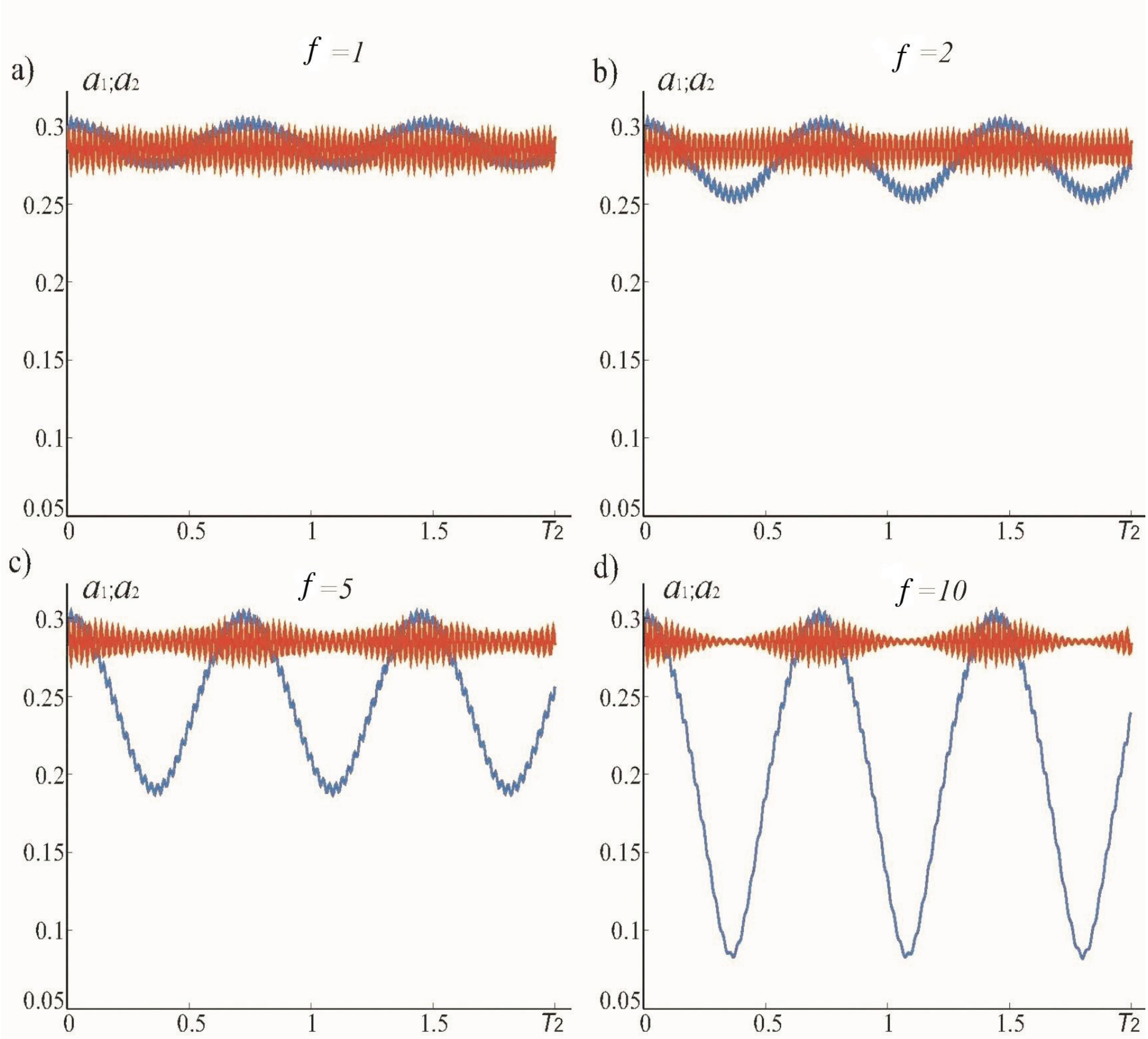

Figure 4. Time-dependence of the dimensionless amplitudes a_1 (blue) and a_2 (orange) at different levels of the external force amplitude.

CONCLUSION

Nonlinear force driven coupled vertical and torsional vibrations of a suspension bridge subject to the combination of external and internal resonances have been investigated for the case when its damping features are described by the fractional derivatives. From the above discussion the following conclusions could be reached.

If the external force is of order of ε^2 and the viscosity coefficients are of order of ε, then it is possible to obtain the approximate analytical solutions for the generalized displacements. As this takes place, the solution for the vertical displacement x_1 involves two parts: the first corresponds to the damping vibrations with damping coefficients and nonlinear frequencies dependent on the fractional parameters and describes the transient process, while the second one is nondamping in character and describes the steady-state regime, i.e., forced vibrations with the frequency of the exciting force and with the phase difference depending on the fractional parameter. The solution for the torsional displacement x_2 consists only from one term describing the transient process.

Moreover, in the transient processes, the damping coefficients and the frequencies of nonlinear vibrations depend on the square of the exciting force amplitude.

If the external force is of order of ε^3 and the viscosity coefficients are of order of ε^2, then the approximate analytical expressions for the generalized displacements x_1 and x_2 have been obtained by the method of successive approximations. The numerical analysis has shown that dimensionless amplitudes decrease with the increase in the fractional parameter γ, and the vertical amplitude and hence vertical displacement are much more susceptible to the higher vertical external force than torsional amplitude.

FUNDING

This research was carried out within the framework of the Government task, Project No 7.4.4 in the 2020 Fundamental Research Plan of RAASN and Ministry of Construction and Municipal Services of the Russian Federation.

REFERENCES

1. **Abdel-Ghaffar A.M.** Suspension bridge vibration: Continuum formulation. // Journal of Engineering Mechanics Division, 1982, Volume 108, pp. 1215-1232.
2. **Abdel-Ghaffar A.M., Rubin L.I.** Nonlinear free vibrations of suspension bridges: Theory and application. // ASCE Journal of Engineering Mechanics, 1983, Volume 109, Issue 1, pp. 313-345.
3. **Rossikhin Yu.A., Shitikova M.V.** Nonlinear free spatial vibrations of combined suspension systems. // Journal of Applied Mathematics and Mechanics, 1990, Volume 54, Issue 6, pp. 823-832.
4. **Rossikhin Yu.A., Shitikova M.V.** Analysis of nonlinear free vibrations of suspension bridges. // Journal of Sound and Vibration, 1995, Volume 186, Issue 3, pp. 369-393.
5. **Rossikhin Yu.A., Shitikova M.V.** Effect of viscosity on the vibrational processes in a combined suspension system. // Mechanics of Solids, 1995, Volume 30, Issue 1, pp. 157-166.
6. **Cevik M., Pakdemirli M.** Nonlinear vibrations of suspension bridges with external excitation // International Journal of Nonlinear Mechanics, 2005, Vol. 40, pp. 901-923.
7. **Nayfeh A.H.** Perturbations Methods. New York: John Wiley & Sons, 1973.
8. **Shitikova M.V., Rossikhin Yu.A.** Dynamics of suspension bridges: Nonlinear free and forced vibrations with internal resonances. // Plenary Lecture at the 5th European Conference of Civil Engineering (ECCIE '14), Florence, Italy Nov 22-24, 2014. In: Recent Advances in Civil Engineering and Mechanics (M.V. Shitikova, L. Vladareanu, C. Guarnaccia, Editors) WSEAS Press 2014, pp. 10.
9. **Arioli G., Gazzola F.** A new mathematical explanation of what triggered the catastrophic torsional mode of the Tacoma Narrows Bridge. // Applied Mathematical Modelling, 2015, Volume 39, pp. 901-912.
10. **Lepidi M., Gattulli V.** Non-linear interactions in the flexible multi-body dynamics of cable-supported bridge cross-sections. // International Journal of Non-Linear Mechanics, 2016, Volume 80, pp. 14-28.
11. **Capsoni A., Ardito R., Guerrieri A.** Stability of dynamic response of suspension bridges. // Journal of Sound and Vibration, 2017, Volume 393, pp. 285-307.
12. **Murphy P.** Retrofit of suspension bridges in the central and eastern United State using distributed supplememtal damping. PhD Thesis, Michigan, 2000, 183 pages.
13. **Strauss J.B.** The Golden Gate Bridge. Report to the board of directors of the

Golden Gate Bridge and highway district, 1937.
14. **Vincent G.S.** Correlation of predicted and observed suspension bridge behavior. // Transactions of ASCE, 1962, Volume 127, pp. 646-666.
15. **Vincent G.S.** Golden Gate Bridge vibration studies. // Journal of Structural Division ASCE, 1958, Volume 84(ST6), 1817.
16. **Vincent G.S.** Golden Gate Bridge vibration studies. // Transactions of ASCE, 1962, Vol. 127, Part II, pp. 667-701.
17. **Baron F., Arikan M., Hamati E.** The effects of seismic disturbances on the Golden Gate Bridge. Report No. EERC 76-31 Earthquake Engineering Research Center College of Engineering University of California, 1976.
18. **Paine C.D.** Supplement to the Final Report of the Chief Engineer – Golden Gate Bridge, Highway and Transportation District, 1970.
19. **Tanaka H., Davenport A.** Wind induced response of Golden Gate Bridge. // Proceedings of the Journal of Engineering Mechanics ASCE, 1983, Volume 109, Issue 1, pp. 296-312.
20. **Abdel-Ghaffar A.M., Scanlan R.H.** Ambient vibration studies of Golden Gate Bridge. I: Suspended structure. // ASCE Journal of Engineering Mechanics, 1985, Volume 111, Issue 4, pp. 463-482.
21. **Abdel-Ghaffar A.M., Housner G.W.** Ambient vibration tests of suspension bridge. // ASCE Journal of Engineering Mechanics, 1978, Volume 104, Issue 5, pp. 983-999.
22. **Rossikhin Yu.A., Shitikova M.V.** Application of fractional calculus for analysis of nonlinear damped vibrations of suspension bridges. // ASCE Journal of Engineering Mechanics, 1998, Volume 124, Issue 9, pp. 1029-1036.
23. Shitikova M.V. The fractional derivative expansion method in nonlinear dynamic analysis of structures. // Nonlinear Dynamics, 2020, Volume 99, Issue 1, pp. 109-122.
24. **Shitikova M.V.** The fractional derivative expansion method in nonlinear dynamics of structures: A memorial essay. // Transmutation Operators and Applications (V.V. Kravchenko and S.M. Sitnik, Editors) Trends in Mathematics, 2020, Chapter 29, pp. 653-670, Springer.
25. **Rossikhin Yu.A., Shitikova M.V.** Vliyanie vyazkosti na svobodnue prostranstvennue kolebaniya visyachei kombinirovannoi sistemu [Influence of viscosity of free spatial vibrations of a suspension combined system]. // News of Higher Educational Institutions. Construction, 1993, No. 4, pp. 26-29 (in Russian).
26. **Samko S.G., Kilbas A.A., Marichev O.I.** Fractional Integrals and Derivatives. Theory and Applications. Minsk: Nauka i Tekhnika, 1988 (in Russian).
27. **Rossikhin Yu.A., Shitikova M.V.** New approach for the analysis of damped vibrations of fractional oscillators. // Shock and Vibration, 2009, Volume 16, pp. 365-387.
28. **Rossikhin Yu.A., Shitikova M.V.** Forced vibrations of a nonlinear oscillator with weak fractional damping. // Mechanics of Materials and Structures, 2009, Volume 4, Issue 9, pp. 1619- 1636.
29. **Rossikhin Yu.A., Shitikova M.V.** On fallacies in the decision between the Caputo and Riemann-Liouville fractional derivatives for the analysis of the dynamic response of a nonlinear viscoelastic oscillator. // Mechanics Research Communications, 2012, Volume 45, pp. 22-27.

СПИСОК ЛИТЕРАТУРЫ

1. **Abdel-Ghaffar A.M.** Suspension bridge vibration: Continuum formulation. // Journal of Engineering Mechanics Division, 1982, Volume 108, pp. 1215-1232.
2. **Abdel-Ghaffar A.M., Rubin L.I.** Nonlinear free vibrations of suspension bridges: Theory and application. // ASCE

Journal of Engineering Mechanics, 1983, Volume 109, Issue 1, pp. 313-345.
3. **Rossikhin Yu.A., Shitikova M.V.** Nonlinear free spatial vibrations of combined suspension systems. // Journal of Applied Mathematics and Mechanics, 1990, Volume 54, Issue 6, pp. 823-832.
4. **Rossikhin Yu.A., Shitikova M.V.** Analysis of nonlinear free vibrations of suspension bridges. // Journal of Sound and Vibration, 1995, Volume 186, Issue 3, pp. 369-393.
5. **Rossikhin Yu.A., Shitikova M.V.** Effect of viscosity on the vibrational processes in a combined suspension system. // Mechanics of Solids, 1995, Volume 30, Issue 1, pp. 157-166.
6. **Cevik M., Pakdemirli M.** Nonlinear vibrations of suspension bridges with external excitation // International Journal of Nonlinear Mechanics, 2005, Vol. 40, pp. 901-923.
7. **Nayfeh A.H.** Perturbations Methods. New York: John Wiley & Sons, 1973.
8. **Shitikova M.V., Rossikhin Yu.A.** Dynamics of suspension bridges: Nonlinear free and forced vibrations with internal resonances. // Plenary Lecture at the 5th European Conference of Civil Engineering (ECCIE '14), Florence, Italy Nov 22-24, 2014. In: Recent Advances in Civil Engineering and Mechanics (M.V. Shitikova, L. Vladareanu, C. Guarnaccia, Editors) WSEAS Press 2014, pp. 10.
9. **Arioli G., Gazzola F.** A new mathematical explanation of what triggered the catastrophic torsional mode of the Tacoma Narrows Bridge. // Applied Mathematical Modelling, 2015, Volume 39, pp. 901-912.
10. **Lepidi M., Gattulli V.** Non-linear interactions in the flexible multi-body dynamics of cable-supported bridge cross-sections. // International Journal of Non-Linear Mechanics, 2016, Volume 80, pp. 14-28.
11. **Capsoni A., Ardito R., Guerrieri A.** Stability of dynamic response of suspension bridges. // Journal of Sound and Vibration, 2017, Volume 393, pp. 285-307.
12. **Murphy P.** Retrofit of suspension bridges in the central and eastern United State using distributed supplememtal damping. PhD Thesis, Michigan, 2000, 183 pages.
13. **Strauss J.B.** The Golden Gate Bridge. Report to the board of directors of the Golden Gate Bridge and highway district, 1937.
14. **Vincent G.S.** Correlation of predicted and observed suspension bridge behavior. // Transactions of ASCE, 1962, Volume 127, pp. 646-666.
15. **Vincent G.S.** Golden Gate Bridge vibration studies. // Journal of Structural Division ASCE, 1958, Volume 84(ST6), 1817.
16. **Vincent G.S.** Golden Gate Bridge vibration studies. // Transactions of ASCE, 1962, Vol. 127, Part II, pp. 667-701.
17. **Baron F., Arikan M., Hamati E.** The effects of seismic disturbances on the Golden Gate Bridge. Report No. EERC 76-31 Earthquake Engineering Research Center College of Engineering University of California, 1976.
18. **Paine C.D.** Supplement to the Final Report of the Chief Engineer – Golden Gate Bridge, Highway and Transportation District, 1970.
19. **Tanaka H., Davenport A.** Wind induced response of Golden Gate Bridge. // Proceedings of the Journal of Engineering Mechanics ASCE, 1983, Volume 109, Issue 1, pp. 296-312.
20. **Abdel-Ghaffar A.M., Scanlan R.H.** Ambient vibration studies of Golden Gate Bridge. I: Suspended structure. // ASCE Journal of Engineering Mechanics, 1985, Volume 111, Issue 4, pp. 463-482.
21. **Abdel-Ghaffar A.M., Housner G.W.** Ambient vibration tests of suspension bridge. // ASCE Journal of Engineering Mechanics, 1978, Volume 104, Issue 5, pp. 983-999.
22. **Rossikhin Yu.A., Shitikova M.V.** Application of fractional calculus for analysis of nonlinear damped vibrations of

suspension bridges. // ASCE Journal of Engineering Mechanics, 1998, Volume 124, Issue 9, pp. 1029-1036.
23. Shitikova M.V. The fractional derivative expansion method in nonlinear dynamic analysis of structures. // Nonlinear Dynamics, 2020, Volume 99, Issue 1, pp. 109-122.
24. **Shitikova M.V.** The fractional derivative expansion method in nonlinear dynamics of structures: A memorial essay. // Transmutation Operators and Applications (V.V. Kravchenko and S.M. Sitnik, Editors) Trends in Mathematics, 2020, Chapter 29, pp. 653-670, Springer.
25. **Россихин Ю.А., Шитикова М.В.** Влияние вязкости на свободные пространственные колебания висячей комбинированной системы. // Известия вузов. Строительство, 1993, № 4, с. 26-29.
26. **Самко С.Г., Килбас А.А., Маричев О.И.** Интегралы и производные дробного порядка и некоторые их приложения. – Минск: Наука и техника, 1987. – 688 с.
27. **Rossikhin Yu.A., Shitikova M.V.** New approach for the analysis of damped vibrations of fractional oscillators. // Shock and Vibration, 2009, Volume 16, pp. 365-387.
28. **Rossikhin Yu.A., Shitikova M.V.** Forced vibrations of a nonlinear oscillator with weak fractional damping. // Mechanics of Materials and Structures, 2009, Volume 4, Issue 9, pp. 1619- 1636.
29. **Rossikhin Yu.A., Shitikova M.V.** On fallacies in the decision between the Caputo and Riemann-Liouville fractional derivatives for the analysis of the dynamic response of a nonlinear viscoelastic oscillator. // Mechanics Research Communications, 2012, Volume 45, pp. 22-27.

Marina V. Shitikova, Advisor of the Russian Academy of Architecture and Construction Sciences (RAACS), Professor, Dr.Sc.; Research Center on Dynamics of Solids and Structures, Voronezh State Technical University; 84, 20-letija Oktyabrya, Voronezh, 394006, Russia; Senior Researcher, RAASN Research Institute of Structural Physics, Moscow, Russia; phone +7 (473) 271-52-68; fax +7 (473) 271-52-68; e-mail: mvs@vgasu.vrn.ru.

Aleks L. Katembo, PhD Student, Research Center on Dynamics of Solids and Structures; Voronezh State Technical University; 84, 20-letija Oktyabrya, Voronezh, 394006, Russia; e-mail: katembo2020@gmail.com.

Шитикова Марина Вячеславовна, советник Российской академии архитектуры и строительных наук (РААСН), профессор, доктор физико-математических наук; руководитель международного научного Центра по фундаментальным исследованиям в области естественных и строительных наук; Воронежский государственный технический университет; 394006, Россия, г. Воронеж, ул. 20 лет Октября, д. 84; Главный научный сотрудник, Научно-исследовательский институт строительной физики РААСН, Москва, Россия; тел. +7 (473) 271-52-68; факс +7 (473) 271-52-68; e-mail: mvs@vgasu.vrn.ru.

Катембо Алекс Лунгили, аспирант, Воронежский государственный технический университет; 394006, Россия, г. Воронеж, ул. 20 лет Октября, д. 84;
E-mail: katembo2020@gmail.com.

DOI:10.22337/2587-9618-2020-16-2-130-142

GEOTECHNICAL FEATURES OF HISTORICAL ARCHITECTURAL MONUMENTS OF CENTRAL ASIA

***A.Zh. Zhussupbekov*[1], *A. Issina*[2], *Y. Iwasaki*[3], *Sh. Kenjaev*[4], *I. Usmankhodjaev*[5]**
[1]L.N.Gumilyov Eurasian National University, Nur-Sultan, KAZAKHSTAN
[2]Saken Seifullin Kazakh Agricultural Technical University, Nur-Sultan, KAZAKHSTAN
[3]Geo-Research Institute, Osaka, JAPAN
[4]Tashkent Institute of Architecture and Civil Engineering, Tashkent, UZBEKISTAN
[5]Tashkent Institute of Architecture and Civil Engineering, Lolazor St. 70, Samarkand, UZBEKISTAN

Abstract: In this paper geoenvironmental problems of the historical cities of Central Asia are considered, climatic, geotechnical, hydrogeological characteristics of the studied objects, their constructive decision and the analysis of deformations of elevated and underground construction designs are provided. Main reasons for deformations of monuments of architecture of Central Asia: uneven rainfall of soil of the basis in the most overloaded sites of designs of the building; seismic influences; violation of temperature moisture conditions and moisture; anthropogenous influence (especially notable in the historical cities of Samarkand and Bukhara where monuments of architecture are influenced by vibrations from traffic). In the paper the offered observation method of monuments of architecture of Central Asia and results of observation of the mausoleum Arystan-Bab and a mosque and minaret Kalon for 2014 is described.

Key words: geotechnical analysis, anthropogenic impacts, constructions of architectural monuments

ГЕОТЕХНИЧЕСКИЕ ОСОБЕННОСТИ ИСТОРИЧЕСКИХ АРХИТЕКТУРНЫХ ПАМЯТНИКОВ ЦЕНТРАЛЬНОЙ АЗИИ

***А.Ж. Жусупбеков*[1], *А.З.Исина*[2], *И.Ивасаки*[3], *Ш.Кенжаев*[4], *И.Усманходжаев*[5]**
[1]Евразийский национальный университет им. Л.Н. Гумилева, г. Нур-Султан, Республика КАЗАХСТАН
[2]Казахский агротехнический университет им. С.Сейфуллина, г. Нур-Султан, Республика КАЗАХСТАН
[3]И. Ивасаки, директор, Институт гео-исследований, Осака, ЯПОНИЯ
[4]Ташкентский архитектурно-строительный институт, г. Ташкент, УЗБЕКИСТАН
[5]Ташкентский архитектурно-строительный институт, г. Самарканд, УЗБЕКИСТАН

Аннотация: В статье рассматриваются геоэкологические проблемы исторических городов Центральной Азии, приводятся климатические, геотехнические, гидрогеологические характеристики исследуемых объектов, их конструктивные решения и анализ деформирования надземных и подземных строительных конструкций. Основные причины деформирования памятников архитектуры Центральной Азии: неравномерное выпадание грунта из основания в наиболее перегруженных участках конструкций здания; сейсмические воздействия; нарушение температурно-влажностного режима и влажности; антропогенные воздействия (особенно заметны в исторических городах Самарканд и Бухара, где на памятники архитектуры влияют вибрации от движения транспорта). В статье описан предложенный метод наблюдения за памятниками архитектуры Центральной Азии и результаты наблюдения за мавзолеем Арыстан-Баб, а также мечетью и минаретом Калон за 2014 год.

Ключевые слова: геотехнический анализ, антропогенные воздействия, конструкции памятников архитектуры

1. INTRODUCTION

The history of our ancient land leaves deep into the millennia. Holding an advantageous geographical position, the connecting North with the South, the East with the West, Central Asia was the important center on the road of a caravan which became history under the name of the Great Silk Way. On branches of this ancient transcontinental highway not only trade developed – there was an active process of mutual enrichment of ideas, cultures, traditions, religions, crafts and technologies.

Considering all importance of the huge cultural heritage, which got to us carrying out numerous researches and monitoring of technical condition of significant monuments of architecture of the Central Asian region for the purpose of its preservation is necessary for descendants.

One of the types of the works directly concerning cultural heritage, demanding greater financial influences, but which aren't receiving the due amount of financing is carrying out engineering-geological and geotechnological researches of historical monuments of architecture of Central Asia.

At the present stage the majority of monuments of architecture of the countries of Central Asia faced a problem of destruction of the bases under the influence of climatic factors. One of the most common causes of deformations are uneven rainfall which, in turn, cause deformations and destructions of the bearing designs – the bases, walls, columns, overlappings, the arches, crossing points window and doorways.

The integrated approach to restoration practically was only designated due to wide use of engineering restoration, and concerning necessary taking note of changes of the geological environment on safety of historical territories is made
so far very little.

2. GEOENVIRONMENTAL PROBLEMS IN THE HISTORICAL CITIES OF CENTRAL ASIA

Environmental problems are connected with changes of historically developed geological and hydrogeological mode. In particular is a raising of ground waters and increase in their structure of concentration of salts, increase in moisture content and salt in the soil. These phenomena started promoting actively deformation of designs and an intensive erosion of walls and bases of monuments of architecture. Especially strongly historical buildings of the cities located in low territories of Central Asia (Bukhara, Khiva) suffer. Now the listed above negative facts negatively influence and the architecture monuments which are in rather favorable foothill territories of Central Asia: in such as Samarkand, Shakhrisabz, Shymkent, etc. however here increase in humidity in soil and raising of ground waters is generally connected with a human factor: urbanization and development of communication systems. For this reason studying of this problem needs to be conducted in two directions: in the global - change of a geoecological situation of Central Asia, in local scale - to look for evidence-based ways of decrease in level of its influence for the purpose of preservation of masterpieces of world famous monuments of architecture. We will begin with the main thing: a geoecological situation in the region (Guseva 2000).

For the last decade there were serious problems connected with preservation of world famous masterpieces of architecture. In particular, the salted ground waters owing to the aggression in relation to construction materials as a result of difficult physical and chemical processes start erodirovat intensively underground and elevated designs of monuments therefore often there are deformations, and in certain cases and their final fracture. As an example, it is possible to bring catastrophic destruction of one of minarets of the Chor-Minor complex, strong deformations of a complex Tim Abdulkhan, a complex Ark and an inclination of minarets in Bukhara or deformations of some monuments in Samarkand, the

Ichang-Kala complex in Khiva (Abdurashidov et al. 2011).

3. GEOTECHNICAL, HYDRO-GEOLOGICAL AND CONSTRUCTIVE CHARACTERISTICS OF MONUMENTS OF ARCHITECTURE OF CENTRAL ASIA

The mausoleum of Hodge Ahmed Yassavi (XIV-XV cen.) (Figure 1).

Figure 1. *The Mausoleum of Hodge Ahmed Yassavi.*

Soils. The prolyuvialny loams with a general power of 5-7 m quarternary allyuvialno containing form the basis of a monument interlay also lenses of sandy loams. They are spread water containing gravel with the power from 4 to 24
m. Sandy loams are developed mainly in the top part of a section. Sandy loams of light brown color, macroporous, loessial, uniform. Loam of brown color, dense with inclusion of carbonate particles. Sand dusty, meets in the form of lenses, mainly on contact with a galechnik, color its gray and brown, uniform. Pebble soil is presented by sedimentary breeds, fragments well rounded, so-so thickened and extended, as filler sand serves.

Ground waters. Ground waters for June, 2011 are opened with developments at a depth of 7,6-7,8 m from an earth surface. In relation to situation level of ground water (LGW) for September, 1997, LGW in June, 2011 is recorded 1,4- 1,5 m below.

Foundations. The main part of a construction is built on clay gulfs, in South side under portal part the rubble foundations up to 7 m in depth are executed.

In 1993 the technology of jet cementation of soil was applied to strengthening of the basis of a monument by the Turkish company. Strengthening and the device of piles was carried out to two stages. At the first stage of work were carried out for walls to 2 m. At the second stage strengthening of the basis of walls up to 4 m thick was made. Total length of a pile is about 15 m. Thus, the support of all construction through piles on thickness of solid soil is reached.

Deformations. Due to the lack of emergence of essential deformations on a monument to the first cycle it wasn't given due consideration though at this moment there was a deep soaking of soil and the basis of the foundations of monuments of the complex. The second cycle of rise in level of ground waters caused already external deformations of the building of a monument, in December, 1982 there was a destruction of the top restoration number of stalactites of a dome of the Main Hall - Kazanlyk.

The mausoleum of Arystan-Bab (XIV-XV cen.) (Figure 2).

Figure 2. *The Mausoleum of Arystan-Bab.*

Soils. The analysis of average values physic mechanical property of soil on holes and an additional driving of holes allow directly under a sole without foundations walls and the bases with depth to 1,0 m to allocate 3 engineering- geological element (EGE):

1. EGE – loam of a firm-semi-firm consistence, not collapsible, uniform, with rare inclusions of fragments of a brick and the vegetable remains in the top part of a layer, 1,0 - 1,5 m (0,9 – 1,0 m – on wells), it is possible to assume that it is the loam layer, or the layer executed by method of "gulf" in a trench width exceeding thickness of walls which is artificially condensed in an open trench; it possesses quite certain and rather close indicators of physic mechanical properties 2 EGE;
2. EGE – loam dark brown a firm-semi-firm consistence, not collapsible, with roots of vegetation, 3,3-3,6 m (on wells);
3. EGE – sandy loam brown, a plastic and fluid consistence with pro-layers of sand dusty (to 0,2 m) with an opened power of 3,5-3,7 m (Report, 2004).

Ground waters. LGW near a contour of the monument is opened at depths of 1,9-2,7 m (August, 1984), 2,75-2,85 m (May, 2004) and 3,14-3,37 m (August, 2004).

Foundations. The foundations are arranged under the most loaded parts of a construction. Under minarets the foundations are executed from a stone-plitnyak on clay solution. Materials of the bases are in a good shape.

On a hole № 10 up to 1,5 m in depth, in a place of a joint of a longitudinal wall on axis A and the left minaret, lack of the foundation under a wall which laying leans on three rows of preparation from a detrital brick is revealed. Their basis is the uniform layer of loam of the first EGE. The hole № 11 from the outer side of a wall on axis 4 up to 0,7 m in depth, opened the concrete plate 17-20 thick see above it the layer of dry, fragile roofing material, and over it one more concrete layer about 9 cm thick, revetted outside with a thin facing tile is found. Over this layer there is a wall bricklaying.

Deformations. In a laying of walls cracks on all facades are noted. During observation it is established that width of disclosure of cracks makes from 0,1 to 2 mm. In a place of interface of a minaret to a wall (a northeast facade) the crack reaches 2 cm and goes mainly on laying seams. All cracks in a laying come to an end, without reaching a socle. Cracks, generally in places of reduction of thickness of walls settle down. Indoors tombs № 1 are noted the deformations in a laying menacing to safety of a construction. These are cracks and smashing of a brick in a laying of basic part of arches, split of a brick in places of support of angular arches in northeast and northwest walls. In a northeast wall of a crack in a laying of basic part of arches have extent to 2 m.

The Registan ensemble (XV-XVII cen.) (Figure 3).

Figure 3. The Registan Ensemble.

Soils. On a site the different depth of weak anthropogenous soil is noted: the greatest depth of 12,6 m takes place directly under the dome foundations at the western wall and is almost twice less (6,8 m) on wall length on the southern site.

Foundations. The foundations under buildings have various constructive decision, depth and are made of different materials. Under walls the tape foundations, and under racks and poles the separate step are, as a rule, executed. For the device of the foundations blocks and rubble stones of Chupan-atinsky slate or marble limestone on ganchevy and limy solution with use in some cases of ashes, and also the foundations of the caravanserai which was earlier existing on this place were used (the burned brick on limy and ganchevy solution). By observations it is established that the lower part of a laying is made of quarrystone on clay solution, all other part of a laying is executed on ganchevy solution. In a design of the foundations the wooden reinforcing elements are found.

Deformations. Judging by the tilted racks of northern and southern galleries and other architectural forms, deformation of a mosque proceeds rather long time. Tool supervision over the building is begun since 1983. It is established that uneven rainfall of soil of the basis in the most overloaded building design sites were the main reason of deformation of the building. In particular more uneven deformations underwent designs of the western wall and foundations under a dome that led to emergence of a huge number of through cracks in walls, coverings, arches and floors.

The Bibi-Hanym mosque (XIV-XV cen.) (Figure 4).

Soils. The quarternary alluvial prolyuvialny loams with a general power of 5-7 m containing form the basis of a monument interlay also lenses the lessovidnykh of sandy loams. They are spread water containing gravel with the power from 4 to 24 m. Sandy loams are developed mainly in the top part of a section. Sandy loams of light brown color, macroporous, loessial, uniform. Loam of brown color, dense with inclusion of carbonate particles. Sand dusty, meets in the form of lenses, mainly on contact with a galechnik, color its gray and brown, uniform. Pebble soil is presented by sedimentary breeds, fragments well rounded, so-so thickened and extended, as filler sand serves.

Foundations. The foundations of small mosques are put from plates of a fragmentary Chupan-atinsky stone by the size on the person (60-80) ×25 cm, on the same solution, as a laying.

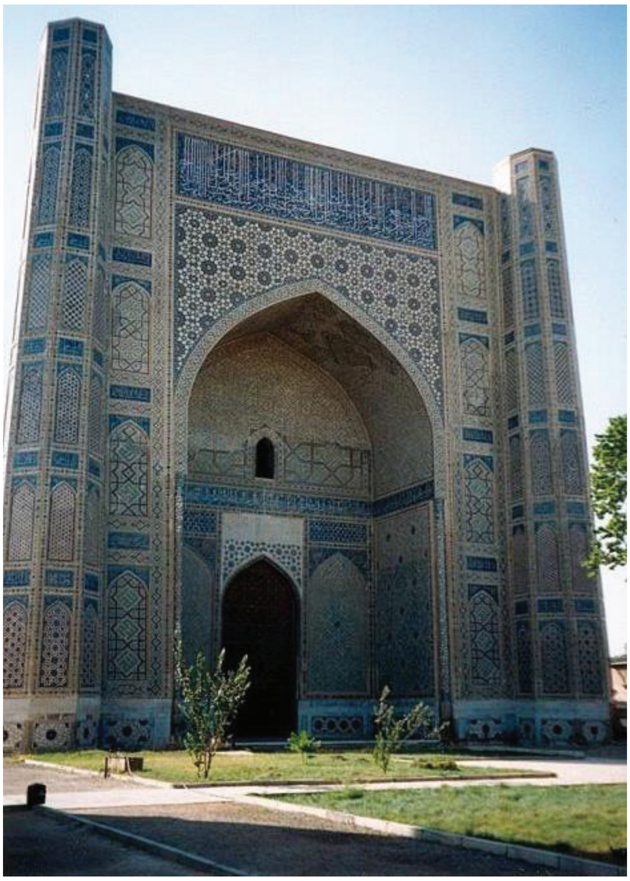

<u>Figure 4.</u> The Bibi-Hanym Mosque.

In the foundations of the Big mosque, various on a laying and upon transition to elevated parts – kyr. Depth of the foundations various, in some places it doesn't exceed 0,5-0,6 m from a day surface of the earth.

Deformations. In a body of old layings and a minaret traces of inclined cracks are visible. It means that before destruction the minaret was strongly rejected from a portal. Existence of cracks in the central dome part of the Big mosque is noted.

The Ishratkhona (XV cen.) (Figure 5).

Soils. The prolyuvialny loams with a general power of 5-8 m quarternary allyuvialno containing form the basis of a monument interlay also lenses the lessovidnykh of sandy loams. They are spread water containing gravel with the power from 4 to 24 m. Sandy loams are developed mainly in the top part of a section. Sandy loams of light brown color, macroporous, loessial, uniform. Loam of brown color, dense with inclusion of carbonate particles. Sand dusty, meets in the form of lenses, mainly on contact with a galechnik, color its gray and brown, uniform.

Figure 5. The Ishratkhona.

Ground waters. Because the minimum level of ground waters during the summer period reaches 3,50-3,80 m, there is a capillary rising of water in solution to its moistening.

Foundations. The foundations of the building have various depth (from 1,3 to 4,2 m) and is presented by a rubble laying from a fragmentary Chupan-atinsky stone on clay solution. Under a portal the rubble laying has power down of nearly 4 m, being lowered on depth about 5,5 m from earth level. Existence in soil of marlaceous layers assumes the assumption that the basis before construction was previously killed and condensed.

Deformations. The building of a monument is strongly destroyed and many elements are bared. The design of an underground crypt is executed from the flat arch leaning on massive side support. Support of the arch aren't connected with the bases of the main building that gives it the chance independently to be deformed irrespective of building rainfall. In 1903 the dome and a drum of the central room failed, and in 1904 the remains of a drum and the top parts supporting its arches finally collapsed. The main reason for long destruction of vaulted and arch designs is connected with gradual decrease in durability of material in the most loaded basic parts and destruction of integrity of designs.

In the course of complex research of historical monuments of architecture of Central Asia the main reasons for an unsatisfactory condition of some constructive elements of a monument are established:

- uneven rainfall of soil of the basis in the most overloaded sites of designs of the building;
- seismic influences;
- violation of temperature moisture conditions and moisture. In our case moisture is formed for the account:
  - absolute and relative humidity of the air environment generally during the winter period;
  - condensation moisture;
  - penetrations of soil moisture into thickness of the protecting designs into the spring period;
  - atmospheric moisture during the autumn and spring periods;
  - technical moisture which arises in the course of performance of construction works.
- anthropogenous influence (especially notable in the historical cities of Samarkand and Bukhara where monuments of architecture are influenced by vibrations from traffic).

4. OBSERVATION METHOD FOR HISTORICAL MONUMENTS OF ARCHITECTURE OF CENTRAL ASIA

The offered observation method of historical monuments of architecture of Central Asia will unite in itself a package of measures on research, preservation and forecasting of behavior of construction designs of historical monuments of architecture:

1. Collecting and an assessment of retrospective engineering-geological information in the territory of a monument and in the territory adjoining

a monument;

2. Carrying out hydrogeological researches for the purpose of specification of a depth of ground waters and its dynamics, definition of a chemical composition;
3. Heatphysical calculation of a monument of architecture;
4. Collecting and the analysis of the deformations given about character and speed of their development; control of shrinkage of a monument or its elements;
5. Identification of the most rational methods of prevention of further development of deformations in the bearing designs;
6. Use of numerical information technologies for drawing up the correct forecast of work of constructive elements of monuments of architecture for the next 10, 20 and 100 years;
7. Preservation of authenticity of object unless development of deformations brings to full of destruction of object of cultural heritage.

Heatphysical calculations are made for definition of optimum temperature moisture conditions of rooms and are aimed at decrease in accumulation of condensation humidity on a surface of walls.

Degree of stability of flying designs or construction in general, durability and deformability of materials on static and dynamic (seismic) influences is made by means of special engineering settlement programs. By results of these calculations the weakest places in designs come to light and issues of their strengthening are resolved.

Systematization of the most often destroyed sites allows to conduct long supervision over a condition of constructive and finishing elements, to reveal and eliminate the main reasons for damage and destruction.

The results of observation of the mausoleum Arystan- Bab in April, 2014

Foundations. Materials of the foundations of a construction are in a good shape, any violations or deformations is noted.

Socle. Separate bricks in a socle are removed. Also laying seams in the lower part of a socle are removed. On a surface of a bricklaying of a socle of northwest, southwest and northeast facades salt spots are noted.

Walls. In general bricks of walls are in a satisfactory condition. Aeration of separate bricks on facades, and also seams on buttresses, in the lower and top parts of walls (parapet), in a laying of a northern minaret is noted (Figure 6).

Figure 6. Destruction of Separate Bricks in a Laying of a Socle and Walls of the Mausoleum Arystan-Bab.

On a surface of a bricklaying of walls of northwest, southwest and northeast facades salt spots (Figure 7) are noted. Walls are moistened in these parts on 1,5-2 m.

On a laying of buttresses of northwest and southeast facades lichens are noted.

Overlappings. In a tomb № 1 seams in a dome laying are removed inside. Outside seams in a laying of domes are also removed in separate places. In an arch laying separate bricks are removed, on a surface of a laying salt spots are from the inside noted. On a parapet in 1996 the plastering of horizontal surfaces was executed by angidridovy solution. During inspection the plastering exfoliated from a surface and was divided into pieces. Possibly, there is no adhesion of solution and a surface of a laying of a parapet.

Figure 7. Moistening of the Lower Part of a Northeast Facade of the Mausoleum Arystan-Bab.

Figure 8. The Interior of Mausoleum Arystan-Bab.

The laying of domes and turrets is covered with lichens. In an interior of a mosque moistening of a blanket of plaster is noted. Floors are carpeted, thus carpets in a half-baked state that testifies to moistening of plates of a floor of a mosque (Figure 8).

Blind area. Round the mausoleum the blind area is executed from a stone-plitnyak on cement mortar. As cement mortar interferes with moisture evaporation, the blind area round a construction was sorted on width of 40-50 cm.

Analysis of results of a chemical composition of ground waters

Comparison of results of the chemical analysis of ground waters of 1984 (on wells 268 and 269 from depths of 2,37 and 2,46 m), 2004 (holes 2 and 3 from depths of 2,8 and 2,7m) and 2014 (from depth of 2,8 m) is executed (Table 1).

Table 1. The Average Values of Indicators of the Chemical Analysis of Ground Waters

Indicator	Dimension	Value			Note
		1984	2004	2014	
Bicarbonate alkalinity (HCO_3)	mg/l	244	814	769	
Hydrogen indicator of PH		7,6-7,8	7,65-7,7	7,2	
Content of magnesian Mg salts	mg/l	468	1232	973	
Content of caustic alkalis (Na+K)	mg/l	2520	1244	728	decrease
The content of sulfates in terms of SO_4 ions	mg/l	5520	2952	819	decrease
General rigidity (Ca + Mg)	mgecu/l	107	129	118	
Dry rest (mineralization)	g/l	13,5	10,2	7,9	

The changes of salt structure at very high mineralization it is seen, are connected with the general falling of LGW, especially after works on cleaning and deepening of the water lowering channels on external borders of the territory of a necropolis. It and reduction of compounds of caustic alkalis and content of sulfates, and also falling of the general mineralization of ground water. The effect of water decrease would be higher at restoration of part of the filled-up canal (up to 250-300 m long) from entrance on the territory of a necropolis (the southeast party). From this party waters from irrigation aryk of the above-located farmland most intensively arrive (Issina and Zhussupbekov 2015).

The results of observation of the complex Poi-Kalyan in July, 2014

This huge vertical pillar dominating over the city put from a zhzhenny brick gives a complete idea of forms of Central Asian minarets – the round, expanded to a bottom tower, below diameter of 10,5 m and 5,7 m above. The general height of a minaret of 47,5 m, but its multimeter basis is hidden in the depth of the earth, under century stratifications, however on the basis of K.S. Kryukov researches. The depth of the foundations makes about 12,0 m, and also the socle part of a minaret which was in an occupation layer of the earth that gave the chance to restore the area level corresponding to time of construction of the Karakhanidsky mosque and a minaret was naked.

Over a trunk of a minaret the sixteen-arch rotunda of a lamp leaning on the acting ranks of a laying issued in the form of stalactite eaves is arranged. On top of a minaret the cool brick ladder leaning on a trunk and external walls of a minaret conducts. Rise on a platform of a lamp is carried out on a spiral staircase in a minaret trunk. The external surface is decorated by terracotta plates and figured bricks the sizes of 260×260×50 mm. on ganch solution with addition of a kyr. The front surface of a minaret is covered with the magnificent relief pattern from a brick broken into ten ornamental belts, any of them doesn't repeat another. The roof is laid out from a zhzhenny brick on ganch solution.

The minaret Kalon is connected by the bridge transition to a roof of a cathedral mosque Kalon from where it is possible to get in a minaret and to rise on the narrow and cool brick spiral staircase numbering 105 steps.

The ladder, 990 mm wide, is arranged round a minaret kernel - an axial trunk of Ø2250 mm (Figure 9). Each step gets married a vaulted arch height on average of 2450 mm the relations of the parties in respect of on average 211/340 mm and equal to a proportion 0,62 (golden ratio) which corresponds, reached us in antique literature division of a piece in the extreme and average relation (ἄκρος καὶ μέσος λόγος). According to Luk Pachuoli of the contemporary Leonardo da Vinci, called this relation "a divine proportion". The term "golden ratio" (goldener Schnitt) was entered into use by Martin Om in 1835.

Figure 9. The Arch of the Spiral Staircase of the Minaret Kalon.

Under the mosque arches Kalon (Maszhidi colon) gathered to 12 thousand people, the building occupies the space 1ga. At uniform type of the building are absolutely various works of architecture. Its construction was complete in 1514.

The mosque on the architecture belongs to type four ayvan, with the big yard and the arch and dome gallery surrounding it. Serves as a support of multidome overlapping of the gallery bypassing the yard of the mosque Kalon monumental poles.

The rectangular yard is framed with the galleries consisting of 288 domes, the basis it 208 columns form. The longitudinal axis of the yard comes to the end with the maksury - the portal and dome volume of the building with the crosswise hall over which the blue massive dome on a mosaic drum rises.

The main entrance – East is decorated with the big portal issued by a mosaic, and on each side it two blue domes tower. On the central part the internal portal of a mosque has an octahedral construction, playing a role of chair. Color facing of facades is created by means of the mosaic and bricks covered with glaze (Report 2014).

Engineering-geological structure of a site

In the geomorphological relation the platform of researches is dated for the second over an inundated terrace of the river Zarafshan in the Central part of the Bukhara oasis and put by alluvial deposits of quarternary age.

Directly on a site in a lithologic section two engineering- geological elements (EGE) are allocated: EGE-1 and EGE-2.

First engineering-geological element EGE-1:

- from a surface it is covered with a powerful layer cultural and city adjournment of sandy and loamy structure with a large number inclusion of fragments of bricks, fights of pottery.

The layer is opened in intervals of depths of 0,0-14,5 m. The opened power changes from 6,8 to 14,5 m.

The second engineering-geological element EGE-2 consists of:

- the loams of gray and dusty color from damp to water- saturated with a sandy loam pro-layer, it is opened in intervals of depths of 6,8-15,0 m the opened power changes from 0,5 to 4,7 m.

Ground waters belong to nonaggressive in relation to concrete on sulfate-resistant brands of cement.

Category of soil – the second. Standard depth of seasonal frost penetration in soil – 0,8 m. Seismicity of the region of 8 points (Conclusion, 1980).

The results of observation

At the observation time of constructions the natural sizes, sections of designs, determination of physic mechanical properties of materials of construction designs, dynamic characteristics of designs, and also over sensitive seism metric devices were defined by devices of nondestructive control and technical diagnostics.

In the course of inspection defects, damages and the deformations which appeared in use were revealed:

• The minaret – destructions of part of a lamp, formation of through cracks 5-10 mm wide in arch locks, over lighting apertures disclosure of 3-5 mm wide were the main types of damages from dynamic (seismic), which are located from the level of the earth 12,60; 17,60; 22,80; 27,60; 31,80 m and in other places of the top part of a construction.

• The laying of a brick corresponds to the II category of equal 0,84-1,25 kg/cm^2, M-75 brick brand.

• overlapping - a lamp floor bricklaying after repair work is in a satisfactory condition. Disruptions of communication with a bricklaying of walls it isn't observed.

• The trabeation of a lamp is in a satisfactory condition.

• the ladder - a brick ladder leans on a trunk and external walls of a minaret. A satisfactory technical condition, steps didn't lose the bearing ability. Deformations and destructions it isn't observed.

• the roof is laid out from a zhzhenny square brick on ganch solution. In places insignificant cracks are observed. Destructions in a roof resulted from influence of an atmospheric precipitation and seismic influences.

• mosque walls brick thickness in the central part of 1200 mm, in lateral walls – 700 mm, back part – 800 mm, the laying of a brick corresponds to the II category of equal 0,70 - 0,95 kg/cm^2, M-75 brick brand.

On perimeter of walls are observed, from outer side the aeration of solution and the humidified sites in internal walls extending from floor level to 1,8-2,0 m on height (Figure 10)

• In walls on perimeter of a mosque and in a main entrance at the level of the second floor vertical and inclined cracks, disclosure of 2,0-8,0 mm wide, owing to seismic influences are observed.

• floors of a mosque are arranged from brick tiles with the sizes 260×270×40 mm. Because of soaking in left-side gallery of a mosque round columns occurred soil shrinkage, and at distance of 1,0-2,0 m from columns the exit of soil of 3,0-5,0 cm is observed. The exit of soil resulted, apparently, from a frost penetration in soil.

Figure 10. Aeration of Solution in Bricklaying Seams of Mosque Kalon.

Further, on the basis of the conducted on-site investigations and theoretical researches, it is planned to carry out:

- additional engineering-geological researches of sites and research by a SIR-3000 system georadar;
- calculation for an assessment of the intense deformed condition of designs at static loadings;
- calculation on seismic influences and an assessment of seismic stability of designs;
- development of constructive actions and recommendations about strengthening of designs.

5. SUMMARY AND CONCLUSIONS

Climatic, geotechnical and hydrogeological features of historical monuments of architecture of Central Asia are considered and was made the analysis of deformations of monuments of architecture of Central Asia;

The comparative analysis of modern ways of strengthening of the bases and foundations, the deformed monuments of architecture was made and was developed the recommendations about geomonitoring, preservation and protection of historical monuments of architecture;

The results of geotechnical researches were used and formed the basis of the offered observation method of monuments of Central Asia.The observation method of monuments of cultural heritage which purpose is monitoring of an actual state and the forecast of behavior of historical monuments of architecture of Central Asia was developed.

The superficial soil layer to 6 m is unstable and can't form the basis for a construction because of effect of a capillary raising of underground ground waters.

Application of numerical information technologies will allow to analyze more deeply the architectural and construction achievements corresponding to this or that historical period of time and to conduct monitoring of the happening processes.

Data on results of purposeful engineering-geological researches are among necessary materials; these surveys of design features of a monument, types of the foundatios and about distribution of loads of soil of the bases; data on nature of deformations and speed of their development; materials of supervision over an shrinkage of a monument or its elements.

Preventive conservation of historical monuments of architecture is pledge of their safe operation taking into account temporary and natural and technogenic factors and influence of environment.

REFERENCES

1. **Abdurashidov K.S., Kabulov F.R., Rakhmonov B. K.** Inzhenernye problemy arhitekturnyh pamjatnikov [Engineering problems of architectural monuments]. Uzbekistan, Tashkent, FAN, 2011 (in Russian).
2. **Guseva L.Yu.** Problema ispol'zovanija vodnyh resursov v Central'noj Azii [Problem of use of water resources in Central Asia]. Scientific paper. Almaty: KISI, 2000, pp. 8-15 (in Russian).

3. **Issina A.Z., Zhussupbekov A.Zh.** Analysis of geotechnical properties of soils and ground water of Mausoleum Arystan-Bab in South Kazakhstan. // Proceedings of 6th International symposium on Disaster Mitigation in Special Geoenvironmental Conditions, Chennai, India, 2015, pp. 277-280.
4. The conclusion "About engineering-geological conditions of a platform". Uzbekistan, Bukhara, 1980.
5. Report on the complex scientific researches "Engineering – geological and Hydrological Researches for the Mausoleum Arystan-Bab in the South Kazakhstan Area". Kazakhstan, Alma-Ata, 2004.
6. The scientific and technical report "An assessment of operational reliability of the mausoleum Samanidov, a minaret and a mosque Kalon in Bukhara". Uzbekistan, Tashkent, 2014.

СПИСОК ЛИТЕРАТУРЫ

1. **Абдурашидов К.С., Кабулов Ф.Р., Рахманов Б.К.** Инженерные проблемы архитектурных памятников. – Ташкент: Фан, 2011.
2. **Гусева Л.Ю.** Проблема использования водных ресурсов в Центральной Азии. Научная статья. Алматы: КИСИ, 2000, с. 8-15.
3. **Issina A.Z., Zhussupbekov A.Zh.** Analysis of geotechnical properties of soils and ground water of Mausoleum Arystan-Bab in South Kazakhstan. // Proceedings of 6th International symposium on Disaster Mitigation in Special Geoenvironmental Conditions, Chennai, India, 2015, pp. 277-280.
4. The conclusion "About engineering-geological conditions of a platform". Uzbekistan, Bukhara, 1980.
5. Report on the complex scientific researches "Engineering – geological and Hydrological Researches for the Mausoleum Arystan-Bab in the South Kazakhstan Area". Kazakhstan, Alma-Ata, 2004.
6. The scientific and technical report "An assessment of operational reliability of the mausoleum Samanidov, a minaret and a mosque Kalon in Bukhara". Uzbekistan, Tashkent, 2014.

A.Zh. Zhussupbekov, Professor, Dr.Sc.; Department of Civil Engineering, L.N. Gumilyov Eurasian National University, 010008, Satpayev street, 2, Nur-Sultan, Kazakhstan;
phone: +7 (7172) 344796;
E-mail: astana-geostroi@mail.ru

A.Issina, PhD, Associate Professor, Department of Architecture and Design, Saken Seifullin Kazakh Agricultural Technical University, 010011, Zhenis ave., 62, Nur Sultan, Kazakhstan; phone: +7 (7172) 31-75-47;
E-mail: isinaasem83@gmail.com

Y. Iwasaki, Director, Geo-Research Institute, Osaka, Japan, 4-3 2, Itachi-bori, Nishi-ku, Osaka 550-0012;
Phone: +81-6-6539-2976;
E-mail:dec19yoshi1+torino@gmail.com

Sh. Kenjaev, Department of Civil Engineering, Tashkent Institute of Architecture and Civil Engineering, Navoi street, 13,Tashkent, Uzbekistan; phone: +7 (7172) 31-75-47;
E-mail: isinaasem83@gmail.com.

I. Usmankhodjaev, Department of Civil Engineering, Tashkent Institute of Architecture and Civil Engineering, Lolazor St. 70, Samarkand, Uzbekistan,140147;
phone: (+998) 93 330-55-66;
e-mail:uzssmge@gmail.com

Жусупбеков А.Ж., профессор, доктор технических наук; Евразийский национальный университет им. Л.Н. Гумилева; 010008, Республика Казахстан, г. Нур-Султан, ул. Сатпаева, д. 2; тел: +7 (7172)344796;
E-mail: astana-geostroi@mail.ru.

Исина А.З., PhD, ассоциированный профессор, Казахский агротехнический университет им. С.Сейфуллина, 010011, пр. Победы, 62, г. Нур-Султан, Казахстан,
Тел: +7 (7172) 31-75-47;
E-mail: isinaasem83@gmail.com.

И. Ивасаки, директор, Институт гео- исследований, Осака, Япония, 4-3 2, Itachi-bori, Nishi-ku, Osaka 550-0012; phone+81-6-653 2976;
E-mail: dec19yoshi1+torino@gmail.com.

Кенжаев Ш., Строительный факультет, Ташкентский архитектурно-строительный институт, ул. Навои, 13, Ташкент, Узбекистан; тел: +7 (7172) 31-75-47;
e-mail: isinaasem83@gmail.com

Усманходжаев И., Строительный факультет, Ташкентский архитектурно-строительный институт, ул. Лолазор, 70, 140147, Самарканд, Узбекистан,
тел: (+998) 93 330-55-66;
E-mail: uzssmge@gmail.com.